TECHNISCHE UNIVERSITÄT MÜNCHEN

Lehrstuhl für Entwicklungsgenetik

Regulation, biochemistry and functional analysis of the conserved Lunapark protein in central nervous system development

Niklas Julius Senghaas

Vollständiger Abdruck der von der Fakultät Wissenschaftszentrum Weihenstephan für Ernährung, Landnutzung und Umwelt der Technischen Universität München zur Erlangung des akademischen Grades eines

Doktors der Naturwissenschaften

genehmigte Dissertation.

Vorsitzende(r): Univ.-Prof. Dr. S. Scherer

Prüfer der Dissertation:

1. Univ.-Prof. Dr. W. Wurst
2. Univ.-Prof. Dr. C. Schwechheimer

Die Dissertation wurde am 22.11.2010 bei der Technischen Universität München eingereicht und durch die Fakultät Wissenschaftszentrum Weihenstephan für Ernährung, Landnutzung und Umwelt am 28.01.2011 angenommen.

I Abstract

Neuronal migration and differentiation are key processes in the development of the vertebrate central nervous system, but many of the involved genes, underlying mechanisms and pathways still remain unknown.

Because of its prominent expression during zebrafish (*Danio rerio*) brain development, we have analyzed the regulation, biochemical interaction, subcellular localisation and function of the novel gene *lunaparkA* (*lnpA*) and its encoded protein.

The *lnpA* gene is highly conserved among vertebrate species concerning its nucleotide sequence and its regulation of expression. In zebrafish *lnpA* mRNA is expressed in the hindbrain, in the developing trunk muscles, in the fin buds, in the inner ear and in the developing eye. In particular in the hindbrain *lnpA* shows a distinct expression pattern with strong expression in the anterior cerebellum, two longitudinal domains close to the ventral midline spanning the entire rhombencephalon and in a repetitive pattern of dorso-ventral stripes along the boundaries of individual rhombomeres. *lnpA* mRNA is expressed during a developmental period of extensive differentiation and migration of neuronal progenitors in the hindbrain of zebrafish embryos but is subsequently downregulated when the central nervous system is terminally differentiated. Cell culture experiments using fluorescent LunaparkA fusion proteins showed that LnpA localises to the endomembrane system of the cell most likely to the late endosomal and lysosomal compartments. Furthermore, we found that LnpA is capable of dimerising or oligomerising which may be important for its proper function.

Several factors known to be involved in vesicle fusion like Syntaxin7 and Vesicle-associated membrane protein-associated protein A and B (VapA/B) were identified to interact with LnpA and this interaction was confirmed by independent biochemical verification.

Membrane fusion is important for processes such as regulation of signal transduction, membrane expansion or transport of intracellular cargo to ensure proper differentiation of neuronal populations. Therefore LnpA could serve an essential role in proper brain development and thus function.

Furthermore we have established two stable transgenic zebrafish strains that express different genetically encoded fluorophores under the control of an *lnp* regulatory element. Reporter gene expression was detected in the same spatiotemporal pattern in hindbrain structures where *lunaparkA* mRNA is expressed. Moreover, we identified *lnp*:reporter expressing cells at the rhombomere boundaries as progenitors of hindbrain commissural interneurons (HCIs) of the sensory system. HCIs are derived from the dorsal most neuroepithelium in the hindbrain, the

athonal1a expressing rhombic lip. They represent the first lower rhombic lip derivative identified in zebrafish. Furthermore, we showed by in vivo time-lapse analysis that HCI progenitors first converge along dorsal rhombomere boundary tissue to subsequently migrate tangentially along the boundaries to ventral hindbrain positions.

These findings reveal a new role for rhombomere boundaries as tracks of circumferential migration from dorsal rhombic lip to ventral midline structures. Despite their common origin and developmental behaviour individual HCIs show very different axonal projections and hence efferent connections.

Conditional pharmacological inhibition or rhombic lip specific prolonged activation of Notch signal transduction using Gal4 combinatorial genetics demonstrated that Notch signalling is required for maintaining the HCI progenitor pool in the rhombic lip preventing their premature differentiation.

In addition, the studies showed that in order to differentiate, HCIs have to downregulate Notch activity, but proper migration of these neurons requires rhombic lip non-autonomous Notch-activity occurring likely along rhombomere boundaries. Thus, Notch signalling plays a two-fold role in the development of HCIs by mediating the balance between progenitor maintenance and neuronal differentiation and by mediating neuronal migration to ensure the proper positioning of these neurons. Notch signalling thereby guarantees correct positioning of the HCI progenitors in the ventral hindbrain and ensures the generation of later born rhombic lip neuronal subtypes by maintaining a progenitor pool. Therefore Notch signalling has to be carefully orchestrated for proper hindbrain development and function.

II Zusammenfassung

Die Migration und die Differenzierung von Nervenzellen sind fundamentale Schritte in der Entwicklung des zentralen Nervensystems von Wirbeltieren. Viele der dafür verantwortlichen zellulären Vorgänge sowie die daran beteiligten Gene und deren Funktion sind jedoch noch unbekannt.

Die vorliegende Arbeit beschäftigt sich mit der Analyse der Expression und Regulation des Zebrafisch-Gens *lunaparkA* sowie mit der Funktion des kodierten LunaparkA-Proteins. Dabei wurde untersucht, welche Signaltransduktionsvorgänge dieses Gen regulieren, in welchem Zellkompartiment das LunaparkA Protein lokalisiert ist, ob und mit welchen anderen Proteinen LunaparkA interagiert und welche Funktion es während der Entwicklung des Nervensystems ausübt.

Ursprünglich wurde das bisher kaum charakterisierte Gen aufgrund seines ausgeprägten Expressionsmusters während der Hirnentwicklung im Zebrafisch für eine Funktionsanalyse ausgewählt. Die bisher fehlenden Daten zur Expression, Regulation und Funktion zu diesem Protein in Vertebraten sind überraschend, da sowohl die Nukleotidsequenz als auch das Genexpressionsmuster von *lnpA* innerhalb der Wirbeltiere hochkonserviert sind. Die mRNA von *lnpA* wird im Klein- und Stammhirn, in der sich entwickelnden Rumpfmuskulatur, in den Flossenanlagen, im Innenohr und im Auge exprimiert. Im Hinterhirnstamm ist das Expressionsmuster von *lnpA* besonders charakteristisch und zeigt eine intensive Expression in zwei longitudinalen Domänen die nahe der ventralen Mittellinie verlaufen und sich durch das gesamte Hinterhirn ziehen. Zusätzlich verläuft die *lnpA* Expression in sich wiederholenden dorsoventralen Streifen entlang der Grenzen zwischen einzelnen Rhombomeren. Interessanterweise wird *lnpA* in einer Entwicklungsphase exprimiert, in der verstärkt Differenzierungs- und Migrationsprozesse neuronaler Vorläuferzellen im Hinterhirn ablaufen.

In Experimenten, in denen fluoreszierende LunaparkA Fusionsproteine zusammen mit subzellulären Fluoreszenzmarkern in Zellkultur exprimiert wurden, stellte sich heraus, dass das LnpA Protein im Endomembransystem von Zellen lokalisiert ist - höchstwahrscheinlich in späten Endosomen und Lysosomen. Des Weiteren konnten wir zeigen, dass LnpA Proteine in der Lage sind zu dimerisiern oder oligomerisieren, was eine wichtige Rolle bei der Funktion des Proteins spielen sollte.

Um zu ermitteln, in welchen biologischen Prozessen LnpA agiert, wurden potentielle Interaktionspartner von LunaparkA mittels massenspektrometrischer Verfahren identifiziert. Auffällig viele der isolierten Bindungspartner, wie zum Beispiel Syntaxin7 oder Vesicle-

associated membrane protein-associated protein A und B (VapA/B), spielen eine Rolle bei der Fusion biologischer Membranen. Betrachtet man diese Daten im Kontext mit der zeitlichen und räumlichen Expression von LunaparkA, seiner Sekundärstruktur sowie der subzellulären Lokalisation, so liegt der Schluss nahe, dass LnpA bei Membranfusionsprozessen in migrierenden und differenzierenden Nervenzellen des sich entwickelnden Hinterhirns eine involviert ist.

In Neuronen ist die korrekte Fusion von Vesikeln von entscheidender Bedeutung unter anderem für die Regulation der intrazellulären Signaltransduktion, beim Transport von biologischen Molekülen in Vesikeln und bei der Erweiterung extrazellulärer Membranen wie dem ausgeprägten Axonwachstum von Nervenzellen. Aus diesem Grund ist es möglich, dass LnpA entscheidend für die korrekte Entwicklung und damit Funktion des Gehirns ist.

Um daher die Funktionsanalyse von LunaparkA zu beginnen, wurden im Rahmen dieser Doktorarbeit zwei stabil transgene Zebrafischstämme etabliert, welche unterschiedlich fluoreszierende Reporterproteine unter der Kontrolle eines regulatorischen Elementes des *lnp* Gens exprimieren. Die Expressionsmuster der jeweiligen Reporterproteine weisen eine zeitlich-räumliche Verteilung von großer Ähnlichkeit mit endogener *lnpA* mRNA auf. Zudem konnten histologische Studien in dieser Arbeit zeigen, dass die fluoreszierenden Reporterproteine in Vorläuferzellen kommissuraler Interneurone des Hinterhirns (HCIs) exprimiert werden. Diese HCIs werden in der Rautenlippe, im dem am meisten dorsal gelegenen Neuroepithel gebildet. Die HCI-Vorläufer verlassen während ihrer Entwicklung die Rautenlippe und migrieren tangential entlang der Rhombomergrenzen in Regionen des ventralen Hinterhirns in die Nähe der ventralen Bodenplatte ein. Damit konnte gezeigt werden, dass Rhombomergrenzen als Migrationspfade für differenzierende Neurone fungieren, ein neuer bisher unbekannter Migrationsweg in Vertebraten, der den Zellen entlang von Rhombomergrenzen neue Funktionen zuschreibt.

Durch pharmakologische Inhibition oder Überaktivierung des Notch Signalweges spezifisch in Zellen der Rautenlippe konnte gezeigt werden, dass die Aktivierung von Notch Signaltransduktion für den Erhalt der HCI Vorläuferzellen in der Rautenlippe notwendig ist. Durch die Aktivierung von Notch wird zudem eine vorzeitige Differenzierung von Zellen der Rautenlippe verhindert. Darüber hinaus zeigt diese Arbeit, dass die Aktivierung des Notch Signaltransduktionsweges herunterreguliert werden muss, um den kommissuralen Interneuronen die Differenzierung zu ermöglichen. Für die korrekte Wanderung dieser Interneurone ist jedoch eine neuerliche nicht-zellautonome Aktivierung von Notch Signaltransduktion erforderlich. Diese Ergebnisse zeigen, dass Notch-Signaltransduktion eine

zweifache Rolle bei der Differenzierung von HCIs spielt. Zum einen steuert er die Balance zwischen der Aufrechterhaltung von Vorläuferzellen und deren Differenzierung in HCIs, zum anderen sorgt er, durch die Regulation der HCI-Migration, für eine korrekte endgültige Positionierung dieser Interneurone. Das bedeutet, dass Notch Signaltransduktion zeitlich und räumlich sehr präzise im Hinterhirn reguliert werden muss, um die korrekte Entwicklung kommissuraler Interneurone im Hinterhirn zu garantieren. Erste weitere Analysen zur Funktion von Lunapark legen tatsächlich eine Rolle dieses Proteins in der Differenzierung von HCI-Neuronen nahe und müssen in der Zukunft weiter detailliert werden. Diese Ergebnisse zeigen die Bedeutung des Zusammenspiels von Signaltransduktion, Mechanismen der Zellschicksalbestimmung und von zellbiologischen Prozessen, um schließlich ein funktionales Hinterhirn zu etablieren, welches die essentiellen Vitalfunktionen in Wirbeltieren steuert.

III Danksagung

Mein größter Dank geht an Prof. Dr. Reinhard W. Köster. Ich danke Ihm für die hervorragende Betreuung. Er stand mir jeder Zeit ohne Ausnahme mit Rat und Tat zur Seite und unterstützte mich mit all seiner Kraft. Er hatte immer ein offenes Ohr und gab mir immer das Gefühl, bei all meinen Entscheidungen hinter mir zu stehen. Von Reinhard Köster habe ich viel gelernt, auch abseits biologisch wissenschaftlicher Fragestellungen, dafür bin ich sehr dankbar. Ich danke Ihm auch dafür, dass er mir viele Entfaltungsmöglichkeiten gegeben hat. Dazu gehört die selbstverantwortliche Arbeit, zahlreiche Fortbildungen (Singapur, Malik) und das Betreuen von Studenten.
Ich gratuliere Reinhard Köster hiermit nochmals zu seiner Professur, ich wünsche ihm alles Gute für die Zukunft und weiterhin viele spannende Ergebnisse und bleibe ihm freundschaftlich verbunden.

Ich bedanke mich bei Mariana Peer, der ich so vieles zu Verdanken habe. Im Zuge der Doktorarbeit möchte ich ihr dafür danken, dass sie auch in den ganz schwierigen Phasen mir Mut und Kraft gegeben hat und vor allem immer an mich geglaubt hat, selbst wenn ich das einmal nicht getan habe.

Ganz herzlich möchte ich auch meinen Eltern für ihre bedingungslose Unterstützung in allen Lebenslagen danken. Außerdem haben sie mir mein Studium, das den Grundstein für diese Arbeit gelegt hat, ermöglicht.

Ein ganz besonders großes Dankschön geht an Barbara Solchenberger, die durch ihr unermüdliches Engagement und ihre wirklich hervorragende Masterarbeit einen wichtigen Beitrag zum Abschnitt über die Notch Regulation und die Charakterisierung der Lunapark Linien in dieser Doktorarbeit beigetragen hat.

Außerordentlich dankbar bin ich für die wirklich netten Arbeitskollegen und die tolle Atmosphäre im Labor. Ich denke nur wenige haben das Glück so eine harmonische und freundschaftliche Verbindung mit dem Großteil seiner Kollegen zu haben.
Besonders danke ich Enrico Kühn für grandiose Gesangs und Pfeifduette und natürlich für seine großartige Unterstützung im Laboralltag.
Ich danke Dr. Sandra Rieger für eine wirklich nette Zeit im Labor und moralische Unterstützung in schwierigen Phasen.
Auch danke ich meinen Bürokollegen Dr. Katrin Volkmann und Dr. Andreas Babaryka besonders für ihre Vorbildfunktion bei der termingerechten Vorbereitung von Vorträgen und Postern.

I want to thank Kaszuhiko Namikawa for giving valuable insights into Japanese pronunciation. I also want to thank Jen especially for reading and correcting my thesis.

Ich danke Rosemarie Söllner dafür, dass sie für mich den Firmenlauf bestritten hat und mich mit ihrer Beharrlichkeit nicht völlig in den Wahnsinn getrieben hat.
Anna-Lena danke ich für ihre Unterstützung dabei und für ihre nette Gesellschaft.
Bei Thomas bedanke ich mich für nette Unerhaltungen wissenschaftlich und privat, wie auch für sein betörendes Flötenspiel.

Allen dreien Danke ich auch nochmals fürs Korrekturlesen.

Ich bedanke mich außerdem bei allen Kollegen, die den beschwerlichen Aufstieg zu Guffert mitgemacht haben.

Bedanken möchte ich mich auch bei Petra Hammerl für ihre großartige Hilfe im Labor und bei den Fischen, sowie bei den Damen in der Fischanlage für deren tolle Arbeit.

Ich möchte mich auch noch bei allen Mitarbeitern im IDG bedanken die ich kennenlernen durfte hier ganz besonders bei Annerose Drexler.
Der ZEN Gruppe möchte ich zuerst mal danken, dass sie Humor verstehen und für viele, viele Tipps und Materialien.

Die Gruppe von Dr. Lie hat des Öfteren ausgeholfen wenn beim Zellkulturmaterial mal wieder Not am Mann war, danke dafür.

Prisca Chapouton möchte ich für Ihre Hilfe und anregende Diskussion beim Notch Projekt danken.

Recht herzlich möchte ich mich auch bei all unseren Kooperationspartner bedanken.
Dazu gehören zum einen Dr. Johannes Glöckner, Felix von Zweidorf und Prof. Dr Marius Üffing und allen anderen die die massenspektrometrischen Analysen für uns durchgeführt haben und zum anderen Yuan Chu und Dr. Ralf Kühn für die Zusammenarbeit beim Caspase Paper.

I am also grateful to everyone being kind enough to provide us with DNA constructs or zebrafish transgenic strains including David Wilkinson, Dirk Meyer, Robert Lodge, Don Lamb, Suzanne Pfeffer, Laure Bally-Cuif, Prisca Chapouton, B. Appel, S. Leach, S. Harris, N. Lawson, R. Bernados, N. Scheer.

Ich bedanke mich ganz herzlich bei Prof. Dr. Wolfgang Wurst, dass er mir die Möglichkeit gegeben hat meine Doktorarbeit in seinem Institut durchzuführen.

Ganz am Ende möchte ich mich noch bei meinen beiden Prüfern Prof. Dr. W. Wurst und Prof. Dr. C. Schwechheimer sowie dem Prüfungsvorsitzendem Prof. Dr. S. Scherer bedanken

IV Table of content

I Abstract 1

II Zusammenfassung 3

III Danksagung 6

IV Table of content 8

1. Introduction 12

1.1. Hindbrain Development 12
1.1.1. The Rhombomeres 12
1.1.2. Key molecules in hindbrain development 14
1.1.3. Rhombomere cells are sorted by adhesion molecules 17
1.1.4. The rhombomere boundaries 18
1.1.5. Segment organisation inside rhombomeres 21
1.1.6. Atonal1 and the rhombic lip 23

1.2. The Notch Signal Transduction Pathway 26
1.2.1. Notch signalling: The core pathway 26
1.2.2. Modulation of Notch activity by processing and trafficking 27
1.2.3. Notch Signalling during development 29

1.3. Neuronal Migration 31
1.3.1. Modes of migration tangential versus radial 31
1.3.2. Differentiation and axonogenesis 32

1.4. Endosomes: their role in signalling processes and cellular dynamincs 34

1.5. Lunapark 39

1.6. Aim of the study 41

2. Materials and Methods 43

2.1. Equipment and Reagents 43
2.1.1. Equipment 43
2.1.2. Suppliers of chemicals and consumables 44
2.1.3. Antibodies 44
2.1.4. Kits, Enzymes and Affinity Purification Reagents 45
2.1.5. Buffers and media 46
2.1.5.1. Protein Biochemistry 46
2.1.5.2. Fish Media 46
2.1.5.3. Histology 47
2.1.5.4. *E.coli* & Cell Culture Medium 47
2.1.6. Software for image procession 47
2.1.7. Bacteria strains and cell culture lines 48
2.1.7.1. Bacteria 48
2.1.7.2. Cell culture 48
2.1.8. Fish Strains 48
2.1.8.1. Wild type 48
2.1.8.2. Mutant strains 48
2.1.8.3. Transgenic lines 48
2.1.9. Antisense Oligonucleotides 48
2.1.10. Plasmid Vectors 49
2.1.11. Oligonucleotides for cloning and sequencing 51

2.2. Experimental Procedures 52
2.2.1. DNA handling and cloning procedures 52
2.2.1.1. Plasmid transformation 52
2.2.1.2. Low scale plasmid preparation from bacteria (Mini Prep) 52
2.2.1.3. Large scale plasmid preparation from bacteria (Maxi Prep) 52

2.2.1.4. DNA concentration measurement 53
2.2.1.5. Restriction digest of plasmid DNA 53
2.2.1.6. DNA ligation 53
2.2.1.7. DNA agarose gel electrophoresis 54
2.2.1.8. RNA gel electrophoresis 54
2.2.1.9. Extraction of DNA fragments from agarose gels after electrophoresis 54
2.2.1.10. DNA purification of PCR products or fragments of restriction digest 54
2.2.1.11. Removal of 5' DNA overhang 55
2.2.1.12. DNA dephosphorylation 55
2.2.1.13. Nippon oligo cloning 55
2.2.1.14. PCR 56
2.2.1.15. Purification of RNA 56
2.2.1.16. RNA extraction from animal tissue 56
2.2.1.17. Preparation of cDNA 57
2.2.1.18. Stratagene blunt cloning 57
2.2.2. Zebrafish maintenance 57
2.2.2.1. Maintenance of zebrafish 57
2.2.3. Methods for genetic and pharmacological manipulation of zebrafish embryos 58
2.2.3.1. Synthesis of capped mRNA for microinjection into zebrafish embryos 58
2.2.3.2. Cytoplasmic microinjection of nucleic acids 58
2.2.3.3. DAPT treatment of zebrafish embryos 59
2.2.3.4. Morpholino injection 59
2.2.4. Histological Techniques 59
2.2.4.1. Whole-mount in-situ-hybridisation (ISH) 59
2.2.4.2. Immuno histohemistry (IHC) wholemount preparation of zebrafish embryos 61
2.2.4.3. IHC acetone permeabilisation and antigen unmasking 61
2.2.4.4. DAB staining 62
2.2.5. Staining applications using fluorescent Dyes 62
2.2.5.1. Membrane staining using Bodipy Ceramide® 62
2.2.5.2. 4',6-Diamidin-2-phenylindol (DAPI) nuclear staining 62
2.2.5.3. TO-PRO® 3 hair cell staining 63
2.2.5.4. Sytox orange (Acridine Orange) nucleic acid stain 63
2.2.6. Biochemical Methods 63
2.2.6.1. Maintenance and transfection of zebrafish PAC2 cells 63
2.2.6.2. Maintenance and transfection of mammalian cells 63
2.2.6.3. Protein lysate preparation from cultured cells 64
2.2.6.4. BCA protein assay reagent 65
2.2.6.5. Co-immunoprecipitation 65
2.2.6.6. SDS-Page (SDS-polyacrylamide gel electrophoresis) 65
2.2.6.7. Silver staining 66
2.2.6.8. Western blot and immuno-detection 67
2.2.7. Proteomics 67
2.2.7.1. Preparation of cell lysates 68
2.2.7.2. SF-TAP Streptavidin FLAG tag tandem affinity purification 68
2.2.7.3. Methanol chloroform protein precipitation 69
2.2.7.4. Sample preparation for mass spectrometry (MS) analysis: in-solution digest 70
2.2.7.5. Mass Spectrometry (MS) Analysis and Data Processing 71
2.2.8. Imaging 71
2.2.8.1. Cell culture 71
2.2.8.2. Imaging of zebrafish embryos 71
2.2.8.3. Kaede Photoconversion in living zebrafish embryos 71
2.2.8.4. Processing 72

***3. Results* 73**

3.1. Lunapark in zebrafish 73
3.1.1. The zebrafish genome contains two highly conserved *lunapark* genes 73
3.1.2. *LunaparkA* is expressed in the CNS and in the muscles of the developing zebrafish embryo 78

3.2. Subcellular localisation of Lunapark protein 80
3.2.1. Fluorescent LnpA reporter proteins localise to large vesicular structures in PAC2 cells 80
3.2.2. LnpA localises to late endosomes and lysosomes in NIH3T3 cells 81
3.2.3. The N-terminus is required for proper localisation of LnpA Protein 85

3.3. Screen for Interaction partners of Lunapark 88
3.3.1. The SF-TAP system 88
3.3.2. Analysis of purification and enrichment of Lnp bait proteins 90
3.3.3. Mass spectrometric analysis of Lnp-SF-TAP pulldowns 92
3.3.4. Syntaxin 7-like (Stx7) 96
3.3.5. Biochemical validation of Syntaxin 7-like interaction with zebrafish LunaparkA 97
3.3.6. Intracellular localisation of Syntaxin 7-like and its co-localisation with LnpA 101

3.4. Morpholino Artefacts – death of a phenotype 102
3.4.1. Three independent Morpholinos effectively target *lunaparkA* mRNA 102
3.4.2. *lunaparkA* Morpholino injection results in an alteration of rhombomere boundary expression and a loss of hindbrain commissural interneurons 105
3.4.3. *lunaparkA* Morpholinos cause *p53* dependent apoptotic hindbrain artefacts 108

3.5. Analysis of the *lnp* enhancer strains identifies a new role for rh boundaries 112
3.5.1. Generation and expression analysis of transgenic *lnp* enhancer reporter strains 112
3.5.2. *lnp*:mRFP cells differentiate into postmitotic interneurons of the sensory system and show a high diversity in their axonal projections. 116
3.5.3. HCIs are derived from the rhombic lip 121
3.5.4. HCIs migrate along the rhombomere boundaries to ventral target regions 122

3.6. Regulation 125
3.6.1. Notch signalling is active in *lnp*:mRFP expressing HCIs 125
3.6.2. Inhibition of Notch signalling impairs HCI differentiation 127
3.6.3. HCI progenitors are not maintained after DAPT-mediated Notch inhibition 129
3.6.4. Activation of Notch impairs HCI differentiation by prolonged progenitor state maintenance 130
3.6.5. Inhibition of Notch signalling leads to premature neuronal differentiation 134
3.6.6. Notch signalling is essential for progenitor maintenance in the hindbrain 136
3.6.7. Over-activation of Notch under control of the *atonal1a* enhancer element may lead to an increase in brain size 138
3.6.8. Inhibition of HCI differentiation impairs escape response after sound and vibration stimuli 139
3.6.9. NICD overexpression in haircells leads to their reduction but does not cause a complete loss of these cells 142

***4. Discussion* 144**

4.1. Zebrafish Lunapark is highly conserved and potentially functions in neuronal development by mediating membrane fusion events 144
4.1.1. Lunapark expression pattern and peptide sequences are highly conserved 144
4.1.2. LunaparkA localises to late endosomal/lysosomal compartments 146
4.1.3. The interactome of Lunapark shows a bias for vesicle trafficking proteins 148
4.1.4. The Morpholino artefacts 151
4.1.5. Lunapark: Summary & Future perspective 152

4.2. *atonal1* expressing rhombic lip cells migrate tangentially along the rhombomere boundaries in the zebrafish hindbrain 154
4.2.1. The global regulatory element of *lunapark* and the *hoxd* cluster drives reporter gene expression in migrating hindbrain commissural interneurons 154
4.2.2. HCIs are derived from the rhombic lip and migrate tangentially along rhombomere boundaries to their ventral target areas 155
4.2.3. HCIs form a complex meshwork of differentially projecting axons 157

4.3. Differentiation and migration of the *atonal1* expressing HCI progenitors depends on Notch signalling 158
4.3.1. Notch signalling is required for RL progenitor maintenance and for the differentiation of late born hindbrain neurons 158
4.3.2. Notch activity in neuronal migration 159
4.3.3. Rhombic lip progenitor and Notch regulation: Summary & Future perspective 160

***5. Appendix* 162**

5.1. Supplementary Figures 162

5.2. Abbrevations 163

5.3. Movie legends **164**

5.4. List of publications **166**

5.4.1. Publications 166

5.4.2. Publications in Preparation 166

5.5. Lebenslauf **167**

6. References **169**

1. Introduction

The vertebrate central nervous system (CNS) has a high degree of anatomical complexity, consisting of hundreds of distinct cell types. These cells are organised in a precise spatial pattern of glia and of neuronal cell bodies. The neurons are connected with each other and target tissues via circuitries of axons and dendrites. The high complexity of the CNS arises progressively during its development from the neural epithelium, an epithelial sheet of cells that is induced in the dorsal ectoderm. The neural epithelium folds to form the neural tube and is maintained as a proliferating cell population adjacent to the inner (ventricular) surface. These proliferating cells are a source of glial cells and postmitotic neuronal precursors. The latter migrate radially or tangentially to specific target sites within the neural tube were they differentiate into distinct types of neurons and establish connectivities (Pasini and Wilkinson 2002). Neuronal migration is a fundamental process that determines the final allocation of neurons in the nervous system. Thus the ability of neurons to migrate to their appropriate positions and to differentiate in the proper neuronal subtypes in the developing brain is critical to brain architecture and function (Metin et al. 2008).

1.1. Hindbrain Development

1.1.1. The Rhombomeres

The hindbrain is the most evolutionary ancient part of the vertebrate brain. In the adult, it is composed of the posteriorly localised medulla, the ventroanterior pons, and the dorsoanterior cerebellum (Figure 1). The cerebellum controls the coordination of movements. It receives a wide variety of sensory inputs and generates motor-related outputs according to internal rules of computation while transmitting information primarily to motor cortical areas (Apps and Garwicz 2005). The medulla and pons form the fourth ventricle of the brain, and together with the midbrain, they are often referred to as the "brainstem." The brainstem contains a conglomerate of cell groups that form a complex network termed the reticular formation, which is involved in controlling basal vital functions such as respiration, circulation, and wakefulness. The reticulospinal neurons of the brainstem provide the major route through which the brain communicates with the spinal cord to control locomotion (Moens and Prince 2002). In addition, cranial nerves projecting from the hindbrain control muscles in the jaw, eye, and face and receive sensory input from these regions (Chandrasekhar et al. 1997 ; Guthrie 2007). In all vertebrates the hindbrain is transiently segmented in compartments

termed neuromeres or rhombomeres. These segments are molecularly and physically defined and already visible under a brightfield microscope as morphological restricted compartments (Figure 2A). Although the clear morphological rhombomeric organisation is lost during

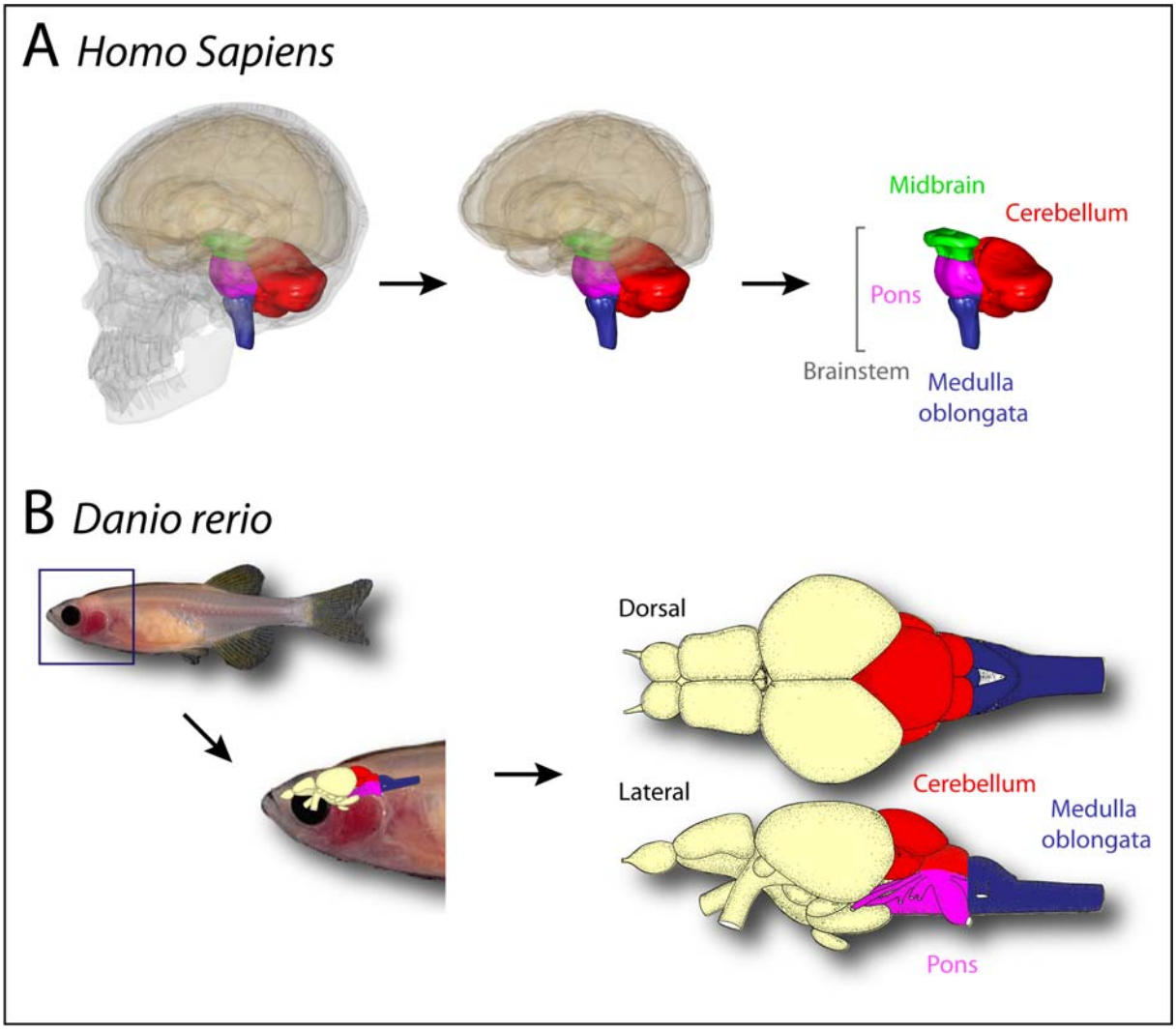

Figure 1 The hindbrain in human and in zebrafish

A 3D reconstruction of the human head highlighting the position and the individual parts of the hindbrain **B** Schematic drawings of the zebrafish hindbrain and its position within the adult animal. Adapted from (Wullimann et al. 1996).

development the initial segmentation is reminiscent e.g. in the patterning of the cranial nerves and reticulospinal neurons (Figure 2B) (Guthrie 2004). The order of these nerves is set up at an early developmental time point when the neuromeric organisation is still present. Moreover the rhombomeres are well established to influence hindbrain neural crest cell migration in general (Kulesa et al. 2005) or direct axon outgrowth of branchio motoneurons (Chandrasekhar 2004). These few examples highlight the relevance of the rhombomeres in coordinating neuronal patterning.

The rhombomers are established rather early in development; at the 18 somite stage they are visible as a series of bulges along the neural tube separated by boundaries (Kimmel et al.

1995). Rhombomeres do not arise in a straightforward anterior to posterior order as somite

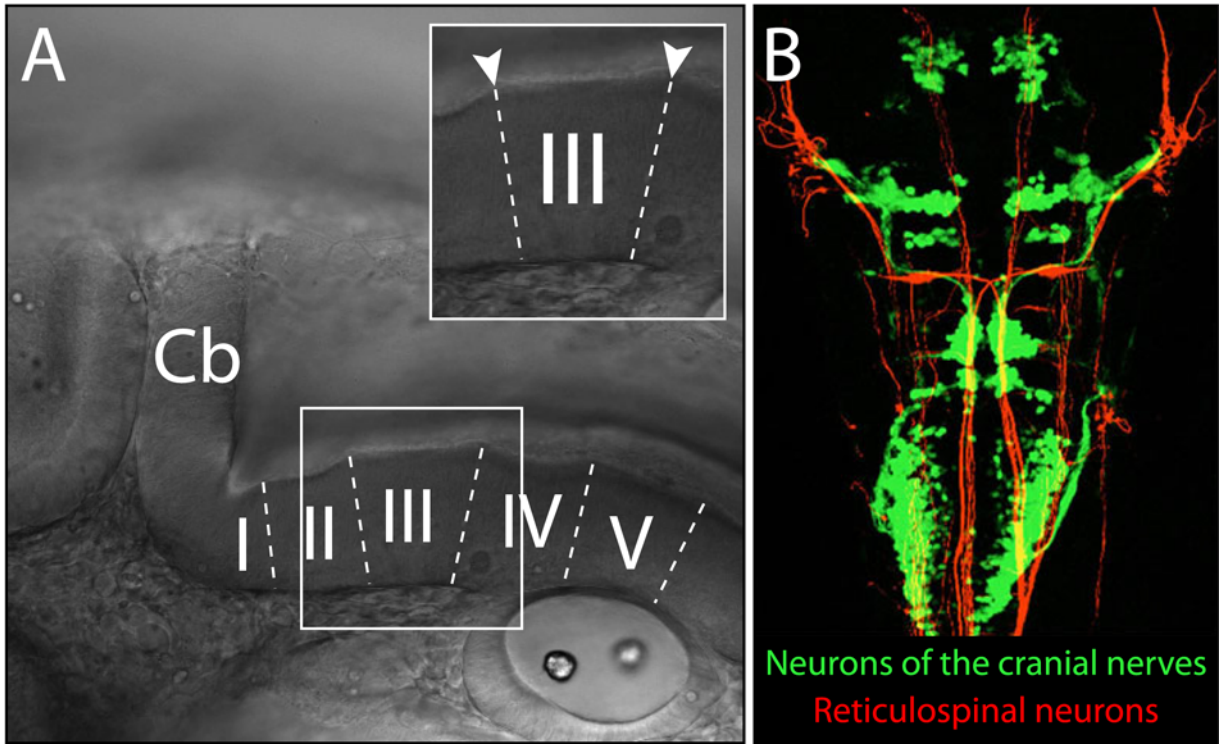

Figure 2 The rhombomeric organisation of the zebrafish hindbrain

A Lateral view of the hindbrain of a 24 hpf zebrafish embryo. Anterior is to the right. The interfaces between individual rhombomeres are indicated by dotted lines. **B** Distribution of different subtypes of branchiomotor neurons expressing *islet1* enhancer driven GFP (green) and reticulospinal neurons labelled by 3A10 antibody(red) zebrafish hindbrain (dorsal image, anterior to the top). Adapted from (Chandrasekhar 2004).

boundaries do in the trunk, but rather in a seemingly erratic order that nevertheless hints at the underlying genetic events. The order of boundary formation is stereotypical for embryos of a given species: in the zebrafish, the r4 territory is defined first with the appearance of the boundary between r3 and r4 (r3/4) and then the r4/5 boundary (Moens and Prince 2002).

1.1.2. Key molecules in hindbrain development

The molecular identity of the rhombomeres is determined much earlier than their morphological appearance. Right after gastrulation the hindbrain is strictly regionalised by the expression of a distinct combination of transcription factors mainly of the *homeobox* (*hox*) family and for example *early response element 2b* (*egr2b/krox20*) or *valentino*/*mafB* in individual compartments later giving rise to the rhombomeres (Figure 3). These factors are highly conserved in their role and in their expression pattern in all vertebrate species. The *hox* genes are initially activated by retinoic acid (RA) derived from the germ ring and the paraxial mesoderm. The enhancers of several *hox* genes contain retinoic acid response elements that are essential for their expression within the mouse hindbrain (Gavalas and Krumlauf 2000). At the onset of somitogenesis the high point of RA is located at the border between the

hindbrain and the spinal chord thereby creating diffusion gradients in both directions. While the posterior gradient is responsible for anterior posterior fates of spinal chord neurons the

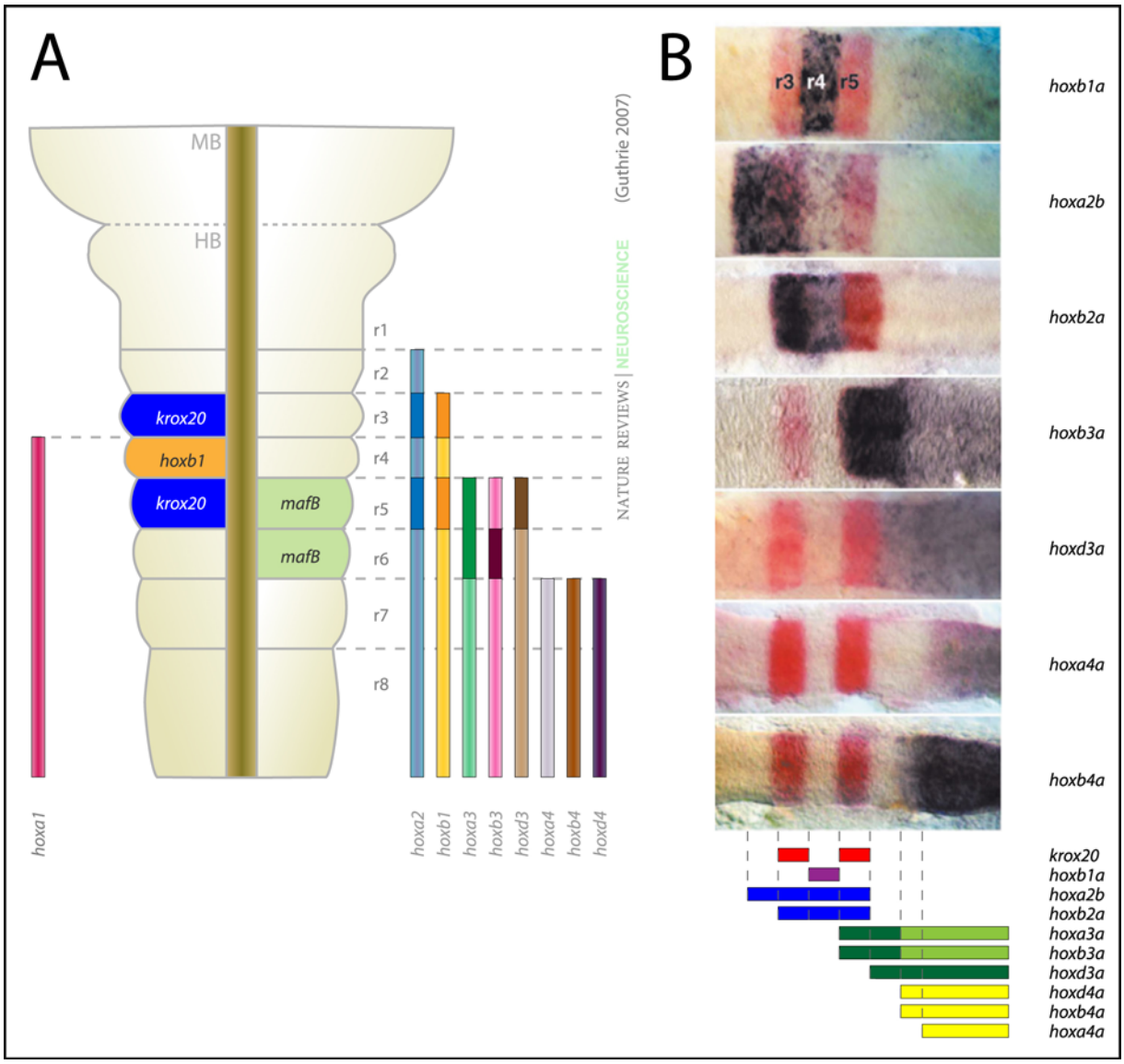

Figure 3 *hox* genes confer segment identity to the rhombomeres.

A Schematic view of the domains of mRNA expression of the *hox* genes *egr2* and *mafb* in the hindbrain of the mouse and chick embryo, at embryonic day 11.5 (E11.5) and E4, respectively. The bars labelled with different *hox* genes show the genes' expression domains, which extend from the caudal hindbrain up to particular rhombomere (r) boundaries. Darker shading indicates higher levels of expression. HB, hindbrain; MB, midbrain (anterior is to the top)
B Expression of zebrafish *hox* genes is rhombomere-restricted. Wholemount *in situ* hybridisation of *hox* genes (purple) together with *egr2b* (*krox20*) (red; r3 and r5) at 14 hours post-fertilisation (hpf), anterior is to the left, dorsal views. Adapted from (Moens and Prince 2002).

anterior gradient induces the hindbrain regionalisation by controlling *hox* gene expression (Hollemann et al. 1998; Maden et al. 1998a; Maden et al. 1998b). This RA diffusion gradient is opposed by an Fgf8 (Fibroblast growth factor 8) signalling gradient originating from the local organizer at the midbrain hindbrain boundary (MHB) also termed the isthmic organizer (IsO) that is involved in specifying r0 and in setting the boundary between r0 and r1.

Moreover Fgf8 together with Fgf3 is required for the specification of r5 and r6 (Joyner et al. 2000; Liu and Joyner 2001; Rhinn and Brand 2001; Maves et al. 2002).

The process of early hindbrain regionalisation is highly conserved in vertebrates. And the opposing morphogenic gradients of Fgf8 and RA signalling are well described in many vertebrate species such as fish, chick and frog (Moens and Prince 2002). In the zebrafish *neckless* mutant, in which the ultimate enzyme in the retinoic acid biosynthetic pathway, Retinaldehyde dehydrogenase 2 (Raldh2), is disrupted the hindbrain posterior to r6 is truncated and *hox* gene expression in this region is delayed and abnormal (Gould et al. 1998; Begemann et al. 2001). In the zebrafish *fgf8* mutant *acerebellar* (*ace*), cell types characteristic of the anterior part of r0 are absent (Ben-Arie et al. 1997). At the same time, the expression domain of *fgfr3*, a marker of r1, is expanded anteriorly (Sleptsova-Friedrich et al. 2001).

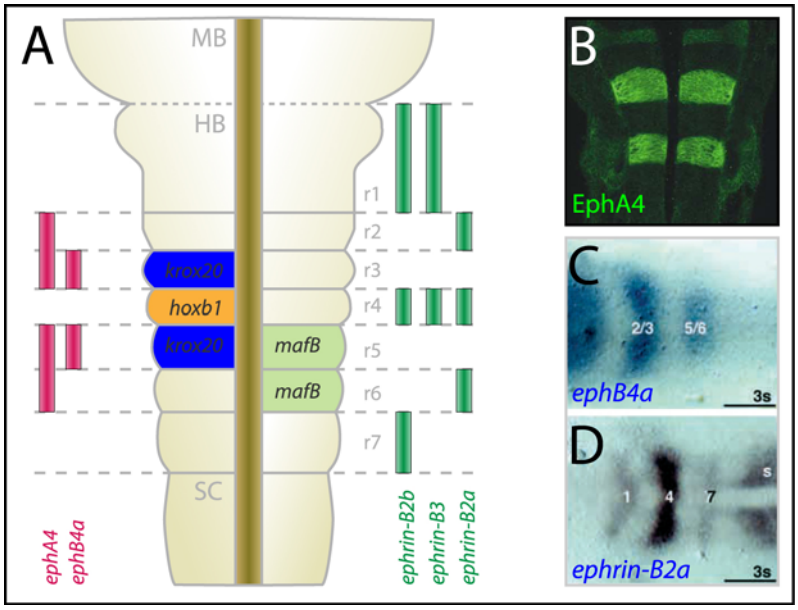

Figure 4 Expression patterns of *eph* and *ephrin* genes in the vertebrate hindbrain

A Schematic showing the domains of mRNA expression of selected *eph* and *ephrin* genes in the zebrafish hindbrain. Modified from (Guthrie 2007) **B** The *ephA4* Receptor is expressed in rhombomere 3 and 5 shown by immunolabeling. Adapted from (Cheng et al. 2004) **C, D** In situ hybridisation against *ephB4a* (**C**) and *ephrin-B2a* mRNA in 24 hpf zebrafish embryos. (Dorsal view image, anterior is to the left). Adapted from (Cooke et al. 2001).

In order to maintain the rhombomere identity, the transcription factors activated by these numerous morphogenes cross-regulate each other. For example in zebrafish the bZip transcription factor Valentino (MafB), positively regulates *hoxa3* and *hoxb3* (Manzanares et al. 1997) while negatively regulating *hoxb1a* (Prince et al. 1998).

Whether the RA and Fgf8 gradients antagonise each other or act either synergistically or independently is still unknown. Analyses in frogs suggest that they act as independent mechanisms in patterning distinct regions along the AP axis and that the *cdx* homeobox genes (vertebrate caudal homologs) are responsible for transducing the Fgf signals (Pownall et al.

1996; Kolm et al. 1997; Isaacs et al. 1998). Evidence is emerging, however, that *cdx* genes are targets of retinoid acid signalling, therefore the RA and Fgf pathways may be integrated at this level. In addition to these two morphogenes, posteriorising factors like Wnts, e.g. Wnt8 in *Xenopus*, or Nodal play a crucial role in the anterior posterior patterning of the rhombencephalon.

In summary it can be said, that during hindbrain development various prominent signalling pathways are carefully orchestrated to activate unique stets of transcription factors in individual rhombomeres and that these transcription factors cross-regulate each other to maintain the rhombomere specification.

1.1.3. Rhombomere cells are sorted by adhesion molecules

During the next step of hindbrain development the transcription factors expressed in individual rhombomeres translate into the expression of again rhombomere specific combinations of Eph receptor tyrosine kinases (Eph) and their Ephrin ligands (Figure 4). These Ephs and Ephrins are membrane proteins that mediate among other functions cell-cell repulsion and attraction in many developmental contexts. The outcome of a given Eph-Ephrin interaction is context dependent, and both in vivo and in vitro, receptor ligand pairs have been

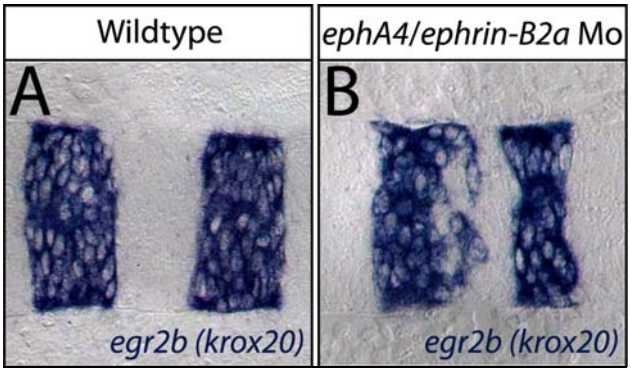

Figure 5 EphA4 and EfnB2a mediate hindbrain boundary sharpening.

Wholemount in situ hybridisations with an *egr2b* (*krox20*) riboprobe. (Anterior is to the left, dorsal views). **A** Brightfield image of an un-injected control embryo **B S**tage matched anti-*ephA4*; *ephrin-B2a* double Morpholino injected embryos. Adapted from (Kemp et al. 2009)

shown to mediate cell-cell repulsion in some instances, while promoting adhesion in others. In the developing zebrafish hindbrain, EphA4 is expressed in rhombomeres 3 and 5 while EphrinB ligands (EphrinB2a and EphrinB3) are expressed in the adjacent even rhombomeres. Knock-down of EphA4 results in the loss of rhombomere boundaries and the disruption of normal segmental hindbrain neuroanatomy, a phenotype that is exacerbated by simultaneous depletion of EphrinB2a, consistent with a critical role for these molecules in regulating the cell sorting behaviours that drive neuromere formation and maintenance (Figure 5) (Kemp et

al. 2009). In order to better understand the sorting process, scientists in the lab of Cecilia Moens performed transplantation experiments in combination with Morpholino mediated *ephA4* knockdown (Cooke et al. 2005). While transplanted wildtype cells were evenly distributed in the entire hindbrain of wildtype host embryos, EphA4 deficient donor cells were excluded from rhombomere 3 and 5 when transplanted in a wildtype background. In contrast, wildtype donor cells that were positioned by chance in the rhombomeres 3 and 5 of anti *eph4A* Mo injected hosts formed tight clusters not intermingling with the surrounding cells showing that the sorting is achieved by a mechanism of adhesion and repulsion. The fact that Eph-Ephrin interaction is capable of mediating adhesion and repulsion simultaneously is due to their unusual ability to initiate signalling in both the receptor-expressing ("forward signalling") and ligand-expressing ("reverse signalling") cells (Cowan and Henkemeyer 2001; Lu et al. 2001; Bong et al. 2004; Cowan et al. 2004).

1.1.4. The rhombomere boundaries

This strong and very restricted Eph-Ephrin mediated adhesion creates boundaries at each interface and shortly after the segmentation and sorting has finished, the boundary cells obtain distinct identities indicated by the expression of boundary-specific genes. They express among others members of the Wnt/β-Catenin signalling pathway e.g. *wnt1* or components of the Notch pathway like *radical fringe* (*rfng*) or *lunatic fringe* (*lnfg*), two modulators of the

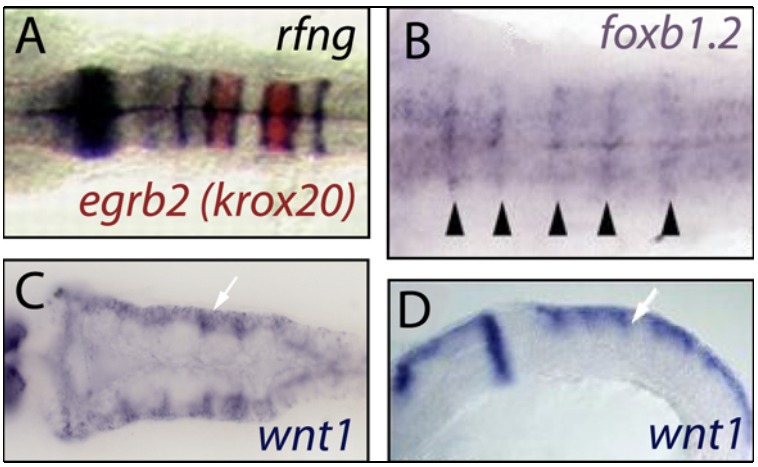

Figure 6 Rhombomere boundary marker genes

Wholemount in situ hybridisations of genes expressed specifically at the rhombomere boundaries. **A** *rfng* (black)/*egrb2* (*krox20*) (red) double staining of mRNA in situ hybridisation (dorsal view) (Skromne et al. 2007). **B** *foxb1.2* staining of mRNA in situ hybridisation (dorsal view) (Amoyel et al. 2005). **C**, **D** *wnt1* staining of mRNA in situ hybridisation. Showing dorsal view (**C**) and lateral view (Elsen et al. 2008) (**D**) images. In all images anterior is to the left.

Notch receptor (Figure 6). In contrast, cells directly adjacent to the boundaries express other factors like *deltaA* or *deltaD* or neurogenic markers like *neurogenic differentiation* (*neuroD*) or *neurogenin* (*ngn*) which promote neurogenesis (Figure 7). The Notch and the Wnt

signalling pathways are essential to maintain the boundaries thereby preventing neurogenesis at the boundaries and they are responsible for the patterning in the hindbrain segments (Cheng et al. 2004; Amoyel et al. 2005; Nikolaou et al. 2009).

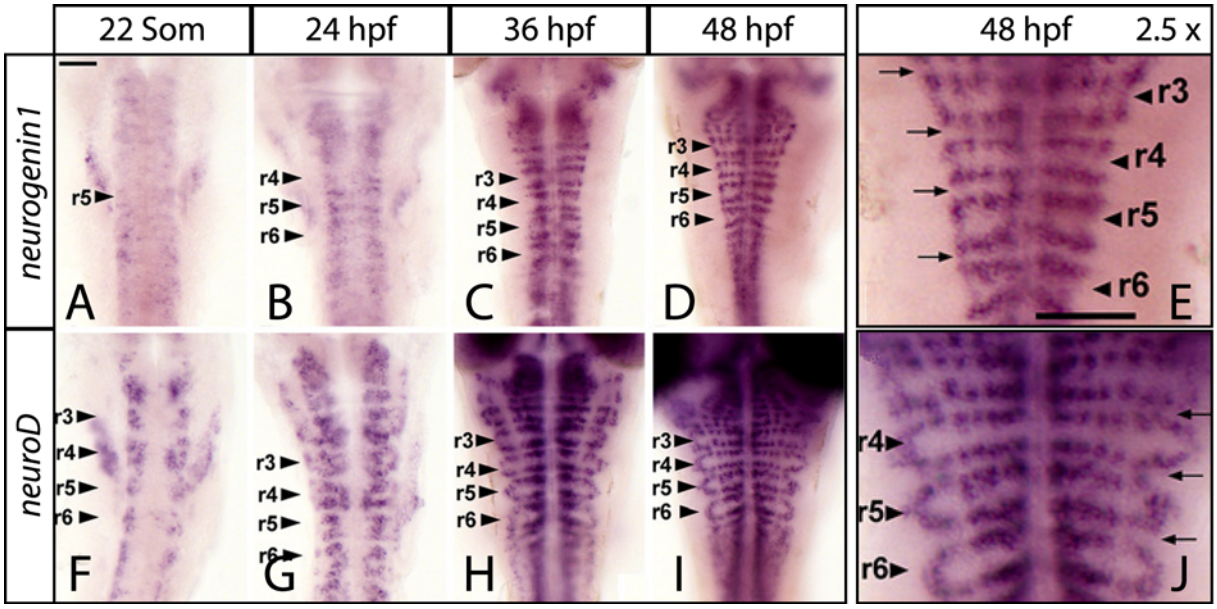

Figure 7 mRNA expression domains of neurogenic markers in the zebrafish hindbrain

A-**E** Whole mount in situ hybridisations against the mRNA of the neurogenic markers *neurogenin1* and **F**-**J** *neuroD* at the indicated developmental stages. Expression of these markers is absent at the boundaries and within the segment centres. Adapted from (Gonzalez-Quevedo et al. 2010).

Rhombomere boundaries have a dual function in development, they prevent the intermingling of cells that are fated to contribute to different parts of the embryo by differential adhesion and they provide positional information to flanking cell populations by regulating signal transduction. During development there are many examples for such cell lineage restriction boundaries (Kiecker and Lumsden 2005). For example both, the abdomen and the wing anlage of insect embryos were found to be segregated into cellular compartments by boundaries that cells do not cross thereby imposing lineage restriction on groups of cells (Garcia-Bellido et al. 1973; Lawrence 1973; Morata and Lawrence 1975). The most prominent example for a boundary having inductive properties in the vertebrate CNS is the midbrain hindbrain boundary (MHB) or isthmic organizer (IsO). The boundary is defined by the junction of the non-overlapping opposing expression of the homeobox genes *orthodenticle homologue 2* (*otx2*) and *gastrulation brain homeobox 2* (*gbx2*) (*gbx1* in zebrafish) at the end of gastrulation. The IsO is necessary and sufficient for the development of mesencephalic and metencephalic structures like the cerebellum or the anterior rhombomeres. (Broccoli et al. 1999; Wurst and Bally-Cuif 2001; Chi et al. 2003; Louvi et al. 2003; Puelles et al. 2003; Jukkola et al. 2006).

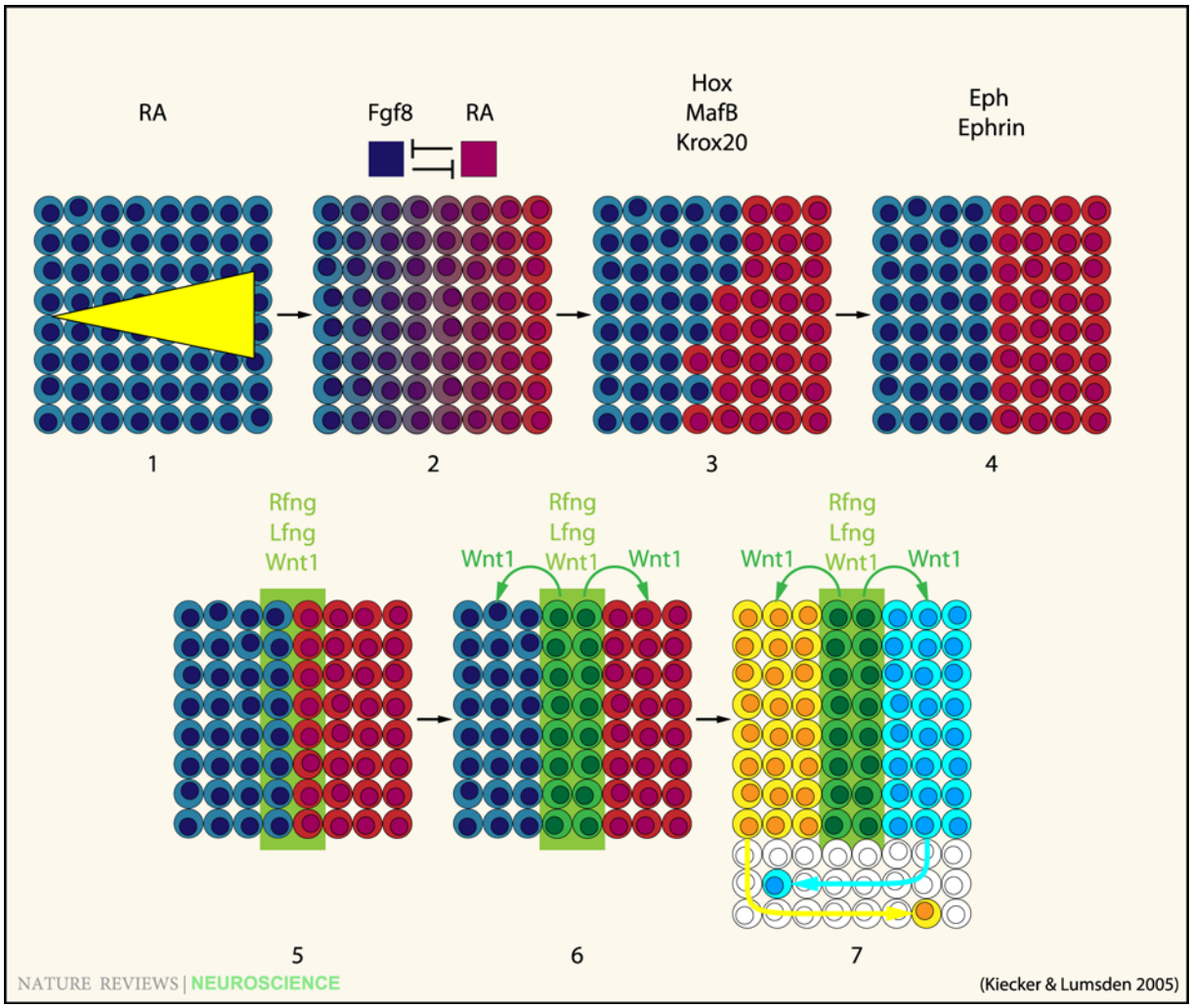

Figure 8 General model for boundary formation.

An initially uniform sheet of cells is polarised by an early signalling gradient (yellow; 1), which results in a coarse prepattern of transcription factor expression (red/blue; 2). Mutual repressive interactions between these factors establish two distinct populations of cells that are separated by a fuzzy interface (3). Cell-sorting processes result in a sharpening of this interface (4), and a specific boundary phenotype (loss of adhesion, expression of specific boundary markers) is generated (shaded area; 5). The boundary cells express signalling factors (green; 6) that induce prepattern-dependent cell fates (yellow/turquoise) in the adjacent territories. Postmitotic cells might be able to cross the boundary, as their fates are sealed (7) (Kiecker and Lumsden 2005). The indicated factors are specific for rhombomere boundary formation.

Due to their ability to induce the fate of adjacent cells in a non-autonomous manner, like the organizer of the gastrula of vertebrate embryos, boundaries like the IsO or the rhombomere boundaries are often referred to as secondary organizers as they appear after the gastrulation. Another key feature of the organizer during gastrulation is the reorganisation of the morphology of the embryo by directing intense migratory processes thereby forming the germ layers and extending the body axis. The organizer could thus be considered as a migratory landmark. Directing migration might also be an additional task for some of the secondary organizers. The mid hindbrain domain for example seems to direct the dorso ventral migration of granule cell precursors (Köster and Fraser 2001a, 2001b). Whether rhombomere boundaries are involved in migratory processes remains elusive so far.

1.1.5. Segment organisation inside rhombomeres

The rhombomeres are very individual and distinct in terms of the transcription factors and adhesion molecules that they express. Neurons derived from different rhombomeres innervate different target areas and are involved in different physiological processes. Despite this individuality of the rhombomeres the anterior posterior organisation of neurons and glial progenitors and their developmental time course is very similar in every segment. Moreover, there are many factors, which are expressed in a repetitive manner and they occur at the same position in every segment. This suggests that despite of their individuality in the adult the hindbrain, neurons follow a similar differentiation program in every segment.

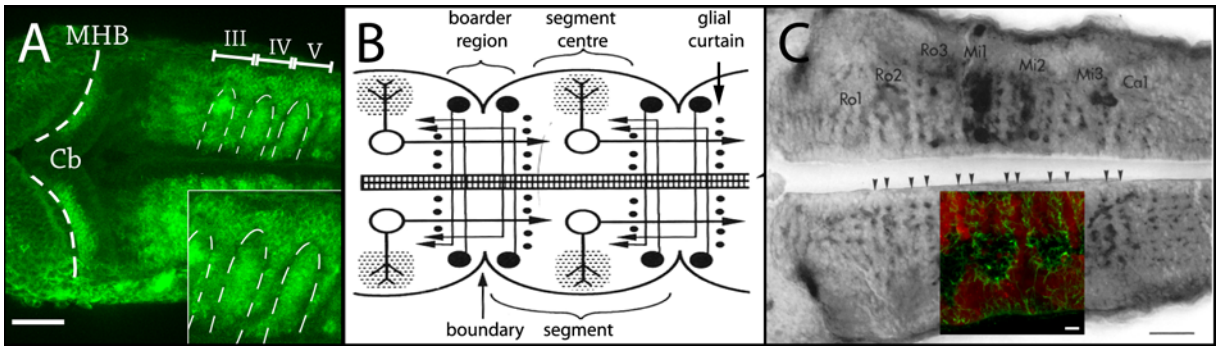

Figure 9 Organisation of the hindbrain

A Pattern of postmitotic neurons during zebrafish early hindbrain development visualised by anti-HuC/D antibody staining. (Dorsal view, anterior to the left). Scale bar 50 µm **B** Proposed structure of hindbrain segments (Trevarrow et al. 1990). A single unit of repetition, consisting of the segment centre and the segment border region (labelled on the right). The segment centres contain the earliest reticulospinal neurons (open circles), and their dendrites are shown projecting into the earliest synaptic neuropil (stippling). The border regions contain commissural neurons (closed circles). Centres are divided from the borders by curtain-like rows of glial fibres (dotted lines). **C** The segment centres and the boarder region are separated by curtain of glial fibres visualised with the Zrf antibodies. (Dorsal view, anterior to the left). Modified from (Trevarrow et al. 1990) Scale bar 25 µm.

The first sign of neuronal differentiation in the zebrafish hindbrain is visible at the 22 somite stage by the expression of proneural genes like *neurogenin1* (*ngn1*) and their downstream targets for example *neuroD* in the segment centres. This initially widespread neurogenic pattern becomes progressively restricted to zones adjacent to hindbrain boundaries, such that at 36 hpf and 48 hpf the domains form horseshoe like shapes and that there is an absence of neurogenic markers in the centre of rhombomeres and at the boundaries were the non-neurogenic zone broadens at lateral positions (Figure 7 I, J white asterisk). (Gonzalez-Quevedo et al.). Additionally these neurogenic markers overlap with the expression of several *delta* genes. Thus the hindbrain shows a very dynamic but distinct pattern of neurogenesis. According to the expression markers of neurogenesis the first postmitotic neurons arise within the segment centre at 24 hpf shown by HuC/D staining. Later, at 32- 48 hpf two domains of

postmitotic neurons can be found in each segment of the hindbrain (Figure 9 A). One domain, that is located in the medial segment centre and looks like a filled U-shape and a second domain in the border region that appears Y-shaped and that is located at the segment boundaries. These two domains are separated by a gap filled with fibres that express glial markers and are emerging from dorsal radial glia cells. These fibre filled gaps are often referred to as the glial curtains (Figure 9 B, C) (Trevarrow et al. 1990). The central U shaped domain nicely correlates with the expression of proneural and *delta* genes which appear at the outline of this domain. The HuC/D positive cells that settle in the centre of the U-Shape might have derived from outer boarder of the U-shaped domain were these cells started to express proneural genes. Once their fate is determined they populate the very centre of the rhombomeres. But what about the postmitotic neurons at the boundaries were no proneural genes are expressed and that are separated by the glial curtain? Do they derive from the *ngn1* and *delta* expressing progenitors in the segment centre and then migrate through the glial curtain in order to settle at the boundaries? Or are they derived from the boundary cells? This would be in contrast to earlier findings which rhombomere boundary cells undergo reduced cell proliferation and interkinetic nuclear migration compared with other neural epithelial cells and that they are late differentiating while inducing neuronal fates in adjacent cells through lateral inhibition (Guthrie and Lumsden 1991; Cheng et al. 2004; Amoyel et al. 2005). An alternative more likely explanation is that the neurons of the Y shaped domain are derived from other hindbrain neurogenic areas not discussed so far. In the vertebrate hindbrain there are two very dorsally located proliferation domains: the ventricular zone (VZ) and the rhombic lip (RL). These domains are un-segmented and expand over the entire hindbrain including the cerebellar anlage. The two areas are molecularly defined by the mutually exclusive bHLH transcription factors Ptf1a (Pancreas Specific Transcription Factor 1a) which is exclusively expressed in the VZ (Lin et al. 2004; Zecchin et al. 2004; Volkmann et al. 2008; Elsen et al. 2009) and Atoh1 (Atonal Homolog 1) expression, which is only present in the rhombic lip (Köster and Fraser 2001a; Adolf et al. 2004). Genetic studies in the mouse and in the zebrafish cerebellum have shown that these regions give rise to a large variety of neuronal subtypes and that especially the rhombic lip progeny shows intense dorso ventral migratory behaviour.(Machold and Fishell 2005; Wang et al. 2005)

1.1.6. Atonal1 and the rhombic lip

The rhombic lip (aka Rautenlippe), was identified 1891 in 2 month-old human embryos by His (His 1891), and is the most dorsal germinal neuroepithelium. Present in all vertebrates it is rimming the opening of the hindbrain fourth ventricle during development (Wingate 2001). It can be divided along the anterior posterior axis into upper or rostral (rRL) and lower or caudal (cRL) portions (Altman and Bayer 1997).

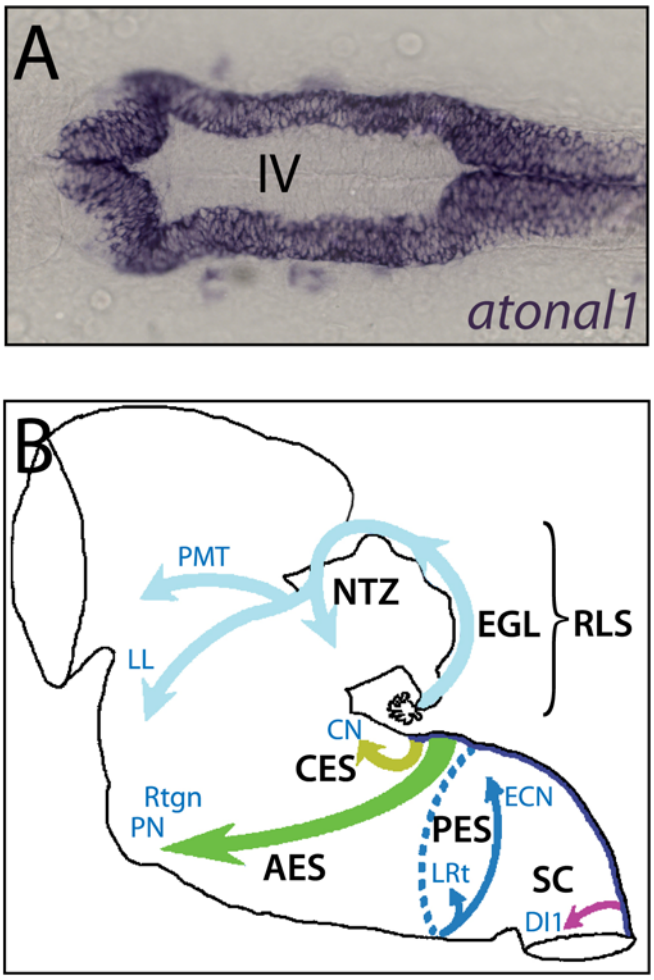

Figure 10 *atonal* and the rhombic lip
A Dorsal view image of in situ hybridisations against *atonal1* mRNA on 22 hpf zebrafish embryos. Zebrafish *atonal1* is specifically expressed in the hindbrain rhombic lip. Anterior is to the left. IV: fourth ventricle.
B Schematic showing rhombic lip migratory streams of *atonal1* expressing neuronal progenitors and the locations in which their cells settle. The dotted line of the PES indicates that these cells migrate from one side of the medulla, cross the midline, and settle on the other side. RLS: rhombic lip migratory stream, CES: cochlear extramural stream, AES: anterior precerebellar extramural stream, PES: posterior precerebellar extramural stream, SC: spinal chord, EGL: external granule layer, NTZ: nuclear transition zone, PMT: pontomesencephalic tegmentum, LL: lateral lemniscus; CN: cochlear nucleus, PN: pontine nucleus, Rtgn: reticulotegmental nucleus, ECN: external cuneate nucleus, LRt: lateral reticular nucleus. Adapted from (Wang et al. 2005).

Since then, extensive studies mostly performed in mice and chick embryos have shown that the rhombic lip produces numerous brainstem neuronal populations unique in their development and functions. While these studies have largely been anatomical in nature, recent applications of newer techniques such as genetic fate mapping and conditional mutagenesis have resolved the rhombic lip into numerous molecularly distinct progenitor domains along spatial and temporal axes that give rise to specific neuronal subtypes and systems (Wingate 2001; Bloch-Gallego et al. 2005; Landsberg et al. 2005; Wang et al. 2005; Ray and Dymecki 2009), while the entire rhombic lip is molecularly defined by the expression of the homologue of the *Drosophila* Atonal bHLH transcription factor (Machold and Fishell 2005; Wang et al. 2005). For the rRL it has been shown that it mainly generates cerebellar granule cell

progenitors (GC) (Altman and Bayer 1997), that migrate superficially from the rRL starting at embryonic day 13 (E13) to first form the external granule cell layer (EGL) on the surface of the cerebellum. These cells proliferate to form the later granule neurons, which subsequently descend into the cerebellum by radial migration (Hatten and Heintz 1995; Wang et al. 2005). For a long time it was believed that the GCs are the only neurons derived from the rRL (Alder et al. 1996), while other cerebellar cell types such as inhibitory Purkinje cells (PCs) and efferent deep nuclear neurons (DNs) begin forming around E10 (Taber-Pierce 1975) and are thought to derive from the more ventro-medially localised ventricular zone (Hallonet et al. 1990; Hatten and Heintz 1995; Mathis et al. 1997; Hoshino et al. 2005). More recent fate mapping studies using tissue specific expression by homologues recombination of *lacZ* into the locus of the mouse *atonal1 homologue* (*atoh1*) showed that cells leaving the rhombic lip prior to the onset of GC migration are part of an early rostral rhombic lip migratory stream (RLS) that is distinct from the later population that forms the EGL. These early born neurons give rise to deep nuclear neurons in the cerebellum and to nuclei in the lateral lemniscus in the pons and in the pontomesencephalic tegmentum (Wang et al. 2005). Whether these different populations are generated by the same progenitor cells or whether two different progenitor cell populations exist in the rhombic lip remains unclear so far.

In the cRL several superficial migratory routes can be distinguished. Most anterior lies the cochlear extramural stream (CES) that gives rise to almost the entire cochlear neuronal populations including deep dorsal and ventral cochlear neurons and the cochlear granule neurons. (Farago et al. 2006; Fujiyama et al. 2009; Maricich et al. 2009). More posteriorly located are the anterior (AES) and posterior precerebellar extramural streams (PES), which give rise to four of the five known brainstem precerebellar nuclei including the pontine nucleus, the reticulo-tegmental nucleus, the lateral reticular nucleus and the external cuneate nucleus (Figure 10). Strikingly all of these four nuclei project mossy fibres to the granule cells and the deep nuclear neurons while the remaining inferior olive precerebellar nucleus, that is not derived from the *atoh1* lineage, projects climbing fibres to the Purkinje cell layer (Wang et al. 2005). In addition, these streams generate brainstem nuclei of the proprioceptive, interoceptive and respiratory system (Machold and Fishell 2009; Rose et al. 2009a; Rose et al. 2009b).

All neuronal nuclei or granule cells have in common that they are positioned in the ventral hindbrain, but they originate in the dorsal rhombic lip and reach their place of terminal differentiation through extramural long distance migration via well defined routes. It has been shown in chicken and zebrafish embryos that this rhombic lip derived migration is conserved

throughout vertebrates. (Cambronero and Puelles 2000; Ono et al. 2004; Wilson and Wingate 2006; Volkmann et al. 2008; Volkmann et al. 2010)

It is also been shown that the rostral rhombic lip produces similar derivatives in zebrafish and mouse embryos (Kani et al. 2010; Volkmann et al. 2010). However, in the zebrafish some of the posterior rhombic lip derivatives such as the pontine nucleus do not exist and the fate and contribution of lower rhombic lip cells in general to hindbrain neuronal circuitries as well as their migratory routes has remained elusive.

During early hindbrain differentiation the *atoh1* expressing cells that stay in the rhombic lip are maintained in a proliferative state, while cells that leave the rhombic lip start to differentiate into many different migrating neuronal populations over time. Thus, the rhombic lip faces the challenge to coordinate neurogenesis while simultaneously maintaining a progenitor pool.

Notch signal transduction is well established to propagate progenitor maintenance in various neuronal (Bertrand et al. 2002; Ross et al. 2003; Kageyama et al. 2009; Kopan and Ilagan 2009) and non-neuronal tissues (Ikawa et al.). For example in the retina of vertebrate embryos Notch activation blocks neuronal differentiation in progenitors (Hashimoto et al. 2006). A similar effect can be observed in mice where conditional inactivation of the Notch transcriptional co-activator Rbpj in the embryonic or adult telencephalon leads to premature differentiation or differentiation into transit-amplifying cells and neurons, respectively (Imayoshi et al.).

In the hindbrain rhombic lip the function of Notch signalling is rather poorly understood. So far, most research efforts concerning this topic have focused on the developing cerebellum where Notch activity in the upper rhombic lip of mice has been shown to prevent induction of *atoh1* expression thereby inhibiting rhombic lip cells to respond to roof plate secreted BMP ligands that induce neuronal fate (Alder et al. 1999; Machold et al. 2007). However, it has also been shown that Atoh1 is required to maintain Notch expression in rhombic lip cells while on the other hand higher amounts of successively accumulating Atoh1 subsequently down-regulate Notch expression in a negative feedback loop (Gazit et al. 2004). Furthermore, maintained Notch signalling in granule neuron progenitors derived from the rhombic lip is required to maintain proliferation and is therefore necessary to expand the pool of later differentiating granule neurons (Solecki et al. 2001).

Thus Notch signalling might play an important role in specifying different neuronal subtypes by promoting the cell fate switch between progenitors and differentiating neurons in the

hindbrain lower rhombic lip, thereby regulating the spatial and temporal organisation of the posterior hindbrain region.

1.2. The Notch Signal Transduction Pathway

1.2.1. Notch signalling: The core pathway

A small number of signalling pathways are used iteratively to regulate cell fates, cell proliferation and cell death during development. Notch is a receptor in one such pathway, and is unusual in that most of its ligands are also transmembrane proteins; therefore signalling is restricted to directly adjacent cells. Although the intracellular transduction of Notch receptor activation is remarkably simple, with no secondary messengers, this pathway functions in an

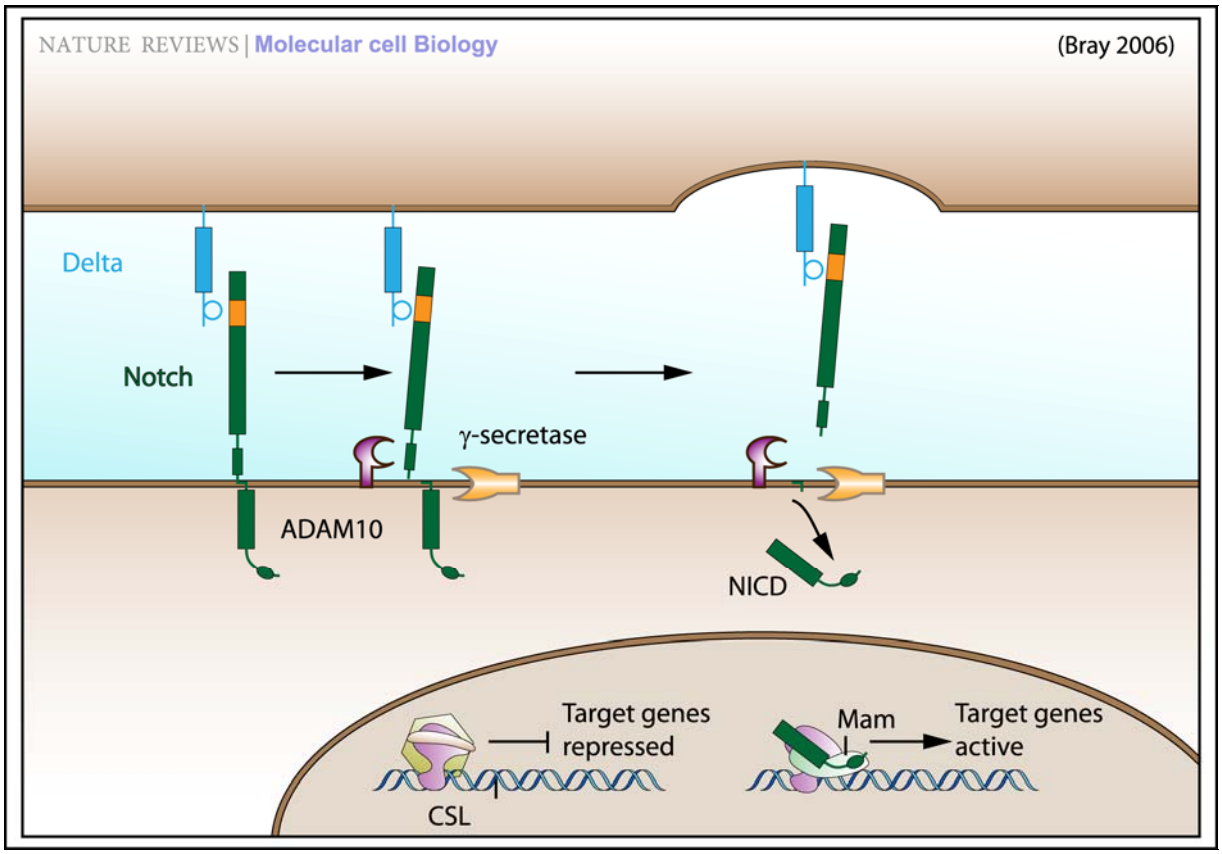

Figure 11 The Notch signal transduction pathway

Binding of the Delta ligand expressed on one cell to the Notch receptor on an adjacent cell results in two proteolytic cleavages of the receptor. The ADAM10 or TACE (TNF-α-converting enzyme) metalloprotease catalyses the S2 cleavage, generating a substrate for S3 cleavage by the γ-Secretase complex. This proteolytic processing mediates the release of the Notch intracellular domain (NICD), which enters the nucleus and interacts with the DNA-binding CSL (CBF1, Su(H) and LAG-1) protein (lilac). The co-activator Mastermind (Mam) and other transcription factors are recruited to the CSL complex, whereas co-repressors are released. Adapted from (Bray 2006).

enormous diversity of developmental processes and its dysfunction is implicated in many cancers and other severe diseases (Bray 2006). The Notch signalling underlies a mechanism that is highly conserved in the animal kingdom (Figure 11). The Notch receptor as well as its

ligands Delta and Jagged are transmembrane proteins. The extracellular domains of these proteins are quite large and consist mainly of Epidermal Growth Factor (EGF)-like repeats. Upon ligand binding, two proteoliytic cleavage processes in the Notch receptor are initiated in a given order. First the extracellular domain is cleaved off by A disintegrin and metallopeptidase (ADAM) -family metalloproteases. This step is followed by a second cleavage promoted by the γ-Secretase complex containing Presenilin, Nicastrin, Presenilin Enhancer 2 (PEN2) and Anterior Pharynx Defective 1 (APH1) which releases the Notch intracellular domain (NICD) of the receptor. NICD then translocates into the nucleus and cooperates with the DNA-binding protein CLS (named after the human CBF1/RBPJ, *C.elegans* LAG-1 and *Drosophila* Su(H) homologues) and its co-activator Mastermind to promote transcription of Notch dependent target genes (Fortini et al. 1993; Mumm and Kopan 2000). The second γ-Secretase mediated cleavage is a critical step in the activation of Notch signalling and therefore a good target for pharmacological inhibitors like DAPT to interfere with the pathway (Geling et al. 2002). Other very established methods to genetically modify the Notch Signalling pathway is by overexpressing dominant active or dominant negative versions of the DNA binding component CLS (Wettstein et al. 1997) or the intracellular domain of the Notch receptor (Fortini et al. 1993; Lieber et al. 1993; Struhl et al. 1993).

1.2.2. Modulation of Notch activity by processing and trafficking

The concept of the core pathway has been established for a long time, but more recently evidence is emerging that post-translational modification and trafficking of the Notch receptor and its ligands affect the activation of the pathway. This might give a reasonable explanation for the context dependency of the integration of the Notch signal. Two especially interesting mechanisms are the receptor maturation and the switch between receptor recycling and degradation regulated by components of the endocytic pathway (Figure 12).

The Notch receptor is translated in the endoplasmic reticulum where it interacts with the O-Fucosyl Transferase (O-Fut) in two ways that are essential for the generation of a functional receptor (Okajima and Irvine 2002; Sasamura et al. 2003; Shi and Stanley 2003). As a first step O-Fut adds a fucose residue to the immature receptor and secondly it acts as a chaperone to promote proper folding of Notch and its transport from the ER to the outer cell membrane (Okajima et al. 2005). On the way to the cellular surface, the Notch protein passes the Golgi apparatus where it is processed by the Furin-like Convertase (S1 cleavage) and glycosylated by O-Fut and other glycosyltransferases like members of the Fringe family. Depending on the nature of this glycosylation the Notch receptor alters its affinity to different ligands.

Glycosylation by one of the Fringe proteins for example potentiates Notch activation by Delta while rendering Notch resistant to Serrate activation in the dorsal cells of the wing in *D.melanogaster* (Haines and Irvine 2003).

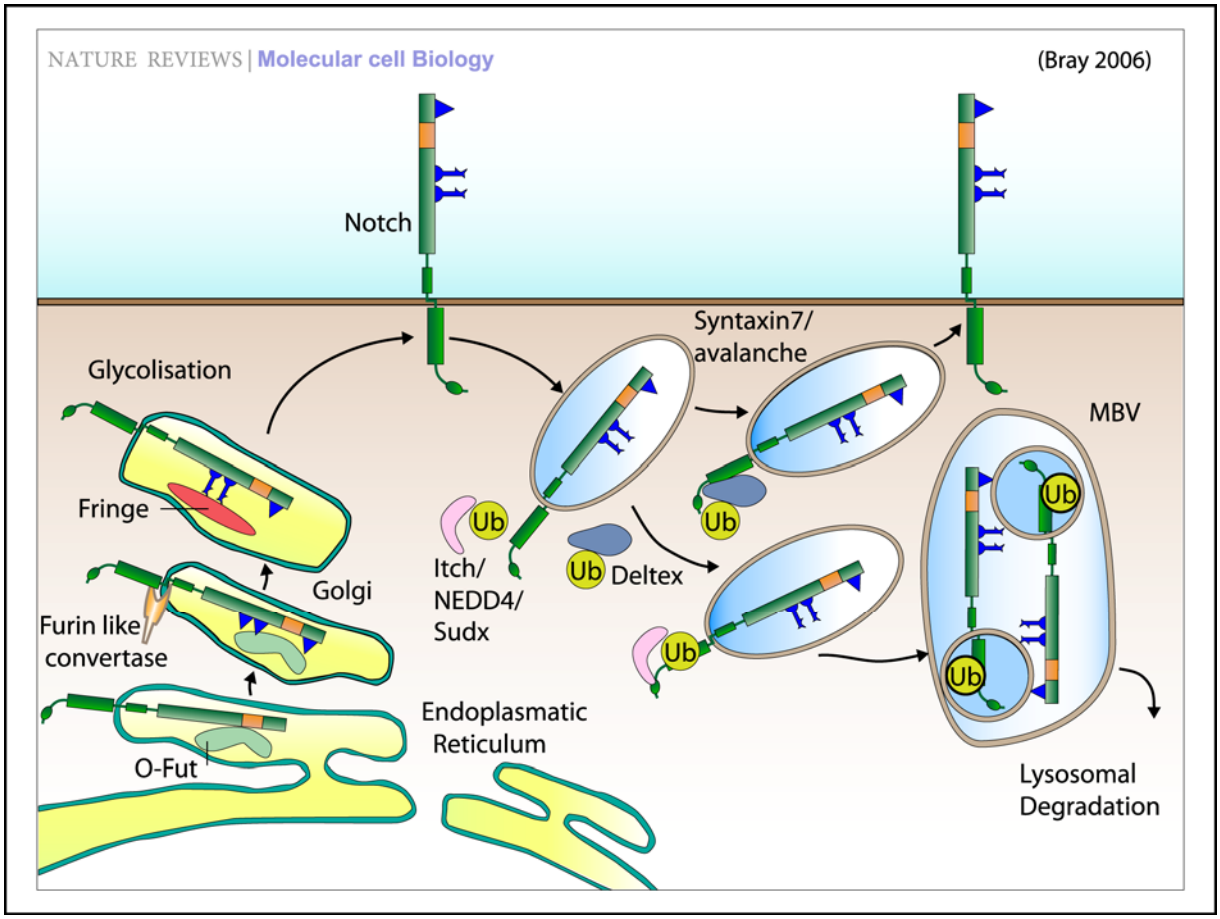

Figure 12 Processing and trafficking regulate Notch-receptor activity.

Notch is produced in the endoplasmic reticulum where it interacts with the O-fucosyl transferase (O-Fut) and is transported to the Golgi. In the Golgi, it is processed by a Furin-like convertase (S1 cleavage) and glycosylated by O-Fut and other glycosyltransferases (for example, Fringe) before export to the cell surface. Notch that is endocytosed from the cell surface can be recycled or degraded through the multivesicular-body (MVB) pathway. Actions of the ubiquitin ligases Deltex and Itch/NEDD4/Su(dx) and the SNARE protein Syntaxin regulate trafficking, although their precise roles are not yet clear. Ub, ubiquitin. Adapted from (Bray 2006).

Notch is a cell surface receptor hence its expected location is the plasma membrane. However, a substantial amount of Notch is targeted for degradation and a large fraction of Notch can be detected in the cytoplasm in compartments of the endocytic pathway. Actions of the ubiquitin ligases Deltex and Itch/NEDD4/Su(dx) regulate trafficking, although their precise roles are not clear yet (Yamamoto et al. 2001; Sakata et al. 2004; Wilkin et al. 2004; Flasza et al. 2006). In addition, studies in *D. melanogaster* have shown that Notch co-localises with the small Rab GTPases Rab5 and Rab7, which are both markers of the endocytic pathway and members of the Ras superfamily of small GTPases that are known to regulate vesicle budding, fusion and motility. Moreover, Notch accumulates in intracellular structures when the endocytic progression is perturbed (Jekely and Rorth 2003; Wilkin et al. 2004). Another factor identified

in *Drosophila* shown to be important in this processes is the protein Avalanche which shows a high degree of sequence similarity to the human t-SNARE family member Syntaxin 7 (Stx7). Syntaxin 7 directs endosomal entry and progression towards the lysosome. If the protein is absent, Notch receptors that are endocytosed from the cell surface are no longer degraded and therefore accumulate in endosomal compartments. (Lu and Bilder 2005)

1.2.3. Notch Signalling during development

The Notch signal transduction pathway functions during diverse developmental and physiological processes, which can broadly be subdivided into three categories all of which can be found in the developing vertebrate central nervous system.

The first functions of Notch activation that have been well characterised are those affecting neurogenesis in the early neural tube. From these studies it became evident that Notch acts at different stages of development even within one tissue. For example, Notch together with its ligands first regulate the number of cells, that acquire neural potential by a mechanism called lateral inhibition and subsequently it determines whether the progeny will adopt neuronal or glial fates by influencing lineage decisions.

Besides lateral inhibition and lineage decisions the third fundamental role of Notch activity during development is the capability of establishing and maintaining compartment boundaries for example in *Drosophila* the maintenance of the wing margins and in vertebrates the maintenance of somite boarders and boundaries between individual rhombomeres. (Cheng et al. 2004; Hashimoto-Torii et al. 2008b; Sibbe et al. 2009). The functions of Notch are further detailed below:

Lateral inhibition

The vertebrate CNS forms over a period of many days or weeks, while progenitor cells differentiate to form distinct cell types at different stages. Consequently, it is essential that a pool of progenitors is maintained in order to ensure subsequent neurogenesis, and that simultaneously an appropriate amount of neuronal differentiation occurs at any specific stage. The correct balance between the maintenance of progenitors and neuronal differentiation is regulated by Notch-mediated lateral inhibition of cell differentiation. Proneural genes up-regulate the expression of Delta or Serrate/Jagged ligands, which activate Notch signalling in adjacent cells. Notch activation leads to the up-regulation of the expression specific members of the Hes/Her family of transcriptional repressors, which in turn inhibit both the expression and function of proneural genes (Ross et al. 2003; Kageyama et al. 2005).

This mechanism converts initially equivalent cells into cells with distinct but different fates. This lateral inhibition of neurogenesis is relieved once the differentiating neurons migrate away from the ventricular zone, such that progenitors can then compete with each other to again initiate neuronal differentiation.

Lineage decisions

Notch signalling between two daughter cells is dependent on asymmetrical inheritance of Notch regulators (for example, Numb). In the mother cell prior to cell division, Numb accumulates in a crescent shaped arc along one side of the cell, oriented toward one end of the mitotic spindle apparatus. During cell division, Numb segregates asymmetrically to one daughter cell, where it inhibits Notch. In the daughter cell that does not receive Numb from the mother cell, Notch activity is not inhibited to the same extent. Asymmetric partitioning of Numb thus biases the outcome of the lateral signalling interactions between the two equipotent daughter cells, allowing the resulting cell fates to be predetermined with respect to their relative spatial orientations.

Boundary induction and maintenance

Notch signalling that occurs between two adjacent populations of cells is able to establish and maintain boundaries by different expression of Delta and Notch in boundary and non-boundary cells. As already discussed the rhombomere compartments form by differentially expressing specific stets of transcription factors that translate into different adhesive properties. Not only the individual rhombomeres differ in their expression profile but also cells at the boundaries differ in this aspect from non-boundary cells, a difference that is induced by signals received from the adjacent compartment.

After specified by adhesive properties rhombomere boundaries express Wnt1, that activates *delta* and proneural genes in cells adjacent to the boundaries, which in turn leads to Notch activation in boundary cells. This sustained Notch activation then regulates cell affinity properties that segregate cells to boundaries (Cheng et al. 2004; Amoyel et al. 2005)

Taken together, Notch is a signal transduction pathway that plays an important role in progenitor maintenance, differentiation decisions and boundary formation in the developing central nervous system and in particular in the hindbrain. In addition, recent findings suggest a role for Notch in regulating neuronal migration. In the developing dentate gyrus Notch was shown to cooperate with Reelin to control neuronal positioning (Sibbe et al. 2009). Further studies in mice also linked Notch signalling to the Reelin pathway, this time in migrating

pyramidal cells where NICD is cell autonomously required for radial migration. Further evidence that Notch signalling directly regulates neuronal migration comes from mice with loss of function of Presenilin-1, a crucial mediator of γ-Secretase activity and thus Notch receptor activation (Louvi et al. 2004). In these mouse embryos the expression of Notch target genes is downregulated in several migratory neuronal populations and among others telencephalic cortical neurons, midbrain dopaminergic neurons, cerebellar granule neurons and lower rhombic lip derived precerebellar neurons are malpositioned. This suggests that severe neuronal migration defects occur, with immature neurons failing to reach their proper locations of terminal differentiation.

1.3. Neuronal Migration

Migration is key feature of embryonic development that is important to create appropriate spatial relationships of cells. In the nervous system, migration during development brings different classes of neurons together so that they can interact and form proper neuronal circuitries. The final location of a postmitotic neuron is very crucial, because neuronal function depends on precise connections made by neurons and their targets. In short, the developing presynaptic and postsynaptic elements must be in the right place at the right time (Purves et al. 2001). Neuronal migration is therefore a fundamental process and the determination of the final allocation of neurons in the nervous system is the basis for the subsequent wiring of neuronal circuitries. From cell polarisation to target identification, neuronal migration integrates multiple cellular and molecular events that enable neuronal precursors to move across the brain to reach their final destination (Valiente and Marin 2010).

1.3.1. Modes of migration tangential versus radial

During the development of the vertebrate brain two major modes of neuronal migration called radial and tangential migration occur (Nadarajah et al. 2001). The best example to describe radial migration is the mammalian cerebral cortex. It is arranged into six layers, which are laid down in an inside-out orientation during development. The majority of neurons that form these layers migrate radially from the ventricular zone, travelling over increasing distances as the cortex expands. Radial migration is further classified into locomotion and somal translocation. Locomotion is characterised by cell migration along the fibres of an extensive network of radial glial cells. Neurons migrating in this mode have a bipolar cell morphology, with an expanded leading process and a thin trailing process. In locomotion, the entire cell remains closely apposed to a glial fibre and the length of the leading process remains more or

less constant as the cell migrates. During somal translocation, the leading process, which is often branched, is anchored to the pial surface of the cortex and the cell body seems to be pulled towards it. The leading process shortens, which could reflect contraction of the process or displacement of the nucleus within the cytoplasm. The mode of migration does not seem to be cell-type-specific, but somal translocation is observed more frequently during the early stages of cortical development, when the distances travelled by the cells are relatively short. Many cells that initially locomote seem to use somal translocation to make final adjustments to their positions. (Miyata et al. 2001; Nadarajah et al. 2001; Tamamaki et al. 2001)

Tangentially migrating neurons move parallel to the brain surface and most importantly they do not use radial glial cell processes but other substrates for migration such as neurons, axons or the extracellular matrix. One example is represented by GABAergic interneurons that originate from the subpallium populating the cortex of the striatum and the olfactory bulb following characteristic migratory streams (Corbin et al. 2001; Marin and Rubenstein 2001).

Tangential migration can occurs homo- and heterophilic, neural precursors are able to move along other cells which serve as a scaffold or they move by forming chain like structures (Rakic 1990).

Chainlike migration was described for zebrafish granule cell progenitors deriving from the cerebellar rhombic lip. These neurons start to migrate at developmental time points when glial cells are absent in the cerebellar primordium. They rely on homophilic N-cadherin mediated cell-cell contact and migrate as clusters along their neighbours to reach their ventral target areas. In N-cadherin deficient *pac2* zebrafish mutants directed migration of granule cell precursors is impaired (Rieger et al. 2009).

A general separation of tangentially versus radially migrating neurons is not possible as many neurons switch the migration mode during development. In many systems neurons first migrate tangential and then radially upon entering their terminal territory (Saghatelyan et al. 2004; Watanabe and Murakami 2009). Cerebellar granule cells in the mouse are one prominent example. Post-mitotic granule cells migrate tangentially within the lower EGL (external granule cell layer). Once they leave the lower EGL and enter the molecular layer (ML) to reach their final destinations a drastic change in GC migration mode from tangential to radial occurs, accompanied by a major modification of GC morphology. (Chedotal 2010).

1.3.2. Differentiation and axonogenesis

The onset of neuronal migration is often accompanied by the initiation of differentiation. The neuronal progenitors leave the proliferative areas and therefore are no longer exposed to

progenitor promoting signals such as Notch activation. On their journey they become postmitotic and start to express early neuronal markers. Once they reach their target areas they terminally differentiate. The ultimate task during the differentiation process of neurons after having migrated considerable distances is to produce dendrites, send out an axon to the right position and establish a synapse in order to create a functional neuronal circuit. Axonogenesis and migration are two processes that can not fully be separated as there are many examples when the axon emerges from the leading or trailing processes of the migrating neuron. Additionally there a many molecular factors known to guide cell migration and axon outgrowth simultaneously.

The relevance of neuronal migration and axonogenesis is also obvious in respect of the numerous diseases caused by defects in those two mechanisms (Morris et al. 1998; Gressens 2006; Valiente and Marin 2010). Additionally precise knowledge of axon outgrowth and path finding might give crucial clues to promote axonal regeneration after axon lesions such as spinal chord injury (Nishio 2009).

Understanding these processes is therefore important and numerous studies have helped so far to identify a variety of extracellular and intracellular cues responsible for controlling migration and axonogenesis and these studies also provided general models of the cellular dynamics of migration (Lambert de Rouvroit and Goffinet 2001; Tsai and Gleeson 2005) and revealed prominent migratory routes of neurons in the CNS (Wang et al. 2005).

Most of what is known today has been either obtained by static methods which means observation of changes occurring in fixed preparations of cells and tissues at different developmental time points or by *in vivo* data that was obtained from isolated biological samples such as cultured cells or tissue explants rather. There is no doubt that these techniques lead to informative developmental and mechanistic insights, but all of them have their limitations as well. Static observations carry the intrinsic danger of missing crucial events of dynamic processes, while experiments using explants and cell cultures might lack crucial factors only present in the environment of the intact embryo (Lichtman and Fraser 2001).

In vivo time lapse imaging using the zebrafish embryo as a model organism has become a powerful tool to circumvent these limitations. The constant improvement of temporal and spatial resolution as well as the discovery and development of a wide variety of fluorescent dyes and genetically encoded fluorescent proteins spanning the whole wavelength spectrum of visible light and also of new applications such as photoconversion or multiphoton imaging allows the observation of highly dynamic cellular processes in vivo. Due to the external

development of the zebrafish embryo, its transparency, its easy access for imaging and the possibility to perform genetic as well as surgical manipulations, these animals are an excellent vertebrate model for *in vivo* imaging applications and therefore for addressing questions concerning neuronal migration and dynamic differentiation processes in its natural context.

1.4. Endosomes: their role in signalling processes and cellular dynamics

Compartmentalisation is crucial for the proper function and survival of every eukaryotic cell and membrane-enclosed compartments in average fill nearly half the cell volume. The endomembrane system represents one such compartment that is further divided in functionally distinct subunits termed organelles including the nuclear envelope, the endoplasmic reticulum, the Golgi apparatus, trafficking vesicles and the cell membrane. The endomembrane system is highly dynamic and constant exchange of material occurs between different organelles and the extracellular space by membrane fission and fusion events. (Alberts et al. 2002)

Endosomes are an important gateway of the endomembrane system. They contribute to the endocytic membrane transport pathway that internalises molecules from the plasma membrane. The molecules are then either transported to the lysosomes for degradation, or they can be recycled back to the plasma membrane. Alternatively proteins produced in the cell can be transported from the ER via the Golgi Network towards the endosomal compartments where they either end up in lysosomes, recycle back to the Golgi or fuse with the plasma membrane (Figure 13). Moreover, molecules can be directed into vesicles that bud from the perimeter membrane into the endosome lumen to form multivesicular bodies (MVB) (Seaman 2008). In addition, endocytosis is the basic mechanism driving the synaptic vesicle cycle that controls neurotransmitter release at the synaptic cleft of neurons and endosomal compartments greatly contribute to neurite outgrowth and guidance. They promote the elongation of axons by fusion with the surface plasma membrane and they deliver cargo that is essential for axonal and dendritic growth and guidance (for review see (Sann et al. 2009))

The endocytic system comprises a series of compartments that have distinct roles in the sorting, processing and degradation of internalised cargo. These compartments include early and recycling endosomes, multivesicular bodies, late endosomes and lysosomes. The compartments are connected with each other and the plasma membrane by mechanistically diverse and highly regulated pathways. (Seaman 2008; Gould and Lippincott-Schwartz 2009).

The early endosomes which are often located in the periphery of the cell are the first station on the endocytic pathway. The early endosomes have a mildly acidic pH and show a

characteristic tubulo-vesicular morphology. They receive most types of vesicles coming from

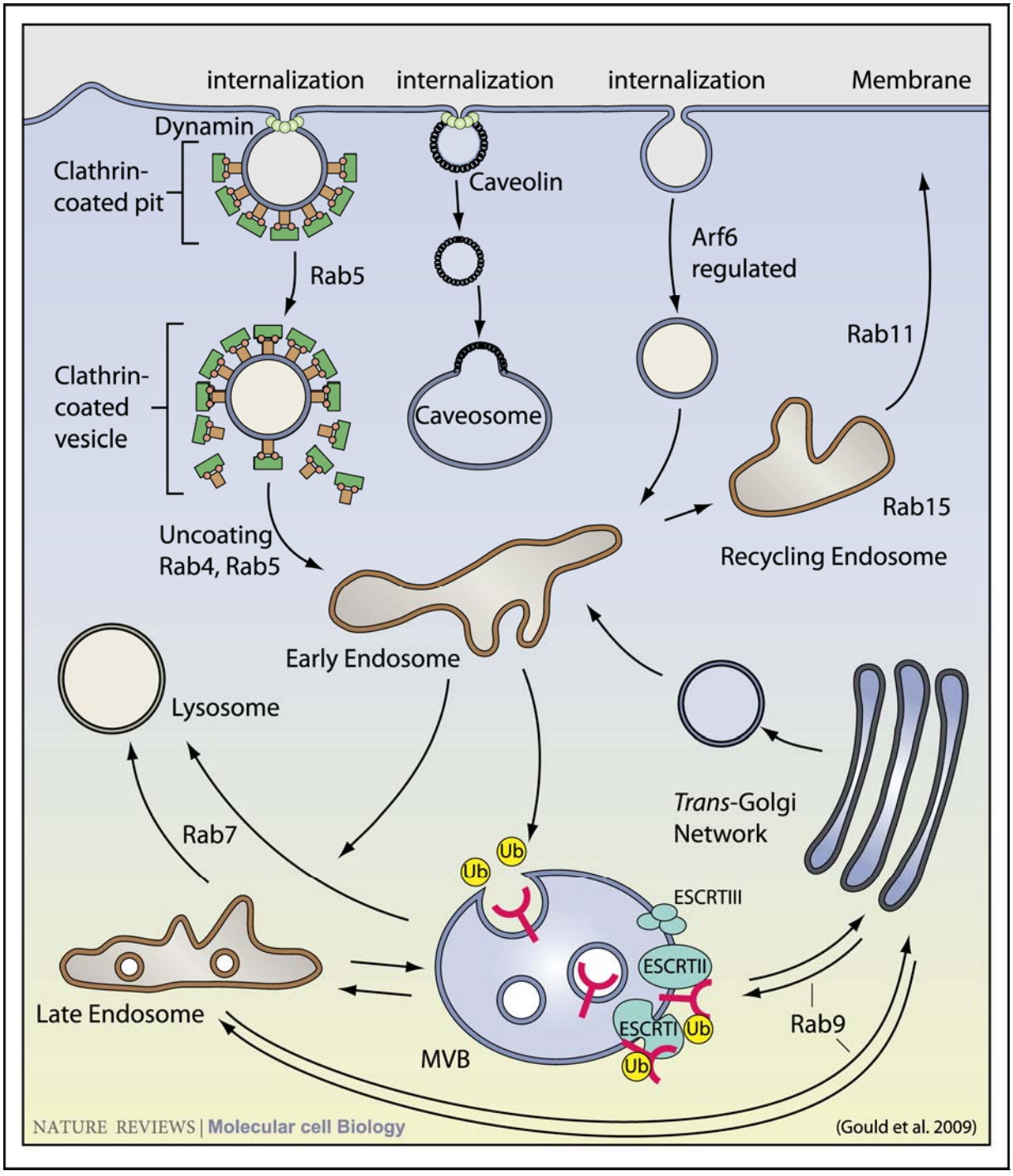

Figure 13 Pathways of endocytosis

Cartoon of the endosomal compartments and the three most prominent modes of endocytosis. Tethering and fusion of different compartments often relies on GTPases of the Rab family. Every compartment is using a specific Rab protein as depicted in the Figure.

the cell surface, from where they are internalised using several routes. These are a) the classic Clathrin-dependent pathway (Bonifacino and Glick 2004), b) the Caveolin dependent endocytosis both named after the scaffolding proteins coating the vesicles and c) a third endocytic mode that is independent from these scaffolding molecules. These vesicles are

subsequently uncoated, if necessary, and fuse with early endosomes (Mayor and Pagano 2007). The early endosomes are sorting organelles in which many ligands dissociate from their receptors due to the acidic pH of the lumen and from which many of the receptors

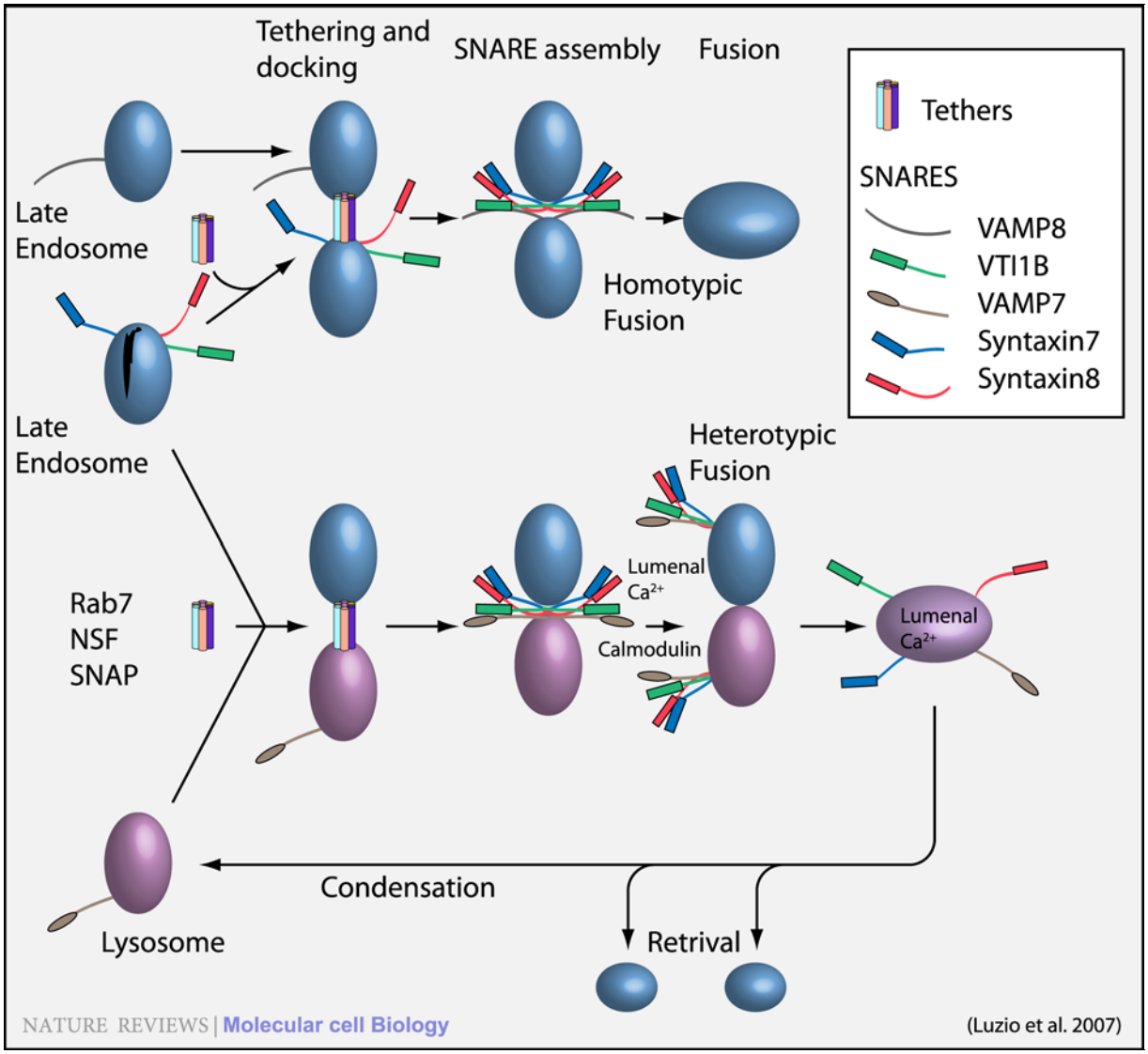

Figure 14 Late endosome-lysosome and homotypic endosome fusion require Syntaxin 7/8 and Rab7

Schematic models of heterotypic late endosome-lysosome fusion and homotypic late endosome fusion. The small GTPase RAB7 is thought to tether endosomes and lysosomes (or endosomes with endosomes). The fusion of late endosomes and lysosomes requires N-ethylmaleimide sensitive factor (NSF) and soluble NSF attachment proteins (SNAPs). Trans-SNARE (SNAP receptor) complex formation requires Syntaxin7, VTI1B (Vps10 tail interactor-1B) and Syntaxin8 in both fusions types. Whereas vesicle-associated membrane protein-8 (VAMP8) is required for homotypic late endosome fusion and VAMP7 is needed for heterotypic late endosome-lysosome fusions. The release of lumenal Ca^{2+} (shown only for heterotypic fusion) leads to phospholipid bilayer fusion.

recycle to the cell surface via the late endosomal components. Proteins that return to the membrane surface are transported via recycling endosomes. Small GTPases of the Rab family play an important role in the sub-specification of the endosomes and therefore are useful markers for their identification. While Rab4 and 5 are specific for early endosomes, recycling

endosomes can by identified by expressing Rab11 and 15 (Figure 13) (Mellman 1996; Mukherjee et al. 1997).

Late endosomes receive internalised material from early endosomes in the endocytic pathway, from the trans-Golgi network (TGN) in the biosynthetic pathway, and from phagosomes in the phagocytic pathway. Late endosomes often contain many membrane vesicles or membrane lamellae and therefore are also referred to as multivesicular bodies (MVB). Late endosomes are thought to mediate a final set of sorting events prior to delivery of material to lysosomes. Characteristic markers are the small GTPases Rab7 and Rab9.

Lysosomes are the last compartment of the endocytic pathway. They are acidic (approx. pH 4.8) and by electron microscopy (EM) usually appear as vesicles containing electron-dense material. They contain a high amount of lysosomal membrane proteins and active lysosomal hydrolases. They are generally regarded as the principle hydrolytic compartment of the cell. (Korner et al. 2006; Fader and Colombo 2009). Additionally lysosomes are required for the digestion of the intracellular material that is segregated during the process of autophagy (De Reuck and Cameron 1963).

All membrane fusions that occur within a cell regardless whether they utilise endosome-lysosome fusion exocytosis or special mechanisms like neurotransmitter release rely on a similar mechanism that requires the presence of *N*-ethylmaleimide Sensitive Factor (NSF), soluble NSF Attachment Proteins (SNAPs) their receptors (SNAREs) and a small GTPase of the Rab family (Figure 13, Figure 14). The fusion process can be generally divided into three sequential steps: 1) Starting with tethering, 2) the formation of a *trans*-SNARE complex that bridges across the two organelles and 3) finally membrane fusion. Tethering, which happens as a prerequisite to organelle/membrane fusion is responsible for the first connection of two organelles. Responsible for this link are the tethering complexes which are composed of small GTPases, SNAPs and NSFs. In the case of endosomal-lysosomal fusion Rab7 seems to play a key role, as Rab7 overexpression can cause clustering of late endocytic organelles and dominant-negative Rab7 mutants cause dispersion (Bucci et al. 2000; Richardson et al. 2004). Following tethering, a *trans*-SNARE complex must form in which the ~16-turn helix of one SNARE wraps around similar helices on three other SNAREs to form a parallel four-helix bundle called a SNAREpin, which is essential for membrane fusion (Weber and Cyran 1998; Weber et al. 1998). The centre of the four-helix bundle contains an ionic layer comprising an arginine (R) and three glutamine (Q) residues, each contributed by a different SNARE. These residues are termed R-SNARE and Qa-, Qb- and Qc- SNAREs, respectively. A functional *trans*-SNARE complex must contain one helix of each type. Antibody-mediated function-

blocking experiments in cell-free systems have provided the most compelling evidence that the same Qa, Qb and Qc SNAREs - Syntaxin-7, VTI1B (VPS10 tail interactor-1B) and Syntaxin-8, respectively - are required both for homotypic late endosome fusions and heterotypic late endosome–lysosome fusions. What distinguishes the two fusion events is the R-SNARE, which is a Vesicle Associated Membrane Protein-8 (VAMP8) for homotypic late endosome fusion, and VAMP7 for heterotypic late endosome–lysosome fusions (Luzio et al. 2007). This indicates that these factors do not only promote the fusion process but are also responsible for choosing the proper organelle as fusion partner. Once the *trans*-SNARE complex has formed the membranes fuse most likely depending on increased Ca^{2+}-ions concentrations.

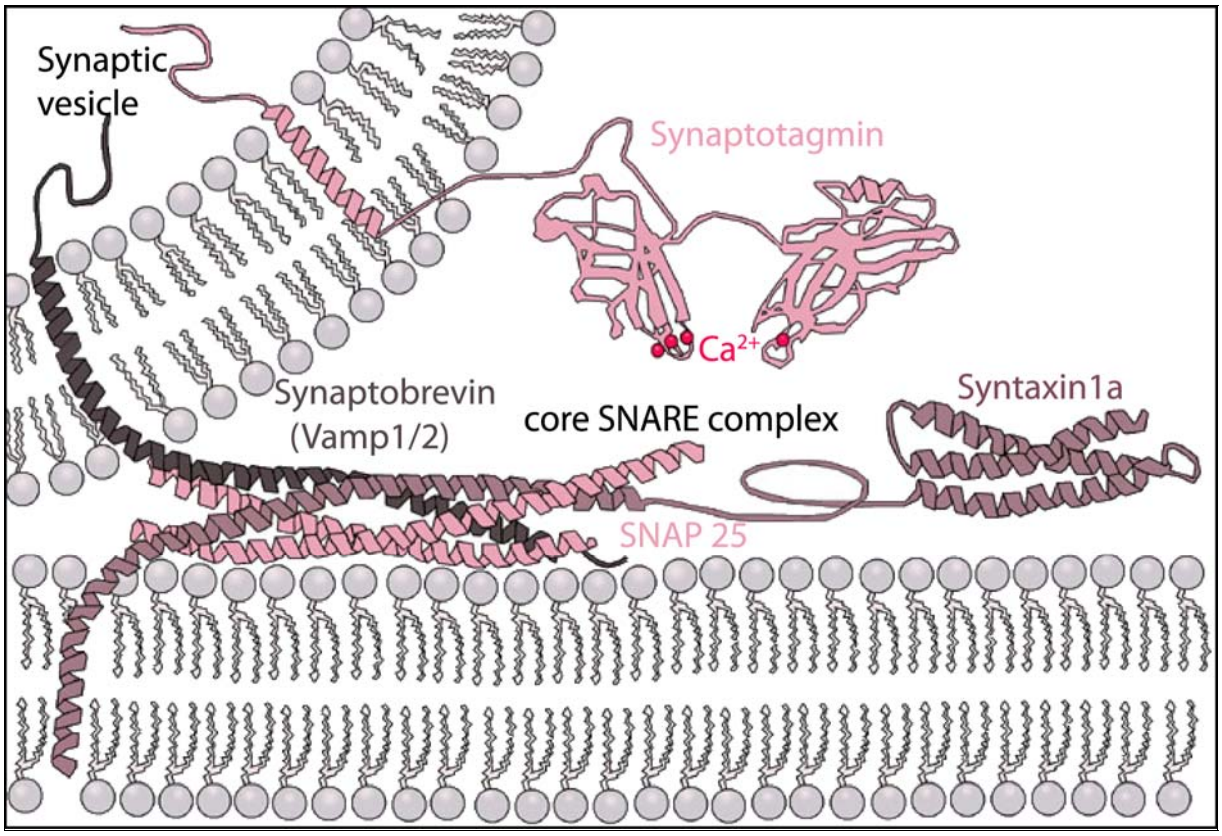

Figure 15 Key players of the synaptic vesicle fusion

Molecular machinery driving exocytosis in neurotransmitter release. The core SNARE complex, which brings the membrane of the synaptic vesicle in close proximity to the cell membrane, is formed by four α-helices contributed by Synaptobrevin, Syntaxin and SNAP-25. Synaptotagmin serves as a calcium sensor and triggers the final release of the neurotransmitter.

The endosomal fusion events are a critical mechanism for the survival of the cell and disturbances in these mechanisms can facilitate the accumulation of aggregate-prone cytosolic proteins. Such aggregates can cause a range of neurodegenerative and other proteinopathies including Huntington's disease, Parkinson's disease and spinocerebellar ataxia (Rubinsztein 2006).

The careful sorting and recycling of membranes and cargo and the intracellular delivery of proteins, toxins and viruses by endocytosis are well-established roles for the endocytic apparatus, which is present in all eukaryotic cells. Furthermore many examples are known where endosomes have important roles in cellular signalling. They function to terminate signalling processes (the internalisation and sorting of the Notch receptors discussed above) and participate in signal propagation by facilitating the recruitment and integration of signalling cascades on the surface of endocytic vesicles. More recently however, it has become clear that endosomes have key roles in such diverse processes as cytokinesis, polarisation, neurite outgrowth, guidance and migration (Gould and Lippincott-Schwartz 2009), functions that are distinct from those classically associated with endosomes. The endosomes are thereby taking advantage of their capability to transport molecular signals and membrane simultaneously one the one hand and on the other hand of the fact that they can localise signals in space due to their compartmentalisation (Gould and Lippincott-Schwartz 2009).

1.5. Lunapark

The development of the hindbrain is a very complex procedure, and many factors are involved, which have to be carefully orchestrated in order to form functional neuronal circuits. Although a lot of these factors are well studied and some mechanisms are understood to a certain extent, many open questions remain. In addition to the described molecules, there are numerous so far undescribed genes that are expressed in the hindbrain and that could therefore be crucial for theses processes. The identification and careful analysis of such factors will increase our understanding of the development of the hindbrain.

In the mouse a candidate has been found recently that promises to play a role during hindbrain development. Spanning over about 100 kb of genomic DNA the *lunapark* (*lnp*) gene containing 13 exons could be identified in the close proximity of the *evx2-hoxd* cluster. Further studies have shown that the *lnp* gene does indeed belong to this genomic cluster and is controlled by the same regulatory element as the *evx2* and *hoxd* genes. This regulatory DNA region showed a pronounced interspecies conservation, including distantly related teleosts like the pufferfish (Spitz et al. 2003). This stretch of regulatory DNA contains a cluster of global enhancers capable of controlling transcription of several genes of unrelated structure or function, thus defining large regulatory domains. Therefore this cluster was referred to as a global control region. Due to the fact that the same enhancer element controls the expression of all of these genes they show similar limb and CNS expression. Especially the expression of

evx2 and *lnp* co-localise in neuronal structures such as the cerebellum and the neural tube (Spitz et al. 2005; Spitz and Duboule 2008).

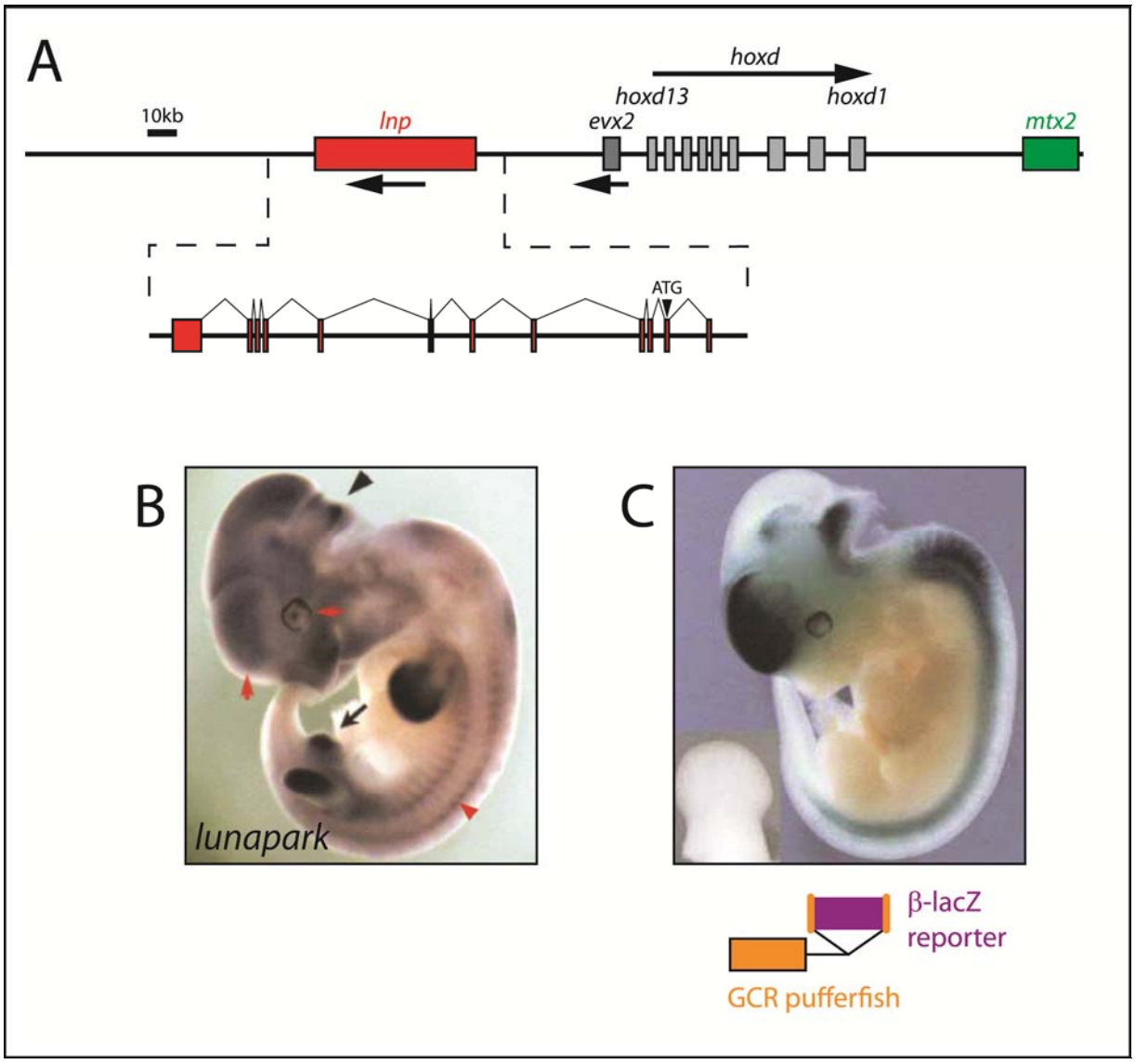

Figure 16 *lunapark* expression in *mus musculus*

A Organisation of the *hoxd* locus on mouse chromosome 2, with the positions of *lunapark* (*lnp*), *evx2*, and *mtx2*. In mouse *lnp* is composed of 13 exons. **B** Lateral view image of in situ hybridisations against *lunapark* mRNA on 11.5 hpf mouse fetuses with expression in the CNS and in the limb anlage. **C** Transgenic embryo at day 12.5 where the β-lac reporter gene was driven by a 7.8 kb fragment containing the *Tetraodon* GCR. GCR: global control region. Images adapted from (Spitz et al. 2003)

Comparison between species revealed that the Lnp Protein has orthologue counterparts in plants, fungi, and in animals such as in *C.elegans*, *Drosophila* as well as in other vertebrates (Spitz et al. 2003; Ghila and Gomez 2008). Despite of the abundance of *lnp* in various species and the high conservation, the precise function of Lnp protein still remains largely elusive. One recent report using *C.elegans* suggested, that Lunapark is involved in synaptic vesicle trafficking and synaptic transmission, although direct evidence is still missing (Ghila and Gomez 2008). While interspecies alignments revealed domains of very high conservation

none of them showed a clear cut similarity to known domains, except for an atypical zinc finger with no assigned function and two transmembrane domains in the N-terminus of Lnp.
Because of the presence, in both vertebrates and arthropods, of the peptide LNPARK in the Lnp amino acid sequence, and its limb and neuronal expression (limb & neuronal pattern) the gene was named *lunapark* (Lnp). Interestingly, neither in the human nor in the mouse genome another Lnp related gene could be identified. Hence, Lnp is a highly conserved single copy gene in mammals with largely unknown function.
Its unique appearance, the high degree of conservation, the absence of known protein domains in combination with its very defined expression pattern suggest that Lunapark plays an important role during development and therefore makes it a very interesting and challenging object for investigation.

1.6. Aim of the study

Spitz and co-workers have identified the novel mouse gene *lunapark* (lnp) with unique properties in respect to its genomic localisation, conservation and gene expression (Spitz et al. 2003). Their preliminary findings suggest a role during early neuronal development. This study aims to further characterise the highly conserved Lunapark in respect to 1) its gene expression and regulation in zebrafish embryos, 2) its biochemical function, 3) its cellular localisation and 4) its role in early neuronal zebrafish development.
1) As the first step we aim to identify and isolated zebrafish *lunapark* orthologues from the genome. The isolated *lnp* cDNA will be used to generate a detailed expression profile of *lunapark* using RT-PCR and mRNA in-situ hybridisation. To address the question if *lnp* expression is conserved and similar to mouse expressed in the CNS.
Furthermore we have generated a transgenic zebrafish line, which expresses a fluorescent reporter under the control of the highly conserved *lnp* enhancer isolated from *Tetraodon*. We will carefully analyse the expression using confocal microscopy and compare the reporter gene expression to endogenous *lnp* expression.
We are interested in the question if *lnp* driven fluorescent reporters are expressed in neurons as suggested by the analysis of the enhancer in mouse (Spitz et al. 2003) and if neuronal expression is detected we aim to characterise precise neuronal subtype. Furthermore we want to find out whether fluorescent reporter expressing cells are migrating and document the possible migratory behaviour.
Finally we aim to identify upstream regulators of the *lnp* expression by interfering genetically or pharmacological with candidate signal transduction pathways.

2) In order to understand the cell biology of the Lunapark proteins and especially its subcellular localisation various fluorescent Lnp fusion proteins are generated and they are overexpressed in combination with known subcellular markers in cultured cells followed by observation using a confocal microscope to determine the location of Lnp within the cell.
3) For the third strategy biochemical methods are applied to identify putative binding partners of the Lunapark proteins. For that purpose a tandem affinity tag based pulldown with subsequent mass spectrometry and bioinformatical analysis will be used to obtain candidates for first and second order Lnp interactions. Promising identified interactions will then be further verified using Immunoprecipitation. Furthermore the individual interactors will be analysed in regards to their cellular context in order to identify functional networks in which Lnp might be integrated.
4) In order to address the function of *lnp* in zebrafish development we aim to interfere with the function of the gene by inducing targeted knockdown of zebrafish *lunapark* mRNA by microinjection of sequence-specific Morpholino phosphorodiamidate antisense oligonucleotides (Morpholinos) followed by a careful analysis of the phenotype.

2. Materials and Methods

2.1. Equipment and Reagents

2.1.1. Equipment

Benchtop thermostats	Thermomixer, 5463/Comfort (Eppendorf, Hamburg, Germany)
Binocular	Stemi SV11 (Zeiss, Jena, Germany)
Centrifuges	Kendro Evolution (Kendro Laboratory Products, München, Germany); Tabletop Centrifuge 5415D and 5415R (Eppendorf, Hamburg, Germany)
Confocal laser scanning microscopes	LSM510 equipped with Argon laser (451, 477, 488, 514nm) and Helium-Neon lasers (561, 594, 633nm), Zeiss LSM510 Meta equipped with Argon laser (451, 477, 488, 514nm) and Helium-Neon lasers (543, 633nm) (Zeiss, Jena, Germany)
Developing machine for radiographs	Curix60 (AGFA, Köln, Germany)
Electrophoresis power supplies	Electron EC105 (Thermo Fisher Scientific, Rockford, IL, USA); Power Pac 3000 (BioRad, München, Germany)
Fluorescent Stereomicroscope	MZ 16FA equipped with filters for UV, GFP, FITC/Cy-3, YFP, Rhodamine and Texas Red (Leica, Wetzlar, Germany)
Gel documentation	(Herolab, Wiesloch, Germany)
Gel electrophoresis chambers	(Shelton Scientific (Sigma-Aldrich Chemie GmbH), Deisenhofen, Germany); (Amersham/BD Biosciences, München, Germany); (PEQLAB Biotechnologie GMBH, Erlangen, Germany)
Microinjection needle puller	(Narishige, London, UK)
Microinjector	FemtoJet Express (Eppendorf, Hamburg, Germany)
Microscope camera	Axiocam HRc digital camera (Zeiss, Jena, Germany)
Objectives	C-Apochromat 40x/NA1.20 water immersion C-Apochromat 63x/NA1.20 water immersion Plan-NeoFluar 5x/NA0.15 Plan-NeoFluar 10x/NA0.3 Plan-NeoFluar 20x/NA0.5 Plan-NeoFluar 40x/NA0.75 DIC Plan-NeoFluar 100x/NA1.3 Ph3 Plan-Apochromat 63x/NA1.4 DIC (Zeiss, Jena, Germany)
PCR machine	PTC 100, MJ Research Inc. (Waltham, MA, USA)
Photometer	Biophotometer (Eppendorf, Hamburg, Germany)
Rotator	(LabInco BV, Breda, Netherlands)
Thermo Incubators	(Memmert, Schwabach, Germany)
Upright compound microscope	Axioplan 2 (Zeiss, Jena, Germany)
XCell II blot module	(Invitrogen GmbH, Karlsruhe, Germany)

2.1.2. Suppliers of chemicals and consumables

Standard chemicals were obtained from Sigma-Aldrich, Fluka, Merck, Roth GmbH, Serva Electrophoresis GmbH, Promega, Waters and Biozym. Enzymes and polymerases were obtained from MBI Fermentas, Invitrogen, Roche, Stratagene and New England Biolabs (NEB). Components used for western blotting were bought from Invitrogen, BioRad, BioTrace, Kodak, and Amersham. Cell Culture Medium and Supplements were delivered by PAA and Gibco. Plastic ware was ordered from NunC, Roth GmbH, Eppendorf and Greiner. Glassware was obtained from Schott.

2.1.3. Antibodies

Table 1

Antibody	Host Species	Antigen	Dilution	Supplier	ID-No.
Histochemistry primary					
α-Ac-Tubulin	Mouse	Acetylated Tubulin	1:500	Sigmas Hybridoma Bank	N/A
α-HuC/D	Mouse	Elavl3/4	1:10	Molecular Probes	A21271
α-PCNA	Mouse	PCNA	1:250	Santa Cruz	sc-25280
Zn8/Zn5	Mouse	Alcama	1:50	Developmental Studies HB	N/A
Zrf-1	Mouse	Glial fibre acidic protein	1:200	Developmental Studies HB	N/A
Zrf-2	Mouse	radial glial fibres	1:200	Developmental Studies HB	N/A
Zrf-3	Mouse	radial glial fibres	1:200	Developmental Studies HB	N/A
Zrf-4	Mouse	radial glial fibres	1:200	Developmental Studies HB	N/A
Rb X RFP	Rabbit	RFP	1:50	Chemicon	AB3216
Histochemistry secondary					
α-mouse Alexa Flour 488	Chicken	mouse IgG	1:200	Molecular Probes	A21200
α-rabbit Cy3	Donkey	rabbit IgG	1:200	Jackson Immuno Research	711-166-152
α-mouse Alexa Flour 546	Donkey	mouse IgG	1:200	Molecular Probes	A10036
α-mouse Alexa Flour 546	Goat	mouse IgG	1:200	Molecular Probes	A11003
Westernblot primary					
3F10	Rat	HA-tag	1:1000	Roche	1 867 423
α-GFP	Chicken	GFP	1:1000	Aves	GFP-1020
Rb X RFP	Rabbit	RFP	1:1000	Chemicon	AB3216
Westernblot secondary					
α-Rat HRP	Goat	IgG Rat	1:10000	Jackson Immuno Research	112-035-063
α-Chicken HRP	Rabbit	IgY Chicken	1:10000	Upstate	12-341
α-Mouse HRP	Goat	IgG Mouse	1:10000	Jackson Immuno Research	156-036-003
α-Rabbit HRP	Goat	IgG Rabbit	1:10000	Jackson Immuno Research	111-036-045
IP					
3F10	Rat	HA-tag	1 µg	Roche	1 867 423
mAb 3E6 α-GFP	GFP	GFP	1 µg	Molecular Probes	A11120
Rb X RFP	Rabbit	RFP	1 µg	Chemicon	AB3216

2.1.4. Kits, Enzymes and Affinity Purification Reagents

Alkaline Phosphatase (1U/µL)	Roche Diagnostics, Mannheim, Germany
Anti-FLAG® M2 agarose	Sigma-Aldrich, St.Louis, MO, USA
BCA Protein assay Kit	Thermo Fisher Scientific, Rockford, IL, USA
Complete – EDTA free	Roche Diagnostics, Mannheim, Germany
dNTPs	Roche Diagnostics, Mannheim, Germany
Desthiobiotin elution buffer	IBA GmbH, Göttingen, Germany
DIG RNA-Labelling mix	Roche Diagnostics, Mannheim, Germany
DNaseI (RNase-free, 1U/µL)	Roche Diagnostics, Mannheim, Germany
ECL Detection kit	GE Lifescience, Upsala, Sweden
3x FLAG® Peptide	Sigma-Aldrich, St.Louis, MO, USA
FuGENE® HD	Roche Diagnostics, Mannheim, Germany
Gel Extraction kit	Eppendorf, Hamburg, Germany
Gel Extraction kit	Quiagen, Hilden, Germany
GeneClean Turbo kit	Q-BIOgene, Heidelberg, Germany
GeneRuler™ 1kb DNA Ladder	Invitrogen GmbH, Karlsruhe, Germany
Klenow-Fragment (10U/µL)	Roche Diagnostics, Mannheim, Germany
Message Machine SP6 Kit	Ambion, Darmstadt, Germany
Nanofectin Transfection Kit	PAA, Pasching, Austria
NucleoBond® Finalizer	Macherey & Nagel, Düren, Germany
NucleoBond® PC100/500	Macherey & Nagel, Düren, Germany
PageRuler™ Prestained Protein Ladder	MBI Fermentas, St. Leon-Rot, Germany
Pfu Ultra II DNA polymerase	Stratagene, La Jolla, CA, USA
Pronase	Roche Diagnostics, Mannheim, Germany
Proteinase K, 20mg/mL	Roche Diagnostics, Mannheim, Germany
Protein G Sepharose™ 4 Fast Flow	GE Lifescience, Upsala, Sweden
QIAGEN Nucleotide Removal kit	Quiagen, Hilden, Germany
QIAquick PCR Purification kit	Quiagen, Hilden, Germany
QIA shredder	Quiagen, Hilden, Germany
RapiGest™ SF	Waters, Milford, MA, USA
Restriction endonucleases	MBI Fermentas, St. Leon-Rot, Germany; New England Biolabs, Frankfurt/M, Germany; Roche Diagnostics, Mannheim, Germany
Rnasin RNase Inhibitor (40U/ µL)	Promega, Mannheim, Germany
RNeasy Mini Kit	Quiagen, Hilden, Germany
SP6 RNA-Polymerase (20U/µL)	MBI Fermentas, St. Leon-Rot, Germany
Strep-Tactin Superflow	IBA GmbH, Göttingen, Germany
StrataClone Blunt PCR Cloning Kit	Stratagene, La Jolla, CA, USA
Super script II, RT (200U/mL)	Invitrogen GmbH, Karlsruhe, Germany
T3 RNA-Polymerase (20U/µL)	MBI Fermentas, St. Leon-Rot, Germany; Roche Diagnostics, Mannheim, Germany
T4 DNA-Ligase (5U/µL)	MBI Fermentas, St. Leon-Rot, Germany
T7 RNA-Polymerase (20U/µL)	MBI Fermentas, St. Leon-Rot, Germany; Roche Diagnostics, Mannheim, Germany

2.1.5. Buffers and media

Standard buffers were prepared according to Sambrook and Fritsch (Sambrook 2001). Embryo solutions and standard zebrafish protocols were derived from M. Westerfield (Westerfield 1995) and Kimmel et al. (Kimmel et al. 1995)

2.1.5.1.Protein Biochemistry

2x HBS (filtered): 280 mM NaCl 1.5 mM Na_2HPO_4 50 mM HEPES 1 M NaOH adjusted pH 7.13	PBS: 10 mM Na_2HPO_4 2 mM KH_2PO_4 137 mM NaCl 2.7 mM KCl pH 7.4 adjusted with 1 M NaOH
2x SDS-Sample Buffer: 125 mM Tris-HCl (pH 6.8) 20% Glycerol (w/v) 4% SDS (w/v) 0.02% Bromphenol blue (w/v) 10% β-Mercaptoethanol (v/v) (add fresh)	IPN_{150}-Lysis Buffer: 50 mM Tris-HCl (pH 7.6) 150 mM NaCl 5 mM $MgCl_2$ 0.1% Nonidet P40 (v/v) 1x Complete Protease Inhibitor Mix 1 mM DTT 1 mM PMSF
SDS-PAGE-Tank Buffer: 25 mM Tris 250 mM Glycine 0.1% SDS (w/v)	TBS-Tween: 20 mM Tris-HCl (pH 7.6) 150 mM NaCl 0.1% Tween20 (v/v)
Dry Milk Blocking Buffer: 2% (w/v) Dry milk powder in TBS-Tween	SF-TAP Wash Buffer: 1x TBS 0.1% NP40.
TEN Buffer: 40 mM Tris-HCl (pH 7.6) 150 mM NaCl 1 mM EDTA	

2.1.5.2.Fish Media

Danieau-stock Solution 300 %: 58 mM NaCl 0.7 mM KCl 0.4 mM $MgSO_4$ 0.6 mM $Ca(NO_3)_2$ 5 mM HEPES (pH 7.2) 1x PTU (optional) Dilute 1:10 for working solutions	Anti-Pigmentation Agent: 0.15 mM 1-phenyl-2-thiourea (PTU)
	Egg Water 0.3 g/L Instant Ocean Salt Mix/osmosis water
	Anaesthesia: 0.002 g/mL Tricaine in 30 % Danieau

2.1.5.3.Histology

20x SSC: Tris-Acetate 3 M NaCitrate 300 mM pH 7.0 adjusted with NaOH	PTW: 0.1% Tween in PBS (v/v)
	PTW DMSO: 1% DMSO in PTW (v/v)
NGS Blocking Solution: 10% NGS (Normal Goat Serum) in PTW DMSO (v/v)	Hybridisation Buffer: 50% Formamide (v/v) 25% 20x SSC (v/v) 150 µg/mL Heparin 5 mg/mL Torula-RNA 0.1 % Tween®20 (v/v)
ISH Staining Buffer: 0.1 M NaCl 0.1 M Tris pH 9.5 50 mM $MgCl_2$ 0.1% Tween ISH Staining Solution: Staining Buffer 3.75 µL/mL BCIP 5 µL/mL NBT	Fixation Buffer: 4% PFA in PTW (v/v)
	Glycine 20 mg Glycine in 1 mL ddH_2O
NBT: 75 mg/mL in 70 % DMF BCIP: 50 mg/mL in DMF	Glycerol 90% Glycerol in ddH_2O

2.1.5.4.*E.coli* & Cell Culture Medium

LB-Medium: 10 g Bacto-Trypton 5 g Yeast Extract 10 g NaCl Water add 1 L In 1 L deionised water pH 7.4.	LB-Agar: 10 g Bacto-Trypton 5 g Yeast Extract 10 g NaCl 15 g Agar In 1 L deionised water
Cell Culture Medium (Mammalian Cells): DMEM Dulbecco's Modified Eagle Medium 10% Fetal Bovine Serum (v/v) 1% Penicilin/Streptomycin (v/v) 1% Glutamin/Glutamax (v/v)	Cell Culture Medium (PAC2 Cells): L-15 Leibovitz 10% Fetal Bovine Serum (v/v) 1% Penicilin/Streptomycin (v/v) 1% Glutamin/Glutamax (v/v)

2.1.6. Software for image procession

Adobe Illustrator CS3 10.0.2 (Adobe, San Jose, CA, USA)
Adobe Photoshop CS3 Extended Version 10.0.1 (Adobe, San Jose, CA, USA)
Axio Vision Software 4.5 SP1 (Zeiss, Jena, Germany)
ImageJ 1.37v + Macro Timestamper (NIH, Bethesda, MD, USA)
LSM 510 Release Version 4.0 SP1 (Zeiss, Jena, Germany)
QuickTime Player Pro Version 7.1.6 (Apple, Cupertino, CA, USA)

2.1.7. Bacteria strains and cell culture lines

2.1.7.1. Bacteria
E. coli-strains of the following genotypes were used:
XL1-Blue (Bullock et al. 1987)
GM4 Dam negative (Bolivar and Backman 1979)
StrataClone SoloPack Competent Cells (Stratagene, LaJolla, CA, USA)

2.1.7.2.Cell culture
293HEK/293-T Human Embryonic Kidney Cells (Graham et al. 1977)
NIH3T3 Mouse Fibroblasts (Todaro and Green 1963)
PAC2 zebrafish Fibroblast Cells (Amsterdam et al. 1999; Senghaas and Koster 2009)

2.1.8. Fish Strains

2.1.8.1.Wild type

Wild type AB strain	(ZFIN)

2.1.8.2.Mutant strains

Brass	(EkkWill Waterlife Resources, Gibbonston, FL, USA)

2.1.8.3. Transgenic lines

Tg[*lnp*:mRFP]	R. Köster, Köster lab	
Tg[*lnp*:Kaede]	R. Köster, Köster lab	
Tg[*olig2*:EGFP]vu12	B. Appel, Appel lab	(Shin et al. 2003)
Tg[*ptf1a*:eGFP]jh1	S. Leach, Leach lab	(Godinho et al. 2005)
Tg[*atoh1a*:Gal4TA4]hzm2	K. Volkmann. Köster lab	
Tg[4xUAS:GFP]hzm3	M. Distel, Köster lab	(Distel et al. 2009)
Tg[*rh3/5*:KalTA4]hzm1	M. Distel, Köster lab	(Distel et al. 2009)
Tg[*wnt1*-GVP-UG]	S. Harris, Nüsslein-Vollhard lab	(Volkmann et al. 2010)
Tg[TP1bglob:GFP]	N. Lawson, Lawson lab	(Parsons et al. 2009)
Tg[*gfap*:GFP]mi2001	R. Bernados, Raymond lab	(Bernardos and Raymond 2006)
Tg[UAS:myc-Notch1a-intra]	N. Scheer, Campos-Ortega lab	(Scheer and Campos-Ortega 1999)

2.1.9. Antisense Oligonucleotides

All Morpholinos were obtained from Gene Tools, LLC Philomath OR USA

Table 2

Morpholino	Sequence
LnpA_Exon2	5'-ACAGGAGCACATACTTACCCTCCAC-3'
LnpA_Exon4	5'-GAATTTACATACTTACAGCAGAGGG-3'
LnpA_ATG	5'-TGTGAGGGCAGTCCTTCCTCTCAGA-3'
P53_Standard	5'-GCGCCATTGCTTTGCAAGAATTG-3'

2.1.10. Plasmid Vectors

#1 pCS2+
(Rupp et al. 1994)

#846 pCRII *lnpA*
The ORF (open reading frame) of zebrafish *lunaparkA* (*lnpA*) was isolated from 32 hpf zebrafish cDNA using primers #165/#166 and subsequently TA-cloned into pCRII (constructed by Reinhard Köster)

#949 pCS *lnpstop*
The ORF of *lnpA* was isolated from plasmid #846 using EclI36II/AgeI and cloned into #1 pCS2 opened with Stu/Xba (constructed by Reinhard Köster)
This plasmid was used to create *lnpA* mRNA for microinjection

#950 pEYFP-N1 *lnpYFP*
The ORF of *lnpA* was isolated from #846 using Ecl136II/AgeI restriction sites and transferred into Ecl136II/AgeI digested pEYFP-N1 (Invitrogen) (constructed by Reinhard Köster)

#959 pCS *lnpYFP*
The open reading frame of *lnpYFP* was isolated from #950 by sequentially digesting with NotI (Klenow blunted) and XhoI and inserted into #1 pCS2 digested with SnaBI/XhoI (constructed by Reinhard Köster)

#979 pCRII *lnpB*
The ORF of zebrafish *lunaparkB* (*lnpB*) was isolated from 16 hpf zebrafish cDNA using primers #215/#216 and subsequently TA-cloned into pCRII (constructed by Reinhard Köster)

#1032 pCS *lnpmCherry*
The *lnpA* ORF was amplified by PCR using primers #254/#256. The PCR product was digests ClaI/SalI, cloned in front of *mCherry* into #952 pCS*uncmCherry* using ClaI/SalI digestion (constructed by Reinhard Köster)

#1269 pCS *NTMmCherry*
The N-terminal fragment of *lnpA* ORF was amplified via PCR from #846 using primers #254/#400 and subsequently digested wit ClaI/SalI. The PCR product was inserted into #952 pCS *uncmCherry* digested with ClaI/SalI (constructed by Reinhard Köster)

#1466 pSC-B *lnpA*
lnpA ORF PCR Fragment was amplified with primers #180/#319 using plasmid #949 and then blunt cloned into pSC-B from Stratagene

#1520 pCS *lnp5'UTR citrine*
Oligos #546/#547 containing the 5'UTR ATG Morpholino target sequence of *lnpA* mRNA were annealed and inserted into #1328 pCS *unccitrine*

#1521 pEGFP *lnpA*
The *lnpA* ORF was isolated by digestion of #1466 with SacI/Asp718 and cloned into #33 digested with SacI/Asp718

#2001 psDNA3 C-SF-TAP *lnpA*
The *lnpA* ORF was PCR amplified from plasmid #846 using primers #832/#833. The PCR product was digested with BamHI/NotI and transferred to #1999 psDNA3 C-SF-TAP (kindly provided by Johannes Glöckner (Gloeckner et al. 2009a))

#2002 psDNA3 N-SF-TAP lnpA
The *lnpA* ORF was PCR amplified from plasmid #846 using primers #830/#831. The PCR product was digested with NheI/XohI and transferred to #2000 psDNA3 N-SF-TAP (kindly provided by Johannes Glöckner (Gloeckner et al. 2009a))

#2418 *lnpHA*
Oligos 804/805 containing a double HA peptide were hybridised and phosphorylated and then cloned into SalI/XbaI digested #1032 pCS *lnpmCherry*

#2286 pSC-B *stx7l N-term*
The N-terminus of zebrafish *stx7l* was amplified from 48 hpf cDNA using primers #997/#1001 thereby introducing ClaI and kozak sequence in front of ATG. The PCR product was blunt cloned into pSC-B (Stratagene)

#2299 pSC-B *stx7l C-term*
The C-terminus of zebrafish *stx7l* was amplified from 48 hpf cDNA using primers #964/#1000 thereby removing the Stop codon and adding a SalI site. The PCR product was blunt cloned into pSC-B (Stratagene)

#2363 pCS *stx7l citrine*
The C-terminus of s*tx7l* was isolated from #2299 using EcoRI/SalI digestion and the N-terminus of *stx7l* ORF was isolated from #2286 ClaI/EcoRI and cloned into the vector #1916 pCS citrine which was opened with ClaI/SalI

#2416 pCS *stx7l HA*
Oligos 804/805 containing a double HA peptide were hybridised and phosphorylated and then cloned into SalI/XbaI digested #2363 pCS *stx7l venus*

#2432 pCS *stx7l tag RFP GI*
The ORF was removed from #2363 using SalI/XbaI digestion and inserted into 2380 digested with SalI/XbaI

#96 pCS2+ *H2BYFP* (obtained from Reinhard Köster)

#1341 pCS*golgicitrine* (obtained from Reinhard Köster)

#1496 pEYFP-ER (obtained from Clonetech)

#1649 pEGFP C1 *rab5* (kindly provided by Robert Lodge/Don Lamb)

#1650 pEGFP C3 *rab9* (kindly provided by Suzanne Pfeffer/Don Lamb)

#1652 pEGFP C1 *rab7* (kindly provided by Robert Lodge)

#1702 pCSII *rfng* (kindly provided by David Wilkinson)

#1895 pBS *deltaA* (kindly provided by Dirk Meyer)

2.1.11. Oligonucleotides for cloning and sequencing

Table 3

No.	Name	Sequence
#165	zf lnpA lo2	5'- TTCTCACTCTACTCGACCTCCATAGCGG -3'
#166	zf lnpA up3	5'- CCTCATAGGATGGGGGCTGTGGTGTCTC -3'
#180	zf koz lnpA	5'- CTGAGCTCCACCATGGGGGCTGTGGTGTCTCGGT -3'
#215	zf lnpB up	5'- CTGACAATGGGAGCCATCATTTCCAGGT -3'
#216	zf lnpB lo	5'- GGTTTAGTTTGATTCATCCTCTTTCTTTTGTTCC -3'
#254	lnpA fusion up	5'- ATTATCGATCCACCATGGGGGCTGTGGTGTCTCGGTGGA -3'
#256	lnpA fusion lo	5'- ATAGTCGACCATAACTTCAGCTGCTTATGGTTC -3'
#319	pCST3lo	5'- GGAAACAGCTATGACCATGATTACGCCAAGC -3'
#400	lnpA NTM lo	5'- TCTGTCGACTTGTTGTATAAAACTATCAGCAGTTTCCTC -3'
#429	zf actin up	5'- ATTGAATTCATGGATGATGAAATTGCCGCACTGGTT -3'
#430	zf actin lo	5'- AATCTCGAGTTAGAAGCATTTGCGGTGGACGATGG -3'
#546	lnp5'UTR up	5'- AATTCAGATCTGCTCTGAGAGGAAGGACTGCCCTCACAG -3'
#547	lnp5'UTR lo	5'- TCGACTGTGAGGGCAGTCCTTCCTCTCAGAGCAGATCTG -3'
#548	lnpA E2/4 up	5'- CGTGCCGCGCGGGGTTGTGGGAACAC -3'
#549	lnpA E2 lo	5'- GCACAGGCCATCAGGTACAGCAGAGCGGAG -3'
#830	lnp N-SF-TAP up	5'- GCCCTTCCTGCTAGCATGGGGGCTGTGGTGTCTCGGTGG -3'
#831	lnp N-SF-TAP lo	5'- CCCCTTTTCTCGAGCTACTCGACCTCCATAGCGGACACGTCC -3'
#832	lnp C-SF-TAP up	5'- CCCTTGGATCCACCATGGGGGCTGTGGTGTCTCGGTGG -3'
#833	lnp C-SF-TAP lo	5'- CCTTTTCGCGGCCGCCTCGACCTCCATAGCGGACACGTCC -3'
#860	lnpA E4 lo	5'- CTCTGCTTTCAGCTCTTCTAACTTTTCATTGTTTCTC -3'
#964	stx7l lo	5'- GAGAGATGTGGTCGACTCTCCTTTGCTGACAGAAGC -3'
#997	stx7l up	5'- GGAGATCGATCCACCATGTATGGATCAAGAGAAGTCGATGCC -3'
#1000	stx7l up seq	5'- CAGAACAGAGGCAAAGAAAGATCCAGCG -3'
#1001	stx7l lo seq	5'- GCCAGAACAGCCACCAGGATGAAAATC -3'

2.2. Experimental Procedures

2.2.1. DNA handling and cloning procedures

2.2.1.1. Plasmid transformation

For transformation of DNA, competent bacterial cells stored at -80°C were thawed on ice. 100 ng-1 µg of plasmid DNA was added to 100 µL of bacteria. The mixture was incubated for 30 min on ice. The bacteria were than heat shocked at 42°C for 45 s to induce plasmid DNA uptake by the bacteria and immediately placed on ice for 2 min, to cool down the cells. 500 µL Luria Bertani (LB) medium was added and the bacteria were incubated for 1 h at 37°C. Additionally the bacteria can be shaken with 250 rpm. The cultures were subsequently plated onto 20 mL LB agar in Petri dishes, containing antibiotics according to the plasmid resistance and incubated over night at 37°C to allow bacteria colonies to grow.

2.2.1.2. Low scale plasmid preparation from bacteria (Mini Prep)

In order to obtain small amounts of purified plasmid DNA for analytical purposes, 3 mL of plasmid-containing bacteria in LB medium were incubated with respective antibiotics at 37°C, shaking at 250 rpm over night. Initial steps of plasmid isolation were performed using buffers obtained from the NucleoBond® PC100/500 Maxi Prep Kit (Macherey-Nagel) (see 2.2.1.3). First, bacterial cultures were transferred into 1.5 mL Eppendorf reaction tubes and pelleted by centrifugation at 13,200 rpm for 1 min. The supernatant was removed and pellets were re-suspended in 200 µL S1 (RNase-containing buffer). After complete resuspension of the pellet, 200 µL S2 alkaline lysis buffer was added. Subsequently, 200 µL of S3 buffer was added for neutralisation to coagulate denatured proteins and to subsequently precipitate the bacteria debris. The debris was removed by centrifugation for 10 min at maximum speed and the supernatant transferred into a fresh 1.5 mL reaction tube. Then 400 µL Isopropanol was added to precipitate the DNA, followed by centrifugation at 13,200 rpm for 30 min. The supernatant was discarded and the pellet washed with 70% ethanol, followed by centrifugation at 13,200 rpm for 20 min. The DNA was finally air-dried and re-suspended in 20 µL ddH_2O.

2.2.1.3. Large scale plasmid preparation from bacteria (Maxi Prep)

For large scale purification of plasmid DNA an individual E. coli colony containing the desired plasmid was cultured in 200 mL LB medium supplemented with the respective antibiotic in a 500 mL Erlenmeyer flask on a shaker (200 rpm) over night at 37°C. The bacteria were then sedimented by centrifugation at 6000 rpm for 15 min at 4°C (Sorvall Evolution, GSA-rotor). All further steps were performed using the NucleoBond® Kit

(Macherey&Nagel) as described by the manufacturer. Alternatively to using centrifugation for the isopropanol precipitation and EtOH washing steps, Finalizer filter membranes from Macherey&Nagel were used as described in the guidelines of the manufacturer. After elution of the DNA, the concentration was determined by photometry. Commonly, the concentration of plasmid DNA was adjusted to 1 µg/µL. Typically 200-400 µg plasmid DNA were obtained from 200 mL cultured bacteria.

2.2.1.4. DNA concentration measurement

The maximum absorbance of DNA occurs at 260 nm. The absorption is proportional to the DNA concentration as described by Lambert-Beers' law. Hence, photometric measurements can be used to determine nucleic acid concentrations. At 260 nm, an extinction coefficient of 1 corresponds to a concentration of 50 µg/µL of double stranded DNA or 40 µg/µL of RNA. As the absorption maximum of aromatic amino acids occurs around 280 nm, it is possible to determine the grade of protein contamination of a DNA sample by measuring the photometric extinction at 260 nm and 280 nm. A sufficient purity of DNA or RNA is given by the ratio of (extinction260 / extinction280) x (ε260 / ε280), which should be above 1.8. The measurements were performed in 100 µL UV plastic cuvettes using a BioPhotometer (Eppendorf).

2.2.1.5. Restriction digest of plasmid DNA

Restriction endonucleases are able to cut double stranded DNA at specific recognition target sequences. For analytical digestions, typically 1µg plasmid DNA was digested with 1-5 units of restriction enzyme and respective 1x buffer provided by the supplier. For cloning and linearization 10 µg DNA with 10-30 Units of Enzyme were used. The reactions were incubated for 30 min at 37 °C for analysis and 3 h for preparatory purposes. Success of the restriction digests was controlled by agarose gel electrophoresis using 1-2 µL of digested DNA.

2.2.1.6. DNA ligation

T4 DNA ligase from Fermemtas was used to ligate DNA fragments. The vector and insert DNA containing solutions were mixed in a 1:3 or 1:4 ratio depending on their individual concentration. 1.5 µL 10 x ligase buffer and 1.5 µL T4 ligase were added. The volume was adjusted to 15 µL by using ddH2O. The reactions were incubated at room temperature for 30 min or at 16°C over night. 50% of the ligation mixture was subsequently used to transform competent bacteria as described above (see 2.2.1.1).

2.2.1.7. DNA agarose gel electrophoresis

The sugar phosphate backbone of DNA is negatively charged. If a steady electric field is applied, the DNA will migrate towards the anode. Larger fragments will migrate more slowly than smaller fragments as they are held back in the agarose meshwork. This leads to a separation of the nucleic acid fragments according to their molecular weight. For gel electrophoresis, DNA (100-200 ng for analytical purposes) or 1-10 µg (for preparative purposes) was diluted 5:1 in 6x loading dye and loaded together with a 1kb standard DNA ladder (MBI or Orange loading dye both from Fermentas) onto 0.8% - 2% agarose gels. The gels were casted and run in Shelton Scientific and PEQLAB gel chamber systems. Electrophoresis was performed at a voltage ranging from 100 V-180 V. Following electrophoresis, the gels were incubated in 1x TAE buffer containing 1 µg/mL ethidium bromide for 10-30 min. DNA fragments containing intercalated ethidium bromide were visualised by UV light at 254 nm and documented on a Herolab gel system.

2.2.1.8. RNA gel electrophoresis

RNA Gel electrophoresis was performed like DNA Gel electrophoresis except for the following differences: To avoid RNase activity, gel chamber and combs were washed in advance with ddH_20 and soap and the gel was pre-run for 10 min at 55V before applying the samples to the slots. RNA-samples of 2 µL were mixed with 8 µL 5x RNA-loading buffer (Ambion). RNA was denatured for 10 min at 95°C to break up secondary structures of the mRNA before applying it to the gel slots.

2.2.1.9. Extraction of DNA fragments from agarose gels after electrophoresis

DNA fragments of the desired sizes were excised from agarose gels and transferred into a fresh 2 mL reaction tube. The slices were extracted according to the manufacturer's protocol using either the Gel Extraction kit from Eppendorf or QUIAGEN.

2.2.1.10. DNA purification of PCR products or fragments of restriction digest

For purification of digested DNA fragments or PCR products either the Nucleotide Removal kit or the QIAquick PCR Purification kit (QIAGEN) were used, according to the manufacturer's protocol.

2.2.1.11. Removal of 5' DNA overhang

Ligation of non complementary double strand DNA ends created by restriction digests can be achieved by blunt end cloning. Therefore the 5'-DNA overhangs were filled using the Klenow fragment of the *E.coli* DNA polymeraseI (Roche). 10x restriction buffer H (Roche), dNTPs (final concentration: 200 µM), 2 µL enzyme and purified DNA were mixed (total volume was usually 40 µL). The reaction mix was incubated at 37°C for 45 to 60 min. Subsequently, the DNA was purified for further processing using gel extraction or Nucleotide Removal Kit (QUIAGEN).

2.2.1.12. DNA dephosphorylation

In order to prevent blunt end or single enzyme digested vector arms from re-ligation, the DNA was dephosphorylated using calf intestinal phosphatase (CIP) in 1x reaction buffer provided by supplier (Roche). The digested plasmid was purified using Nucleotide Removal Kit (QUIAGEN) and eluted with 30 µL ddH_2O. 4 µL 10 x buffer, 3 µL ddH_2O and 1 µL CIP were mixed and incubated 30-45 min at 37°C. Subsequently, the DNA was purified for further processing using gel extraction or Nucleotide Removal Kit (QUIAGEN).

2.2.1.13. Nippon oligo cloning

Oligo cloning can be a very efficient method to add small nucleotide sequences <100 bp to a gene of interest, alternative to restriction fragment or PCR cloning. The oligonucleotides are designed to create restriction site overhangs on both ends upon annealing. It is also suggested to add a unique internal restriction site into the oligo that successful cloning can be controlled easily. In order to enhance ligation efficiency the oligos were phosphorylated. Each oligo was prepared in an extra vial. 1 µL 100 pm/µL primer, 1 µL T4 Polynucleotide Kinase (PNK)(Roche), 1 µL 10x Buffer, 1 µL 10 mM ATP (Roche) and 6 µL ddH_2O were mixed and incubated for 1 h at 37° C. After the incubation the two samples were mixed together and denatured for 10 min at 95°C in an Eppendorf thermomixer. For annealing the reaction was cooled down slowly by turning off the thermomixer. At approximately 40°C the sample was removed from the mixer and left at RT for 5 min. For ligation the annealed oligos were diluted 1:20 in water. 1-2 µL of the dilution was mixed with the following reagents: 1 µL cut vector, 1.5 µL T4 ligase, 1.5 µL T4 ligase buffer and ddH_2O to a total volume of 15 µL.
Ligation and transformation were performed as described above (2.2.1.1, 2.2.1.6).

2.2.1.14. PCR

All PCR reactions were performed with proof reading Polymerases, either Pfu Ultra or Herculase both from Stratagene. Pfu Ultra was used for high accuracy; the Herculase provided a higher yield.

cDNA isolated from zebrafish or cultured cells by RNA extraction and subsequent RT-PCR (2.2.1.15, 2.2.1.16, 2.2.1.17) or plasmid DNA was used as template for the PCR reaction and prepared as followed

20 ng plasmid DNA/ or 10 µL cDNA
5 µL 10x PCR buffer
5-10 µL 2 mM dNTP mix
1 µL upper and lower primer (50 pmol/µL)
1 µL DNA-polymerase
Add ddH2O to a total volume of 50 µL

The PCR conditions were chosen according to the primers and template lengths used. In general, DNA was first denatured at 94°C. The temperature for primer annealing depended on the melting temperature of the oligonucleotides and was therefore determined empirically. Usually 45 s were sufficient for annealing. Elongation occurred at 72°C for 1 min/kb fragment length. As a standard 35 cycles were performed. All PCR reactions were performed using a MJ Research Thermocycler PTC-100.

2.2.1.15. Purification of RNA

For purification of in vitro transcribed RNA or total RNA extracted from tissue, RNeasy Mini Kit (QIAGEN) was used as described in the manufacturer's protocol.

2.2.1.16. RNA extraction from animal tissue

For total RNA extraction from cultured cells or zebrafish embryos RNeasy Mini Kit in combination with QIAshredder columns was used according the manufacturers guidelines. In order to achieve sufficient yields 25 embryos were homogenised in 50 µL RLT buffer (RNeasy Mini Kit) using either a syringe or a pestle-homogeniser fitting into Eppendorf reaction tubes. Additional 300 µL RLT were added before transferring the lysate onto QIAshredder columns.

Chromosomal DNA was eliminated by DNaseI digest (50 µL nucleic acid extract, 6 µL 10x transcription buffer (Roche), 2 µL RNAsin (Promega), 2 µL DNaseI (RNase free) (Roche, 10

U/µL), incubation for 30 min at 37°C). Afterwards, the RNA was purified using the RNeasy kit (Qiagen). Quality of the RNA was controlled by agarose gel electrophoresis. Integrity of the two major rRNA-bands indicated that RNA degradation did not occur.

2.2.1.17. Preparation of cDNA

In order to generate cDNA from total mRNA extracts 5-11 µL RNA template and 1 µL random hexamer primers (Promega) were incubated at 70°C for 5 min. Meanwhile the following reagents were mixed together:

10 µL 5x Superscript II Buffer (Invitrogen)
1 µL RNAsin (Promega)
5 µL 2 mM dNTPs
5 µL 0.1 mM DTT (Invitrogen)
+ RNase free water to a total volume of 50 µL

This reaction mixture was added to the annealed RNA/primer solution at 25 °C followed by 5 min incubation. Subsequently, 1 µL SuperScript reverse transcriptase was added and the following incubation steps were performed

25°C - 10 min
42°C - 60 min
70°C - 10 min
4°C - ∞

The cDNA was now ready for use. Alternatively it was kept at -20°C for long term storage.

2.2.1.18. Stratagene blunt cloning

In order to clone PCR amplicons without flanking restriction sites, they were cloned into the pSC-B vector using the Cre recombinase based Stratagene Blunt Cloning Kit. The procedure was performed according to the guidelines of the manufacturer. http://www.stratagene.com/manuals/240207.pdf

2.2.2. Zebrafish maintenance

2.2.2.1.Maintenance of zebrafish

Raising, spawning and maintaining of zebrafish strains was performed as described previously (Kimmel et al. 1995; Westerfield 1995).

2.2.3. Methods for genetic and pharmacological manipulation of zebrafish embryos

2.2.3.1. Synthesis of capped mRNA for microinjection into zebrafish embryos

In order to synthesise capped mRNA templates from pCS2+ plasmids, 10 µg plasmid-DNA were linearised by single enzyme restriction digest were used. The digested plasmids were purified using the Nucleotide Removal kit (QIAGEN) and eluted in 30 µL RNase free water. In order to ensure that all plasmid was digested, an aliquot of the reaction was analysed by gel electrophoresis on a 0.8% agarose gel (2.2.1.7). In vitro synthesis of capped mRNA was performed using mMESSAGE mMACHINE® SP6 Kit (Ambion) according to the manufacturer's protocol. 6 µL of linearised DNA template, 10 µL 2x NTP/CAP, 2 µL 10x reaction buffer and 2 µL enzyme mix were mixed. The reaction was incubated at 37°C for 3 h followed by digestion of the template DNA by treatment with 1 µL RNase free DNase (Roche) for 15 min. Capped mRNA was purified using the RNeasy Mini kit (QIAGEN) and eluted with 30 µL RNase-free water. The efficiency of RNA synthesis was analysed on a 0.8% agarose gel as described above (2.2.1.7). The concentration of the mRNA was further determined using a BioPhotometer (see 2.2.1.4). The described reaction generated a general yield 6-15 µg of synthesised mRNA.

2.2.3.2. Cytoplasmic microinjection of nucleic acids

The standard method for genetic manipulation of zebrafish embryos is the microinjection of nucleic acids into the cytoplasm of one cells stage embryos. For transient mosaic expression plasmid DNA from maxi preparations (2.2.1.3) additionally purified using the GENECLEAN® Turbo Kit (QBIOgene) according to the specifications of the manufacturer was used. For transient non-mosaic expression capped mRNA was injected. In order to achieve a specific knockdown of the mRNA of target genes antisense oligonucleotides aka Morpholinos were used as described below (1.2.2.5). mRNA and DNA were diluted in water to the desired final concentration (typically 50-250 ng/µL for RNA and 30-50 ng/µL for DNA). Phenol red was added to the solution to facilitate monitoring of the injection (1/10 of a 0.5% stock solution, Sigma). The mix was injected into the cytoplasm of zygotes using a micromanipulator supported by the use of a binocular. To keep the embryos in a fixed position during the injection procedure they were placed into grooves formed by agarose. After injection the embryos were removed from the grooves and transferred into a conventional Petri dish. The embryos were incubated at 28°C until they reached the desired developmental stage for further investigations.

2.2.3.3. DAPT treatment of zebrafish embryos

DAPT (*N*-[(3,5-Difluorophenyl)acetyl]-L-alanyl-2-phenyl]glycine-1,1-dimethylethyl ester) is a chemical compound that is able to block the cleavage of notch intracellular domain (NICD) by inhibiting γ-Secretase activity. As a result of the inhibition NICD cannot be released from the membrane and is therefore not translocated to the nucleus. Thus activation of Notch specific target genes is impaired (Geling et al. 2002). Solid DAPT (Alexis Biochemicals) was dissolved in DMSO and stored at -20°C as 10 mM aliquots. Zebrafish embryos of different stages were treated with 100 µM DAPT, 1% DMSO in 30% Danieau-PTU until they were fixed in 4% PFA/PTW. Control embryos were treated with vehicle only.

2.2.3.4. Morpholino injection

The injection of Morpholino antisense oligonucleotides (Genetools) was performed in analogy to the injection of mRNA or DNA (2.2.3.2). The Morpholinos were stored as 2 mM aliquots at -20°C. For injection 1 µL of a 2 mM Morpholino solution was mixed with 8 µL RNase free water and then heated for 5 min at 65°C in order to solubilise precipitates. After the samples cooled down to room temperature 1 µL phenol red was added to complete the injection mixture.

2.2.4. Histological Techniques

2.2.4.1. Whole-mount in-situ-hybridisation (ISH)

Most genes are expressed in a very specific spatio-temporal pattern within the organism. Antisense riboprobes carrying UTP nucleotides conjugated with e.g. digoxygenin or fluorescine can be used to visualise gene expression in whole-mount preparations. The antisense probe is hybridised to endogenous mRNA and complementary annealed products are subsequently detected by antibodies coupled to Alkaline phosphatase (AP). Visualisation is accomplished by a chromogenic reaction carried out by the AP.

In vitro transcription of antisense riboprobes

Antisense riboprobes were generated from linearised DNA template and labelled by *in vitro* transcription with modified nucleotides using the DIG RNA-labelling mix (Roche), according to the manufacturer's instructions. The DNA template was subsequently digested with 1 µL RNase free DNase at 37°C for 15 min and DIG-labelled RNA was purified using the RNeasy Mini kit (QIAGEN), as described in the manufacturer's protocol.

Fixation and storage of zebrafish embryos

Dechorionated zebrafish embryos were fixed over night in 4% PFA/PTW at 4°C or for 4 h at RT on a shaker. They were washed two times in PTW 5 min each and dehydrated in 100% MeOH and subsequently stored in fresh 100% MeOH. Ahead of ISH the embryos were rehydrated by washing for 5 min each in 75%, 50%, 25% MeOH/PTW followed by washing two times with PTW to remove residual MeOH.

Proteinase K-treatment of embryos

To permeabilise the tissue for RNA probes and antibodies, fixed embryos were treated with the proteolytic enzyme Proteinase K (Roche). The embryos were incubated in Proteinase K/ PTW (10 µg/mL) for the respective time interval depending on the developmental stage of the embryos (listed below). The digest was stopped by washing in 2 mg/mL Glycine/PTW and subsequent fixing in 4% PFA for 20min. To remove excessive PFA, embryos were washed 5 times in PTW for 5 min each.

Developmental stage:	Time of proteinase K digest:
24 hpf	12 min
36 hpf	20 min
48 hpf	30 min
3 dpf	25 min
4 dpf	45 min

Hybridisation

The embryos were first transferred to 2 mL Eppendorf reaction tubes and prehybridised in 2mL of hybridisation buffer for 1 h in a water bath preheated to 60°C. Meanwhile the hybridisation probe consisting of 4 µL of the labelled antisense RNA and 200 µL hybridisation buffer was prepared. The probe was then incubated at 95°C for 10 min to break up secondary RNA structures. From the 95°C incubation the probe was directly transferred on the embryos in exchange of the prehybridzation buffer. The hybridisation was performed over night at 60°C. The following day the embryos were washed two times for 45 min at 60°C in 2mL with 50% formamide/2x SSCT, once in 2x SSCT and two times using 0.2x SSCT.

Antibody detection

After the last wash in 0.2x SSCT, unspecific binding sites for anti-digoxygenin Fab-fragments were blocked by incubating the embryos in 10 % NGS in PTW with 1% DMSO for 1 h on a

rotator at room temperature. The embryos were then incubated over night at 4°C in a 1:2000 solution of the anti-digoxygenin antibody (Roche) in 10 % NGS in PTW while rotating. For the detection reaction the embryos were transferred to a six-well plate and rinsed five times with 5 mL of PTW for 15 min each at room temperature on a shaker in order to remove excess antibody. The embryos were then equilibrated in the freshly prepared ISH staining buffer two times for 5 min each. The buffer was filtered using a 22 µm syringe filter (Millipore) prior to use. After the equilibration step ISH staining solution was added in exchange. The staining reaction was performed in a range from 3 h up to over night at room temperature. For probes with high background the temperature of the chromatogene reaction was reduced to 18°C. During the staining procedure the staining solution was exchanged several times. To stop the chromogenic reaction the embryos were rinsed 3-5 times for 5 min in PTW. For long term storage and observation, the embryos were transferred into 90% glycerol (v/v).

2.2.4.2. Immuno histohemistry (IHC) wholemount preparation of zebrafish embryos

For standard fluorescent immuno-histochemistry the following protocol was performed. Fixation and rehydration of the embryos was performed as described in the protocol for ISH (2.2.4.1). If the antibody required further permeabilisation of the tissue or antigen unmasking was necessary, additional steps as described below (2.2.4.3) were applied. The rehydrated embryos were incubated in 10% NGS in PTW/DMSO blocking solution for 1 h at RT in order to block unspecific binding sites. The embryos were subsequently incubated with the primary antibody diluted in blocking reagent (For dilutions see 2.1.3). Incubation was performed over night at 4°C. The next day, the embryos were washed 5 times or more in PTW/DMSO for 15 to 60 min each at RT. Subsequently the samples were incubated with the secondary antibody diluted in blocking reagent. Incubation conditions were the same as for the primary antibodies. For immuno-fluorescence, samples were incubated with secondary antibodies conjugated to fluorophores such as Cy3, Cy5 or FITC. After incubation, the embryos were washed again at least five times in PTW/DMSO prior to microscopy analysis.

2.2.4.3. IHC acetone permeabilisation and antigen unmasking

To obtain a better penetration of the antibody into the tissue, fixed embryos were transferred directly from their methanol into -20°C cold acetone and they were incubated at -20°C for 7 min. To disrupt cells, the embryos were briefly rinsed and incubated in deionised water for 1 min. Subsequently the specimens were washed 2 times for 5 min with PTW or alternatively subjected to antigen unmasking. For this purpose, the embryos were transferred into preheated

sodium citrate (10 mM, pH 6.0) or 50 mM Tris/HCl, pH 8.2, with 0.1% Tween and incubated at 95°C in a 2 mL reaction tube for 10 to 30 min. After cooling down to RT, the embryos were washed twice in PTW. The following blocking and antibody incubation was performed as described in the standard protocol. (2.2.4.2)

2.2.4.4. DAB staining

Primary antibody staining was performed as in (2.2.4.2). Secondary antibodies conjugated to Peroxidase were visualised by DAB (3,3'-Diaminobenzidine) staining. After over night incubation with the secondary antibody the embryos were washed 5 times for 15 min in PTW followed by 5min incubation in 0.1 M Tris-HCl, pH 7.4 staining buffer. For the staining reaction, the medium was exchanged to 5 mL DAB staining reagent. After a delay of 30 min to allow DAB to penetrate the tissue the reaction was started by addition of 20 µL of 0.3% H_2O_2 (Sigma). The specimens were then stained until the desired intensity was reached. To enhance the staining additional H_2O_2 could be applied if necessary. The chromogenic reaction was stopped by washing twice in PTW.

2.2.5. Staining applications using fluorescent Dyes

2.2.5.1. Membrane staining using Bodipy Ceramide®

Bodipy Ceramide FL C5 is a fluorescent lipophilic vital dye, which labels membranes in living zebrafish embryos. It is available in a wide range of different colours. A 1 mM stock solution dissolved in DMSO. For staining, zebrafish embryos were soaked for a minimum of 30 min at room temperature in a 1:1000 dilution of the stock solution in the desired medium. Staining was followed by three washing steps to remove excess dye prior to fluorescence detection.

2.2.5.2. 4',6-Diamidin-2-phenylindol (DAPI) nuclear staining

DAPI is a fluorescent dye which intercalates with DNA and is well established to label the nuclei of fixed cells. DAPI is excited with ultraviolet light. When bound to double-stranded DNA its absorption maximum is at 358 nm and its emission maximum is at 461 nm. To stain zebrafish embryos, DAPI (Roche) was added to the medium to a final concentration of 1µg/µL. After 30 min incubation at room temperature unbound dye was removed by three 5 min washing steps.

2.2.5.3. TO-PRO® 3 hair cell staining

Hair cells of 4-5 day old zebrafish embryos were labelled with the far red dye TO-PRO® 3 (Invitrogen). The living embryos were soaked for 2 h in 30% Danieau/PTU 1µM TO-PRO® 3. Before imaging the fish were washed three times for 5 min each with 30% Danieau/PTU.

2.2.5.4. Sytox orange (Acridine Orange) nucleic acid stain

Acridine orange (AcO) is a marker for dead cells in living embryos. Only if the cell is permeabilised as a result of ongoing apoptosis, Acridine Orange is able to pass the membrane (Tucker and Lardelli 2007). Within the cell it binds to nucleic acid. For Acridine Orange staining embryos were soaked in 30% Danieau/PTU containing 5 µg/mL Acridine Orange for 30 min, followed by three washes each 1 min in 30% Danieau/PTU. For stock solution 5 mg AcO was solved in 1 mL DMSO.

2.2.6. Biochemical Methods

2.2.6.1. Maintenance and transfection of zebrafish PAC2 cells

Zebrafish PAC2 cells were maintained, transfected and imaged as described in (Chu et al. 2008; Rieger et al. 2009; Senghaas and Koster 2009). The preferred reagent for transfection was FuGENE HD from Roche.

2.2.6.2. Maintenance and transfection of mammalian cells

Two different mammalian cell lines were utilised during this work: Human embryonic kidney 293T cells and NIH3T3 mouse fibroblast cells. 293Tcells were used for protein production because they are easy to maintain, show a high transfection efficiency and are able to produce large amounts of protein from transfected expression plasmids; NIH3T3 cells were used for microscopy because they show a spread out morphology and are resistant to climate changes, a property predesigned for imaging. All mammalian cell lines were maintained at 37°C and 5% CO_2 in DMEM medium supplied with 1% PEN/STREP, 1% Glutamin/Glutamax and 10% fetal bovine serum (FBS). The cells were passaged similar to PAC2 cells described in (Senghaas and Koster 2009) with the exception that the time of trypsin incubation was generally shorter and 293T cells were trypsinised only at room temperature for no longer than 5 min.

NIH3T3 cells were transfected using FuGENE HD as described for PAC2 cells in (Senghaas and Koster 2009). 293T cells were transfected using Calcium Phosphate as reagent. Calcium Phosphate transfection is explained in the following: This protocol is designed for 10 cm

culture dishes for differently sized ones, please adjust volumes accordingly. First, three to five million 293T cells were plated into a 10 cm culture dish. They were incubated for 6 h up to over night to allow cell attachment to the plastic surface of the culture dish. Cells were grown until they reached a confluence of 50-70%. Before the cells could be transfected the DNA/reagent mixture had to be prepared. For the preparation of the transfection mix first 500 µL 2x HBS were added to a snap cap tube. Second 62.5 µL 2M $CaCl_2$, 20 µg total DNA and ddH_2O to at total volume of 500 µL were mixed in a 1.5 mL reaction tube by vortexing.
Under mild vortexing the DNA/$CaCl_2$ mix was added to the HBS buffer in a drop wise manner.
The mixture was incubated at room temperature for 30 min and then applied to the cultured cells again drop wise. After incubating the cells over night the transfection reagent was removed by washing the cells with 1x HBS. 48 h after transfection the cells were harvested as described in 2.2.6.3. Imaging of mammalian cells was performed like PAC2 cell imaging described in (Senghaas and Koster 2009).

2.2.6.3. Protein lysate preparation from cultured cells

In order to extract proteins from cultured transfected cells to perform biochemical analysis such as IP, WB or mass spectrometry the cells were lysed using non ionic detergents. The following protocol describes the lysis of cells plated onto a 10 cm culture dish. For different amount of cells the volume has to be adjusted accordingly.
First the medium was removed from the plates then the cells were washed with 10 mL PBS. All following steps were performed on ice, centrifugation was performed at 4°C. To facilitate detachment 800 µL TEN buffer was pipetted on the cells. They were then removed from the plastic surface using a cell scraper and transferred to a 1.5 mL reaction tube. In order to remove the TEN buffer, the cells were pelleted by centrifugation at maximum speed for 30 s. The supernatant was removed and 1 mL IPN_{150} Lysis buffer was pipetted on the cells. The cells were lysed for 30 min on ice. During incubation the solution was mixed several times by inverting the tubes. After 30 min the cell debris was pelleted by centrifuging 10 min at maximum speed. The pellet could be re-suspended in 1x SDS and denatured for 2 min at 95°C and subjected to SDS-PAGE in order to analyse the insoluble protein fraction. The supernatant was transferred to a fresh tube. For long term storage the lysates were frozen in liquid nitrogen and kept on -20°C. For over night preservation the lysates were stored on ice at 4°C. Samples for mass spectrometry were cleared by filtration through 0.22 µm syringe filters (Millipore).

2.2.6.4. BCA protein assay reagent

Protein concentrations were determined using BCA Protein Assay Kit (Pierce) according to the manufactures protocol (http://www.piercenet.com/files/1296as8.pdf) with the exception that the sample volume was reduced to 12.5 µL and the working reagent volume to 200 µL.

2.2.6.5. Co-immunoprecipitation

Co-immunoprecipitation (Co-IP) is a protein purification method that takes advantage of the specific binding of an antibody to its antigen. If the procedure is performed under native conditions, intact protein complexes can precipitate with the target protein and subsequent analysis allows identifying binding partners. Co-IP is a powerful technique that is used regularly by molecular biologists to analyze protein-protein interactions.

For all Co-IPs 293T cells were used. They are easy to transfect by using the rather cheap calcium phosphate protocol described in (2.2.6.2), and they produce a high amount of protein compared to other cell lines.

Lysates were generated as described (2.2.6.3) and the protein concentration was determined by BCA protein assay (2.2.6.4). From each sample 20 µg of total protein were mixed with an equal volume of 2x SDS buffer and denatured for 2 min at 95°C to serve as an input control.

For the Co-IPs lysate containing 500-1000 µg total protein were mixed with protein G sepharose beads equilibrated three times with IPN_{150} lysis buffer and 1 µg antibody in 1.5 mL reaction tubes. The volume was adjusted to 1 mL by adding additional IPN_{150}.

The samples were incubated for minimum of 3 h up to over night at 4°C on an overhead rotator. After incubation the beads were sedimented by careful centrifugation (30 s, 2.100 g, 4°C) and the supernatant was removed. For washing, the beads were re-suspended in 1 mL IPN_{150} and again centrifuged for 30 s at 2.100 g, 4°C. The washing step was performed three times. After the last centrifugation step the supernatant was removed completely and the beads were re-suspended in 20 µL 1xSDS buffer followed by 2 min denaturing at 95°C.

The denatured input control samples and beads were applied to a SDS-PAGE for immuno detection.

2.2.6.6. SDS-Page (SDS-polyacrylamide gel electrophoresis)

SDS Page is a technique that allows for the separation of protein mixtures according to their electrophoretic mobility (depending on the length of the polypeptide chain or molecular weight). SDS is a strong detergent that is able to denature proteins and charging them

negatively. The samples are forced to migrate through the meshwork of polyacrylamide by applying an electrical field. The larger the polypeptide chain the more slowly it is able to migrate through the pores which leads to a fractioning by size. Polyacrylamide gels consist of two parts, an upper stacking gel with low percentage containing the pockets for sample loading and a larger separating gel. Depending on which mass range should be resolved, the acrylamide percentage of the separating gel was adjusted between 6-12%.The composition of the stacking and separating gel is listed in (Table 4)

Table 4

	Separating Gel	Stacking Gel
30% Acrylamid-Mix	6-15%	3%
1.5 M Tris (pH 8,8)	375 mM	-
1.0 M Tris (pH 6,8)	-	125 mM
10% SDS	0.1%	0.1%
10% APS	0.1%	0.1%
TEMED	0.1%	0.1%

The SDS-Page was performed in Mini-Protean-III Chambers from BioRad filled with SDS-running buffer at a voltage ranging from 140V-180V for 1-2 hours. All samples were denatured for 2 min at 95°C in 2x SDS-loading buffer prior to loading.

2.2.6.7. Silver staining

Kerenyi and Gallyas introduced silver staining as a sensitive procedure to detect trace amounts of proteins in gels (Kerenyi and Gallyas 1972). It is approximately 50 times more sensitive than classical Coomassie Brilliant Blue staining of which the detection limit is around 50 ng protein per band. Silver staining is therefore used to analyse samples with low protein content like tandem affinity purified ones.

After completion of electrophoresis the SDS-Page was removed from the glass cassette and transferred to a suitable dish on a shaker where all the following washing steps were performed. The gel was washed two times for 30 min each with a fixative containing 50% MeOH, 12% acetic acid and 0.0185% formaldehyde. The fixative was removed and 50% EtOH was added to the Gel for approximately 20 min. The EtOH washing step was repeated three times. Next, 0.8 mM $Na_2S_2O_3$ in water was applied for only 20 s followed by two quick washing steps with water. After the water was removed, the staining solution (11.8 mM $AgNO_3$, 0.028 % formaldehyde) was added to the gel. After 20 min the staining solution was removed and the gel was quickly rinsed with water. To develop the gel 0.57 mM Na_2CO_3/0.8 mM $Na_2S_2O_3$, 0.0185% formaldehyde was applied and once a strong staining was visible the developing solution was replaced by the fixative solution described above. The fixative was

applied for at least 10 min. For preservation of the staining the gel was subsequently washed in 20% EtOH containing 2% glycerine.

2.2.6.8.Western blot and immuno-detection

Polyacrylamide gels were blotted on PDVF membranes using the XCell II™ Blot Module from Invitrogen life technologies. All steps were performed as described by the manufacture for Tris-Glycine type gels (http://tools.invitrogen.com/content/sfs/manuals/blotmod_pro.pdf). To control for the efficiency of the protein transfer, PonceauS solution was added to the membrane. PonceauS S is a temporary stain that can easily be removed by rinsing the blot with water or 1x TBS buffer. For subsequent immuno detection of proteins, first unspecific binding sites were blocked by applying blocking reagent (1x TBS with 2% dry milk) for 10-20 min at room temperature. The blocking reagent was replaced by blocking solution containing 1:1000 dilution of primary antibody stock solution recommended by the supplier. Incubation of the primary antibody was performed at 4°C over night. After incubation over night the primary antibody was removed and the blot was quickly washed three times and three times for 5 min each with 1x TBS buffer. Subsequently the secondary peroxidase coupled antibody was applied for 30 min-1h at room temperature followed by the same washing steps as after the primary antibody incubation.

For detection ECL™ Western Blotting Detection Reagents (Amersham) were used. These reagents use enhanced luminol based detection, which is suitable for all routine Western blotting. The detection reagent consists of two components that were mixed together shortly before use in a 1:1 ratio. For the standard membrane size 1 mL of detection reagent is sufficient. The membrane was dried using tissue paper and then soaked for one minute in the detection reagent. This elicits a peroxidase-catalyzed oxidation of luminol and subsequently enhanced chemiluminescence where the peroxidase coupled antibody is bound to the antigen on the membrane. Excess solution was removed using tissue paper. The membrane was transferred into an autoradiography cassette. Hyperfilm was placed on the membrane in the dark room. As standard exposure times 1 min and 5 min were used. For stronger or weaker signal the time was adjusted accordingly. The films were developed in a Curix 60 developing machine (AGFA).

2.2.7. Proteomics

Characterizing the interactome of a protein of choice gives valuable information about its cellular context and biological mechanisms in which it is involved. The following protocol describes the isolation of the native protein complex from cell lysates via Tandem Affinity

Purification and the subsequent sample preparation for mass spectrometric analysis. The process involves five major parts which include a) the overexpression of SF-TAP tagged protein in culture cells b) a two step column purification, c) trypsinisation and sample preparation d) mass spectrometry analysis and e) data processing.
(For reference and a more detailed protocol please refer to (Gloeckner et al. 2009a))

2.2.7.1. Preparation of cell lysates

293T cells were plated into 15 cm dishes and transfected according to the transfection protocol described above (2.2.6.2.). For each purification sample three 15 cm dishes were used. The lysates were prepared as explained above using IPN_{150} lysis buffer (2.2.6.3)

2.2.7.2. SF-TAP Streptavidin FLAG tag tandem affinity purification

In recent years several methods have been developed to analyse protein-protein interactions under native conditions. One of them, the tandem affinity purification (TAP), combines two purifications based on two different affinity matrices in order to reach the optimal purity of the isolated protein complexes (Rigaut et al. 1999; Gloeckner et al. 2009a). Therefore, tandem affinity purification can significantly reduce the background caused by nonspecific binding of proteins compared to single step purification. Due to the high purity achieved by this two step purification methods TAP samples are ideal for subsequent mass spectrometry analysis. The tandem affinity tag used in this approach consists of two Streptavidin peptide sequences and a FLAG tag. The advantage of this TAP compared to others is the small size of the peptide and the possibility to elute the tag by competition rather than by proteolytic cleavage. Desthiobiotin is used for the elution of tagged proteins from the Strep-Tactin resin in the first step and the FLAG octapeptide for the elution from the anti-FLAG resin in the second step (Gloeckner et al. 2009b).
First, Strep-Tactin beads (Strep Tactin Superflow IBA Cat. No. 2-1206-025) were equilibrated by adding them to 600-800 µL SF-TAP wash buffer provided in a 1.5 mL Eppendorf tube (50 µL beads for each 15 cm dish were used). The resin was centrifuged 1 min at 5000 g at 4° or RT. The overflow was discarded. Subsequently the beads were re-suspended and washed two times with SF-TAP wash buffer and once by adding 500 µL IPN_{150} lysis buffer.
The equilibrated beads were transferred to a 15 mL falcon tube and the filtered cell lysates were added. To allow binding of the tagged protein to the beads the samples were incubated at 4°C for 1-2 hours on a shaker. After the incubation the solution was centrifuged for 1 min at 4°C using 5000g. The overflow was discarded with exception of the last 2 mL. The beads were re-suspended and loaded onto microspin columns (GE Healthcare). The remaining liquid was removed by

centrifugation of the microspin columns for 5 s at 0.1 g. (Centrifugation steps are very crucial. The beads should never fall dry).

The beads were then washed 3 times by adding 500 µL wash buffer each followed by centrifugation of 5 s at 0.1 g. After the last washing step the protein was removed from the beads using 400 µL strep-elution buffer (10x Strep-tag elution buffer with D-Desthiobiotin diluted in dH_2O). The buffer was added to the column, which was then incubated 10 min on ice while shaking the column gently once in a while. Subsequently, the column was placed into an Eppendorf reaction tube and the eluate was collected by centrifugation for 1 min at 1000 g. The column and the beads were discarded and the eluate was used for the second purification step using agorse beads conjugated to the anti-FLAG antibody.

Before the eluate could be applied to the FLAG beads they had to be equilibrated. Therefore, a 1.5 mL Eppendorf reaction tube with 600-800 µL 1x TBS was prepared, the FLAG beads were added (50 µL beads for each 15 cm dish) and centrifuged for 1 min at 1000 g at 4° or RT. The overflow was discarded and the beads were washed 3 times by resuspension followed by centrifugation and discarding the supernatant. First they were washed two times in SF-TAP wash buffer and then one time with IPN_{150}. After the washing of the beads they were re-suspended in ~300 µL 1x TBS and loaded onto microspin columns. Shortly before adding the strep eluates to the columns, they were centrifuged at 0.1g for 3-5 s in order to remove the remaining 1x TBS. Immediately after removal of the TBS, the strep-eluate was added in order to prevent the beads from drying out. For binding the columns were incubated on a shaker for 1-2 h at 4°C. Their incubation was followed by three washing steps with 500 µL wash buffer each and once with 1x TBS added to the column and removed by centrifugation for 5 s at 0.1 g. For elution, 200 µL FLAG peptide elution buffer (1x TBS buffer, 200 mg/mL Flag peptide (Sigma)) was applied to the column. After incubation for 10 min on ice the purified proteins were eluted by centrifugation for 1 min at 1000 g.

20 µL aliquots were used for analysis on SDS-PAGE followed by silver staining. The remaining sample was precipitated using chloroform methanol protein precipitation. (See 2.2.7.3)

2.2.7.3. Methanol chloroform protein precipitation

Methanol chloroform protein precipitation is a rapid method based on a defined methanol chloroform water mixture for the quantitative precipitation of soluble as well as hydrophobic proteins from dilute solutions (e.g. column chromatography effluents) (Wessel and Flugge 1984).

The 200 µL eluate obtained from the SF-TAP purification was transferred into a 2 mL sample tube and 0.8 mL of methanol was added. The suspension was mixed and then centrifuged for

20 s. All centrifugation steps during this protocol were performed at 9.000 g. Next 0.2 mL chloroform was added to the solution again followed by mixing and 20 s of centrifugation. After that 0.6 mL of water were added. The mix was vortexed until a homogeneous milky consistence could be observed and subsequently centrifuged for 1 minute. The upper layer (aqueous phase) was carefully removed and 0.6 mL of methanol were added. The solution was mixed very gently and centrifuged for 2 min. The supernatant was removed cautiously and the pellet was dried. Subsequently, the sample could be wrapped with parafilm for long term storage at -20°C or re-suspended for in-solution digestion.

2.2.7.4. Sample preparation for mass spectrometry (MS) analysis: in-solution digest

The in-solution digest is a quick and efficient method to digest the whole SF-TAP eluate after protein precipitation. The use of a MS-compatible surfactant helps to solubilise the precipitated proteins. In order to allow the identification of cysteine containing peptides, random oxidation is prevented by alkylation, applying a DTT/iodoacetamide treatment prior to digestion, leading to a defined mass-adduct. The digested protein sample can be directly subjected to the analysis by a Liquid Chromatography (LC) coupled mass spectrometer (Gloeckner et al. 2009a).

The protein pellet prepared in by Methanol Chloroform precipitation (2.2.7.3) was dissolved in 30 µL of freshly made 50 mM ammonium bicarbonate by extensive vortexing. Then 3 µL of a RapiGest^{TM} SF stock solution (Waters) (final concentration 0.2 %) followed by 1 µL of 100 mM DTT (freshly made) were added. The samples were vortexed and then incubated for 10 min at 60°C. Afterwards the solution was cooled to room temperature and 1 µL of freshly prepared 300 mM iodoacetamide was added. The samples were vortexed and subsequently incubated for 30 min at room temperature in the dark. Subsequently 2 µL trypsin stock solution (Promega) was added and the samples were vortexed and incubated at 37°C over night. Next, 2 µL of concentrated HCl (37%) were added for hydrolysis of RapiGest^{TM} SF . The samples were transferred to polypropylene inserts (Supelco) (remove spring) and incubated for 30 min at RT. The inserts were placed in 1.5-mL reaction tubes and centrifuged for 10 min (13,000 × *g*, RT). After the centrifugation the solution between the upper oleic phase and the pellet was carefully recovered by using gel-loader tips. After that the samples could be directly subjected to C-18 HPLC (high pressure liquid chromatography) separation prior to MS analysis.

2.2.7.5. Mass Spectrometry (MS) Analysis and Data Processing

Mass spectrometry is a technique used to analyse the elemental composition of a sample or molecule, e.g. peptides. The underlying principle of all MS techniques is the ionisation of the sample to generate charged molecules or molecule fragments and measure their mass-to-charge ratios. The accuracy of the measurement is high enough to determine the peptide sequence by *in silico* comparison of the data to peptide databases.

Samples in these studies were analysed by the Proteomics Core Facility at the Helmholtz Zentrum München in collaboration with Dr. Christian Johannes Glöckner using the ESI-Orbitrap (Electronspray Ionisation) technique. The spectra that were received by the analysis were processed using MASCOT and Scaffold Viewer software in order to identify the peptides. The hereby revealed functional interactome was illustrated using CYTOSCAPE.

2.2.8. Imaging

2.2.8.1.Cell culture

Culture cells prepared for fluorescent microscopy were grown in custom-made sterilised or commercially available (MatTek) imaging chambers. Observation was performed using a LSM 510 confocal microscope (Zeiss). Details of this procedure are described in Senghaas and Köster 2009 (Senghaas and Koster 2009).

2.2.8.2.Imaging of zebrafish embryos

In-vivo imaging

Living zebrafish embryos were anesthetised using 30% Danieau/PTU containing 0.01% tricaine. The anaesthetised embryos were embedded in 1.2% ultra low melting agarose/30% Danieau in custom-built imaging chambers with a glass bottom. The mounted embryo was covered with 30% Danieau/PTU/0.01% tricaine. Detailed information about embedding and imaging can be found in Distel el al. (Distel and Köster 2007; Fraser and Koster 2009).

Imaging of fixed samples

Fixed embryos were treated accordingly with the exception that they were kept in PTW or PTW DMSO instead of Danieau medium.

2.2.8.3. Kaede Photoconversion in living zebrafish embryos

Kaede is a fluorescent protein derived from the stony coral, *Trachyphyllia geoffroyi*. This fluorescent protein was discovered in 2002 in the laboratory of A. Miyawaki (Ando et al. 2002). Initially Kaede is a green fluorescent protein with an emission maximum at 518 nm

when excited with blue light. The fluorophore has a special feature as it is photoconvertible. Kaede is highly sensitive to irradiation of UV or violet light (370-400 nm) and due to an irreversible photoreaction if the fluorophore its emission peak is altered to 582 nm after UV excitation. As a consequence there is a 2000 fold increase in green to red ratio.
Both the green and red emitting forms of Kaede show a reliable fluorescence with comparable signal intensity. Photoconvertible fluorescent proteins are useful tools for example to identify the morphology or trace the behaviour of individual neurons inside a large cell cluster from which they are indistinguishable (Hatta et al. 2006; Sato et al. 2006).
Transgenic Kaede expressing embryos have to be kept in the dark to protect them from UV light in order to prevent unwanted premature conversion of Kaede prior to imaging.
The embryos were embedded in agarose as described above (2.2.8.2). Kaede conversion was performed using a 405 nm diode on a Zeiss LSM 510 confocal microscope and the Edit Bleach tool of the Zeiss software.
Laser power of the 405 nm diode was set to a value of 80-90%. The area that was aimed for conversion was defined by the region of interest (ROI) tool. As a starting point scan speed was set to 5 units and 6 iterations were executed. Subsequently, the scanning parameters were adjusted for optimal conversion efficiency.
Finally, the conversion step was performed with the bleach feature implemented in the time series tool of the microscope. This routine scans the adjusted ROI repeatedly under user defined conditions. For subsequent time lapse imaging, it was important to keep the laser power of the green and red excitation to a minimum because otherwise bleaching occurred rapidly.

2.2.8.4. Processing

Confocal images were acquired with a LSM 510 confocal microscope (Zeiss). Subsequently, these images were processed with specific modules implemented in the LSM 510 software in order to obtain maximum projections, 3D reconstructions, 3D depth coding and orthogonal sections. The resulting raw data was exported as Tagged Image File Format (TIFF) and further processed with Adobe Photoshop CS3, Adobe Illustrator CS3, ImageJ and QuickTime Player Pro 7.4.5.

3. Results

3.1. Lunapark in zebrafish

3.1.1. The zebrafish genome contains two highly conserved *lunapark* genes

Recently, the highly conserved *lunapark* (*lnp*) gene was identified in the mouse genome, where it is located in close proximity to the *hoxd/evx2* gene cluster, even sharing the same regulatory elements (Spitz et al. 2003). The gene was named *lunapark* because of the presence, in both vertebrates and arthropods, of the conserved peptide LNPARK and because of the limb and neuronal pattern of its mRNA expression in mouse (*lnp*). In order to identify possible zebrafish orthologues of the mouse *lunapark* gene, the genome of *Danio rerio* was searched using Ensembl blast. In contrast to other non teleost vertebrates, where the gene is only present as a single copy, the blast search revealed that two copies of *lunapark* exist in zebrafish. The fact that two *lunapark* homologues exist is due to a genome duplication that occurred during *teleost* evolution (Amores et al. 1998; Robinson-Rechavi et al. 2001; Taylor et al. 2003). One of the genes was localised on Chromosome 23 and termed *lunaparkA* (*lnpA*); the second one was discovered on Chromosome 6 and named *lunaparkB* (*lnpB*). The cDNA of the two genes were cloned and isolated using RT-PCR on 24 hpf zebrafish cDNA. The corresponding DNA and peptide sequences of the identified open reading frame are displayed in Figures 1 and 2.

The *lunapark* gene can be found in all species ranging from yeast to men. Alignment of the Lunapark protein sequences from different vertebrate species using (fish, amphibian, avian, mammals) Meg Align software from Lasergene showed a high degree of sequence similarity with more than 50% between all compared vertebrate species (Figure 3 A).

More detailed analysis of the deduced amino acid sequence revealed that the Lunapark proteins share an 80 AA stretch in the C-terminus, representing a highly conserved domain (Figure 3 B). An alignment of this domain retrieved from selected vertebrate Lunapark protein sequences revealed a level of similarity equal to or larger than 88.8% (Figure 3 C). This high degree of similarity suggests that this domain has been conserved during evolution due to an important function. During the course of these studies, it was found in *C.elegans* that this conserved 80 AA domain contains an atypical zinc finger motif (C_2HC_2) (Krishna et al. 2003; Ghila and Gomez 2008). The precise function of the zinc finger, however, remains elusive. Zinc fingers are small protein structural motifs that can coordinate one or more zinc ions to help stabilise their folds. They are interaction modules that bind DNA, RNA, proteins, or small molecules such as lipids (Krishna et al. 2003; Kadrmas and Beckerle 2004).

Secondary structure prediction analysis using the TMHMM transmembrane prediction software provided by the Centre for Biological Sequence Analysis (CBS) at the Technical University of Denmark (http://www.cbs.dtu.dk/index.shtml) showed that both zebrafish Lnp

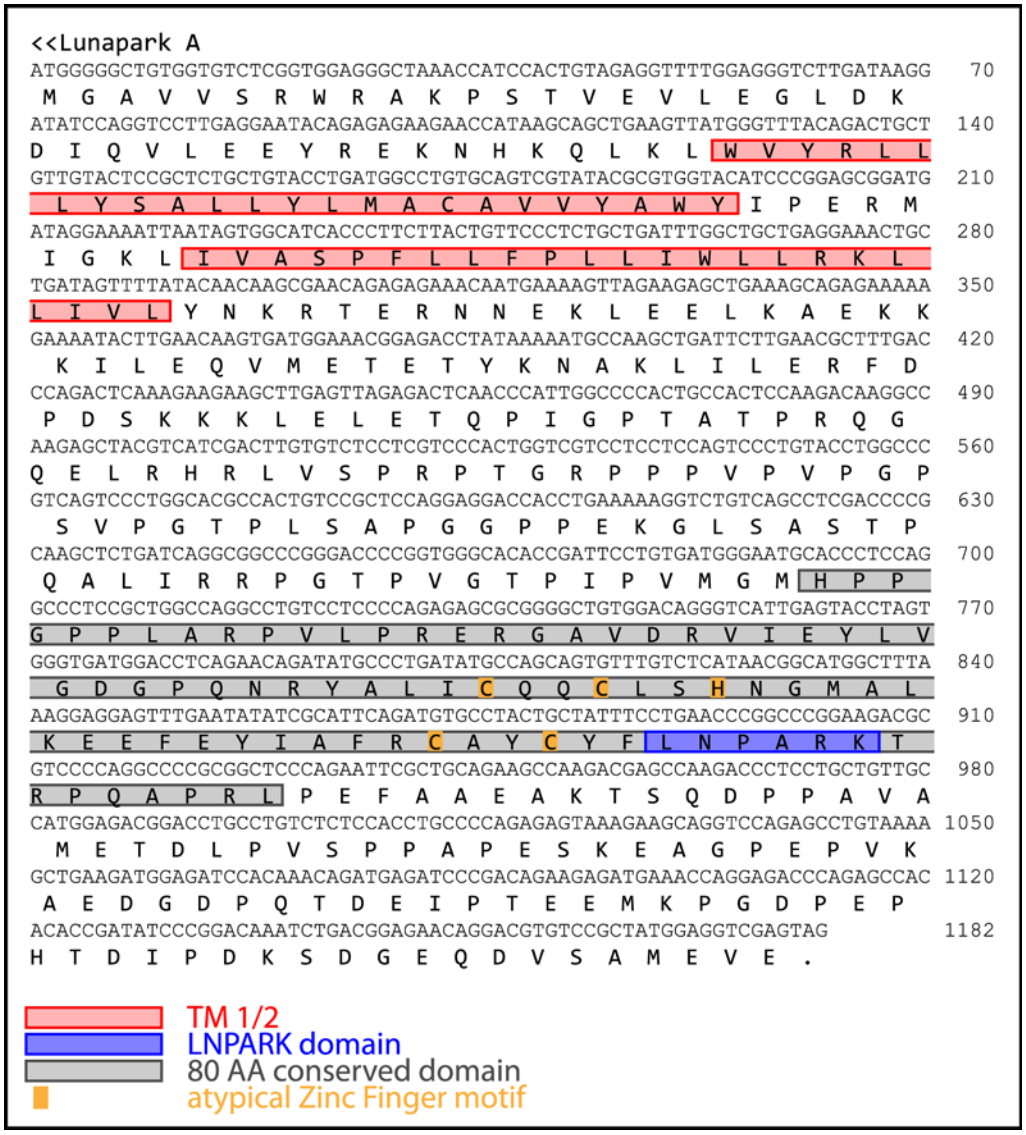

Figure 1 *lunaparkA* (*lnpA*) cDNA and amino acid (AA) sequence.

Nucleotide and deduced amino acid sequence of isolated zebrafish *lunaparkA* cDNA

proteins harbour two adjacent transmembrane (TM) helices in the N-terminus. The TM domains are positioned between AA 42 and 96 in LnpA and between AA 44 and 98 in LnpB (Figure 4 A,B; Figure 5). The majority of the amino acid sequence of both Lnp proteins is predicted to be located within the cytosol (Figure 4 A, B; Figure 5). An exception are eight AAs (LnpA AA 65-72, LnpB AA 67-75) that serve as linker between both TM domains that are located of the opposite membrane site. Depending on the subcellular location of the Lnps this could be the outer surface or the lumen of the organelle. (Figure 5)

The sorting and transport of proteins to their subcellular localisations depends on intrinsic signals -“zip codes”- determined by the peptide sequence. The best known protein ‘‘zip

code'' is the secretory signal peptide (SP). In eukaryotes it targets a protein for translocation across the endoplasmic reticulum (ER). It is an N-terminal peptide, typically 15-30 amino acids long, which is cleaved off during translocation of the protein across the membrane.

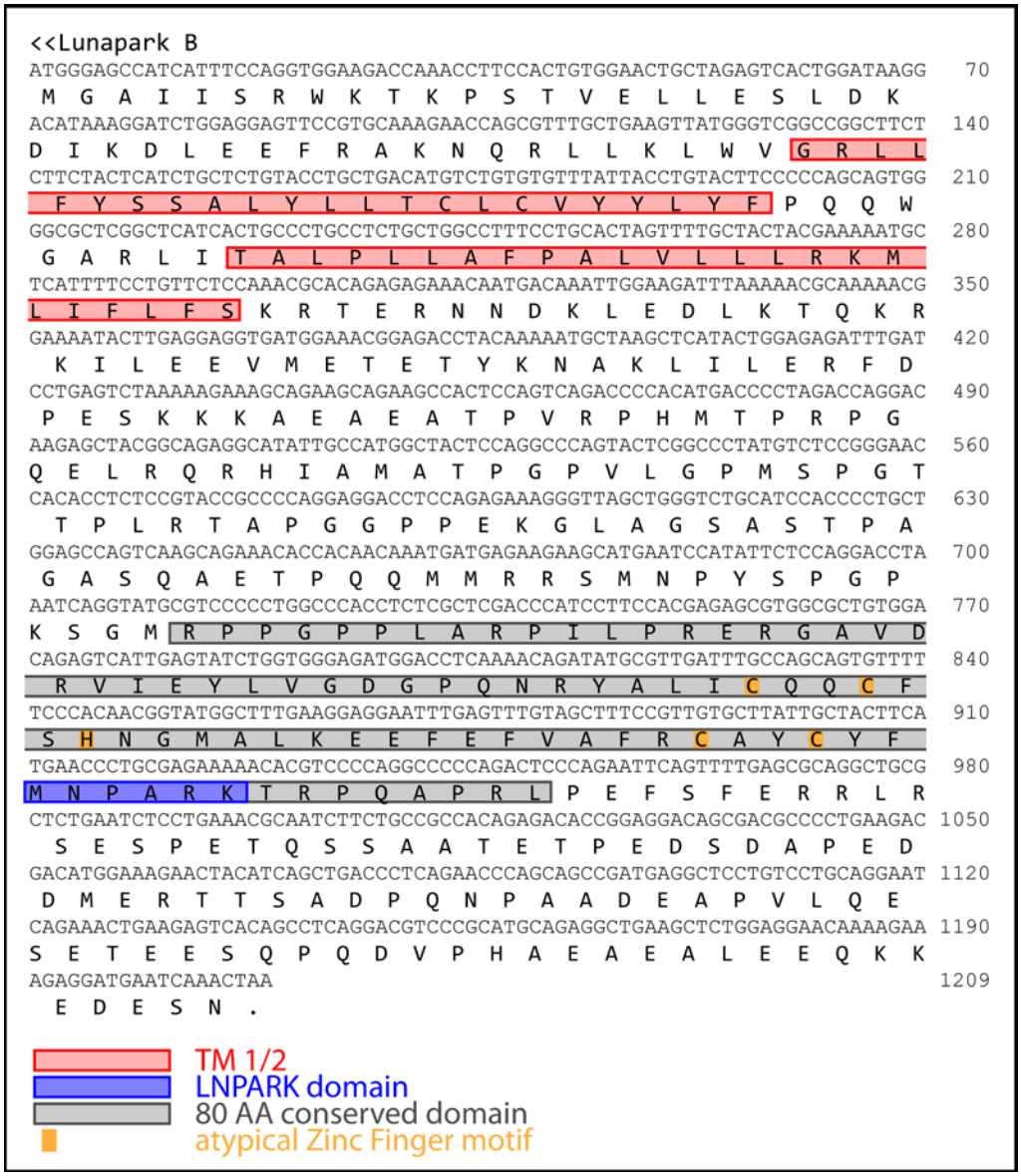

Figure 2 *lunaparkB* (*lnpB*) cDNA and amino acid (AA) sequence.

Nucleotide and deduced amino acid sequence of isolated zebrafish *lunaparkB* cDNA

There is no simple consensus sequence for SPs, but they typically show three distinct compositional zones: an N-terminal region (n-region) which often contains positively charged residues, a hydrophobic region (h-region) of at least six residues and a C-terminal region (c-region) of polar uncharged residues with some conservation at the +3 and +1 positions relative to the cleavage site (Emanuelsson et al. 2007). In eukaryotes, proteins translocated across the ER membrane are by default transported through the Golgi apparatus and exported by secretory vesicles some proteins have specific retention signals that hold them back in the ER or the Golgi or divert them to the lysosomes. In general, these retention signals are poorly

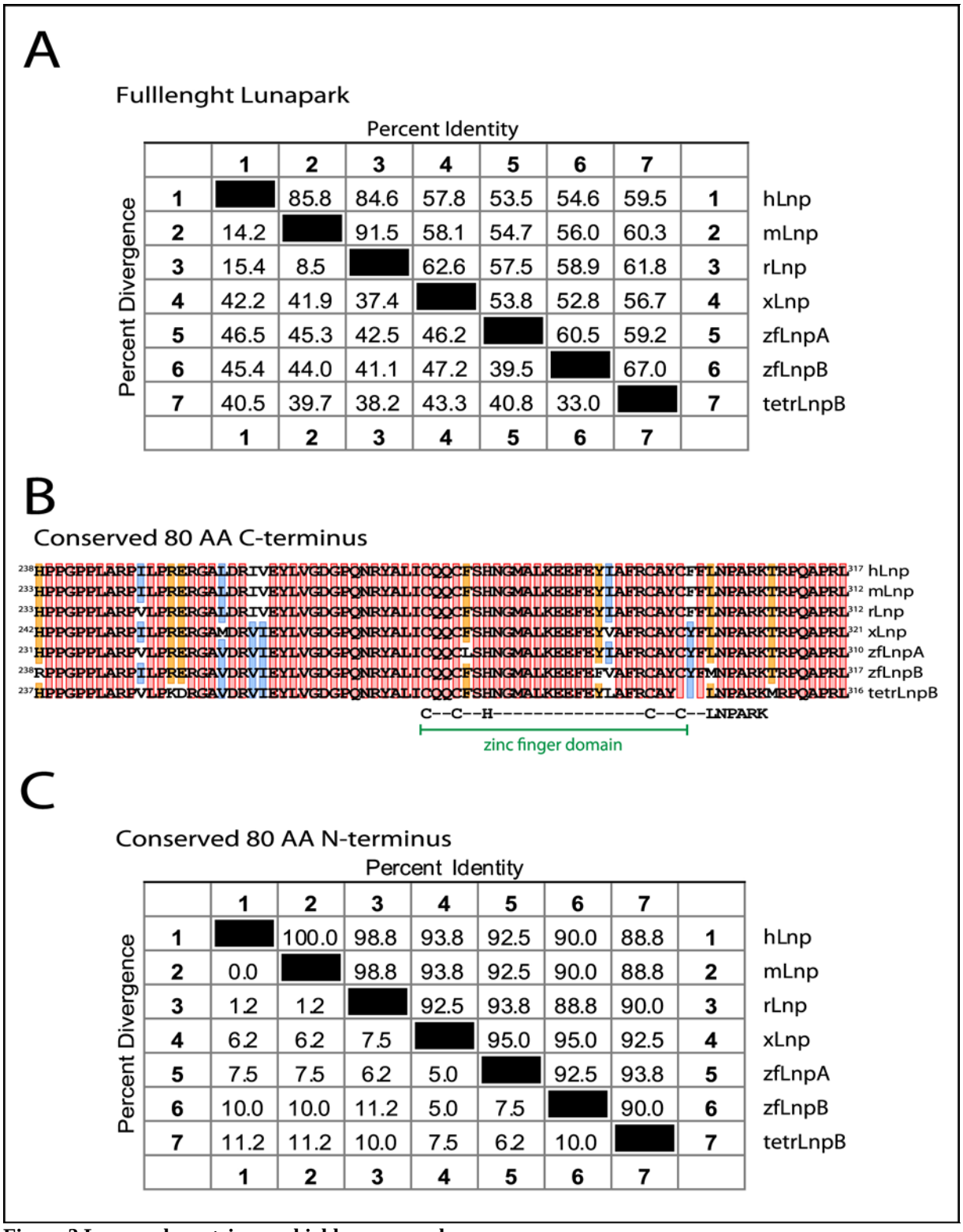

Figure 3 Lunapark proteins are highly conserved

A Alignment summary of several vertebrate full length Lunapark amino acid sequences.
x axis indicates the percent sequence identity. The y axis gives the divergence of the sequences in percent. All full length sequences are at least 53.5 % identical to each other. **B** Alignment of the highly conserved 80 AA C-terminal domain of Lunapark from selected vertebrate species. **C** Sequence distances of the aligned peptides shown in **B**. The AA sequence similarity between single vertebrate species is higher than 88.8 %. h (*Homo sapiens*); m (*Mus musculus*); r (*Rattus norvegicus*) ; x (*Xenopus laevis*); zf (*Danio rerio*); tetr (*Tetraodon nigroviridis*)

characterised, one exception being the ER lumen retention signal, which has the consensus sequence KDEL or HDEL (Emanuelsson et al. 2007).

The peptide sequences of the Lunapark genes were further analysed to determine if they contain a signal peptide in combination with a putative cleavage site and are therefore secreted. Therefore the sequence was evaluated using the SignalP algorithm, a software program also available on the CBS protein prediction server and designed to detect possible

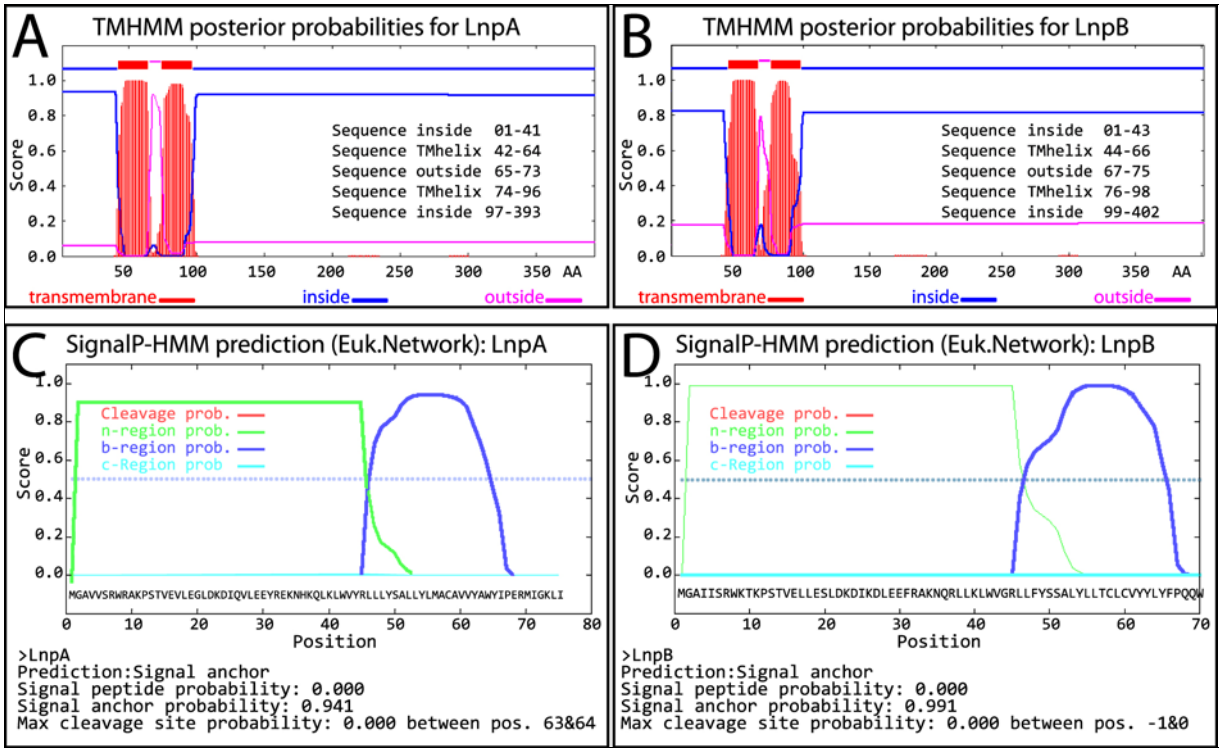

Figure 4 Lunapark proteins contain a signal anchor and two N-terminal transmembrane domains

A, B Transmembrane domain prediction for LnpA and LnpB using the TMHMM prediction software (CBS prediction server Technical University of Denmark). Red peaks indicate hydrophobic regions capable of forming transmembrane helices. The blue line shows the probability for amino acids to be located in the cytosol. The pink line indicates a likelihood of AA to be found outside the cytosol. (The higher the value the grater is the likelihood.) **C, D** SignalP-HMM algorithm output chart for the N-termini of LnpA and LnpB. This method calculates the probability of a given sequence to contain a signal peptide which directs secretion and putative cleavage sites. Both Lnp proteins have a very high signal anchor probability LnpA 94.1% and LnpB 99.1 % in contrast to a value of 0 for signal peptide and cleavage site probability. Thus Lnp proteins are likely targeted to the membrane but are not likely to be secreted.

signal peptides and their corresponding cleavage sites by analysing the peptide sequence in respect to the occurrence of the three distinct compositional zones (n-, h-, and c-region). The analysis of the Lnp proteins using this software revealed that the probability for a signal peptide or a cleavage site within the Lnp proteins is 0.0% and that therefore it is unlikely that the Lnp proteins are secreted. In contrast, both proteins showed a very high probability of containing a signal anchor sequence in the N-terminal region (94.1% for LnpA and 99.1% for LnpB) (Figure 4 C, D). A signal anchor, just like an SP, contains a region of hydrophobic residues close to the N-terminus, but it is not cleaved. Instead, it remains as a transmembrane

α-helix in the membrane and anchors the protein to the membrane. A protein anchored in this way is translocated to the ER but it will not be secreted. These proteins are called type II membrane proteins (Heijne 1988). The Lnp sequence does not contain an ER retention signal and it is therefore unlikely that it is an ER protein.

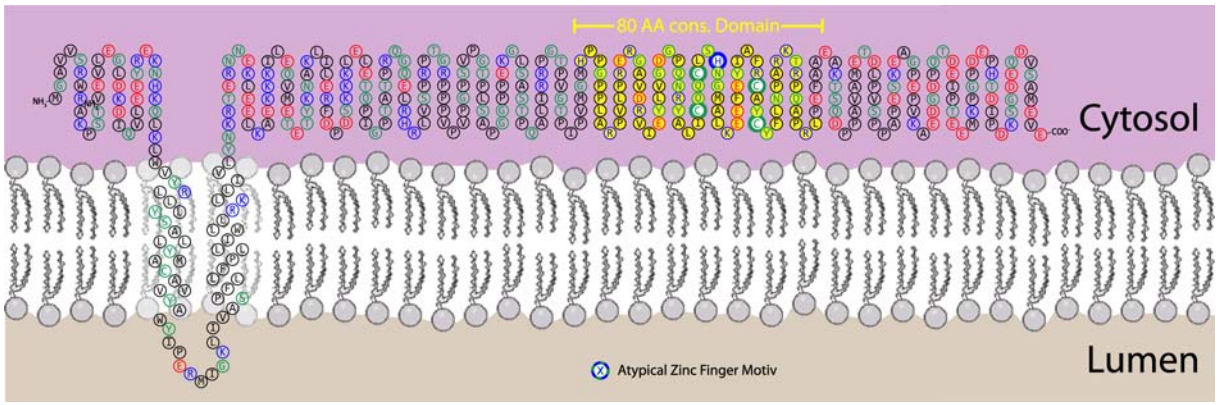

Figure 5 The Lunapark protein domains

Schematic drawing showing LunaparkA protein topology within the membrane. Representative also for LunaparkB. The majority of the AA sequence is located within the cytosol. The protein is anchored to the plasma membrane with two N-terminal helices.

Taken together these results show that the Lunapark proteins are signal anchor type II transmembrane proteins. Due to their large cytosolic domain, (Figure 5) rather than acting as an extracellular signal receptor lunapark proteins likely to receive intracellular signals or act as adapter or scaffolding proteins on the surface of internal membranes.

3.1.2. *LunaparkA* is expressed in the CNS and in the muscles of the developing zebrafish embryo

In situ hybridisation studies in mice showed that the *lunapark* gene is expressed in the central nervous system in the limb buds and the urogenital system of the developing embryo (Spitz et al. 2003). In order to clarify if this expression pattern is also conserved for both genes in zebrafish and to learn more about the spatio-temporal function of these uncharacterised genes, zebrafish embryos were analysed for the expression of the two *lunapark* genes (*lnpA* and *lnpB*) at different developmental stages. RT-PCR analysis using specific primers for *lnpA* and *lnpB* on cDNA generated from whole zebrafish embryos demonstrated that both genes are expressed already maternally (Figure 6 I). *lnpB* shows the highest expression at the 16 cell stage and slowly decreases until 24 hpf, when no more *lnpB* transcript could be detected. However, all attempts to examine *lnpB* by anti-sense mRNA in situ hybridisation failed. This indicates that *lnpB* is only required at low expression levels during early developmental stages. In contrast to *lnpB*, *lnpA* is more persistently expressed throughout early developmental stages, as shown by RT-PCR (Figure 6 I). Starting at 24 hpf, it was also possible to detect the

transcript by in situ hybridisation (Figure 6 A-C). Consistent with the mouse data, *lnpA* was strongly expressed in the hindbrain, exhibiting a very distinct pattern of well-defined domains

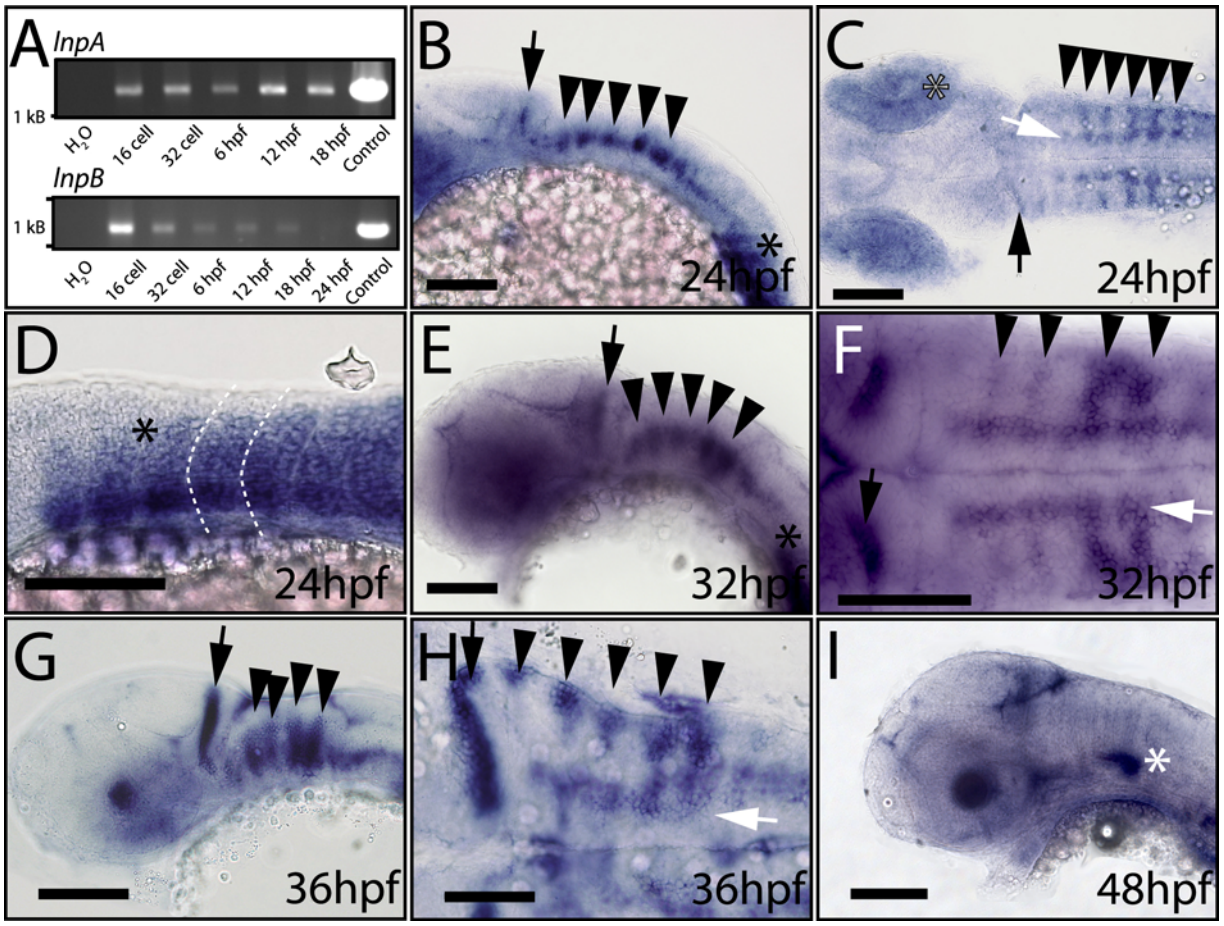

Figure 6 Expression profile of the two zebrafish *lunapark* homologues

A Agarose gel from RT-PCR with *lnpA* and *lnpB* primers. The cDNA template was generated by reverse transcription of mRNA extracted from whole zebrafish embryo lysates at the indicated time points. In addition, a no-template control (H_2O) and a positive control using plamids of the respective genes as templates are shown. This RT-PCR analysis shows that both genes are expressed maternally. *lnpB* transcripts disappear at 24 hpf while *lnpA* transcripts persist. kB (kilo basebair). **B-I** *In situ* hybridisation against *lunaparkA* mRNA at 24 hpf (**B-D**), 32 hpf (**E-F**), 36 hpf (**G-H**) and 48 hpf (**I**). Images were recorded from lateral (**B**, **D**, **E**, **G**, **I**) or dorsal view (**C**, **E**, **G**). *lnpA* is expressed in the anterior cerebellum (black arrows), along the rhombomere boundaries (black arrowhead), in two continuous medio-lateral domains in the hindbrain (white arrow), in the inner ear (white asterisk) and in the developing muscles (black asterisks) at the indicated time points. Scale bars 100 µm.

including the anterior cerebellum (Figure 6 black arrows), two rostro-caudal stripes spanning the entire rhombencephalon close to the ventral midline of the hindbrain (Figure 6 white arrows), and the ventro-lateral rhombomere boundaries (Figure 6 black arrowheads). In addition to the CNS expression, *lnpA* is very strongly expressed in the developing muscles of the zebrafish trunk (Figure 6 black asterisks) in the eye (Figure 6 grey asterisks) and in the fin buds (Ahn and Ho 2008).

This characteristic expression pattern remains until around 36 hpf. After two days, the expression in the hindbrain and muscle has disappeared and *lnpA* transcripts are then only present in the inner ear (Figure 6 white asterisks). Comparing the expression of the two

zebrafish *lnp* genes reveals striking differences. While *lnpA* resembles CNS expression of the mouse orthologue, *lnpB* is only expressed maternally and is therefore not playing a role in neuronal development. In contrast *lnpA* is present in a striking pattern during developmental stages when important neuronal lineage decisions are made and differentiation processes are initiated. For that reason, this study focuses on *lnpA* and all of the constructs used for the analysis of interaction partners and cellular localisation are based on the *lnpA* cDNA sequence.

3.2. Subcellular localisation of Lunapark protein

3.2.1. Fluorescent LnpA reporter proteins localise to large vesicular structures in PAC2 cells

Sequence analysis clearly showed that Lunapark proteins have two transmembrane domains in their N-terminus and that it is likely that are translocated to the ER and therefore are integrated into a lipid bilayer somewhere in the cell. Either they can be found at the outer plasma membrane or in one of the numerous compartments of the endomembrane system within the cell. It is although unlikely that they are ER proteins themselves as they do not have an ER retention signal within their sequence. The next set of experiments aimed to identify the precise subcellular localisation of Lunapark. Therefore several fusion proteins of full length and truncated LnpA with fluorescent proteins were generated (Figure 7). These constructs were overexpressed in cell culture together with various subcellular fluorescent markers.

In an initial experiment, full length LnpA fused to yellow fluorescent protein (YFP) or a monomeric red fluorescent protein called mCherry at the C-terminus or green fluorescent protein (GFP) at the N-terminus (Figure 7) were transfected into zebrafish PAC2 fibroblast cells and images were recorded by confocal microscopy (Figure 8 A-B’’). Co-expressed LnpA fusion proteins showed a complete overlap of their fluorescent signals (Figure 8 A-B’’) and were present within huge vacuole-like structures in the cell (Figure 8 A-B’’; Movie 1). In contrast, no signal on the outer cell membrane could be detected.

In addition, Lnp-mCherry and Lnp-YFP full length fusion proteins did co-localise with fluorescent reporters proteins that are targeted to the ER membrane, as shown by images recorded from transiently transfected PAC2 cells using a confocal microscope (Figure 8 C-D’’; white arrows) This findings further confirm the data obtained from the protein prediction analysis, described above, that Lnp proteins translocate to the ER after their translation. Unexpected was although that LnpA itself was actually found within the ER. Due to the lack of an ER retention peptide we rather suggested that LnpA would transit through the ER to

reach its final target organelle presumably in the endomembrane system. The vacuole like structures that are formed after expression of fluorescent LnpA fusion proteins are relatively large. Membrane structures with that size and shape are usually not observed in normal animal cells. Therefore it is possible that the observed structures are a result of LnpA

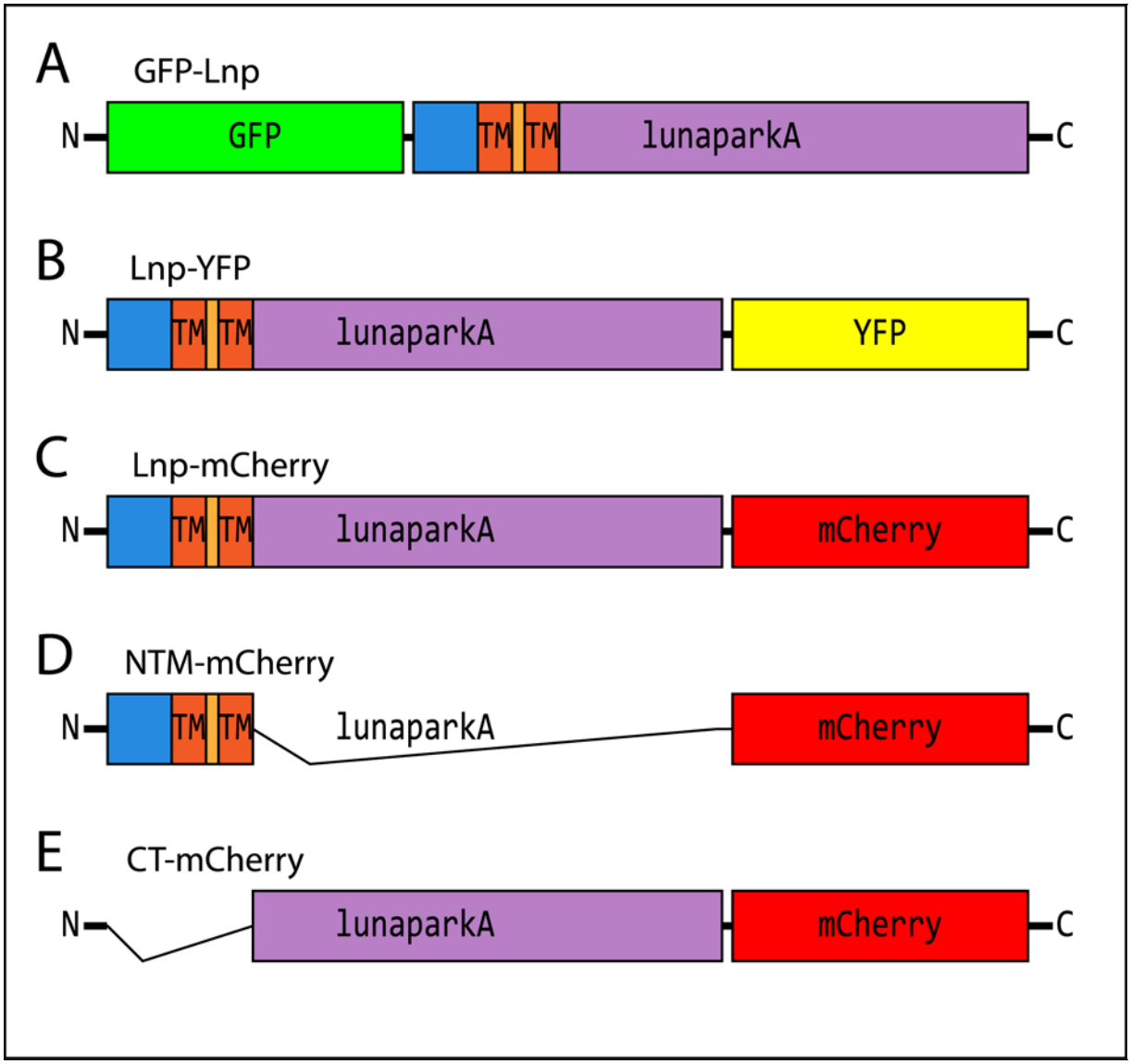

Figure 7 Schematic drawings of LunaparkA fluorescent fusion proteins

A Schematic drawings of N-terminal GFP fusion of full-length LunaparkA (GFP-LnpA) **B** N-terminal YFP fusion **C** mCherry C-terminally fused to full-length LunaparkA. **D**, **E** Truncated versions of LunaparkA fused to mCherry.

overexpression either showing a protein folding artefact or a gain of function effect of LunaparkA.

3.2.2. LnpA localises to late endosomes and lysosomes in NIH3T3 cells

In order to determine if the endogenous localisation of LnpA are the observed vacuole like structures of or if these structures are rather a result of the overexpression, we tested a second

cell type. Instead of PAC2 cells, NIH3T3 mouse fibroblasts were used. These cells are rather large and have a spread out morphology that is advantage for imaging and they are also resisted to overexpression. Confocal images of NIH3T3 cells transfected with Lnp-mCherry

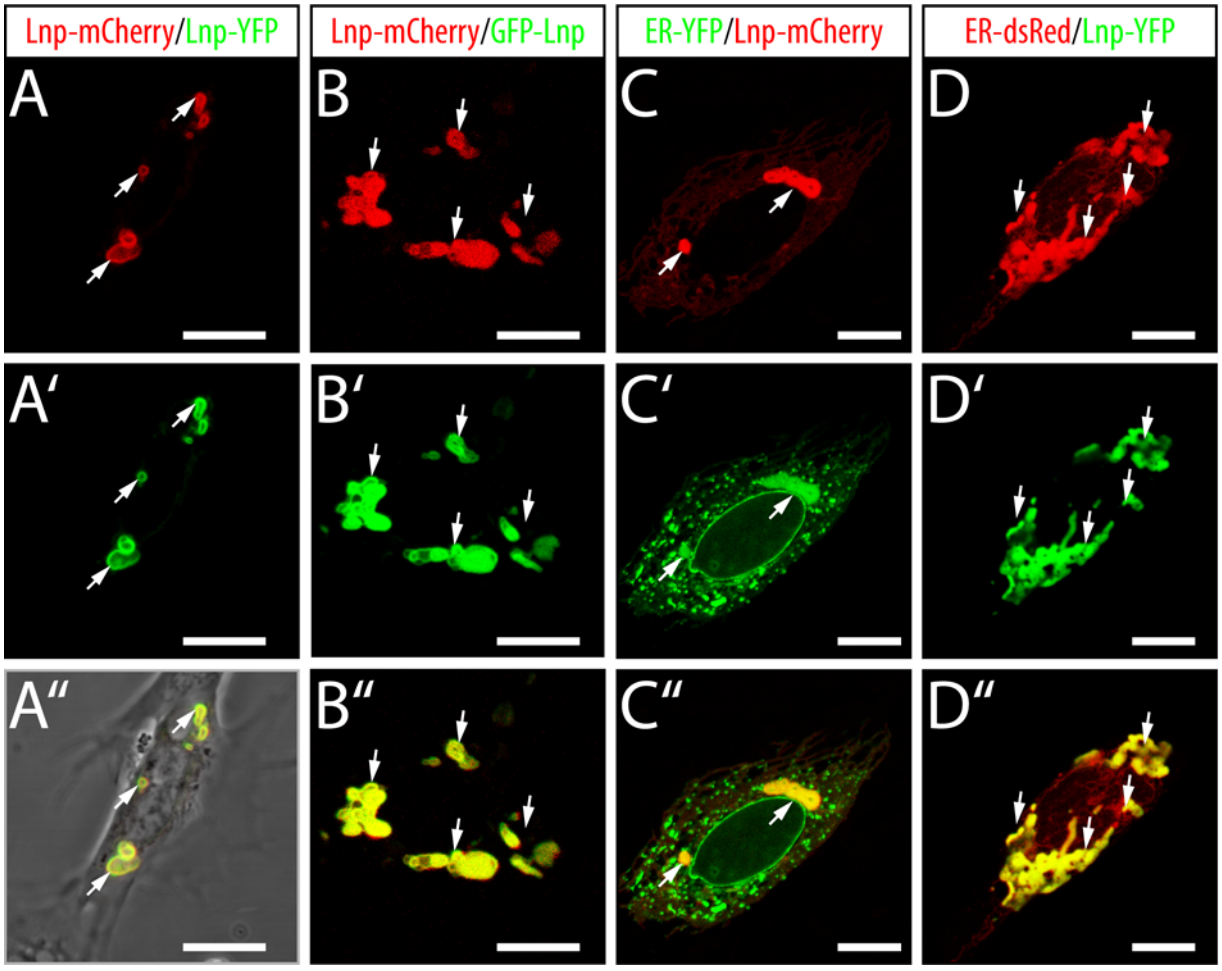

Figure 8 Overexpression of full-length Lnp-fusion constructs generates large vacuole like structures

A-B'' PAC2 cells co-expressing two different fluorescent Lnp reporters simultaneously showing their co-localisation (white arrows). **C-D''** PAC2 cells transfected with Lnp fluorescent reporter in combination with ER-marker constructs. Overexpressed Lnp accumulates in the ER (white arrows). Images show single confocal sections of PAC2 cells transfected with the indicated fluorescent fusion proteins. Scale bars 10 µm.

in combination with ER-YFP or Golgi-YFP showed that the formation of the large vacuole like structures is reduced (Figure 10, Figure 11) and appears only occasionally in individual exceptionally strong expressing cells (Figure 11 F asterisk). In addition, the ER-YFP signal shows a characteristic ER morphology (Figure 10 3 A). The Lnp-mCherry still shows partial overlap with the ER, but this might be LnpA proteins that are transiting through the ER in order to reach its target locations (Figure 10 A'-A'' arrows). In contrast, LnpA was excluded from the Golgi apparatus (Figure 10 A'-A'' dashed circle). These results show that LnpA is initially translocated to the ER but the ER is probably not the site of the final LnpA subcellular localisation. Furthermore the findings indicate that the Lnp-mCherry and Lnp-

YFP positive vacuole like structures observed in PAC2 cells are therefore likely to be a consequence of LnpA overexpression.

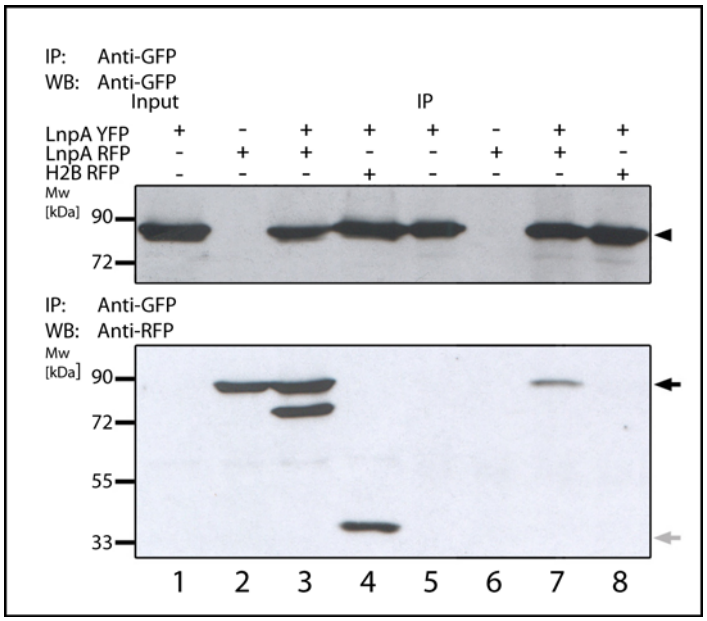

Figure 9 Co-immunoprecipitation of Lunapark shows homophilic interaction

Westernblot analysis of co-immunoprecipitation against Lnp-GFP. 20 µg total protein from lysates obtained from 293T cells transfected with the indicated constructs were used as input control (Lane 1-4). 500 µg total protein was incubated together with a GFP antibody and protein G-Sepharose (Lane 5-6). All samples were separated by SDS-PAGE and transferred to a PDVF membrane for immuno-detection with GFP (upper blot) and RFP (lower blot) antibody. Lnp-GFP (black arrowhead) as bait could efficiently bind to the GFP antibody (Lanes 5, 7-8 black arrowhead). Lnp-mRFP (black arrow) could be precipitated from the lysate only in the presence of Lnp-GFP (Lane 3, 7) and not if transfected alone (Lane 2, 6).
H2B-RFP was used as negative control and it was not precipitated by Lnp-GFP (Lane 4, 8)

There are several explanations why the observed structures are formed, that also give hints towards a possible LnpA function within the cell. Co-immunoprecipitation assays with Lnp-mCherry and Lnp-YFP expressed in 293T cells for example showed that Lunapark proteins can strongly bind to one other (Figure 9) suggesting that LnpA proteins are capable of forming homodimers or oligomers. This is further supported by the complete co-localisation of LnpA protein fused to different fluorescent reporters. Strong overexpression induced by transient transfection might enhance the homophilic binding thereby creating oligomers or even aggregates that are stuck in the ER. Alternatively it might be that Lunapark promotes organelle fusion or membrane expansion. Overexpression of the protein could result in a misregulation of these processes, thereby producing the huge vacuole structures. Another explanation might by that the LnpA proteins are not folded properly once they are translocated into the ER and are therefore retained in the ER by chaperones. It is also possible that LnpA requires specific interaction partners to fold properly that are not present in PAC2 cells. This hypothesis could be tested by co-expressing putative interaction partners of LnpA

in PAC2 cells. Reduction of enlarged vesicular structures would indicate the requirement of that particular binding partner for proper LnpA protein folding.

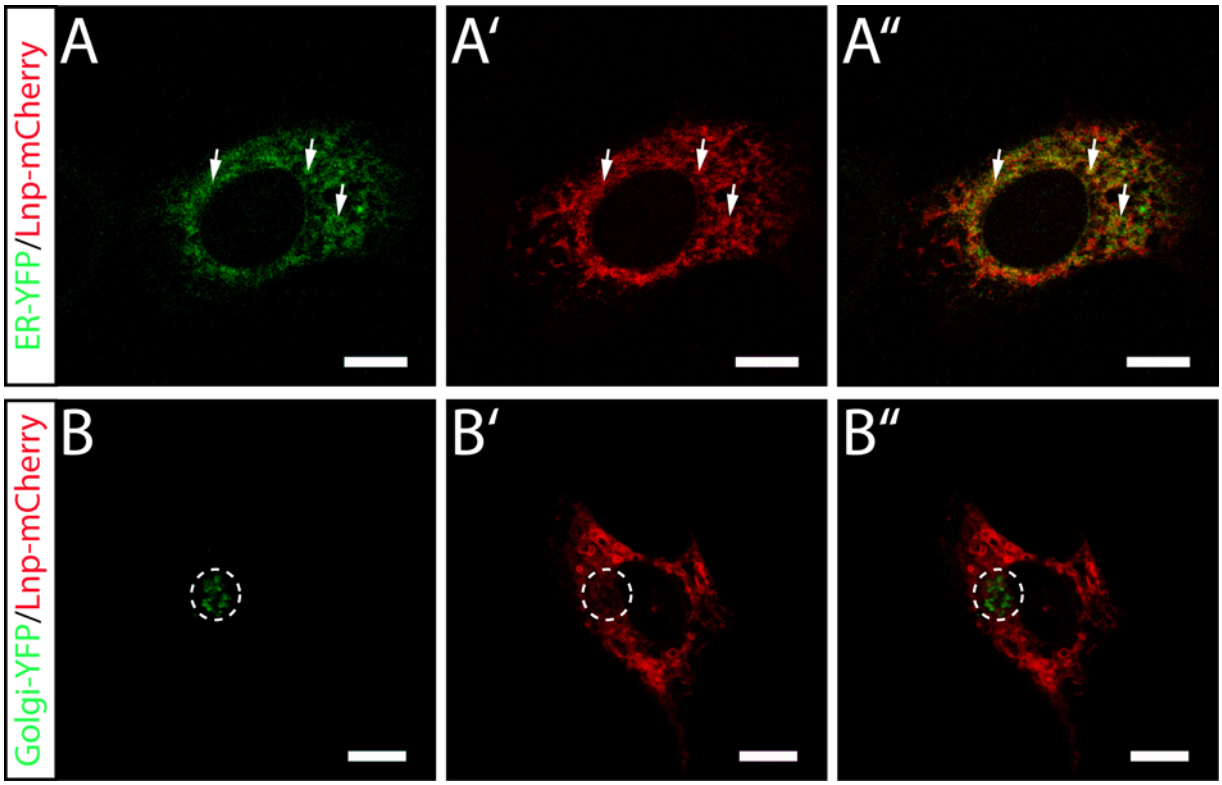

Figure 10 Lnp-mRFP shows strongly reduced overexpression phenotype in NIH3T3 cells

Image sections of NIH3T3 cells recorded by confocal microscopy transfected with **A-A''** Lnp-mCherry and ER-YFP or **B-B''** Lnp-mCherry and Golgi-YFP. In NIH cells less Lnp-mCherry aggregates were detected compared to PAC2 cells. ER-YFP and Lnp-mCherry fluorescent signal show a partial overlap (white arrow) whereas Golgi-YFP and Lnp-mCherry signals do not overlap. (Circle indicates position of the Golgi apparatus). Scale bar 10 µm.

In order to further determine the cellular compartment where full length LnpA fusion proteins localise the small GTPases Rab5 as marker for early endosomes, Rab7 for late endosomes and lysosomes and Rab9 for late endosomes were used (Gould and Lippincott-Schwartz 2009). YFP fusions of these markers were transfected in combination with full length Lnp-mCherry into NIH3T3 cells (Figure 11). Confocal images showed that Lnp-mCherry did not overlap with Rab5-YFP (Figure 11 A-C). In contrast, Rab7-YFP and Rab9-YFP fluorescence showed partial overlap with the mCherry signal (Figure 11 D-O white arrows). Furthermore, if Lnp-mCherry expressing cells were analysed using brightfield microscopy, Lnp-mCherry was represented by small dark round structures within the cell (Figure 12 A-C). Lysosomes are known to contain electron dense material and therefore appear as dark structures in images recorded with an electron microscope. Strikingly, these compartments did also co-localise with the vital dye lysotracker which is used as a marker for lysosomes (Figure 12 D, E). Thus full length LnpA is mostly localised in lysosomes and late endosomes.

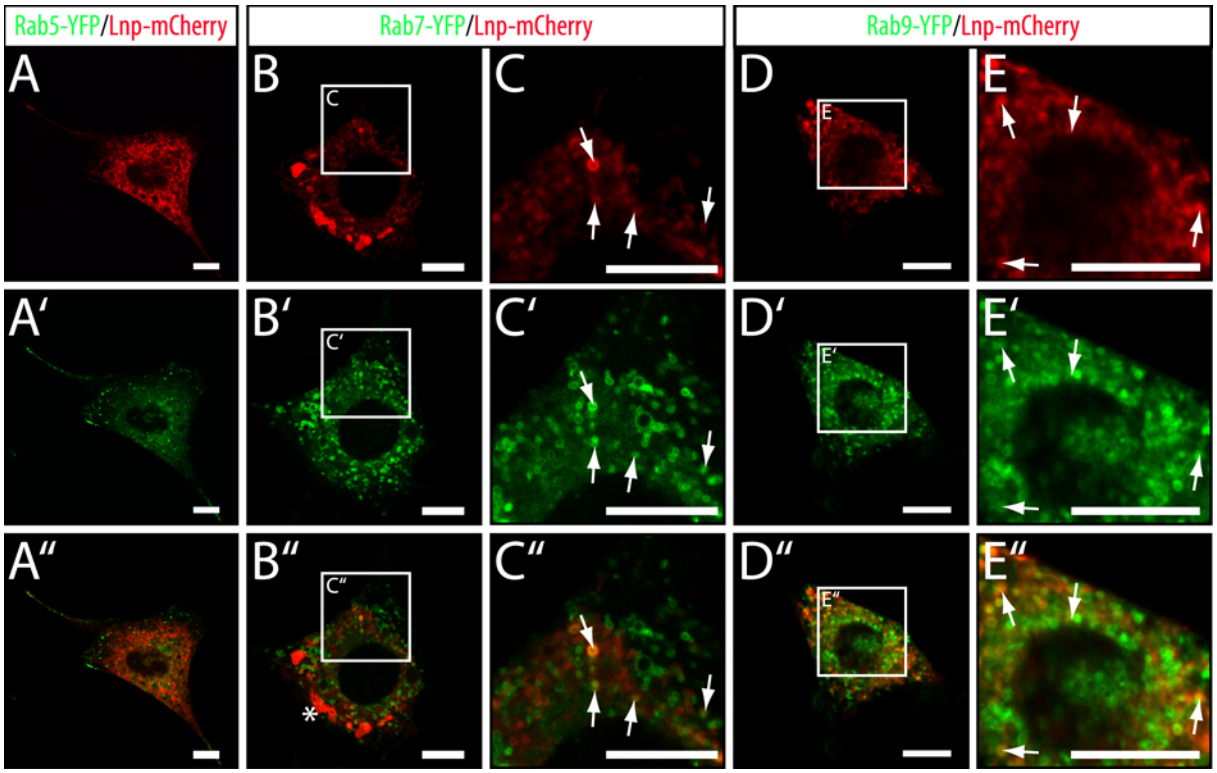

Figure 11 Lnp-mRFP co-localises with late endosomal and lysosomal markers
A-E'' Images of NIH3T3 cells transfected with plasmids expressing Lnp-mCherry in combination with fluorescent protein fusions of small GTPases of the endocytic pathway recorded by confocal microscopy. **A-A''** The fluorescent signals of Lnp-mCherry and Rab5-YFP, a marker for early endosomes, do not co-localise. In contrast, partial overlap of Lnp-mCherry fluorescence with the YFP expression signal of the late endosomal/lysosomal marker Rab7-YFP and the late endosomal marker Rab9-YFP could be detected. (**B-E''**; white arrows). **C-C''** Magnification of the region indicated by the white boxed area in figure (**B-B''**). **D-D''** Magnification of the region indicated by the white boxed area in figure (**E-E''**)

3.2.3. The N-terminus is required for proper localisation of LnpA Protein

Above, it was hypothesised that the transmembrane domain containing N-terminus sequence acts as a signal anchor required for proper localisation, whereas the C-terminus is responsible for the function of the protein (e.g. protein-protein interactions). In addition, the C-terminus, when overexpressed alone, was distributed over the entire cytosol, indicating that this structure is not involved in targeting localisation (Data not shown). In order to address this hypothesis we created a fusion protein consisting of the N-terminus of Lunapark truncated after the two TM domains and C-terminal mCherry (Figure 7 D), which is referred to as NTM-mCherry. First, NIH3T3 cells were transfected with NTM-mCherry in combination with ER-YFP or Golgi-YFP (Figure 13 A-A''). Confocal images revealed that the fluorescent signal of the NTM-mCherry fusion proteins appeared as small punctate structures distributed over the entire cell. Large vesicular structures could not be observed in cells expressing NTM-mCherry. Additionally, NTM-mCherry fluorescent signal did not co-localise with ER-YFP or Golgi-YFP expression. This indicates that the lack of the C-terminus prevents LnpA from forming large vacuole like structures within the ER.

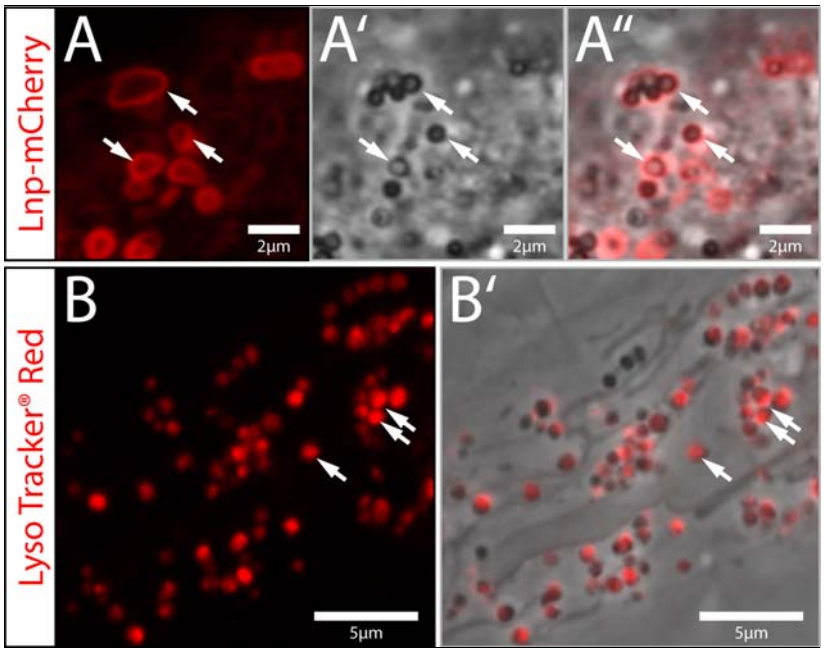

Figure 12 Lnp-mRFP localises to the membrane of Lyso Tracker® positive vesicles
A-A'' High magnification images recorded by bright-field and confocal fluorescent microscopy from the cytosol of NIH3T3 cells transfected with Lnp-mRFP showing red fluorescence in small round dark appearing vesicle like structures. **B-B'** NIH3T3 cells counterstained with the dye Lyso Tracker® Red. The red Lyso Tracker® signal is present in photon dense small round vesicle like structures (white arrows) identifying them as late endosomes/lysosomes. Scalebar 10 µm.

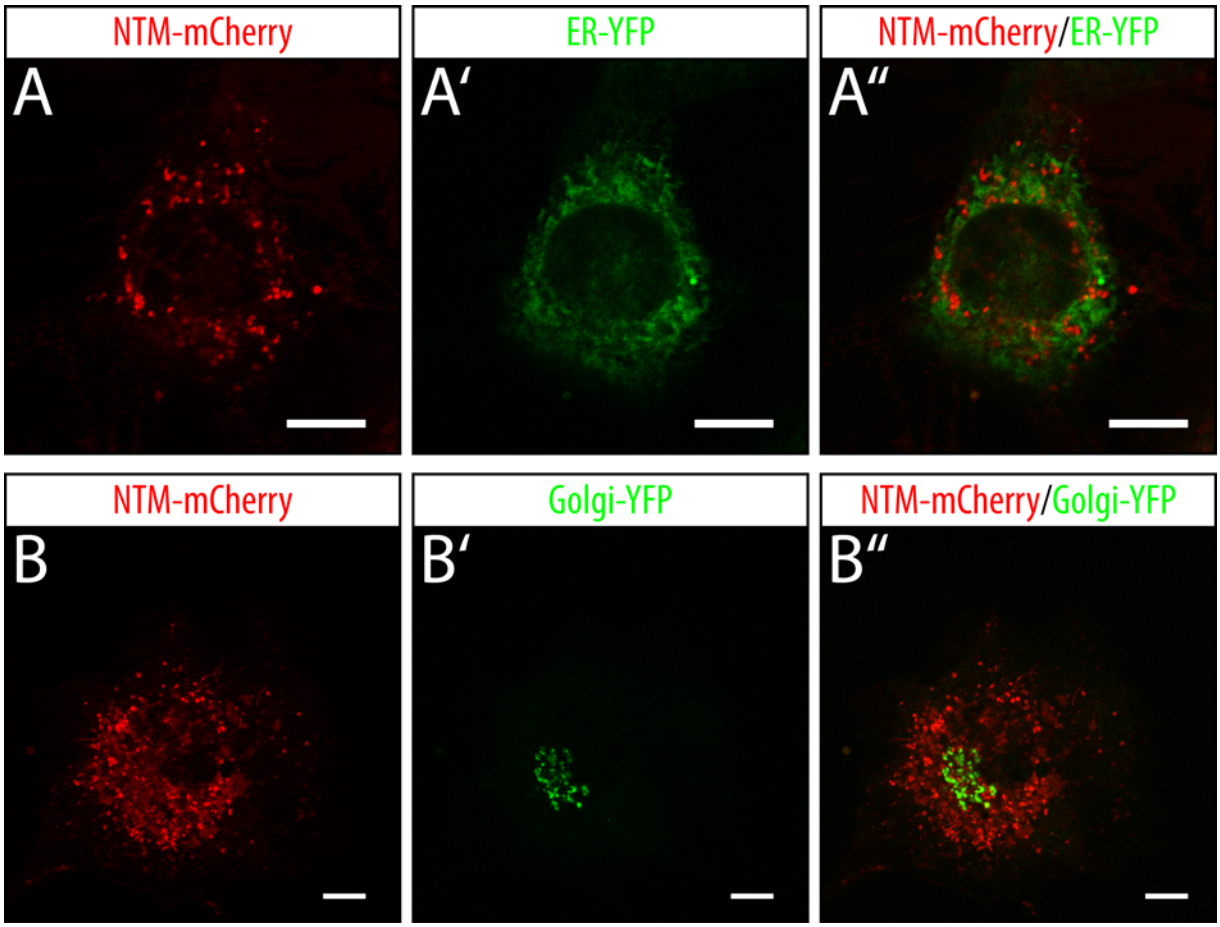

Figure 13 Lnp N-terminus is required for proper intracellular localisation

A-B'' Images of NIH3T3 cells expressing NTM-mCherry in combination with ER-YFP or Golgi-GFP recorded by confocal microscopy. The NTM-mCherry fluorescent signal appeared as small punctate structures that did neither co-localise with ER-YFP (**A-A''**) or Golgi-YFP (**B-B''**) fluorescent signal.

Furthermore, time lapse recording of individual cells transfected with NTM-mCherry showed that the small punctate structures are highly motile (Figure 14; Movie 2). Analysis

images recorded by brightfield microscopy revealed that NTM-mCherry co-localises with

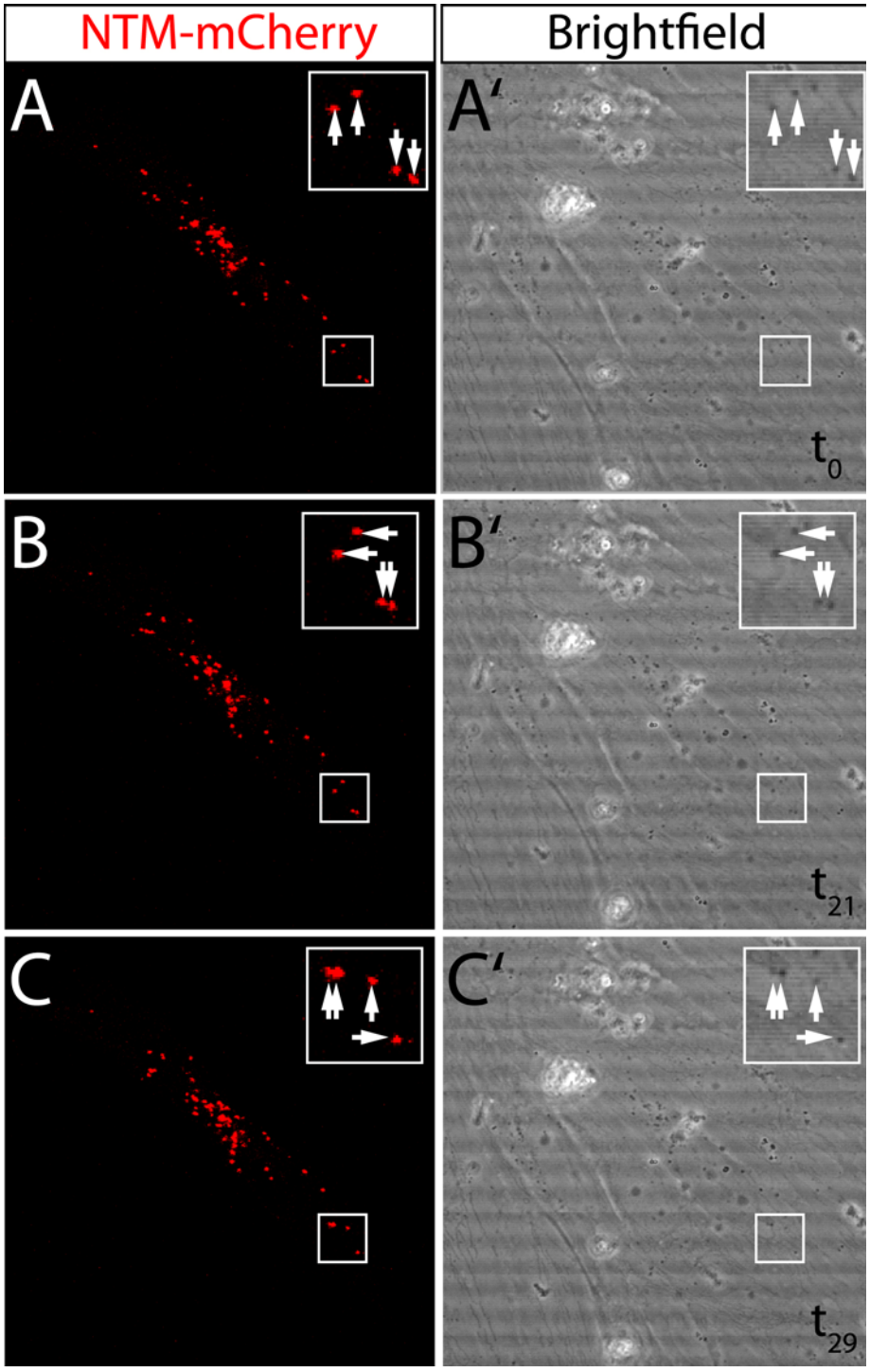

Figure 14 NTM-mCherry co-localises with highly motile photon dense vesicular structures
A-C Image series of a NTM-mCherry over expressing NIH3T3 cells recorded over time by confocal microscopy. NTM-mCherry (white arrows) fluorescent signal co-localises with highly motile dark vesicular structures most likely representing late endosomes/lysosomes (black arrows).

dark vesicle-like structures that likely represent late endosomes/lysosomes. Further evidence for an endosomal/lysosomal co-localisation of NTM-mCherry is derived from confocal images of NIH3T3 cells transfected with NTM-mCherry together with either Rab7-YFP or Rab9-YFP expression constructs. Red NTM-mCherry fluorescence overlaps to a large extend with fluorescent signal of the small GTPase Rab7-YFP and shows partial overlap with the Rab9-YFP reporter fluorescence (Figure 15). Interestingly, vesicles that express NTM-mCherry alone are often found in close proximity to ones that are positive for Rab9-YFP

expression only, perhaps representing kissing and fusion events between late endosomal and lysosomal vesicles (Figure 15 C, D).

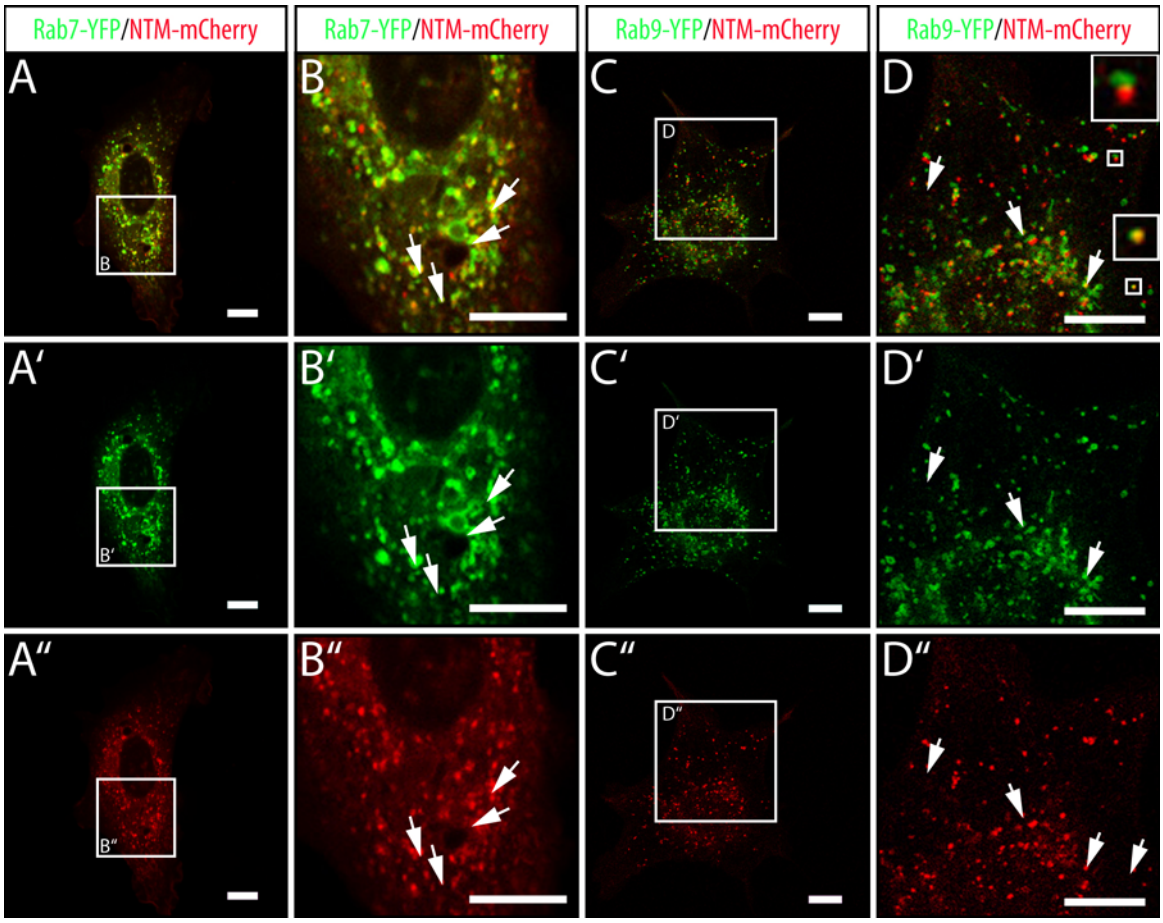

Figure 15 NTM-mCherry co-localises with small GTPases of late endosomes and lysosomes

Images of NIH3T3 cells recorded by confocal microscopy expressing NTM-mCherry in combination with **A-B''** Rab7-YFP or **C-D''** Rab9-YFP. **B-B''** and **D-D''** show magnifigation of the area indicated by the white box in the corresponding image. The YFP fluorescent signals of small GTPases YFP reporter proteins show a clear overlap with the NTM-mCherry signal (white arrows). Scale bars 10 µm.

Taken together these results using full length and NTM LnpA suggest that endogenous Lunapark is most likely localised to late endosomal and lysosomal vesicles of the endomembrane system. Furthermore, these results support the idea of Lunapark being subdivided into an N-terminal cellular targeting domain and a C-terminal domain of biological function including a potential protein dimerisation domain.

3.3. Screen for Interaction partners of Lunapark

3.3.1. The SF-TAP system

The *in silico* analysis of the Lunapark peptide sequence revealed that, other than an atypical zinc-finger postulated by Ghila and Gomez (Ghila and Gomez 2008) and two N-terminal transmembrane domains (Figure 5), no known functional domains could be identified in the C-terminus. In addition there is not many information available concerning the biological

function of the protein. So far we now that Lnp-1 might play a role in vesicular transport in *C.elegans* (Ghila and Gomez 2008) and we have determine the subcellular localisation of zebrafish LnpA. In order to learn more about the function of the LnpA protein we screened for putative binding partners of LunaparkA using a mass spectrometry (MS) based pulldown assay. These assays are a very powerful method used to screen for protein-protein interaction.

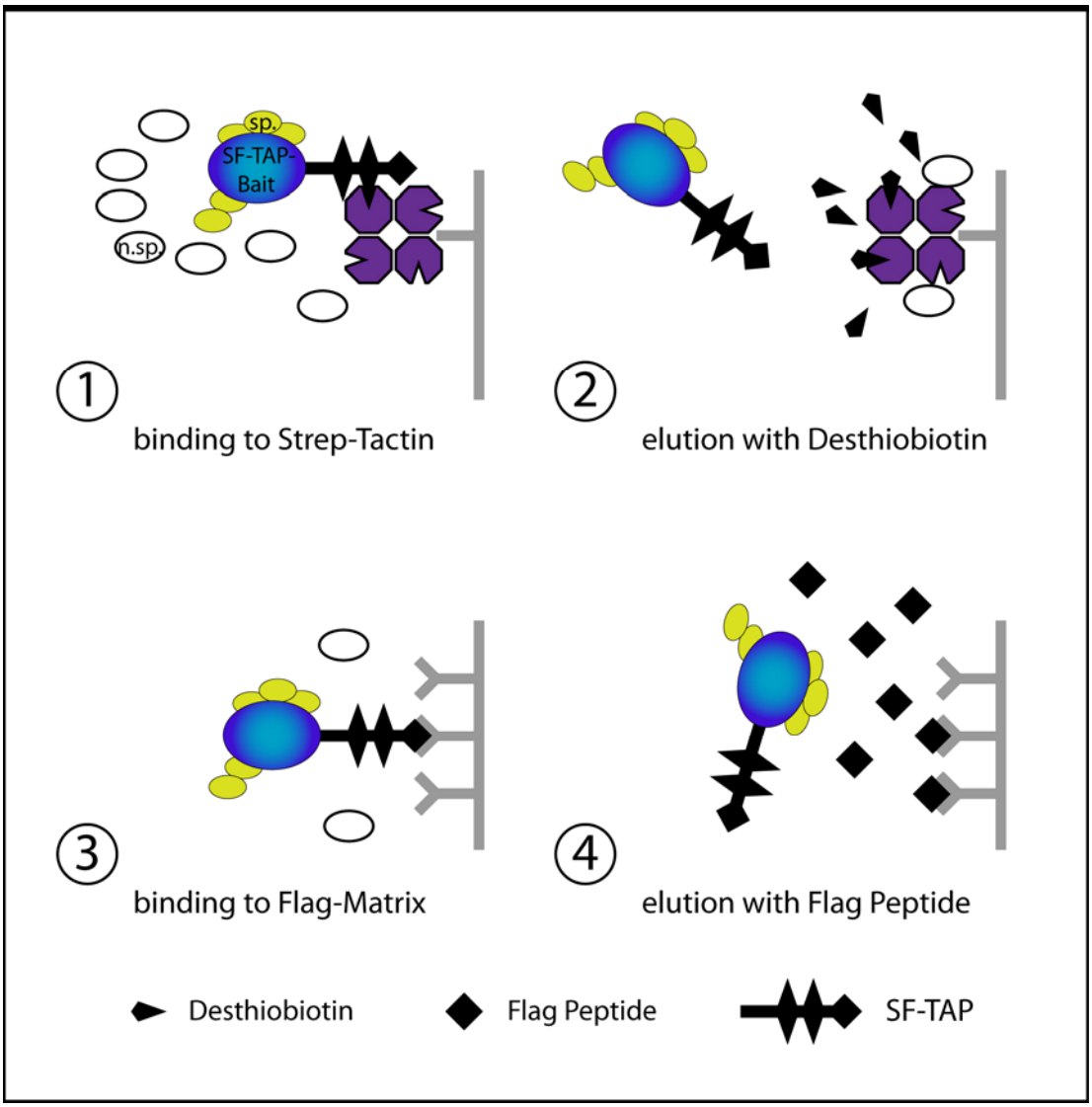

Figure 16 The Strep/FLAG tandem affinity purification

Schematic representation of the SF-TAP purification workflow. Overview of both purification steps. First purification step by the tandem Strep-tag II moiety: **1** Binding to Strep-Tactin matrix, **2** Elution with desthiobiotin. Second purification by the FLAG-tag moiety: **3** Binding to anti FLAG M2 affinity matrix, **4** Elution with FLAG peptide. sp.: specific interactors are represented by green ovals, n.sp.: non-specific proteins (contaminants) are shown as white ovals. Modified from (Gloeckner et al. 2009a)

One advantage of these assays is that they can be performed under native conditions and therefore the entire complex containing also indirect interaction partners of the bait protein can be extracted. Additionally, the high sensitivity of mass spectrometric analysis allows for the detection of small amounts of protein. However, a high purity of the protein samples is

required, and thus a two step affinity purification pulldown approach was chosen. The tandem affinity tag used for LnpA consisted of a doublet Strep-tag II and a FLAG moiety, the so called SF-TAP-tag, optimised for rapid as well as efficient tandem affinity purification of native proteins and protein complexes in higher eukaryotic cells. The workflow of the purification is described in Figure 16. The lysates from HEK293T cells overexpressing the LnpA bait protein were applied to Strep-Tactin coated beads (Figure 16; Step 1), non-specific binding partners were removed by washing and finally the bait/interactor complex was eluted with a buffer containing Desthiobiotin (Figure 16; Step 2). For the second purification step, the eluate was then incubated with beads coated with the FLAG antibody (Figure 16; Step 3). Remaining unspecific bound proteins were removed by washing, and the interaction complexes were finally eluted using a buffer containing the FLAG peptide (Figure 16; Step 4).

3.3.2. Analysis of purification and enrichment of Lnp bait proteins

In order to perform the pulldown, two different vectors were created. Each vector contained the full open reading frame of zebrafish *lnpA* fused to the tandem affinity tag either N-terminally (N-SF-TAP-LnpA) or C-terminally (LnpA-C-SF-TAP) (Figure 17). Before the first

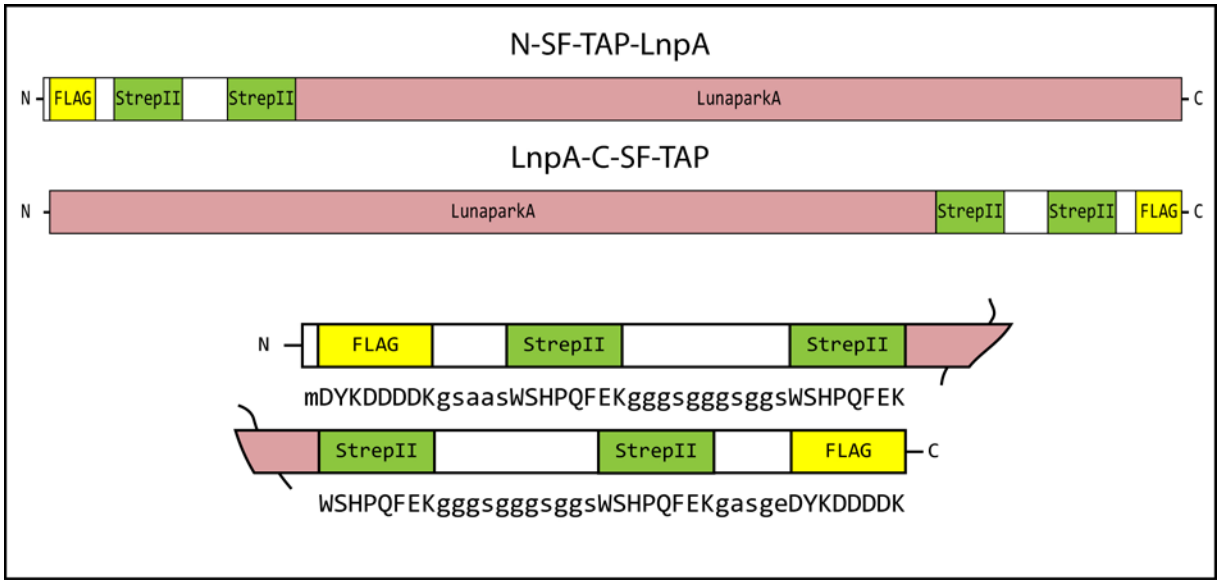

Figure 17 N- and C-terminal SF-TAP tagged LunaparkA

Schematic drawings of LunaparkA with N- and C- terminal SF-TAP tags. Adapted from (Gloeckner et al. 2009a)

mass spectrometry analysis was performed, the vectors were tested to examine if they show robust expression in cell culture and if the purification yield of the bait proteins is sufficient for the downstream mass spectrometric analysis. The two TAP plasmids, or an empty vector as a control, were transfected into HEK293T cells. The high purity achieved by a two-step purification like in the SF-TAP system is usually at the expense of the resulting yield. Thus, an input of 6-10 mg total protein was required, which was achieved by using three 15 cm

dishes of transfected cells for each sample. 48 hours after transfection, the cells were lysed using non-ionic detergents and the insoluble fraction was removed by centrifugation and by

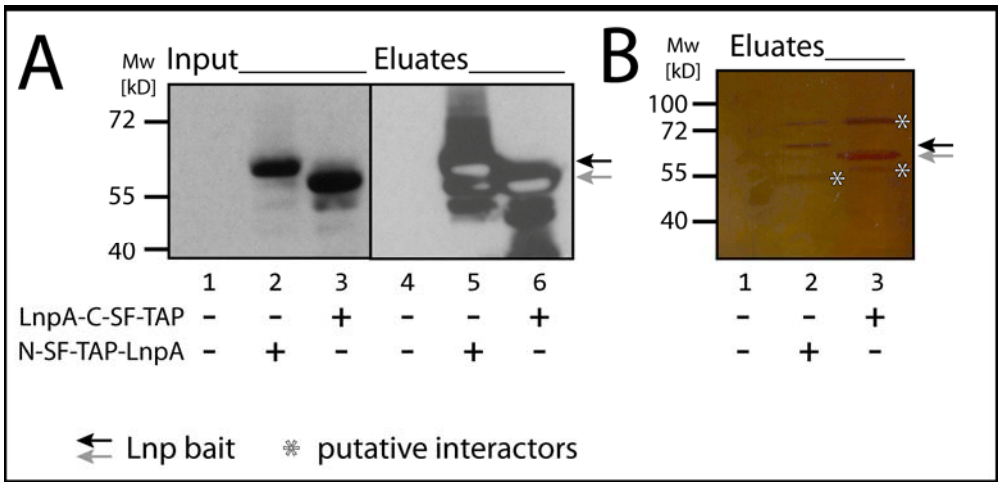

Figure 18 Expression and purification test of Lnp-SF-TAP constructs
A SDS-PAGE and Westernblot analysis with anti-FLAG antibody of crude lysates from 293T cells transiently transfected with empty vector (lanes 1, 4), N-SF-TAP-LnpA (lanes 2, 5) or LnpA-C--SF-TAP (lanes 3, 6). From each sample 20 µg total protein were used as input control (lanes 1-3) and subjected to a SDS-PAGE together with the tandem purified eluates (lanes 4-6). Both tagged LnpA constructs were robustly overexpressed in 293T cells and appeared as two strong bands at 60 kD (arrows) in the total protein lysates (Input lane 2, 3). Successful purification and enrichment is shown by two bands of similar size in the eluted fraction (eluates lane 5, 6).
B Tandem purified eluates of N-SF-TAP-LnpA (lane 2), Lnp-C-SF-TAP (lane 3) and control (lane 1) from 239T lysates were subjected to SDS-PAGE and silver staining. In comparison to the control, the purified bait samples show prominent bands at a molecular weight of 60 kD similar to the western blot in **A** (arrows). These bands weight represent the Lunapark bait proteins. Additional specific bands of different molecular that are not appearing in the control lane are putative interaction partners (asterisks).

ultra filtration. Subsequently, 20 µg total protein from the filtered lysate was used as input control (Figure 18 A; Lane 1-3). The rest of the cleared lysates were subjected to microspin affinity columns and then purified using the two-step protocol described above. At last, 10% of the final eluate was used for analysis (Figure 18 A; Lane 4-6). The input as well as the eluted samples were loaded on a SDS gel. After the electrophoresis, the SDS gel was blotted on a PDVF membrane and labelled with FLAG antibody (Figure 18 A). The Western blot showed that the lysates obtained from cells transfected with one of the TAP vectors showed a very prominent band at approximately 60 kD, which was not present in the control lane (Figure 18 A; black and grey arrow). The two bands were still present after the purification process. Therefore we concluded that both vectors could be robustly overexpressed in 293T cells and that both versions of the bait protein bind efficiently to and can easily be eluted from the beads.

Additionally 10% of the purified protein from each sample was loaded on a SDS gel and stained with silver solution to check the quality of the purification (Figure 18 B). In the control lanes (Figure 18 B Lane 1), no bands could be detected indicating a low background. In contrast, in lanes transfected with N-SF-TAP-LnpA or LnpA-C-SF-TAP, several bands were visible. In every sample lane there is a strong band at 60 kD represent which represent

the bait proteins (Figure 18 B; Lane 2-3 black and grey arrow) as they have the same molecular weight as the bands detected by the anti-FLAG antibody (Figure 18 A). In the sample lanes (Figure 18 B; Lane 2-3 asterisks) several other bands appear. These bands are absent in the control and therefore most likely represent specific interaction partners of LnpA. It can be concluded that both LnpA bait proteins are robustly express in HEK293T cells and that the affinity tags are able to bind to the corresponding matrix and are therefore not masked by the fused protein. Furthermore, the bait could be efficiently eluted from the beads and also additional bands representing potential interaction partners could be detected by silver stain analysis. Moreover, no contaminants could be observed in the control lane. Thus the vectors are well suited for SF-TAP mass spectrometric analysis.

3.3.3. Mass spectrometric analysis of Lnp-SF-TAP pulldowns

After having established LnpA protein isolation, several pulldowns were performed to subject them to mass spectrometry. Following every single purification 10% of the eluted fraction was used for analysis on a silver stained SDS gel to control successful purification. Subsequently, these samples were prepared for mass spectrometric analysis by overnight trypsin digestion and were then implemented into the workflow of the Proteomics core facility at the HelmholtzZentrum München. In total, five independent analyses were performed. Each of the five approaches contained three affinity purification samples: one control sample without bait protein, one purification using the N-terminal (N-SF-TAP-LnpA) and one sample using the C-terminal (LnpA-C-SF-TAP) LunaparkA SF-TAP fusion protein as bait. The resulting spectra were analysed with the Mascot software and mapped to peptide sequences. The results were summarised as Scaffold Viewer files. Figure 19 shows a part of a Scaffold viewer results list of two simultaneously conducted pulldown assays. Each of the two assays consisted of three samples: control sample, N-SF-TAP-LnpA and LnpA-C-SF-TAP. An indication of a successful purification process was the identification of the LnpA bait protein which was found in all purifications without exception. Moreover, LnpA was absent in control lanes indicating specificity of the affinity binding process (Figure 19 #1). In addition various putative binding partners of LunaparkA could by identified by mass spectrometric analysis.

In order to extract promising interactors from the obtained list the results were sorted using several steps. First we first removed proteins that appeared not only in cells overexpressing the bait, but also in the control samples (Figure 19 #7, #16) and are therefore unspecific

contaminants, from the list. For example keratin contaminants (Figure 19 #2), which are derived from skin and hair particles and highly abundant in the environment were excluded. Additionally hypothetical or so far uncharacterised proteins were removed, as they will not

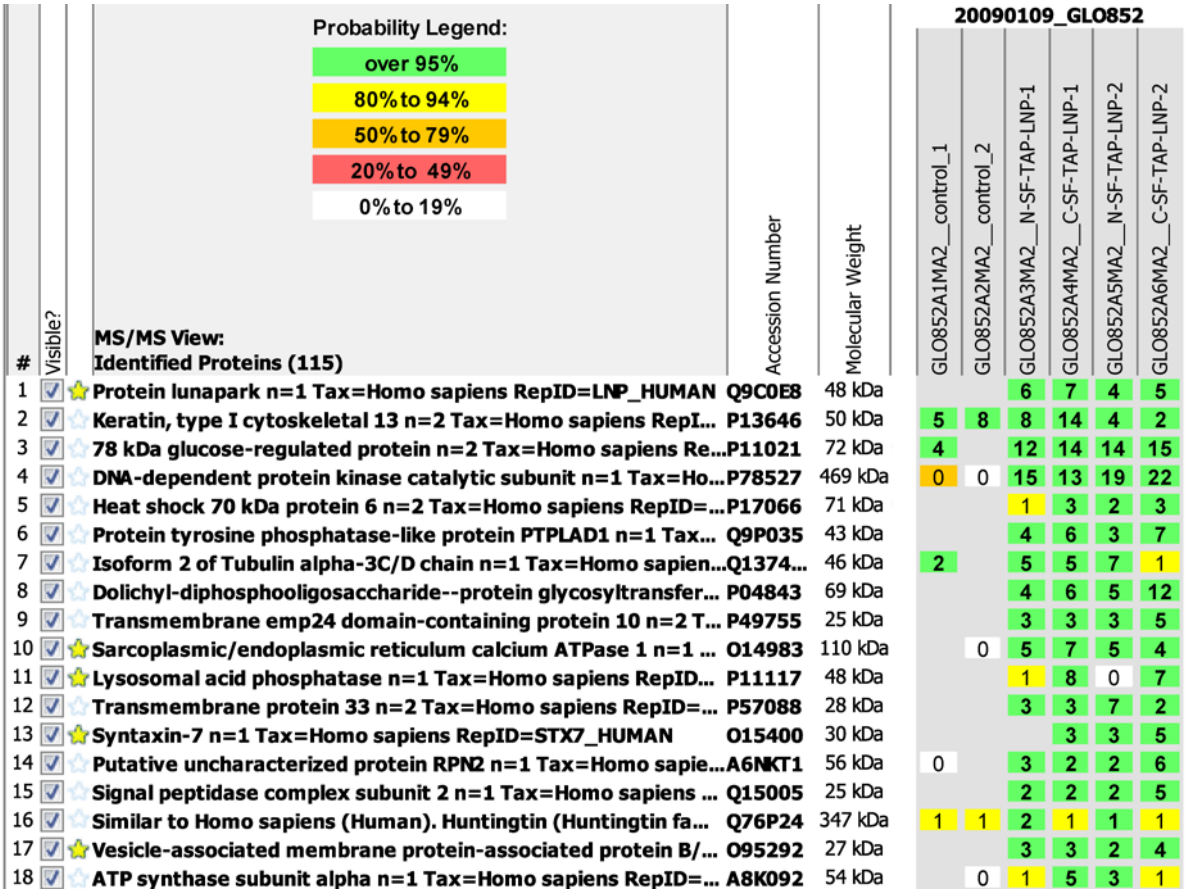

Probability Legend:
over 95%
80% to 94%
50% to 79%
20% to 49%
0% to 19%

#	Visible?	MS/MS View: Identified Proteins (115)	Accession Number	Molecular Weight	20090109_GLO852 GLO852A1MA2__control_1	GLO852A2MA2__control_2	GLO852A3MA2__N-SF-TAP-LNP-1	GLO852A4MA2__C-SF-TAP-LNP-1	GLO852A5MA2__N-SF-TAP-LNP-2	GLO852A6MA2__C-SF-TAP-LNP-2
1	☑	Protein lunapark n=1 Tax=Homo sapiens RepID=LNP_HUMAN	Q9C0E8	48 kDa			6	7	4	5
2	☑	Keratin, type I cytoskeletal 13 n=2 Tax=Homo sapiens RepI...	P13646	50 kDa	5	8	8	14	4	2
3	☑	78 kDa glucose-regulated protein n=2 Tax=Homo sapiens Re...	P11021	72 kDa	4		12	14	14	15
4	☑	DNA-dependent protein kinase catalytic subunit n=1 Tax=Ho...	P78527	469 kDa	0	0	15	13	19	22
5	☑	Heat shock 70 kDa protein 6 n=2 Tax=Homo sapiens RepID=...	P17066	71 kDa			1	3	2	3
6	☑	Protein tyrosine phosphatase-like protein PTPLAD1 n=1 Tax...	Q9P035	43 kDa			4	6	3	7
7	☑	Isoform 2 of Tubulin alpha-3C/D chain n=1 Tax=Homo sapien...	Q1374...	46 kDa	2		5	5	7	1
8	☑	Dolichyl-diphosphooligosaccharide--protein glycosyltransfer...	P04843	69 kDa			4	6	5	12
9	☑	Transmembrane emp24 domain-containing protein 10 n=2 T...	P49755	25 kDa			3	3	3	5
10	☑	Sarcoplasmic/endoplasmic reticulum calcium ATPase 1 n=1 ...	O14983	110 kDa		0	5	7	5	4
11	☑	Lysosomal acid phosphatase n=1 Tax=Homo sapiens RepID...	P11117	48 kDa			1	8	0	7
12	☑	Transmembrane protein 33 n=2 Tax=Homo sapiens RepID=...	P57088	28 kDa			3	3	7	2
13	☑	Syntaxin-7 n=1 Tax=Homo sapiens RepID=STX7_HUMAN	O15400	30 kDa				3	3	5
14	☑	Putative uncharacterized protein RPN2 n=1 Tax=Homo sapie...	A6NKT1	56 kDa	0		3	2	2	6
15	☑	Signal peptidase complex subunit 2 n=1 Tax=Homo sapiens ...	Q15005	25 kDa			2	2	2	5
16	☑	Similar to Homo sapiens (Human). Huntingtin (Huntingtin fa...	Q76P24	347 kDa	1	1	2	1	1	1
17	☑	Vesicle-associated membrane protein-associated protein B/...	O95292	27 kDa			3	3	2	4
18	☑	ATP synthase subunit alpha n=1 Tax=Homo sapiens RepID=...	A8K092	54 kDa		0	1	5	3	1

Figure 19 Putative interactors of LunaparkA

Image shows a Scaffold viewer output file listing selected putative interactors from two independent LunaparkA pulldown assays (No.1 and 2) identified by mass spectrometry. Each assay consists of three samples: a control sample without bait protein (control) and two independent affinity purifications using the N-terminal (N-SF-TAP-LNP) or the C-terminal (C-SF-TAP-LNP) Lunapark SF-TAP fusion protein as bait. The columns on the right show in which purification sample the listed protein was found by coloured and numbered boxes. Numbers give quantity of unique peptides identified for a given protein. The colours specify the probability that a given protein has been identified correctly.

provide any further information on the functional context of LunaparkA (Figure 19 #14). Nevertheless, they represent a very interesting pool of candidate factors to be analysed as soon as the physiological function of LnpA is understood.

Furthermore we removed all candidates from the list that were identified as heat shock (Figure 19 #3, #5) or other stress related proteins (Figure 19 #4). These proteins are often activated if large amounts of transgenic protein are overexpressed. The heat shock proteins are enriched in these samples. Although the heat shock proteins bind to the overexpressed proteins, in this case LnpA, the binding is probably not very specific, because it is a result of the overexpression.

The remaining candidates were further sorted in respect to their confidence in binding and concerning their properties in regard to function and expression.

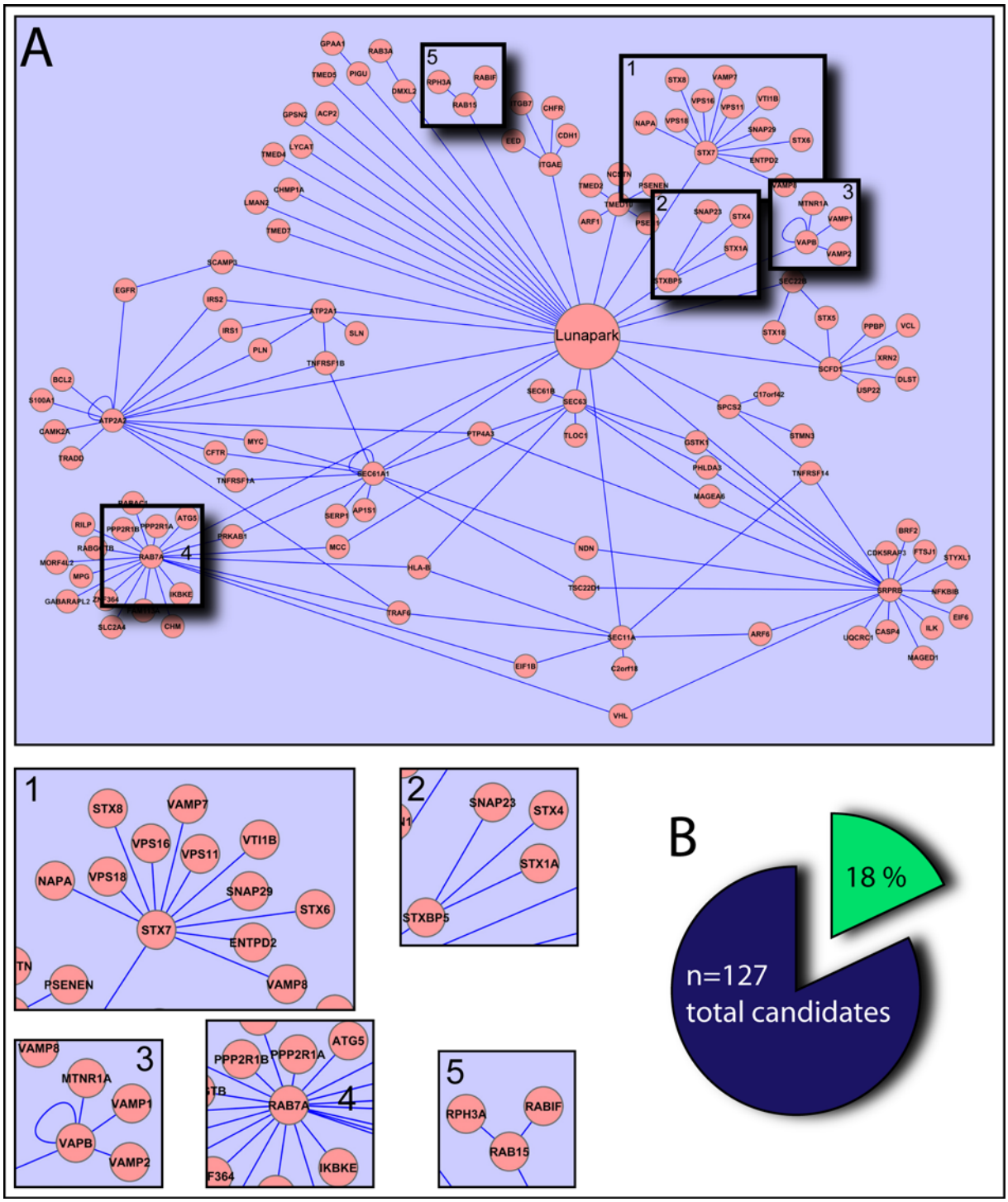

Figure 20 Global view of the LunaparkA vesicle-associated interaction networks

A Selected interactions of LunaparkA summarised in a functional interactome. 1-5 Higher power views of interactions of special interest. **B** 18% of all interactors are vesicle or membrane associated proteins.

In order to determine the confidence three criteria were considered: Number of unique peptides, probability value and reproducibility. By default settings of the Scaffold Viewer software, all candidates that were identified by only a single peptide were excluded from the list. Furthermore, only peptide sequences with a probability value higher then 95% (Figure

19; indicated by green labels) were considered for further analysis. The probability value specifies the likelihood that a given protein has been identified correctly.

The remaining candidates were classified in either having a high or a low confidence or excluded. Proteins were considered to have a high interaction confidence if they were able to bind to both N-SF-TAP-LnpA as well as LnpA-C-SF-TAP and if they were identified in at least two of the five analyses performed, also indicating a high reproducibility of the binding. Examples for interactors with high confidence are e.g. Syntaxin 7 (STX7) (Figure 19 #13), Sarcoplasmatic/endoplasmatic reticulum calcium ATPase 1(SercA) (Figure 19 #12) or Vesicle-associated membrane protein-associated protein B/C (VAPB) (Figure 19 #3).

Candidates with lower confidence, for example Rab7A or Rab15, appeared only a single purification assay but also showed a peptide sequence probability higher than 95%. Candidates with probability value lower than 95% or less then two unique identified peptides were excluded from further investigations.

Analysis of all putative interactors revealed that approximately 18% of these candidates are proteins membrane associated and/or involved in vesicular trafficking (Figure 20 B).

After the classification of the putative interactors, all identified membrane proteins with high and low confidence were further analysed using Cytoscape Software to create a functional interactome (Figure 20 A). This software integrates the received data into a network of interactions already described, revealing additional putative second order interactions or functional relations between individual binding partners (Figure 20). Strikingly, a very large set of these primary and secondary order interaction partners are members of the SNARE family known to be involved in vesicle docking and fusion events (Figure 20 A 1, 2, 3).

For example the Vesicle-associated membrane protein- associated protein B/C (VAPB/C) is known to interact with v-SNARES Vamp1 and Vamp2, (also known as Synaptobrevin1 and 2) (Figure 20 A 3) or Syntaxin Binding Protein 5 (StxBP5), which is known to bind to Snap23, Syntaxin 4 and 1A (Figure 20 A 3). A third SNARE protein that was identified as a putative direct binding partner is Syntaxin 7, which has many confirmed interaction partners that belong to the family of SNARE proteins, such as Syntaxin 6 and 8 and Vesicle-associated membrane protein 7 and 8.

In addition to the various SNARE proteins, two small Rab GTPases could be identified in the LnpA SF-TAP pulldown: Rab7A, localised to late endosomes/lysosomes, and Rab15, a marker for recycling endosomes.

These findings on the one hand further underline the results from the co-localisation assays, indicating that Lunapark is an endomembrane protein. Further, the composition of the

putative interactors suggests that LnpA is involved in vesicle trafficking in particular vesicle fusion events.

Taking the developmental expression in the CNS into account, Lnp could play a role in neuronal differentiation processes that are highly dependent on vesicle trafficking and material transport such as axonogenesis, synptogenesis and dendrite formation.

Therefore the goal of the proteomic approach in identifying cellular processes in which LnpA might be involved was achieved. Not only in associating Lnp with vesicle trafficking and fusion but also providing specific interaction partners of well characterised function.

3.3.4. Syntaxin 7-like (Stx7)

As the first candidate for a more detailed analysis of the interaction with LnpA and its possible biological relevance we choose Syntaxin 7 (Stx7). First, Syntaxin 7 is a candidate

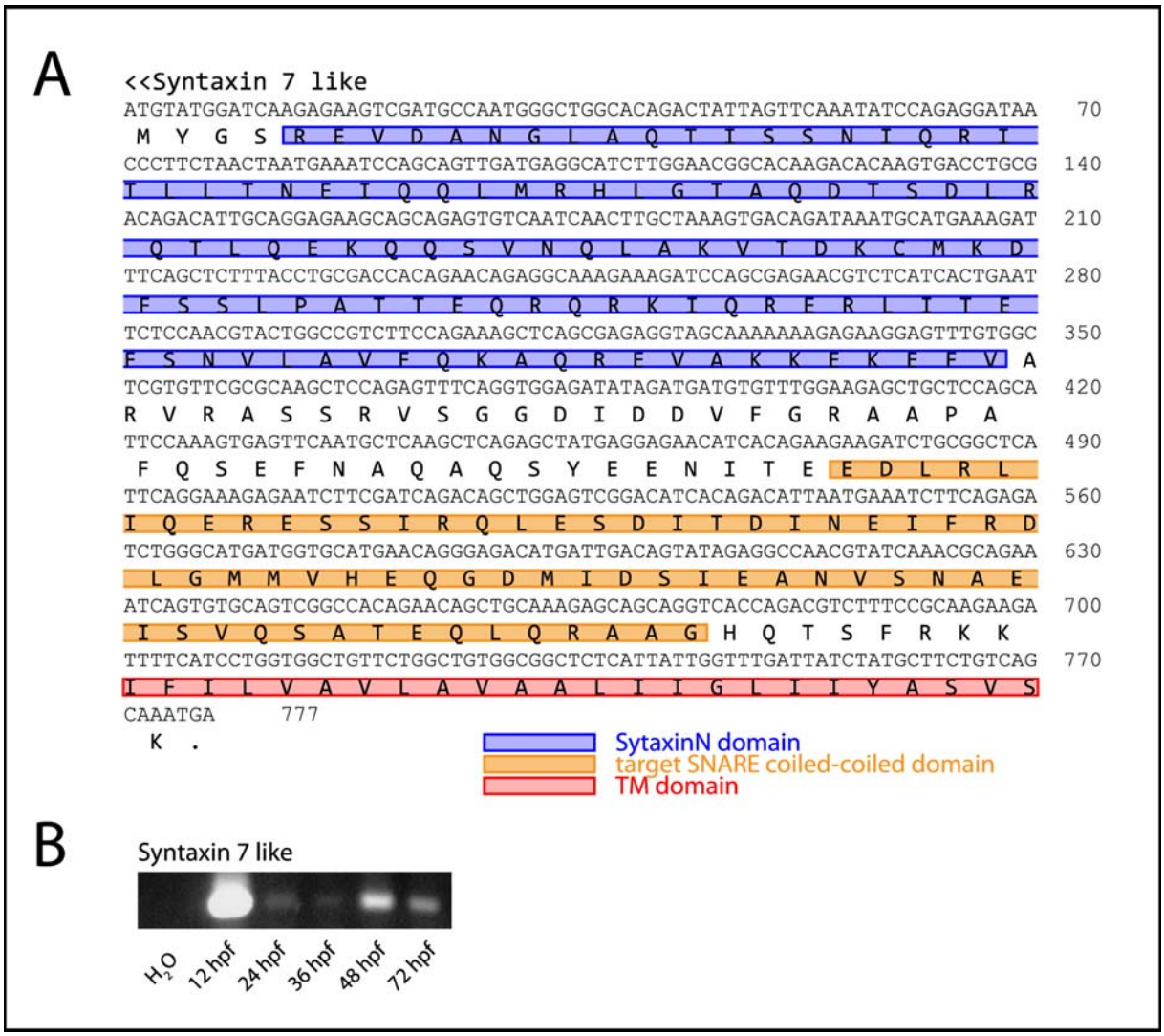

Figure 21 The putative LnpA interaction partner Syntaxin 7 like is expressed during early developmental stages in zebrafish.
A Nucleotide and deduced amino acid sequence of isolated zebrafish *syntaxin 7 like* (Stx-7l) cDNA. **B** *syntaxin 7-like* RT-PCR on mRNA extracted from wildtype zebrafish embryos at the indicated developmental stages.

with a very high confidence in the interaction. It was identified in 7 out of 10 independent purifications but it was never found in control samples. Furthermore, if Syntaxin 7 was detected, at least 3 unique peptides were identified and the probability value for the interaction was higher than 99.9% indicating strong and specific binding of Syntaxin 7 to the LnpA bait proteins showing a high reproducibility.

Syntaxin 7 is a member of the t-SNARE protein family known to be important for vesicle docking and fusion events. Syntaxin 7 in particular was shown to be present in late endosomes/lysosomes responsible for the fusion of these organelles (Prekeris et al. 1999) These observations further motivate the choice to first concentrate on Syntaxin 7 and to characterise its involvement in LnpA dependent processes.

Initially, it had to be clarified if a homologue of the *syntaxin 7* gene exists in zebrafish. Therefore, human *stx-7* cDNA sequence was aligned with the zebrafish genome using the Ensembl genome browser and a gene called *syntaxin 7-like* (*stx7l*) could be identified on chromosome 20: 45,409,147-45,424,026 forward strand. According to the sequence annotated in Ensembl, primers were designed to amplify the *syntaxin 7-like* open reading frame. Using degenerate RT-PCR a 777 bp fragment could be obtained from 48 hpf cDNA (Figure 21 A).

Furthermore, RT-PCR using cDNA from zebrafish embryos of different developmental stages revealed that Syntaxin 7-like is expressed from 12 hpf until at least 72 hpf (Figure 21 B).

Taken together, from these results we can conclude that a s*yntaxin 7* homologue exists in zebrafish embryos and that it is expressed in all early stages of development, similar to the developmental expression profile of zebrafish *lunapark*.

3.3.5. Biochemical validation of Syntaxin 7-like interaction with zebrafish LunaparkA

The SF-TAP pulldown screen repeatedly identified Syntaxin 7 as a putative interaction partner of the Lnp SF-TAP bait proteins with both N- and C-terminally tagged Lunapark bait. A second independent approach was performed in order to both confirm these results and clarify whether the interaction also occurs in zebrafish or if it is exclusive to human Syntaxin 7. Thus, two independent LnpA/Stx7l co-immunoprecipitation (coIP) assays were performed. In the first assay, the Lnp protein tagged at its C-terminus to the HA (Lnp-HA) epitope was used as bait in order to co-precipitate. Plasmids containing these two constructs were transfected alone or in combination in HEK293T cells. H2B-YFP was transfected as a negative control instead of Syntaxin 7l-Citrine. 48 hours after transfection, the cells were lysed and the insoluble fraction was removed by centrifugation. 20 µg total protein was reserved for the input control, while 500 µg of total protein was incubated with the 3F10 high

affinity anti-HA antibody (Roche). After incubation and washing, the input samples and sepharose beads were subjected to SDS-PAGE and analysed by western blot using anti-GFP (also detects Citrine and YFP) and anti-HA antibodies (Figure 22).

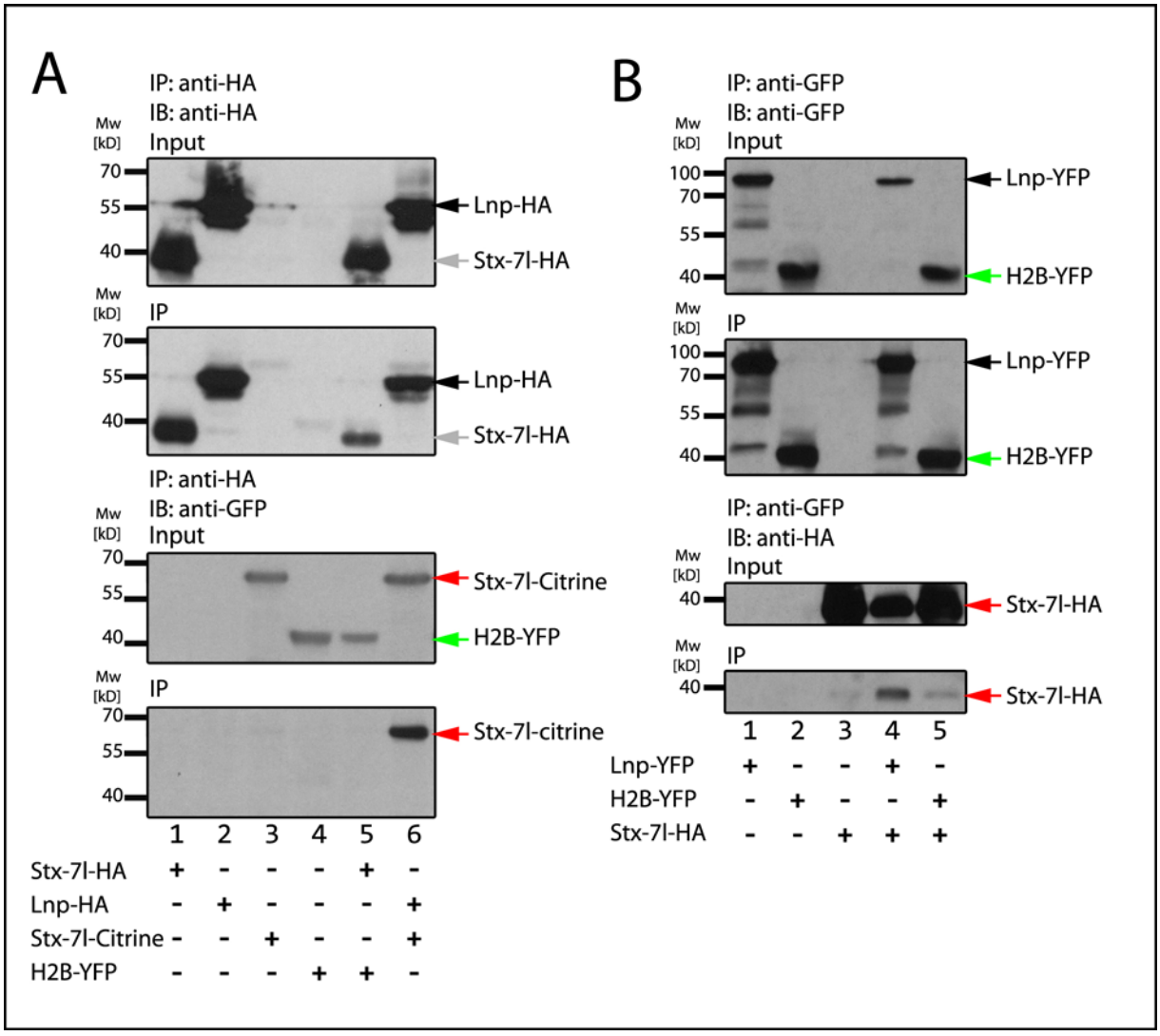

Figure 22 Co-immunoprecipitation of Syntaxin 7 like with LnpA baits

A SDS-PAGE and Westernblot analysis of a co-immunoprecipitation assay with Lnp-HA used as bait. 20 µg total protein from lysates obtained from 293T cells transiently transfected with the indicated constructs were used as input control. 500 µg total protein was used for immunoprecipitation with anti-HA antibody and protein G-Sepharose for precipitation (IP). The western blot was subsequently analysed with anti-HA (upper panel) and anti-GFP antibody (lower panel). Stx-7l-HA (grey arrow) and Lnp-HA (black arrow) could be precipitated using anti-HA antibody. Stx-7l-Citrine (red arrow) was co-precipitated with Lnp-HA. H2B-YFP was used as negative control (green arrow).
B SDS-PAGE and Westernblot analysis of a co-immunoprecipitation assay with Lnp-YFP used as bait. 20 µg total protein from lysates obtained from 293T cells transiently transfected with the indicated constructs were used as input control. 500 µg of total protein was incubated together with anti-GFP antibody and protein G-Sepharose. The western blot was subsequently analysed with anti-GFP (upper panel) and anti-HA antibody (lower panel). H2B-YFP (green arrow) and Lnp-YFP (black arrow) could be precipitated using anti-GFP antibody. Stx-7l-HA (red arrow) was co-precipitated with Lnp-YFP but not with H2B-YFP.

The western blot analysis showed that Lnp-HA as well as Stx7l-HA proteins were able to bind to the sepharose beads in the presence of HA antibody (Figure 22 A lanes 1, 2, 5, 6 HA blots), whereas Stx7l-citrine or H2B-YFP did not (Figure 22 A 3, 4 GFP blots) indicating efficient

and specific immunoprecipitation of HA-tagged proteins. In addition, H2B-YFP did not co-precipitate with Lnp-HA (Figure 22 A Lane 5 GFP blots). In contrast, when Stx7l-citrine was overexpressed together with Lnp-HA, a clear GFP band could be detected in the IP western blot indicating a direct biochemical interaction of both tagged proteins. (Figure 22 A lowest blot). As an additional verification, a second independent coIP was performed using an anti-

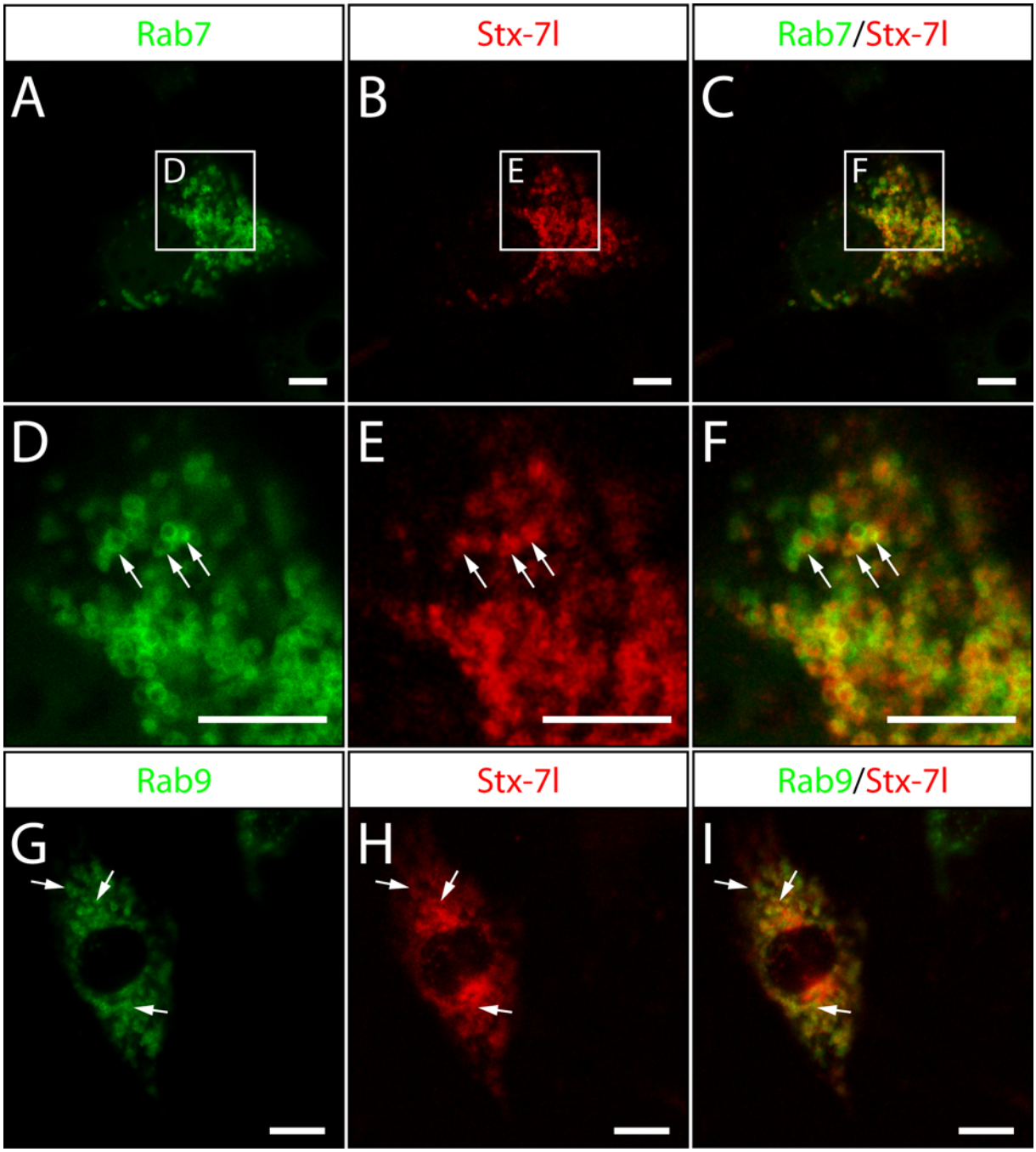

Figure 23 Syntaxin 7 like localises to late endosomes/lysosomes

Images recorded by confocal microscopy of NIH3T3 cells transfected with Stx-7l-TagRFP in combination with **A-F** Rab7-YFP or **G-H** Rab9-YFP demonstrates that Stx-7l is localised to the late endosomal/lysosomal compartment within the cell. (**D-F**) High magnification image of the boxed areas in the corresponding figure. Scale bars 10 µm.

GFP antibody and either H2B-YFP and or Lnp-YFP as bait in an attempt to co-precipitate Stx7l-HA. Again HEK293T cells were transfected, incubated for 48 hours and subsequently lysed. 20 µg total protein from the cleared lysates were used as input control and 500 µg were incubated with anti-GFP antibody and protein-g-sepharose beads. Subsequently, the samples were denatured using SDS and subjected to PAGE, followed by western blot analysis using anti-GFP (Figure 22 B two upper panels) or anti-HA antibody (Figure 22 B two lower panels).

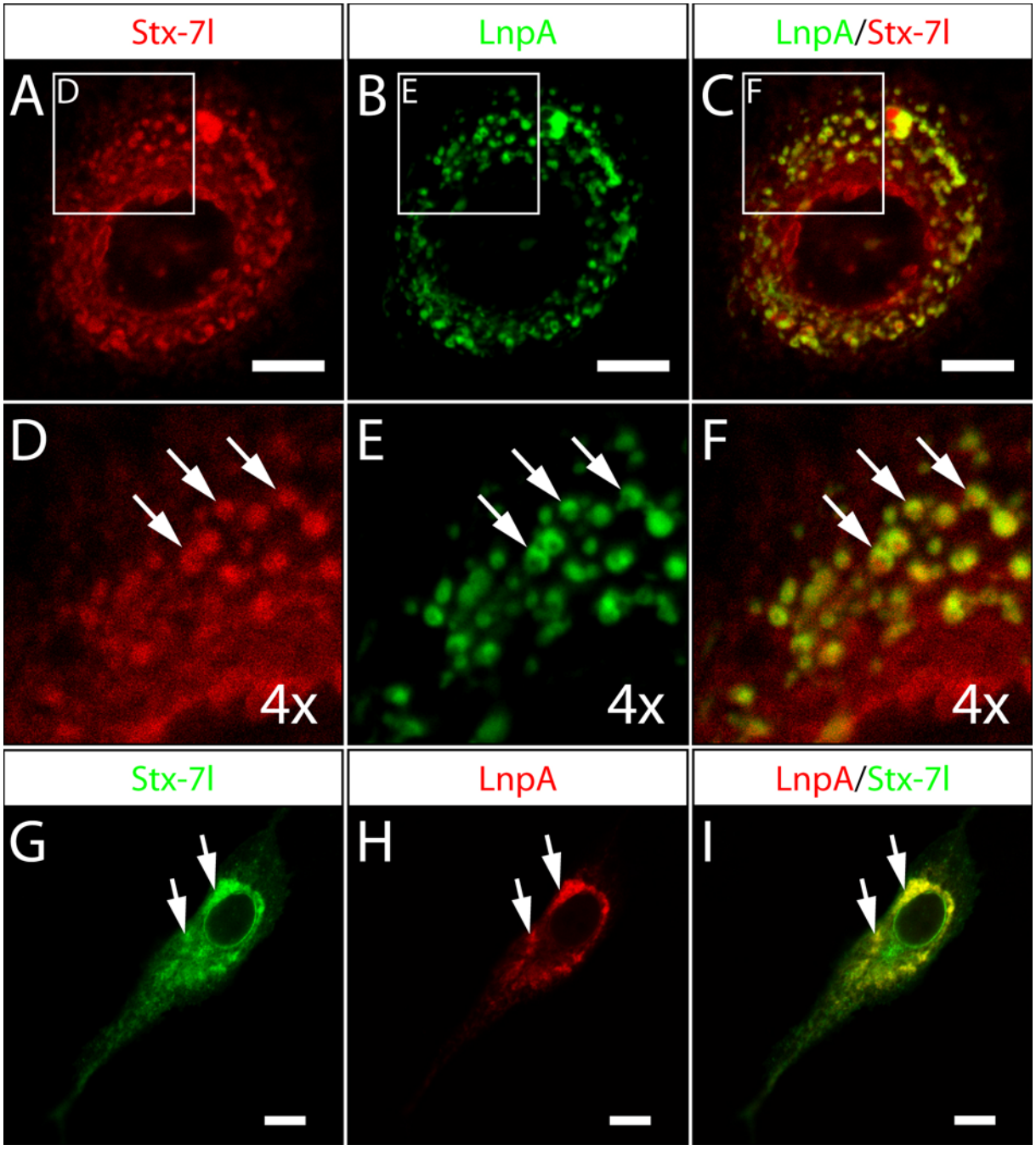

Figure 24 Syntaxin 7 like and LunaparkA co-localise in PAC2 cultured cells in vivo

Images recorded by confocal microscopy of PAC2 cells transfected with **A-F** Stx-7l-Citrine and LnpA-mCherry or **G-H** Stx-7l-tagRFP and LnpA-YFP demonstrate co-localisation of the fusion two proteins (white arrows). **D-F** high power image of boxed areas in the corresponding figure. Scale bars 10 µm.

In this assay Lnp-YFP and H2B-YFP could be extracted from the lysate (Figure 22 B Lane 1, 2, 4, 5 black and green arrow) and only the LnpA bait was able to pulldown Stx7l-HA (Figure 22 B Lane 4 red arrow) whereas Stx7l-HA alone or in combination with H2B-YFP did not result in precipitation of Lnp. (Figure 22 B Lane 3, 5). In summary, our results from the immunoprecipitation assays clearly verified the Syntaxin 7-like and LunaparkA interaction initially identified by the SF-TAP-screen. Furthermore our data provides convincing evidence that this biochemical interaction also occurs between the zebrafish homologue Syntaxin 7-like and the LnpA protein.

3.3.6. Intracellular localisation of Syntaxin 7-like and its co-localisation with LnpA

In initial experiments, it could be biochemically validated that LnpA and Syntaxin 7-like specifically interact. We next addressed whether Stx7l could be found in the same cellular compartments as described for LnpA, which would suggest that the biochemical interaction is indeed biologically relevant based on subcellular co-localisation. Several Stx7l fluorescent fusion proteins were created and subsequently overexpressed together with different subcellular markers as well as LnpA constructs in zebrafish PAC2 cells, followed by confocal microscopy analysis. First Stx7l-tagRFP was co-expressed with either Rab7-YFP or Rab9-YFP, which label lysosomes and late endosomes respectively. Images recorded by confocal microscopy showed that Stx7l-tagRFP co-localise to a large extent with Rab7-YFP (Figure 23 A-F), as well as Rab9-YFP (Figure 23 G-H). This results support earlier findings showing that Stx7 plays a role in late endosome/lysosome fusion (Prekeris et al. 1999).

Furthermore, single optical sections recorded by confocal microscopy of PAC2 cells transfected with Stx7l-tagRFP and full length Lnp-YFP or Stx7l-citrine and Lnp-mCherry show a clear co-localisation of these two proteins (Figure 24). Thus, it can be concluded that Stx7l and Lnp have the same subcellular localisation in cultured cells derived from zebrafish. Interestingly, the characteristic Lnp-YFP aggregate formation usually observed after expression in PAC2 seemed to be reduced in size as well as in number suggesting that co-expression of one of its binding partners facilitates LnpA protein folding.

In Summary, these results show that the zebrafish proteins LnpA and Syntaxin 7-like interact biochemically, they are expressed at the same developmental time point and they are located in the same subcellular compartment indicating that LnpA and Syntaxin 7-like interaction might be important for their individual developmental function.

Interestingly, Avalanche the *Drosophila* Syntaxin 7 homologue has been assigned to attenuate Notch signalling by removing the receptor from the cell membrane. Thus Lnp could well play

a role in this process and may be an important component in regulating Notch signal transduction.

3.4. Morpholino Artefacts – death of a phenotype

3.4.1. Three independent Morpholinos effectively target *lunaparkA* mRNA

In order to determine the function of lunapark in the developing zebrafish and in particular within the hindbrain, a Morpholino (Mo) based knockdown approach was used. Morpholinos are antisense oligonucleotides with a modified sugar phosphate backbone that enhances their stability (Summerton 1999; Nasevicius and Ekker 2000). In general, Morpholinos can be divided into two types. On the one hand there are the Morpholinos that block translation by

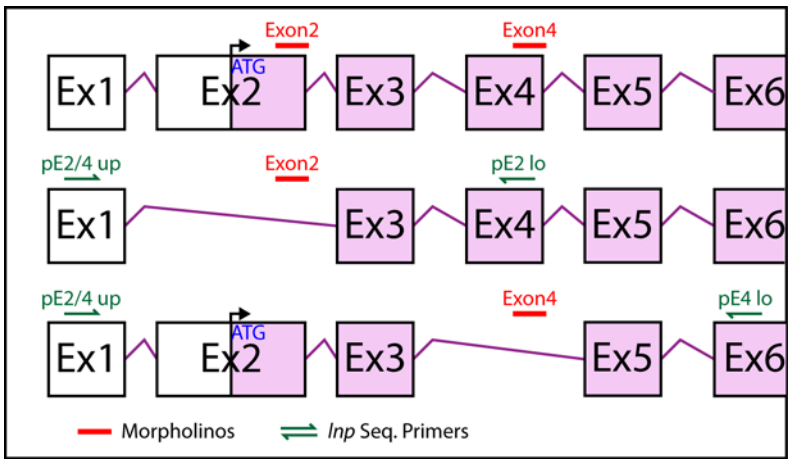

Figure 25 Mechanism of Exon2 and Exon4 *lunaparkA* splice Morpholinos
Schematic drawing of the *lunaparkA* exon intron-structure and the expected splice alterations after application of the Exon2 Mo and Exon4 Mo.

specifically binding the 5' region in close proximity to the ATG start codon, thereby preventing the initiation complex from binding to the mRNA (Figure 27). The second group of Morpholinos are splice Morpholinos. Splice Morpholinos are designed in such a way that they target either splice junctions (splice acceptor or splice donor) or splice regulatory sites, thereby impairing binding of the splicing machinery. As a consequence, the affected exon cannot be recognised and is spliced out together with the neighbouring introns, resulting in a shortened mRNA sequence. Less likely are cryptic splice products which can occur as intronic cryptic, exonic cryptic or splice stopped forms. (For further information please refer to the GeneTools Morpholinos web site www.gene-tools.com)

In the case of *lunaparkA,* two different splice Morpholinos were designed. Exon2 Mo targets the splice donor of the ATG start codon-containing second exon, while Exon4 Mo targets the splice donor of the relatively large Exon4 (Figure 25). According to Ensembl, Exon4 has a length of 188 base pairs in total and is therefore indivisible by 3, which should result in a frame shift and causing a nonsense mutation. The efficiency of these Morpholinos was tested by injecting them into one cell stage wild type embryos, homogenising the embryos at 24 hpf

and performing RT-PCR with primers targeted to the flanking *lnpA* sequence (Figure 26). Gel electrophoresis of the PCR products revealed that injection of Exon2 Mo (Figure 26 A lane 2) and Exon4 Mo (Figure 26 B lane 1) splice Morpholinos each resulted in a size-reduced

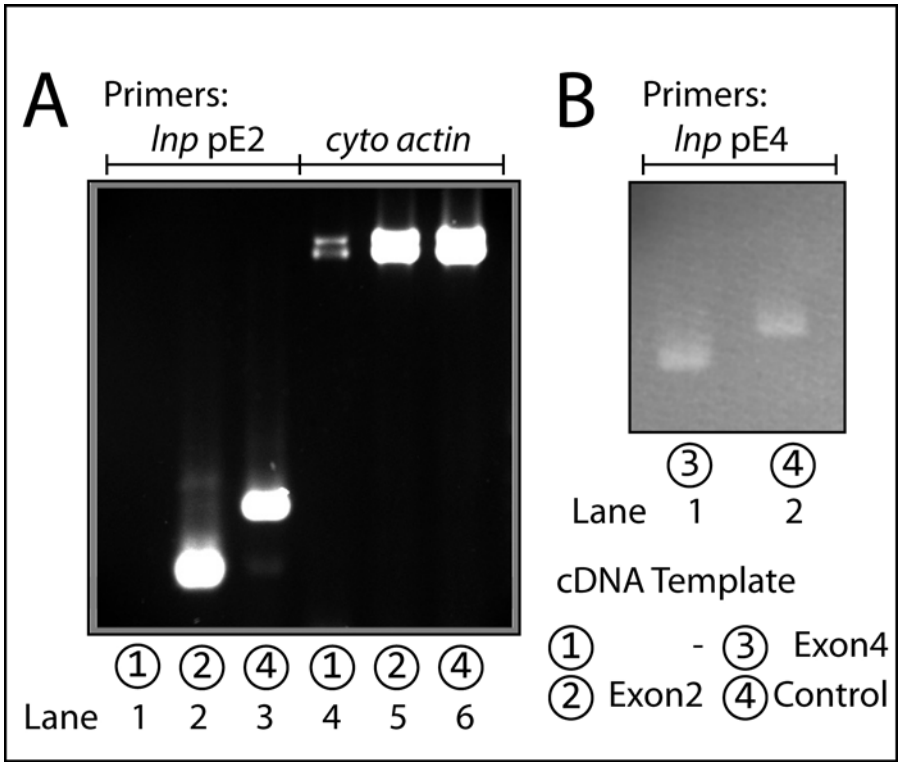

Figure 26 Injection of Exon2 Mo and Exon4 Mo results in truncated *lnpA* mRNA transcripts
Zebrafish embryos were injected with Exon2 Mo, Exon4 Mo or control solution at the one cell stage. cDNA was extracted from 24 hpf embryos. Subsequently, the cDNA was used for PCR with *lnpA* specific primers (see Figure 25) to detect splice alterations in Exon 1 **A** Lane 1-3 or Exon 3 **B** Lane 1-2. Integrity of cDNA was analysed with primers for *cytoskeletal actin* **A** (lanes 4-6). In samples acquired from Mo-injected embryos the lnpA transcript was shorter than compared to control injected littermates.

mRNA fragment as compared to control (Figure 26 A Lane 3 B Lane 2). This splice alteration occurred with a very high efficiency, as no wild type PCR product could be observed in the splice Morpholino samples. PCR with primers targeting the ubiquitously expressed *cytosolic actin* were used to determine the quality and quantity of the PCR template (Figure 26 A Lane 4-6; not shown for Exon4 Mo). Additionally the PCR products were extracted after the gel electrophoresis and the fragments were further analysed by sequencing (Appendix 1). Alignment of the sequences obtained from these transcripts showed that, as expected, the entire Exon2 of the *lnpA* transcript was missing on embryo samples injected with Exon2 Mo. This exon contains the ATG start codon of *lunaparkA* and therefore injection of Exon2 Mo should shift the translation to the next open reading frame (orf). The next open reading frame starts with an ATG sequence in exon3 producing 66 amino acid sequence. This altered orf does not have the same reading frame as LunaparkA. Therefore the injection of Exon2 Morpholino should result in a 66 AA nonsense mutation producing an effective knockdown of LnpA protein. Exon4 Mo in contrast only deleted a part of Exon4, creating an in frame deletion. This result was rather surprising, as we expected a complete loss of the Exon4 sequence and suggested that there is a cryptic splice site in the *lnpA* mRNA, which is used if the proper splice donor for Exon4 is blocked. Moreover, our sequence analysis revealed a

discrepancy with the Ensembl annotation, where Exon5 starts with a guanine. This guanine was removed after Exon4 Mo injection. Intriguingly, the intron between Exon4 and Exon5

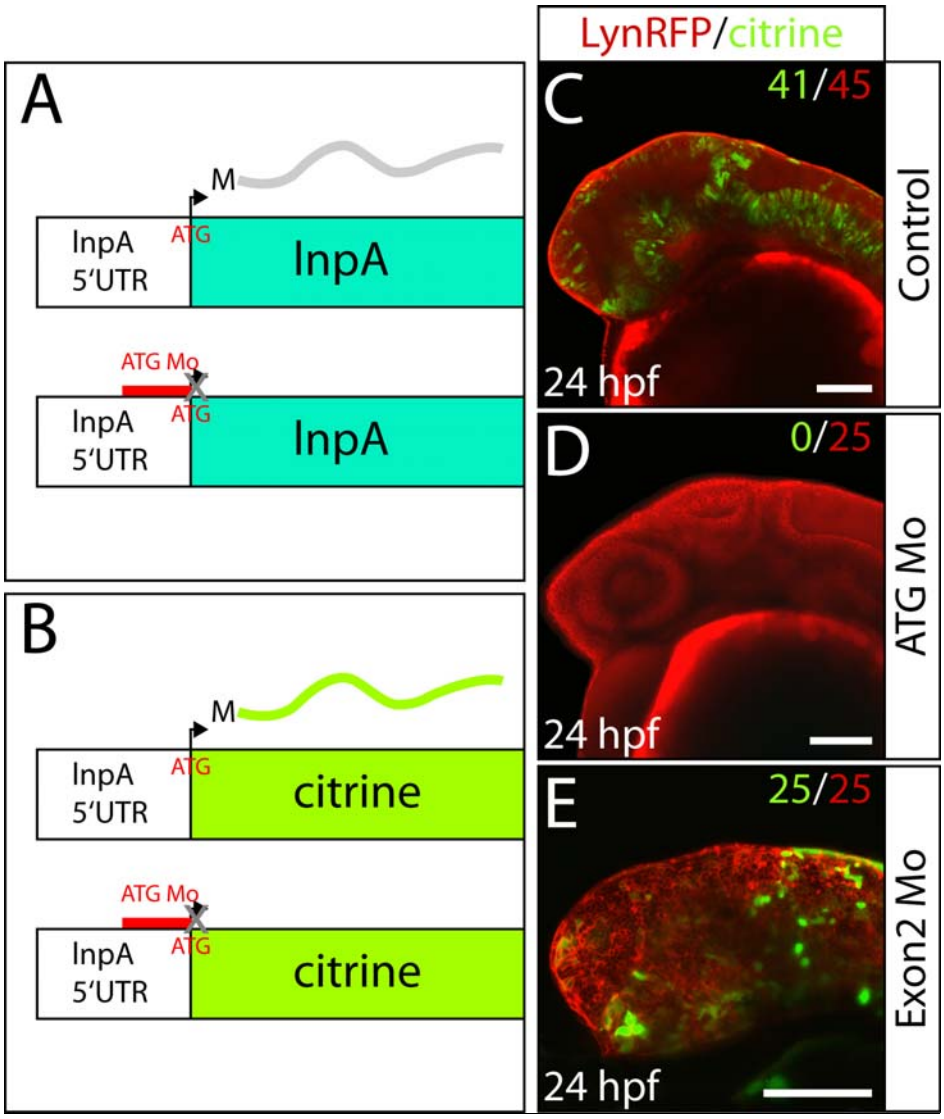

Figure 27 ATG Morpholino specifically blocks translation of *lnpA* mRNA
A Schematic drawing of the blocking mechanism of *lnpA* translation by the ATG Morpholino (ATG Mo). The Morpholino binds to the 5' region in direct proximity to the ATG start codon thereby sterically preventing the initiation complex from binding the mRNA and inhibiting its translation into protein. **B** Cartoon showing the reporter construct used to test the efficiency of the ATG Mo. *citrine* cDNA was fused downstream to the *lnpA* 5' ATG Mo target region. **C-E** Images recorded by confocal microscopy of 24 hpf zebrafish embryos injected with the *citrine* reporter construct and *lyn*RFP encoding a membrane targeted red fluorescent protein, at the one cell stage (**C**) or co-injected with the ATG Morpholino (**D**) or with Exon2 splice Morpholino (Exon2 Mo). Reporter expression could be detected in control (n=41/45) (**C**) and Exon2 (n=25/25) (**E**) Morpholino injected embryos but was absent in animals co-injected with the ATG Morpholino (n=0/25) (**D**). Scale bar 50 µm.

also starts with a guanine. This indicates that the guanine at the beginning of exon 5 is rather part of the preceding intron and the guanine at the beginning of this intron belongs to Exon4. Therefore, the splice pattern of this intron has to be shifted one base pair in the 3' direction. This is of crucial importance because the Morpholinos are designed to create a frame shift and an additional base pair could jeopardize that goal. Therefore, the intron exon borders have to be checked carefully in advance of choosing Morpholino target sequences. Nevertheless, the sequence targeted by *lnpA* Exon4 is part of the sequence encoding the two transmembrane domains. The loss of this sequence stretch after Exon4 Mo injection leads of the condensation

of the two transmembrane domains in wildtype LnpA to only a single TM-domain in the peptide sequence translated from the alternate transcript. As a consequence of this loss of one transmembrane domain, the C-terminus is now on the opposing membrane site in respect to the N-terminus.

In addition to the splice Morpholinos, a Morpholino that sterically blocks translation (ATG Mo) was designed. This type of Morpholino binds to the 5'UTR region of the already spliced transcript and therefore does not alter the length of the mRNA transcript (Figure 27 A). This also means the functionality of the ATG Mo could not be tested by RT-PCR analysis. Thus, a construct was created that contained the 5' UTR region of *lunaparkA,* where the Mo is expected to bind, directly upstream of a sequence encoding Citrine, a yellow fluorescent protein. Efficient Morpholino binding should prevent the translation of the fluorescence reporter (Figure 27 B). Wild type zebrafish embryos were injected with the reporter construct and Lyn-mRFP, a red membrane targeted fluorescent protein, alone or in combination with the *lnpA* ATG Mo. Co-injection of the Exon2 Mo was used as a negative control. Images of the injected embryos recorded by confocal microscopy at 24 hpf showed that animals co-injected with ATG Mo did not exhibit any citrine fluorescence (Figure 27 D; n=0/25). In contrast, control injected embryos (Figure 27 C; n=41/45) or embryos injected with the splice Morpholino (Figure 27 E; n=25/25) showed broad expression of the reporter protein. This demonstrates that the ATG Morpholino is capable of efficiently blocking translation of target mRNA containing the 5' UTR of *lnpA*.

In summary these results revealed that all three Morpholinos could efficiently target the *lnpA* transcript, as shown by either RT-PCR for the splice Morpholinos or using a fluorescent reporter assay for start codon Morpholino. The injection of the *lnpA* ATG Morpholino blocked translation with high effectiveness (n=25/25) and injection of the Exon2 splice Morpholino induced loss of second ATG containing exon. This suggests that the injection of both these Morpholinos results in an efficient knock down of LnpA protein. Injection of the *lnpA* Exon4 Mo in contrast does result in the loss a one transmembrane domain with a switch of the C-terminus to the other side of the membrane. An alteration that promises to have a strong effect on the function of the protein although it is difficult to predict of it will create a neomorph, hypermorph or amorph. Therefore, in our further analysis we used the ATG and Exon2 Morpholinos for injection, as they are capable of knocking down the LnpA protein.

3.4.2. *lunaparkA* Morpholino injection results in an alteration of rhombomere boundary expression and a loss of hindbrain commissural interneurons

Once the efficiency of the *lnpA* Morpholinos could be successfully demonstrated, injected embryos were next screened for possible phenotypes. As *lnpA* is expressed at the rhombomere boundaries (Figure 6), the rhombomere boundary marker *radical fringe* (*rfng*) was chosen for an initial analysis of affected gene expression. Therefore, in situ hybridisation with antisense

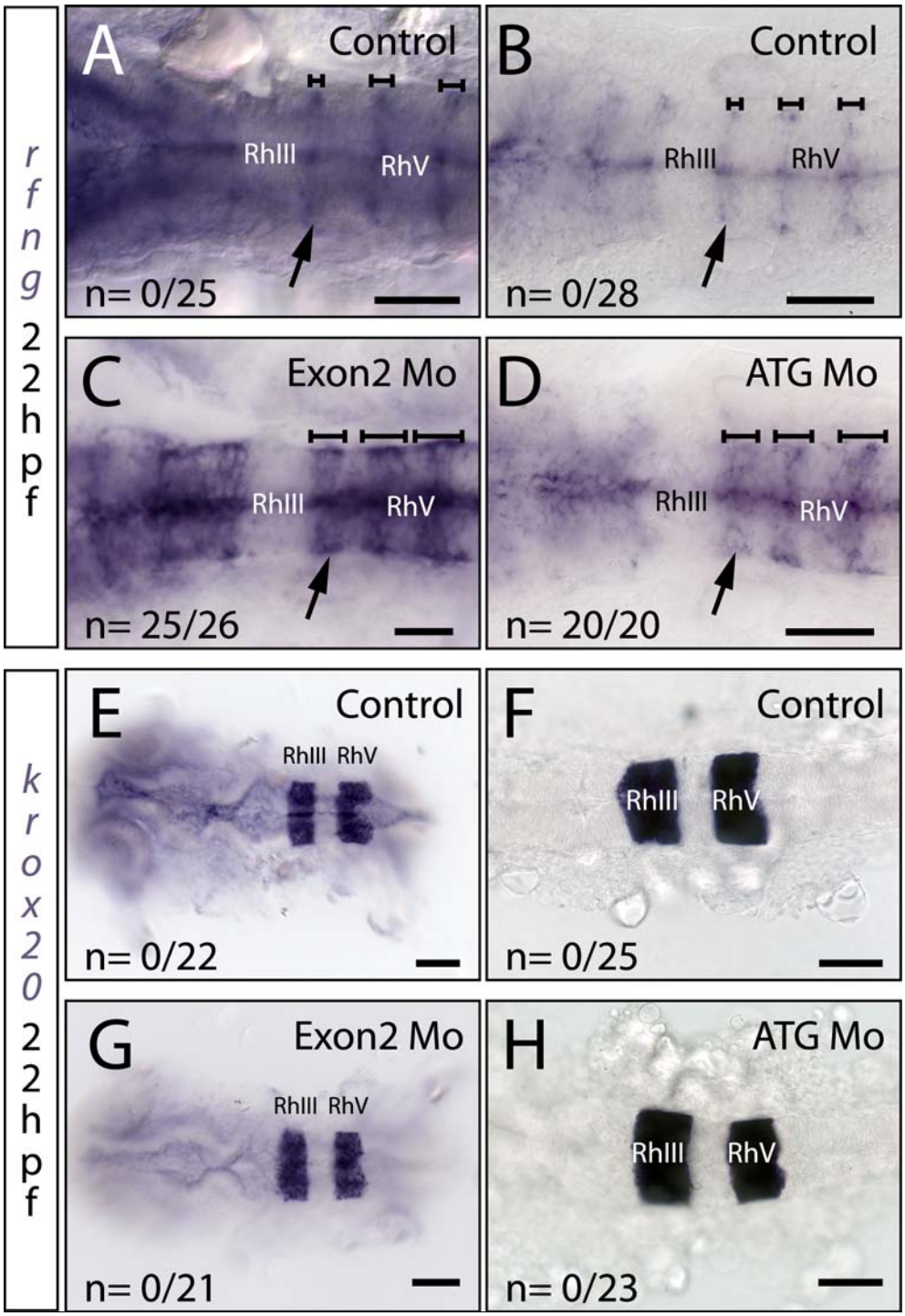

Figure 28 *lnpA* Mo injections results in an expansion of the *rfng* expression domain
A-D mRNA *in situ* hybridisation to detect *rfng* or **E-H** *egr2b* (*krox20*) gene expression on 22 hpf zebrafish embryos either control injected (**A-B**, **E-F**) ATG Mo injected (**D**, **H**) or Exon2 Mo injected (**C**, **G**). Brightfield images show an expansion of *rfng* expression domain in Morpholino injected embryos (**C-D**) (black arrows brackets), whereas *egr2b* (*krox20*) expression is unaltered in these animals, indicating that the rhombomeric organisation of the hindbrain remains intact. Scale bars 50 µm.

RNA probes against *rfng* was performed using 22 hpf embryos injected with either Exon2 Mo or ATG Mo and compared with RNase free water injected control embryos. Dorsal view images recorded by Brightfield microscopy showed an intense broadening of the *rfng* expression domain in Exon2 Mo and ATG Mo injected embryos as compared to control

(Figure 28 A-D). In contrast, the expression of *egr2b* (*krox20*), which specifically labels rhombomeres 3 and 5, was unaltered at 22 hpf in Mo-injected embryos, suggesting that the gross hindbrain morphology is normal (Figure 28 E-H) and the altered *rfng* expression represents a specific effect of downregulated *lnpA* expression. We further analysed ATG Mo injected embryos using anti-HuC/D and the Zn8 antibodies. HuC/D is expressed in postmitotic neurons, while the Zn8 antibody labels hindbrain commissural interneurons (HCI).

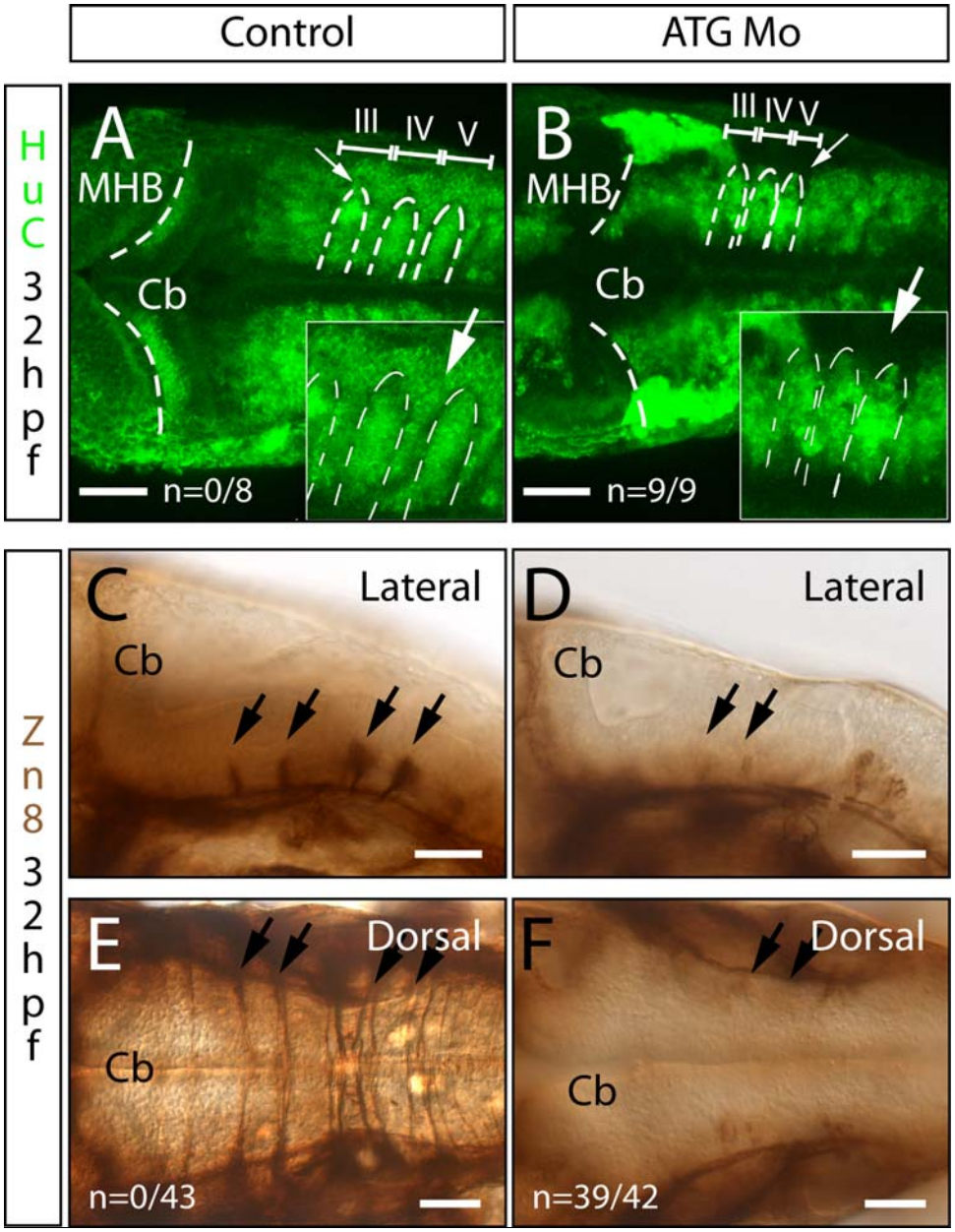

Figure 29 *lnpA* Mo injection induces loss of HCIs in injected embryos
A, **B** Maximum intensity projections of image stacks recorded by confocal microscopy from wholemount fluorescent immuno-staining against HuC/D on 32 hpf control or ATG Mo injected zebrafish embryos show the loss of the HuC/D positive neurons representing the HCI domains. **C-F** DAB (Diaminobenzidine) wholemount immuno-staining using Zn8 anti-Neurolin antibody on 32 hpf control or ATG Morpholino injected zebrafish embryos. Images show dorsal or lateral view of the hindbrain. Commissural projections are lost in embryos injected with Morpholinos. Scale bars 50 µm.

Images of ATG Mo injected embryos stained with the anti-HuC/D antibody and recorded by confocal microscopy at 32 hpf revealed that a population of post mitotic neurons normally present at the rhombomere boundaries was missing (Figure 29 A-B white arrows n=18/19). These neurons usually give rise to HCIs, and Zn8 immunostaining indeed confirmed a dramatic loss of HCIs in embryos injected with the *lnpA* ATG Morpholino (Figure 29. C-F

black arrows n=39/42). These observations opened the question why these neurons are lost. A possible explanation might be that the HCIs are unable to adopt their fate due to defects in differentiation. Alternatively, proliferation in the hindbrain may be impaired resulting in a reduction in the total number of neurons or HCIs may be lost due to enhanced apoptosis.

3.4.3. *lunaparkA* Morpholinos cause *p53* dependent apoptotic hindbrain artefacts

Morpholinos are commonly used and widely accepted platforms to study gene function by sequence-specific knockdown. During the course of this thesis, reasonable doubts arouse concerning severe undesirable off-target effects of this method (Robu et al. 2007). It was demonstrated that Morpholinos can lead to *p53*-mediated apoptosis, an effect particularly pronounced in the hindbrain. As shown above, injection of *lnpA* Morpholinos caused the loss of commissural interneurons in the hindbrain of zebrafish embryos. In addition these embryos

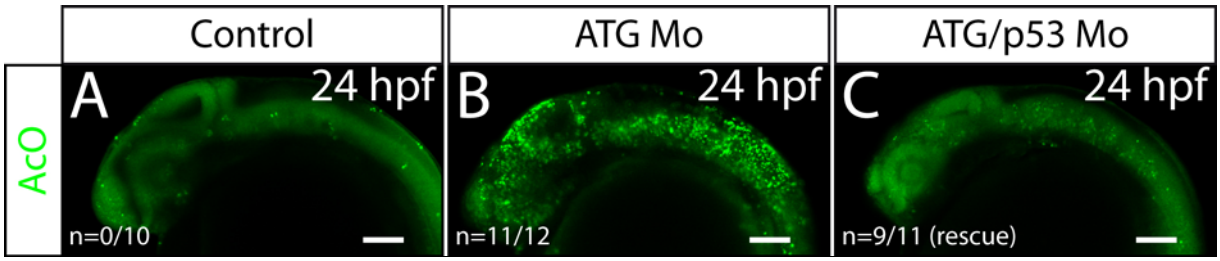

Figure 30 *lnpA* ATG Mo causes unspecific cell death in the zebrafish hindbrain

A Lateral view images recorded by confocal microscopy of 24 hpf control injected embryos and **B** embryos injected with the ATG Mo or **C** co-injected with ATG Mo and *p53* Mo. Dying cells were visualised using Acridine orange staining (AcO). Dramatic increase of cell death could be observed after injection of the *lnpA* ATG Morpholino (n=11/12). Cell death could be mostly rescued be co-injection with the *p53* Morpholino (n=9/11 rescue). Scale bars 50 µm.

showed elevated cell death in the hindbrain as revealed by acridine orange (AcO) staining (Figure 30 A, B). Therefore it was uncertain whether this was a result of the specific knockdown of *lnpA* mRNA or a non-specific side effect of the Morpholino. In order to distinguish between these two possibilities, we attempted to rescue the Morpholino-injected embryos by inhibiting *p53*-mediated apoptosis. Single cell wildtype zebrafish embryos were injected with the ATG Morpholino alone or in combination with an anti-*p53* Morpholino (*p53* Mo). These embryos were raised until 24 hpf, and then soaked in the dye acridine orange (AcO) to detect dying cells. Injection of RNase-free water was used as a control. Lateral view images recorded by confocal microscopy demonstrated that embryos injected with ATG Morpholino alone showed a dramatic increase in cell death throughout the entire CNS (Figure 30 B; n=11/12) as compared to control embryos (Figure 30 A; n=0/10). However, embryos co-injected with the *lnpA* ATG Mo and the *p53* Mo did show only mildly elevated cell death (Figure 30 C; n=9/11(rescue)), suggesting that the ATG Mo induces unspecific *p53* mediated apoptosis in the hindbrain.

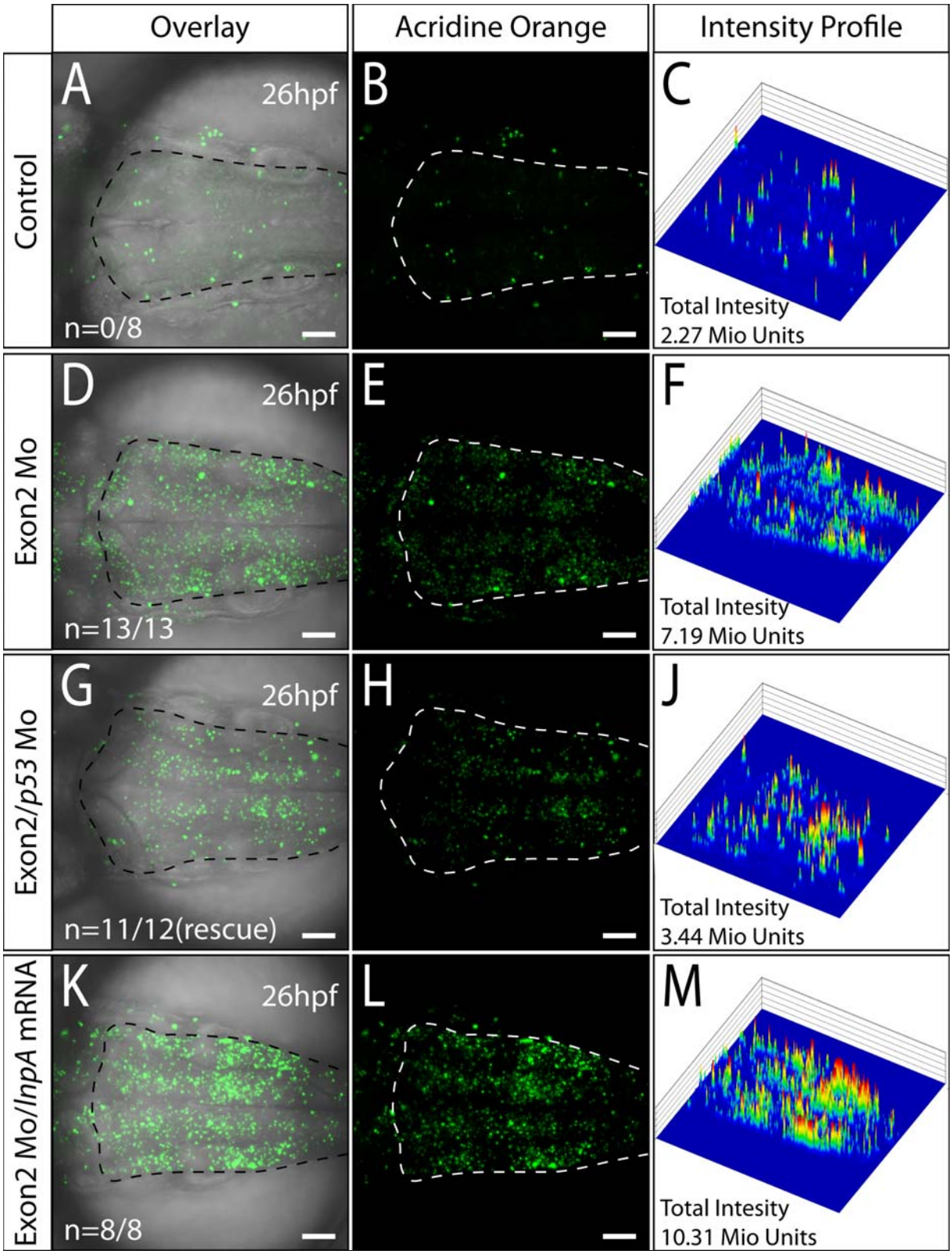

Figure 31 Injection *lnpA* Exon2 Mo induces apoptotic off target effects in the hindbrain
Maximum intensity projections of image stacks recorded by confocal microscopy of the hindbrain from **A**, **B**, control **D**, **E**, Exon2 Mo **G**, **H**, Exon2 Mo/*p53* Mo or **K**,**L**, Exon2 Mo/*lnpA* mRNA injected 24 hpf zebrafish embryos stained for cell death with acridine orange (AcO). Left panel shows the overlay of the AcO signal with the brightfield images. Middle panel shows AcO fluorescence only. **C**, **F**, **J**, **M** Intensity profiles of the AcO Signal of the maximum intensity projection displayed in the corresponding row. Peaks represent intensity of individual pixels normalised against the background. The intensities were added up to the total intensity value. Injection of Exon2 Mo increases the hindbrain AcO more than 3 fold if compared to wildtype. Co-injection of *p53* Morpholino partially rescues cell death. In contrast combined injection of Exon2 Mo and *lnpA* mRNA did not counteract the apoptotic effect. Scale bars 50 µm.

We similarly analysed if the *lnpA* Exon2 Morpholino is also inducing *p53* mediated cell death in the developing zebrafish hindbrain (Figure 31). And indeed, embryos injected with Exon2 Mo showed strong acridine orange signals and thus elevated cell death if compared to wildtype (n= 13/13). Co-injection of the *p53* Mo reversed this effect by reducing the cell death in 11 out of 12 embryos. To better illustrate the differences in the AcO fluorescent signal the image stacks of two representative embryos taken from each batch were further

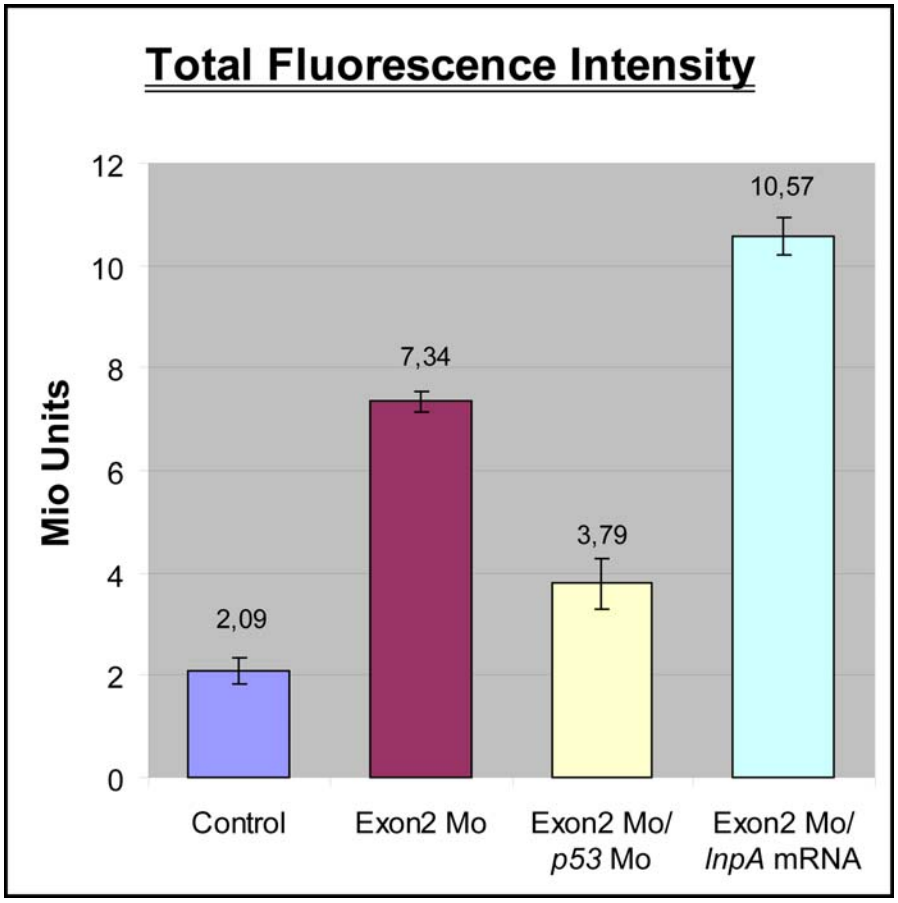

Figure 32 Summary of total intensities of Exon2 Mo-induced apoptosis
Chart shows the total intensities calculated from the intensity profiles in Figure Mo 6. Arrow bars indicate Standard deviation.

analysed with the LSM software in order to create intensity profiles of the AcO signal. The relative intensity values of every individual pixel was calculated and translated into a corresponding number of units. These units were added to obtain a total intensity values (Fig 31 C, F, J, M). The total intensity values were summarised in a diagram (Fig 32). In summary this data shows that ATG Mo and Exon2 Mo cause cell death inducing artefacts in the zebrafish hindbrain. A possible explanation for this observation could also, that knockdown of *lunaparkA* specifically induces *p53*-mediated apoptosis. To address this option, we attempted to rescue cell death that was induced by the Exon2 Mo by co-injecting *lunaparkA* mRNA. However, this rescue attempt did not result in a decrease of apoptosis but rather in an increase of cell death, further supporting the idea that the cell death is a side effect of the Morpholino and does not represent a specific phenotype caused by downregulation of *lunaparkA* expression.

Injection of the Exon3 Morpholino showed the same apoptotic phenotype as the other two tested Morpholinos (Data not shown).

In summary, these results show that three independent anti *lunaparkA* Morpholinos induce unspecific cell death in the hindbrain and that this apoptotic effect could be rescued by co-injection of the *p53* Morpholino but not by expression of *lnpA* mRNA.

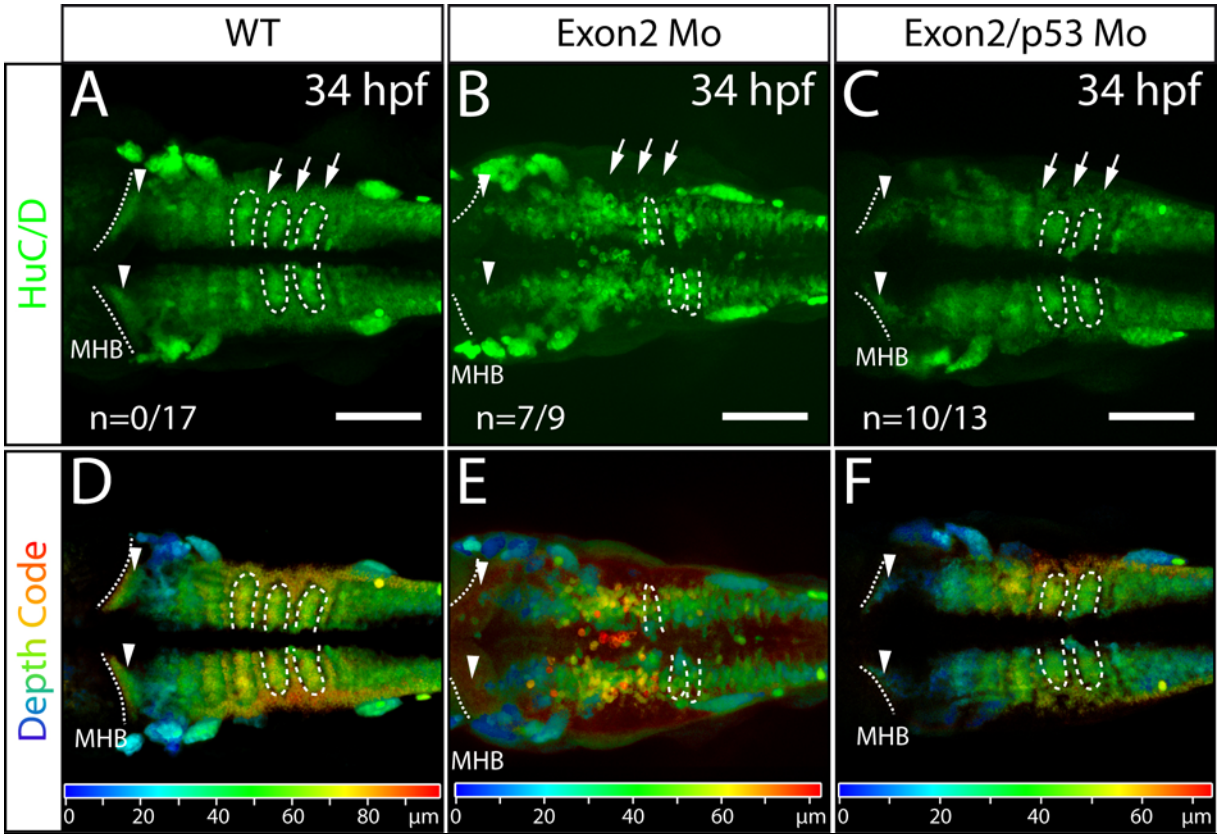

Figure 33 *lnpA* Mo-induced HCI loss is rescued by *p53* Mo co-injection

A-C Maximum intensity projections or **D-F** false coloured depth coding of image stacks recorded by confocal microscopy from wholemount embryos labelled with anti-HuC/D antibodies. Images show either control embryos (**A**, **C**) Exon2 Mo Morpholino injected (**B**, **E**) or embryos co-injected with Exon2 and *p53* Morpholino (**C**, **F**). Loss of lateral HuC/D positive neurons after *lnpA* Mo injection is reverted by co-injected *p53* Morpholino.

Although the *lnpA* Morpholinos induced non-specific cell death, the question remained as to whether the initially observed phenotypes (a broadening of the *radical fringe* domain and a loss of HCIs) were maintained following co-injection with the *p53* Mo. Therefore, wildtype zebrafish embryos were injected with RNase-free water or the Exon2 Mo, alone or in combination with *p53* Mo. After developing to 34 hpf, the embryos were fixed and processed for anti-HuC/D immunochemistry. Maximum intensity projections as well as depth coding of dorsal view image stacks show that injection of the Exon2 Mo resulted in a loss of HuC/D-expressing postmitotic neurons that are normally localised at the rhombomere boundaries (Figure 33 B, E; n=7/9). This effect was rescued by co-injection of the *p53* Morpholino (Figure 33 C, F; n=10/13). In addition Zn8 staining, that labels commissural axons, is also

reappearing after *p53* Mo mediated rescue (data not shown). Thus *p53* co-injection is able to rescue the Exon 2 Morpholino-induced loss of rhombomere boundary commissural interneurons. The same results were obtained when using the *lnpA* ATG Mo (data not shown). This suggests that the loss of HCIs is rather due to Morpholino off-target effects rather than caused by a specific knockdown of LnpA. In order to achieve a knock down of *lnpA* two address its function in development alternative strategies to Mo-injection, that are discussed below, have to be pursued

3.5. Analysis of the *lnp* enhancer strains identifies a new role for rhombomere boundaries

3.5.1. Generation and expression analysis of transgenic *lnp* enhancer reporter strains

The vertebrate hindbrain is responsible for regulating several vital functions such as respiration, circulation, and wakefulness. These functions are controlled through the activity of intricate arrays of neuronal circuits and connections (Narita and Rijli 2009). The

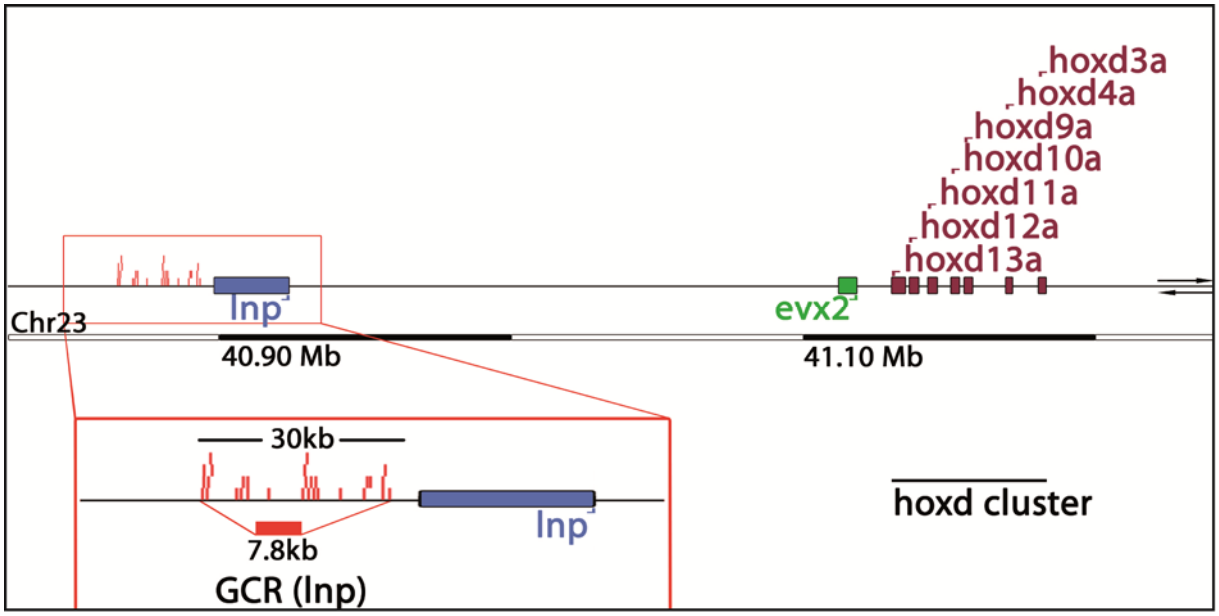

Figure 34: The GCR and the genomic organisation of the *hoxd* cluster are conserved in zebrafish

Ensembl zebrafish genomic blast of the Fugu 7.8 kB GCR/*lnp*-enhancer. The *hoxd* cluster and the *evx2* and *lnpA* gene show a highly conserved genomic organisation in comparison to other vertebrate species.

establishment of ordered patterns of neuronal specification, migration, and axonal topographic connectivity during development is crucial to build such a complex network of circuits and functional synapses in the mature hindbrain (Narita and Rijli 2009). The early development of the vertebrate hindbrain proceeds according to a fundamental metameric partitioning along the antero-posterior axis into cellular compartments known as rhombomeres. The rhombomeric organisation has a strong impact on the anterior posterior organisation of

neurogenesis during the early hindbrain development (Ray and Dymecki 2009). In addition, it is well understood, that dorso ventral migration e.g. emanating from the dorsal rhombic lip has a great influence on the generation of neurons within the hindbrain (Krumlauf et al. 1993; Lumsden and Krumlauf 1996; Moens and Prince 2002).

We wondered how the migration processes and the metameric organisation are interfering. We therefore used the zebrafish as a model to address this question. Zebrafish in vivo neuro-imaging in combination with a growing number of tissue specific gene regulatory elements gives the possibility to observe these processes.

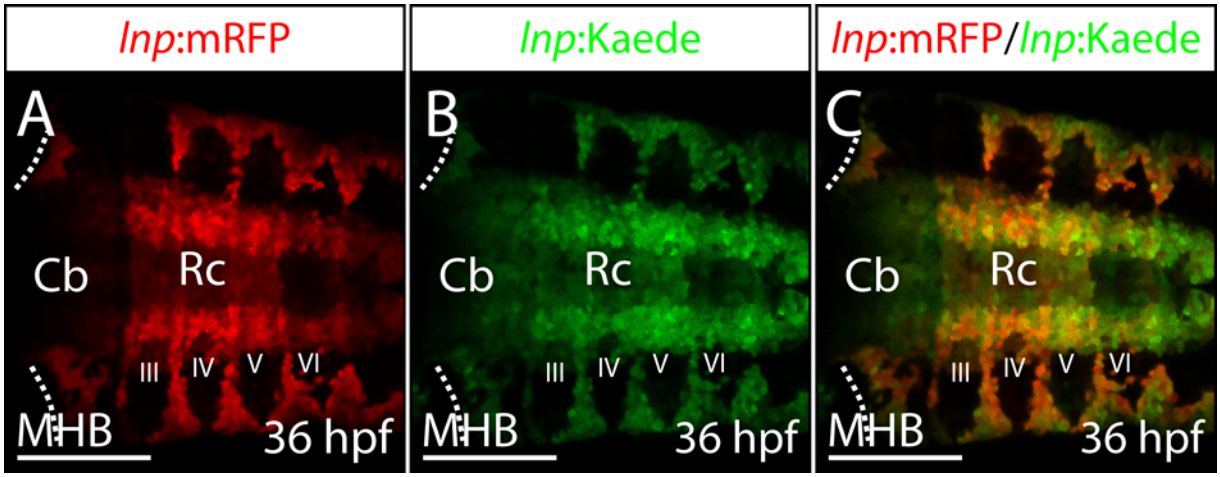

Figure 35 *lnp*:mRFP and *lnp*:Kaede transgenic embryos show identical expression patterns

A-C Comparison of the expression pattern of *lnp*:mRFP and *lnp*:Kaede embryos. Images show dorsal projections of image stacks recorded by confocal microscopy of *lnp*:mRFP/*lnp*:Kaede double transgenic embryos. Scale bars 100 µm

Recently, a 7.8 kB enhancer fragment was isolated from the pufferfish *Tetraodon nigroviridis* (Figure 34). The enhancer is conserved throughout vertebrates and known to act as a global control region (GCR) of the *hoxd* cluster and two other genes, *even-skipped homeobox2* (*evx2*) and *lunapark* (*lnp*) (Spitz et al. 2003; Gonzalez et al. 2007; Spitz and Duboule 2008). From reporter studies in transgenic mice, it is known that the isolated Tetraodon enhancer drives expression in a pattern resembling that of *evx2* and *lunapark* transcripts and therefore specifically in the central nervous system (Spitz et al. 2003).

We first analyzed whether the GCR is also conserved in zebrafish by performing an Ensembl blast search on the zebrafish genome using the sequence of the Tetraodon enhancer element. The 7.8 kB fragment mapped to zebrafish chromosome 23 in close proximity to the *hoxd* cluster directly upstream of *lunapark,* showing a synthenic organisation compared to other vertebrate species (Figure 34) and thus suggesting a conserved function for this regulatory region (Spitz et al. 2003). To test the conservation of gene regulation we generated transgenic zebrafish strains driving expression of different fluorescent reporter proteins by this

regulatory element. The 7.8 kB fragment was cloned in front of the minimal promoter E1b,

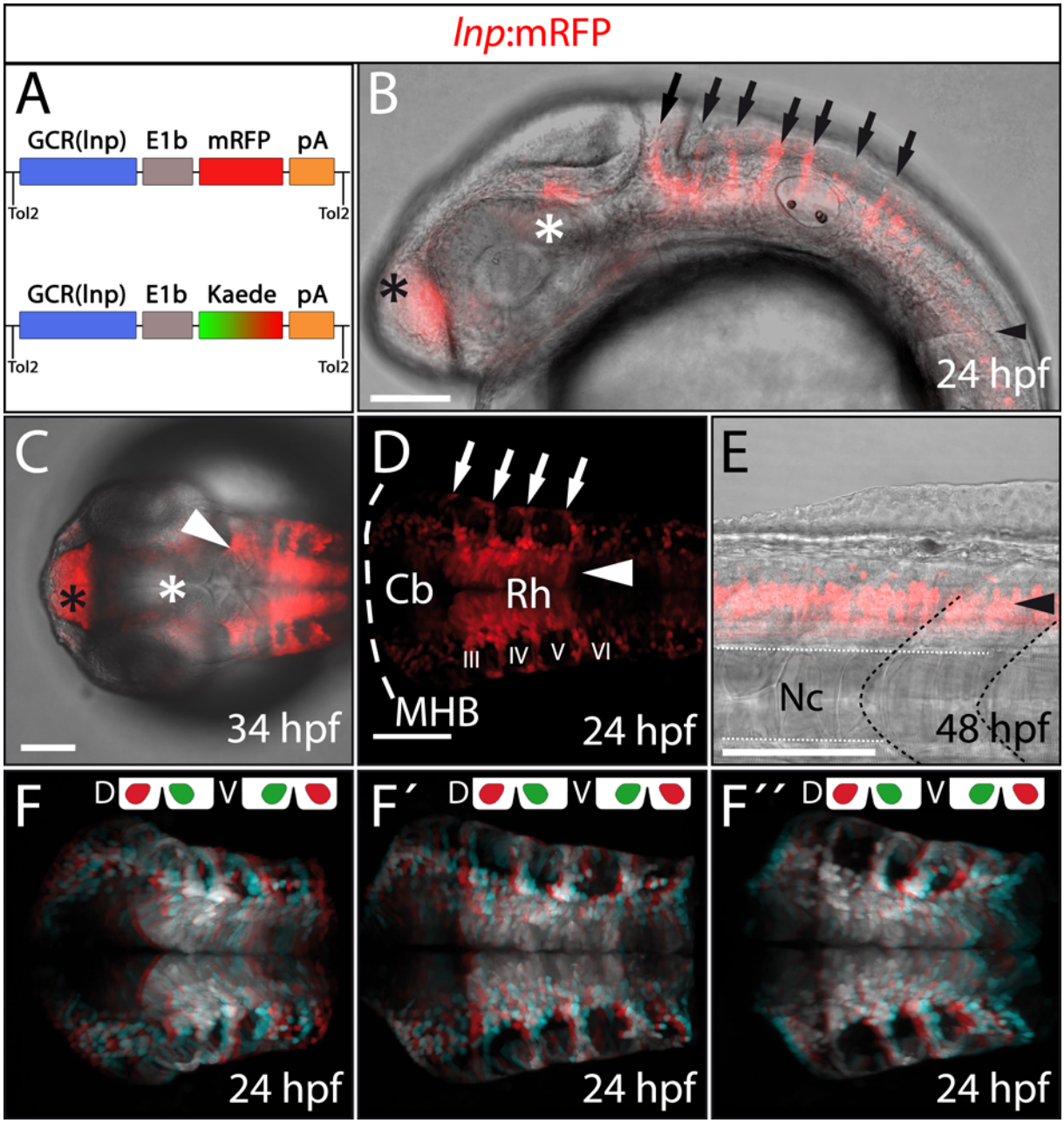

Figure 36 Expression pattern of the transgenic *lnp* enhancer reporter strains
A Schematic representation of constructs used to generate the transgenic *lnp*:mRFP and *lnp*:Kaede lines. **B** Lateral view of *lnp*:mRFP embryo at 24 hpf and dorsal view of the head of a 34 hpf *lnp*:mRFP transgenic animal. mRFP expression was detected in the telencephalon (black asterisks), the tectum (white asterisks), in the cerebellum , in iterative stripes in the hindbrain (arrows), in two broad longitudinal patterns along the ventral midline (white arrowheads) and in neurons of the spinal cord (black arrowhead).
C, **D** Maximum intensity projections of images recorded from the forebrain and the hindbrain of a 24 hpf *lnp*:mRFP embryo which show expression in iterative stripes in the hindbrain (white arrows).
E Lateral view image of the trunk recorded by confocal microscopy of a 48 hpf *lnp:*mRFP embryo shows reporter expression in spinal chord interneurons (black arrow).
F-F'' 3D anaglyph images computed from image stacks recorded by confocal microscopy of a 24 hpf *lnp*:mRFP expressing zebrafish embryo. Images from 3 different angles show the boundary restriction and the bow like architecture of the lateral *lnp*:mRFP expressing cells. Red/green goggles required. Dorsal or ventral view depends on orientation of goggles as indicated in figure. Abbr.: Cb cerebellum; D dorsal; MHB midbrain-hindbrain boundary; Nc notochord; Rh rhombenchephalon; V ventral. Scale bars 100 µm

followed by a cDNA expression cassette followed either mRFP or Kaede and flanked with inverted repeats of the Tol2 transposon (Figure 36 A). Both constructs were injected in combination with *Tol2* transposase mRNA into single cell zebrafish embryos (Kawakami et al. 1998; Kawakami and Shima 1999; Kawakami 2004), resulting in two stable transgenic lines expressing either mRFP or Kaede under the control of the GCR. Due to the expression pattern, which was comparable to endogenous *lnp,* and the close genomic proximity of the GCR to the *lnp* gene in the zebrafish genome, we termed the strains *lnp*:mRFP and *lnp*:Kaede. The two transgenic lines showed identical expression patterns (Figure 35), with strong reporter gene expression starting at 22 hpf in the telencephalon (Figure 36 B, C black asterisks), tectum (Figure 36 B ,C white asterisks), hindbrain (Figure 36 B, D arrows) and neural tube interneurons (Figure 36 E arrowhead). In the hindbrain, two characteristic expression domains were present. Running along either side of the ventral midline, a broad longitudinal pattern could be observed (Figure 36 D white arrowheads) and from the anterior cerebellum to the most posterior rhombomere 7, seven thin dorso-ventral stripes of two to three cell widths were observed (Figure 36 B ,D arrows). Three dimensional anaglyph images show that these lateral iterative stripes form a bowlike structure running from dorsal to ventral at the outer neuroepithelium (Figure 36 F-F'').

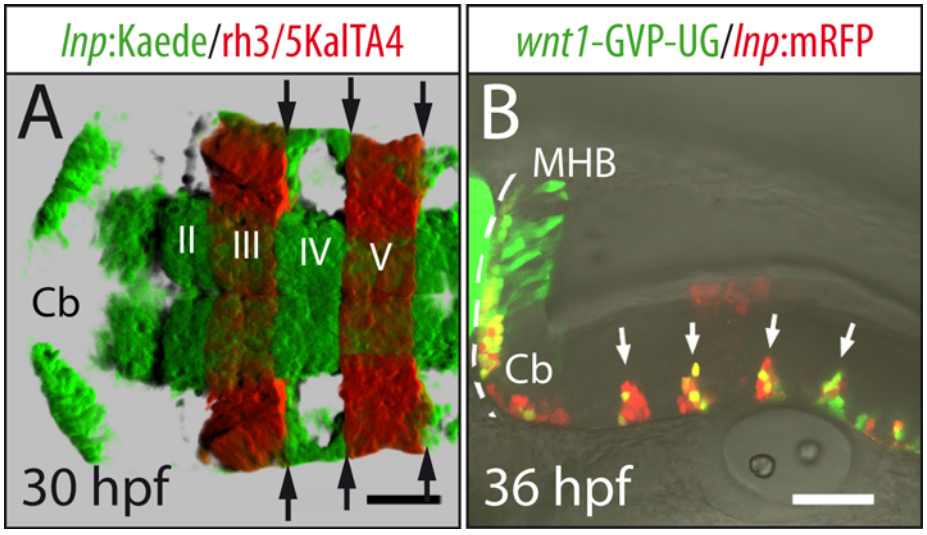

Figure 37 Reporter gene expression of transgenic *lnp* enhancer reporter strains along rhombomere boundaries.
A 3D reconstruction of a dorsal view of an image stack recorded by confocal microscopy of a 30 hpf *lnp*:Kaede/rh3/5 KalTA4/UAS:cherry double transgenic embryo **B** *wnt1*-enhancer mediated GFP expression co-localises with that *lnp*:mRFP expression at the rhombomere boundaries. Scale bars 50 µm.

To further analyse the cells in the iterative vertical stripes in the hindbrain, carriers of the *lnp*:Kaede transgene were crossed with a fishes of a transgenic strain expressing mCherry under the control of the *egr2b* (*krox20*) enhancer element *Tg*(*rh3/5*:KalTA4)hzm1, and thus showing red fluorescence exclusively in rhombomeres 3 and 5 (Distel et al. 2009; Nikolaou et

al. 2009). 3D-reconstruction of an image stack recorded by confocal microscopy from a 30 hpf double transgenic *lnp*:Kaede/rh3/5:KalTA4 embryo shows that the vertical rows of cells expressing the fluorescent reporter mRFP under the control of the *lnp* enhancer are located along rhombomere boundaries (Figure 37 A, black arrows).

Due to the fact that *lnp*:mRFP expressing cells in the cerebellum resembled in their localisation the recently characterised pattern of GFP positive cells in embryos of the transgenic *Tg(wnt1:GVP-UG)* strain (Volkmann et al. 2008) and that Wnt1 expression is a marker for rhombomere boundaries (Amoyel et al. 2005), we generated *lnp*:mRFP/*wnt1*:GVP-UG zebrafish embryos (Figure 37 B). Lateral view images recorded by confocal microscopy of 36 hpf embryos show a clear co-expression of the *wnt1*-enhancer driven GFP expression and the *lnp*:mRFP expressing cells in the cerebellum and along the rhombomere boundaries. The co-localisation of mRFP and GFP in both the cerebellum and along rhombomere boundaries suggest that *lnp* and *wnt1*-expressing cells display a similar developmental behaviour, while also providing further evidence that the *lnp*:mRFP cells of the lateral hindbrain domains are located at the rhombomere boundaries.

Although rhombomere boundary cells have previously been characterised by their expression of *wnt1*, these cells arise earlier during hindbrain development and are located further ventrally than the *lnp*:mRFP or *wnt1*- enhancer driven GFP expressing cells (Amoyel et al. 2005; Nikolaou et al. 2009). In addition, embryos of the *wnt1*:GVP-UG strain do not show GFP expression throughout the entire rhombomere boundaries, as seen with endogenous *wnt1* expression. This suggests that the *wnt1* enhancer used for generating this strain does not fully activate the entire endogenous expression domains of *wnt1*. Thus, it is unlikely that *lnp*:mRFP cells are rhombomere boundary cells themselves, but rather represent a later developing cell type that is specifically positioned along rhombomere boundaries.

3.5.2. *lnp*:mRFP cells differentiate into postmitotic interneurons of the sensory system and show a high diversity in their axonal projections.

Our expression analysis in embryos of the *lnp*:mRFP and *lnp*:Kaede lines showed that fluorescence expression was present at the rhombomere boundaries, but the identity of the expressing cells remained unclear. At 24 hours, the major brain compartments have formed in the developing zebrafish and cells start to differentiate into neurons. However, a large proportion of cells within the hindbrain still remain in a progenitor state. These cells divide symmetrically or asymmetrically and show some glial features, such as fibre formation and GFAP expression, and are therefore known as radial glia cells (Kageyama et al. 2005). They

are positioned in the dorsal germinal areas, whereas differentiated neurons can be found in the ventral part at the rhombomere boundaries and in the centre of each rhombomere. The

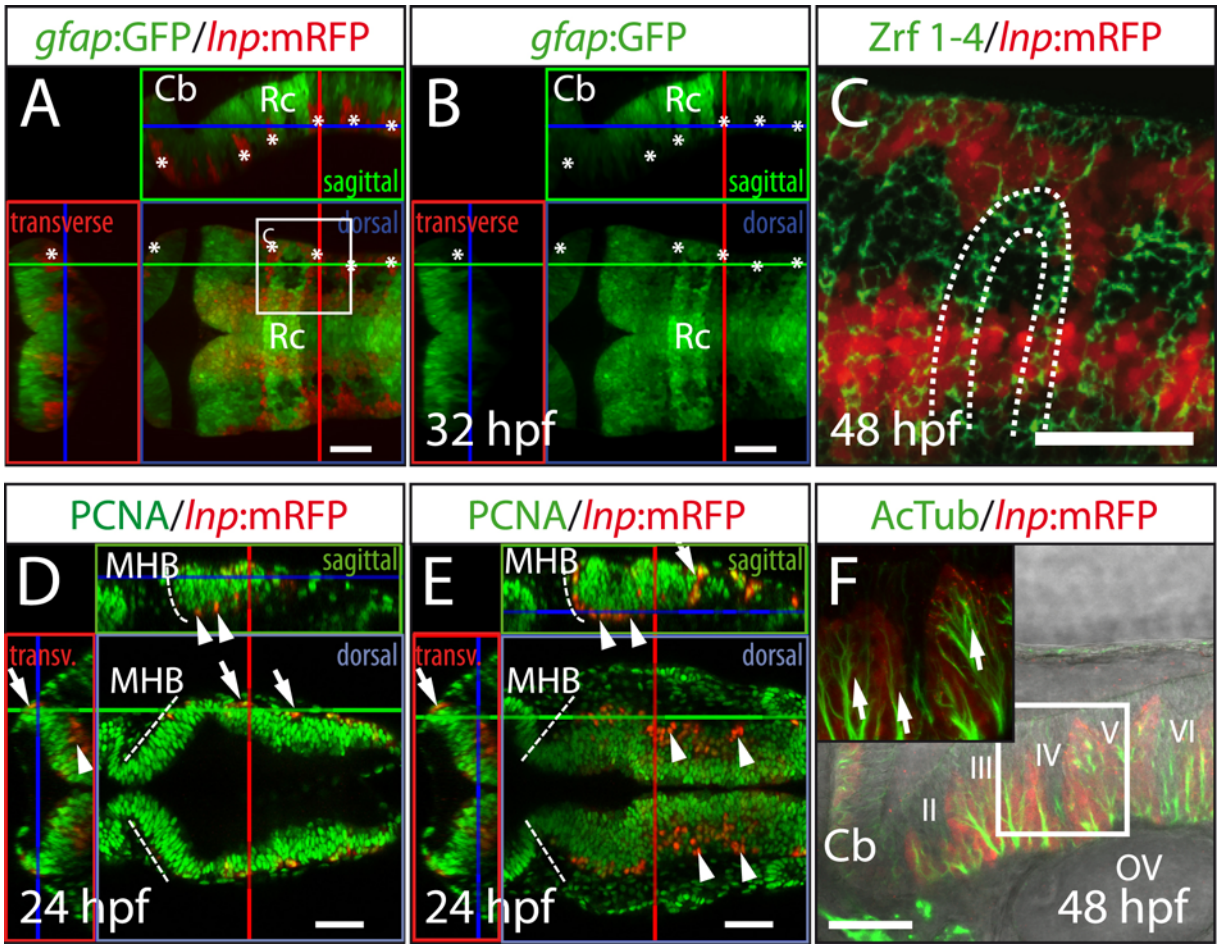

Figure 38 *lnp* enhancer driven mRFP expression is not localised in dorsal radial glia cells and does not co-localise with the expression of the proliferation marker PCNA
A, **B** Dorsal (blue box), sagittal (green box) and transversal (red box) digital sections of an image stack recorded by confocal microscopy of a *gfap*:GFP/*lnp*:mRFP double transgenic embryo at 32 hpf, coloured lines indicate the section plane shown in the corresponding box. Expression of GFP and mRFP (asterisk) were mutually exclusive and showed no co-localisation. **C** Dorsal view of the hindbrain of an 48 hpf *lnp*:mRFP transgenic embryo immuno-stained with a Zrf 1,2,3,4 antibody cocktail and anti-RFP recorded by confocal microscopy. Image was recorded from an area indicated by the white box in figure (**A**).
D, **E** Digital sections of image stacks recorded by confocal microscopy of *lnp:*mRFP expressing embryos at 24 hpf immunostained with anti-PCNA antibody. Coloured lines indicate section planes shown in the corresponding box. Except for few of the dorsal most cells (arrows) mRFP does not overlap with PCNA (arrowheads). **C** Lateral confocal image of a *lnp*:mRFP embryo at 48 hpf stained with anti ac-Tubulin antibody shows that the *lnp*:mRFP domains are interspersed with axonal tracks (arrows). (Inset: magnification of boxed area). Scale bars 50 µm.

neurons in the rhombomere centre are separated from those at the boundaries by a layer of fibres forming a curtain emerging from the dorsal radial glia progenitors (Trevarrow et al. 1990). Regarding the primarily ventral location of the cells expressing mRFP under control of the *lnp* enhancer it is unlikely that they are a part of the radial glia population, which is positioned more dorsally. To further exclude this possibility, carriers of the *lnp*:mRFP line were crossed into a *gfap*:GFP transgenic background. Image stacks recorded by confocal microscopy of these double transgenic embryos showed that the *lnp*:mRFP expression domain

is excluded from the *gfap*:GFP labelled region (Figure 38 A, B). Furthermore, immunolabelling using a cocktail of Zrf 1-4 antibodies, which visualise the curtain-forming fibres emerging from radial glia cells, was performed (Figure 38 C dotted lines) on 48 hpf lnp:mRFP embryos. Images recorded by confocal microscopy revealed that the mRFP expressing cells were located outside of this area and are therefore not radial glia cells.

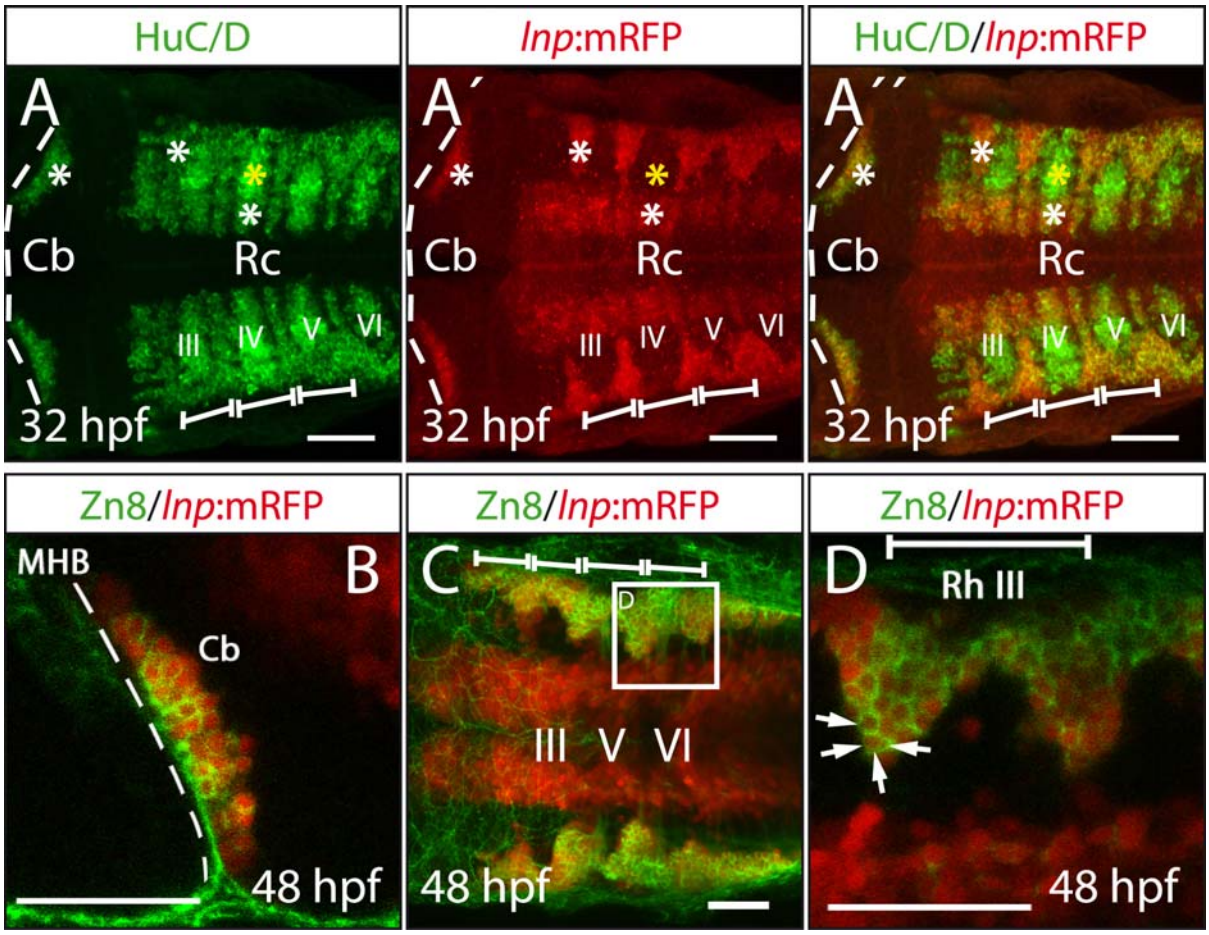

Figure 39 *lnp*:mRFP expressing cells different into hindbrain commissural interneurons (HCIs) of the sensory system.
A-A'' ** Maximum intensity projections of dorsal image stacks recorded by confocal microscopy of double immunolabeling with anti-HuC/D and anti-RFP antibodies on *lnp*:mRFP embryos at 32 hpf show a complete overlap of mRFP and HuC/D signals in the hindbrain. **B-D Whole-mount immunostaining in 48 hpf *lnp*:mRFP embryos using the anti-Neurolin antibody (Zn8). Images show a dorsal cerebellar half (**B**) the rhombencephalon (**C**) and a magnification of the region indicated by the white boxed area in figure (**C**) (**D**). mRFP expressing cells in the cerebellum and at the rhombomere boundaries co-express Neurolin as indicated by Zn8 antibody staining (white arrows). Scale bars 50 µm

In addition, the majority of the *lnp*:mRFP expressing cells have already exited the cell cycle, as they could not be labelled with the anti-PCNA antibody at 24 hpf (Figure 38 D, E). Only the few dorsal-most *lnp*:mRFP expressing cells (Figure 38 D arrows), which are located in close proximity to the upper rhombic lip, were found to be PCNA positive. This overlap decreases during ongoing development (Figure 50). Taking together, these results suggest that the *lnp*:mRFP expressing cells are born during early hindbrain development, and that they have already at 24 hpf started to differentiate into neurons.

In order to prove the neuronal differentiation of *lnp*:mRFP expressing cells, several antibody stainings were performed. Labelling of neuronal processes and axonal tracts in the hindbrain of 48 hpf *lnp*:mRFP zebrafish embryos using an anti-acetylated tubulin (α-T) antibody (Chitnis and Kuwada 1990) revealed that the mRFP expression domains are invaded by axons (Figure 38 F). Additionally, all *lnp*:mRFP expressing cells in the hindbrain were positive for HuC/D (Elav1) expression, identifying them as postmitotic neurons (Figure 39 A-A'', white asterisk). (Marusich et al. 1994; Okano and Darnell 1997; Wakamatsu and Weston 1997).

To address the question of the neuronal identity of the *lnp*:mRFP expressing cells, the *lnp*:mRFP line was crossed into the *Isl-1*:GFP transgenic line (Higashijima et al. 2000) or stained with the Znp-1 antibody (Trevarrow et al. 1990; Fox and Sanes 2007; Pagnon-Minot et al. 2008). Neither the double transgenic embryos nor the Znp-1 antibody stainings in *lnp*:mRFP showed an overlap of the two fluorescent signals, concluding that *lnp*:mRFP is not expressed in hindbrain motoneurons (Data not shown).

As described above *lnp*:mRFP expressing cells are located at the rhombomere boundaries. For that reason they might be commissural interneurons of the sensory system which are known to be localised at the rhombomere boundaries (Trevarrow et al. 1990). Therefore, *lnp*:mRFP embryos were labelled with the Zn8 antibody to detect Neurolin (Alcama /DM-Grasp), a cell adhesion molecule of the immunoglobulin superfamily (Fashena and Westerfield 1999) expressed in the rhombencephalon by commissural interneurons that receive sensory input from the auditory and lateral line system (Sassa et al. 2007). Dorsal view image stacks recorded by confocal microscopy of Zn8 antibody staining on 48 hpf *lnp*:mRFP transgenic embryos showed a clear overlap of the two signals at the lateral rhombomere boundaries (Figure 39 C, D white arrows). Thus, *lnp*:mRFP expressing cells differentiate into hindbrain commissural interneurons (HCIs). However, the mRFP expressing domain along the ventral midline did not show Neurolin expression, indicating that the medial cells have a different identity and maybe also a different origin. Interestingly, the *lnp*:mRFP expressing cells in the cerebellum also showed co-expression of Neurolin (Figure 39 B), underscoring the close relationship to their rhombomeric counterparts, as already shown by the *wnt1*:GFP co-expression.

Neurolin expressing HCIs form a complex meshwork of axonal projections in the zebrafish hindbrain (Trevarrow et al. 1990). Previous studies showed that these neurons project commissural axons and either terminate on the contralateral side of the hindbrain or turn rostrally after crossing the ventral midline to join a single longitudinal fascicle, which projects to the midbrain torus semicircularis. The strong fluorescence detected by either antibody staining or by fluorescent protein expression in the transgenic embryos precluded any analysis

of the axonal trajectories (Sassa et al. 2007). In order to better understand the network formed by the axons, the cell bodies of *lnp*:Kaede expressing cells at adjacent rhombomere

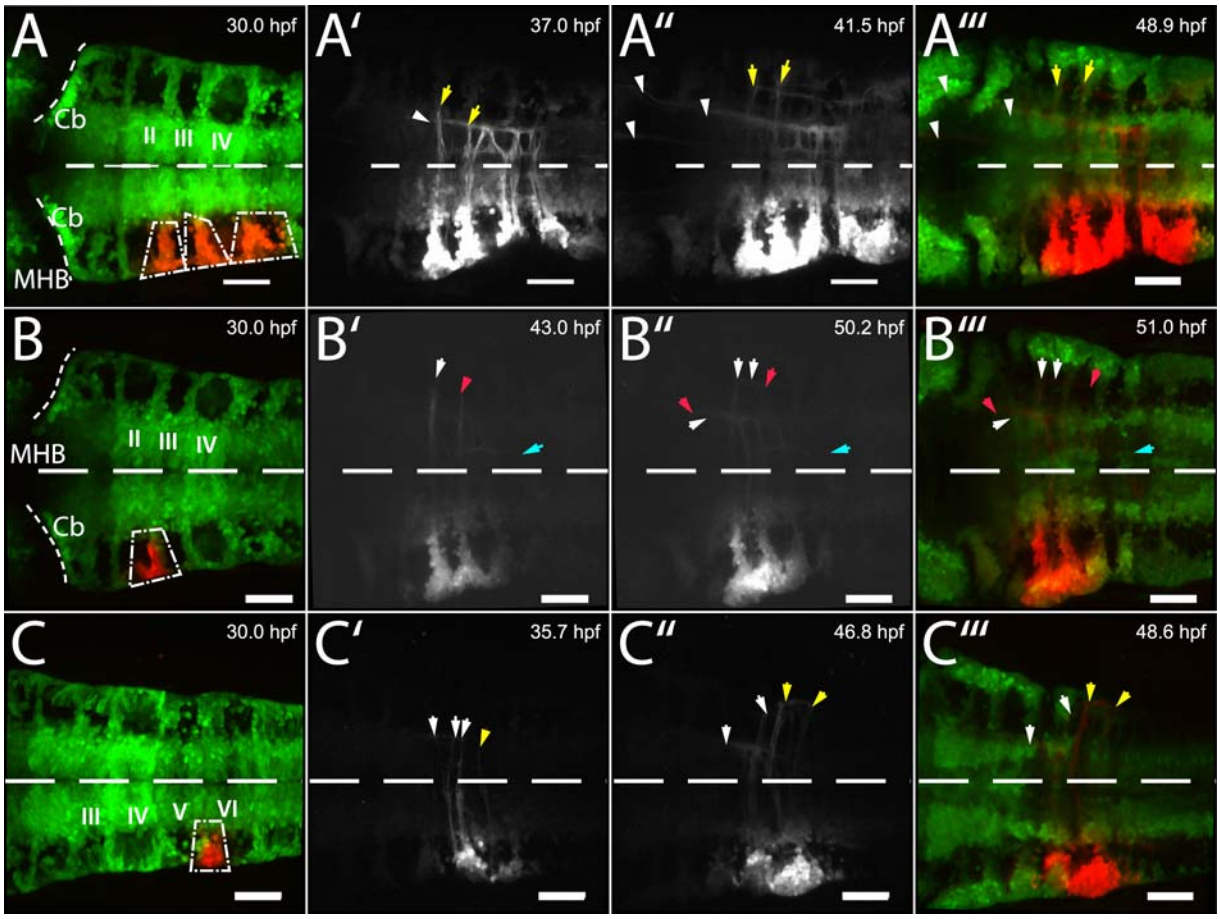

Figure 40 Axonal projections of *lnp:*Kaede expressing commissural interneurons

A-C’’’ Dorsal view projections of image stacks recorded by confocal microscopy of *lnp:*Kaede embryos. Cells at multiple (**A**) or individual rhombomere boundaries (**B-C**) have been repetitively converted by UV laser light excitation in areas indicated by dotted rectangles and recorded over time. Images were extracted from movie sequences that can be found in the supplementary material as follows **A:** Suppl. Movie1; **B:** Suppl. Movie2; **C:** Suppl.Movie3. Arrows indicate axonal growth cones. Scale bars 50 µm.

boundaries on one side of the embryo were converted from green to red fluorescence using UV light excitation. Outgrowth of the colour converted axons was subsequently followed by confocal microscopy time-lapse imaging (Movie 3). In the resulting movies, it could be observed that the axons grew in bundles and crossed the midline without exception. In addition, axons extending from neurons at one particular boundary always projected to their contralateral counterpart (Movie 3-5). Some axons left the commissural tract at certain exit points and followed at least 3 different longitudinal fascicles (Figure 40 A-A’’’ arrows). The medial and the medio-lateral fascicle project rostrally to midbrain target areas of the torus semicircularis (Movie 3 white arrowheads). The axons in the very lateral tracts only extend over short distances connecting HCI clusters in adjacent rhombomere boundaries. In contrast to earlier findings, axons that projected caudally were also detected (Movie 4, Figure 40 B-

B''' blue arrow). Some of these axons first targeted the contralateral side before turning caudally, growing over the rhombomere and its boundaries to connect with adjacent boundary neurons (Movie 5, Figure 40 C-C''' yellow arrows). Other axons followed the medial fascicle directly after crossing the midline.

Summarizing these results, it can be concluded that the projection pattern of the HCIs is far more complex than initially postulated. Although these cells migrate and differentiate together into commissural interneurons, they do not form a homogenous neuronal population. HCIs rather represent a conglomerate of co-developing commissural interneurons with very different efferents and connectivities.

3.5.3. HCIs are derived from the rhombic lip

During early development the hindbrain neuroepithelium is separated into two different proliferative zones: the ventrally localised ventricular zone (VZ) and the dorsally positioned rhombic lip (RL). These two areas are molecularly defined by the mutually exclusive bHLH transcription factors: Ptf1a, which is exclusively expressed in the VZ (Lin et al. 2004; Zecchin et al. 2004; Volkmann et al. 2008; Elsen et al. 2009) and Atonal1, which is only present in the rhombic lip (Köster and Fraser 2001a; Adolf et al. 2004). Each of these defined regions gives rise to distinct neuronal populations of the hindbrain. Strikingly, in the cerebellum *lnp*:mRFP expressing cells co-express *wnt1* and Neurolin (Figure 37 B), and these cells have recently been identified as immature neurons of the tegmental hindbrain nuclei of the secondary gustatory/viscerosensory system derived from the *atonal1a*-expressing cerebellar rhombic lip (Volkmann et al. 2010). This suggests that *lnp*:mRFP expressing HCIs are also derived from the hindbrain rhombic lip *atonal1* expressing lineage, which correlates with the finding that PCNA co-expressing *lnp*:mRFP expressing cells are only present in dorsal hindbrain regions.

To further confirm that the *lnp*:mRFP expressing HCIs indeed arise from the rhombic lip and not the ventricular zone, we generated double transgenic *lnp*:mRFP/*ptf1a*:GFP and triple transgenic *lnp*:mRFP/*atoh1a*:KalTA4/UAS:GFP zebrafish embryos. Images recorded using confocal microscopy revealed that *lnp*:mRFP expressing cells were excluded from the *ptfa1*:GFP expressing ventricular zone (Figure 41 A). In contrast, GFP expressing mediated by the *atonal1a* enhancer (Figure 41 B,C) co-localised with the HCIs located at the rhombomere boundaries. This overlap could be observed starting at 24 hpf (not shown). At that time point, GFP expression was distributed all over the rhombic lip and only a few GFP expressing cells occupied the boundaries. These boundary cells were positive for mRFP expression. With ongoing embryogenesis, the *atonal1a* enhancer mediated GFP expression

becomes more and more restricted to the boundaries, and as a consequence the overlap between mRFP and GFP expression increased (Figure 41 B-C). At 48 hpf, GFP expressing cells were exclusively found at the boundaries and co-expressing mRFP (data not shown).

Taken together, these results show that HCIs are derived from the *atonal1a*-expressing rhombic lip in the dorsal hindbrain and that they differentiate into ventral commissural interneurons. This suggests that HCIs migrate from dorsal to ventral, a behaviour characteristic of many rhombic lip derived neurons.

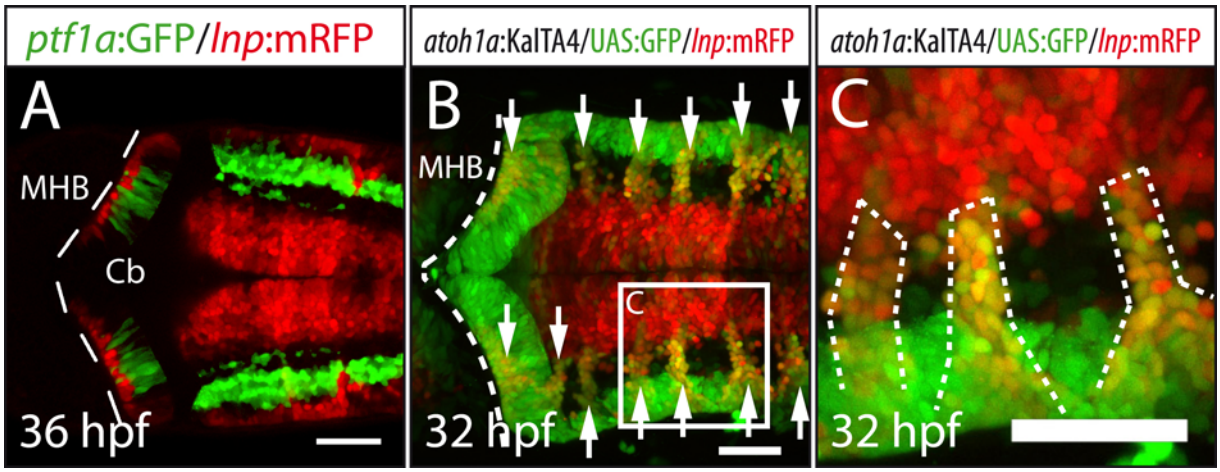

Figure 41 Hindbrain Commissural Interneurons (HCIs) are derived from the hindbrain lower rhombic lip

A HCIs are excluded from the ventricular zone as demonstrated by projections of image stacks recorded by confocal microscopy of 36 hpf *ptf1a:*GFP/ *lnp:*mRFP embryos **B**, **C** Projection of dorsal view image stacks recorded by confocal microscopy of triple transgenic *atonal1a*:KalTA4/ *lnp*:mRFP/ UAS:GFP embryos at 48 hpf show co-localisation of GFP and mRFP expression at the rhombomere boundaries. (**C**) is a higher magnification of the boxed area in (**B**). Scale bars 50 µm.

3.5.4. HCIs migrate along the rhombomere boundaries to ventral target regions

Previous studies in the mouse have shown that *math1*, the mouse homologue of *atonal1,* is required for central and peripheral components of the proprioceptive, vestibular and auditory sensory network. Lineage tracing showed that the Math1-expressing LRL progenitors follow dorso-ventral extramural migratory routes within the posterior hindbrain in order to form

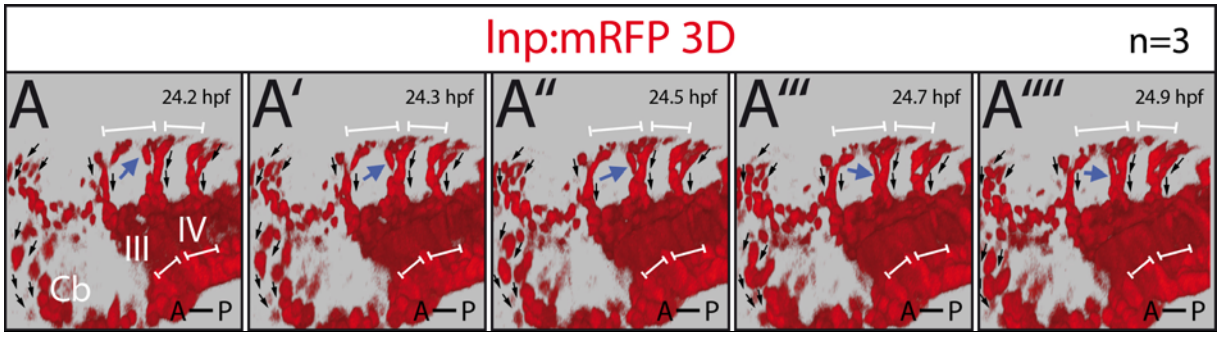

Figure 42 HCIs show dorso-ventral migration behaviour

A-A’’’’ 3D reconstruction of image stacks recorded by confocal microscopy over time from the hindbrain of a *lnp*:mRFP expressing transgenic embryo (Suppl. Movie4). Images show individual time points. Black arrows depict the general migration routes the blue arrow shows an individual migrating cell. (Lateral view slightly twisted around the x axis.).

precerebellar and auditory nuclei located in the ventral hindbrain (Wingate 2001; Wang et al. 2005; Millimaki et al. 2007; Maricich et al. 2009; Rose et al. 2009b).

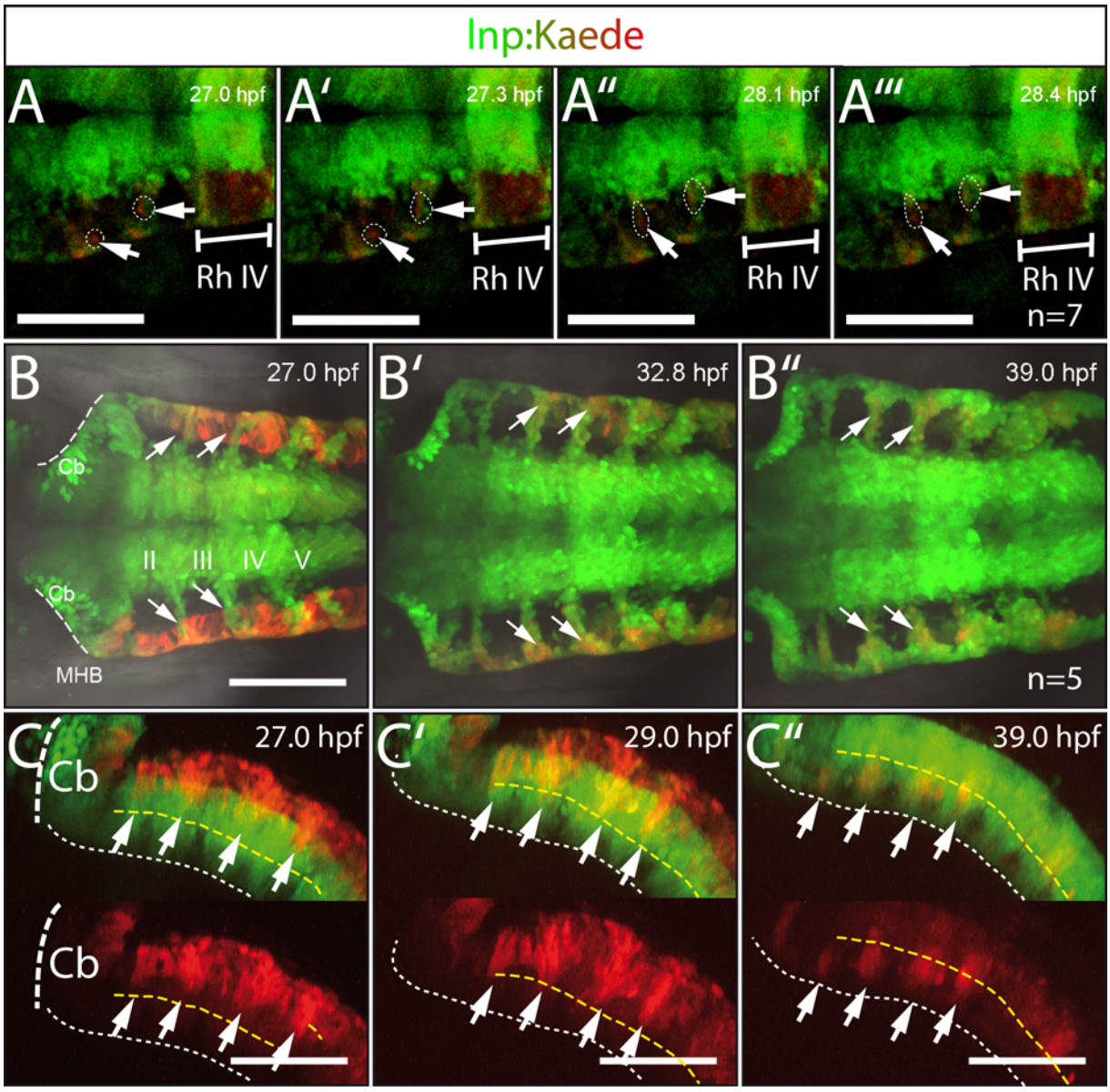

Figure 43 HCIs migrate from dorsal the rhombic lip to ventral regions of differentiation by following narrow and distinct routes along the rhombomere boundaries

A-A''' Dorsal view image stacks recorded over time of a *lnp:*Kaede embryo with clusters of cells converted using a UV laser at 24 hpf in the dorsal hindbrain. Images show different time points of Suppl. Movie5. Converted cells (dotted circles; white arrows) migrate along the rhombomere boundaries from dorsal to ventral in a bow like stream.

B-B'' Dorsal view projections of image stacks recorded by confocal microscopy of a *lnp*:Kaede expressing embryo. The dorsal population of Kaede expressing cells was converted by UV radiation at 24 hpf and migration of the cell population was monitored over time. Images show different time points of Suppl. Movie6

C-C'' Lateral view projections of confocal image stacks of a *lnp*:Kaede embryo. The dorsal population was converted by UV light excitation at 24 hpf. Images show individual time points taken from Suppl. Movie7. Dashed yellow line indicates dorso-ventral midline of the hindbrain. (Upper panel shows overlay of red and green Kaede fluorescence. Lower panel shows red channel only).

Earlier studies in our laboratory (Volkmann et al. 2010) demonstrated that *wnt1*/*atonal1a*-expressing cells in the cerebellum show intense cerebellar rhombic lip derived dorso-ventral migration behaviour, similar but prior to granule cell precursors (Volkmann et al. 2008;

Rieger et al. 2009). Considering the findings in mouse and in the zebrafish cerebellum, it can be assumed that developing neurons of the *atonal1a* lineage in the zebrafish rhombencephalon also undergo extensive migratory processes.

In order to directly observe the predicted ventral migration of HCIs, we performed in vivo time lapse analysis using embryos from transgenic lines with *lnp* enhancer driven fluorescent reporter protein expression. As shown above, HCIs represent progeny of the *atonal1a* expressing positive cells in the hindbrain, and 4D reconstructions of 24 hour dorsal confocal image recordings from *lnp*:mRFP zebrafish embryos revealed that the *lnp*:mRFP expressing HCIs are in fact generated across the entire lower rhombic lip. They initially converge towards the rhombomere boundaries, where they form a highly dynamic stream following a narrow extramural bow-like tangential path along the individual rhombomere boundaries (Movie 6, Figure 42). Similar to the lineage derived from atonal expressing cells in mouse, HCIs follow an extramural route, but in zebrafish they do so in a pattern that is strictly segmented and confined to rhombomere boundaries.

Due to the strong mRFP fluorescence and the tight chain-like migration of HCIs, it is difficult to distinguish individual cells using the *lnp*:mRFP line. Thus, to image the migration of individual HCIs, small clusters of expressing cells in the hindbrain of *lnp*:Kaede transgenic embryos were converted from green to red fluorescence using a restricted illumination by UV laser at 405 nm, and confocal images were recorded over time (Movie 7, Figure 43 A). These in vivo data demonstrated that HCIs indeed migrate from dorsal to ventral in a bowlike structure along the outer neuroepithelium. After being born at locations throughout the lower rhombic lip, HCI progenitors converge towards the rhombomere boundaries and then travel ventrally. The migration stream is especially narrow during this initial phase, covering only 1-2 cell diameters in width (Movie 7, Figure 43 A). Migrating HCIs finally reach their targets close to ventral midline where longitudinal *lnp*:Kaede expression domains are located. Here they stop, begin to differentiate terminally and send out commissural axons.

From the initial analysis, it was still unclear as to whether the entire *lnp*:Kaede expressing cell population in the dorsal hindbrain migrates ventrally along rhombomere boundaries or whether some cells remain in dorsal positions. Therefore, the dorso-lateral expression domain of 27 hpf *lnp*:Kaede embryos was completely UV-converted from green to red. Subsequently, dorsal view confocal image stacks were recorded over time and the data was processed to obtain 3D anaglyph images of the red channel (Movie 8), dorsal view maximum intensity projections of the green and the red signals (Movie 8; Figure 43 B) and lateral projections of both signals (Movie 9; Figure 43 C). The resulting movies show that every converted cell

migrated ventrally along rhombomere boundaries to populate the ventral HCI clusters and none of the cells remained in dorsal positions.

These results demonstrate that HCIs are derived from the dorsal *atonal1a* expressing rhombic lip. While they emigrate from the rhombic lip, they become postmitotic start to express neuronal markers and migrate to their ventral target regions where they terminally differentiate into clusters of commissural interneurons of diverse projection patterns.

Rhombomere boundaries are known to act as local signalling centres with inductive properties and as physical borders preventing interchange of cells between adjacent rhombomeres (Cheng et al. 2004; Baek et al. 2006; Kageyama et al. 2008). Our time lapse data assigns a new role to rhombomere boundaries being of pathways for directed cell migration.

3.6. Regulation

3.6.1. Notch signalling is active in *lnp*:mRFP expressing HCIs

Above it has been shown, that HCIs are born throughout the rhombic lip, but then they strictly follow a migratory pathway along rhombomere boundaries, during which they also undergo differentiation. A question that is now arising is which molecular signalling processes could be active within the rhombic lip that coordinates the migration and differentiation of HCIs? Notch signalling is one pathway that is known to be involved in many developmental processes. The most important role is perhaps the regulation of cell fate decision and progenitor maintenance (Lewis 1998; Bray 2006). In the developing central nervous system, cells with active Notch signalling suppress proneural genes and keep neuronal progenitors in a proliferative state. Therefore we wondered if Notch signalling is involved in regulating the cell fate decision between differentiation and progenitor maintenance also in *lnp*:mRFP HCIs in the lower rhombic lip.

Tp1bglob:GFP transgenic embryos indicate cells in which Notch signalling is active by expressing GFP under control of Notch responsive elements (Parsons et al. 2009). Therefore, double transgenic *lnp*:mRFP/Tp1bglob:GFP embryos were generated to address the state of Notch signalling in *lnp*:mRFP expressing cells. Confocal sections of the double transgenic embryos recorded at different time points revealed co-expression of GFP and mRFP in HCIs along their entire pathway of differentiation. Already at 24 hpf, co-expression could be observed in dorsal hindbrain regions (Figure 44 A). This correlates with the onset of HCI emigration from the rhombic lip. Overlap of the two fluorescent signals continued until 48 hpf along the rhombomere boundaries and in ventral regions, where HCIs terminally differentiate

(Figure 44 B-D white arrows). The delay between Notch mediated activation of the reporter

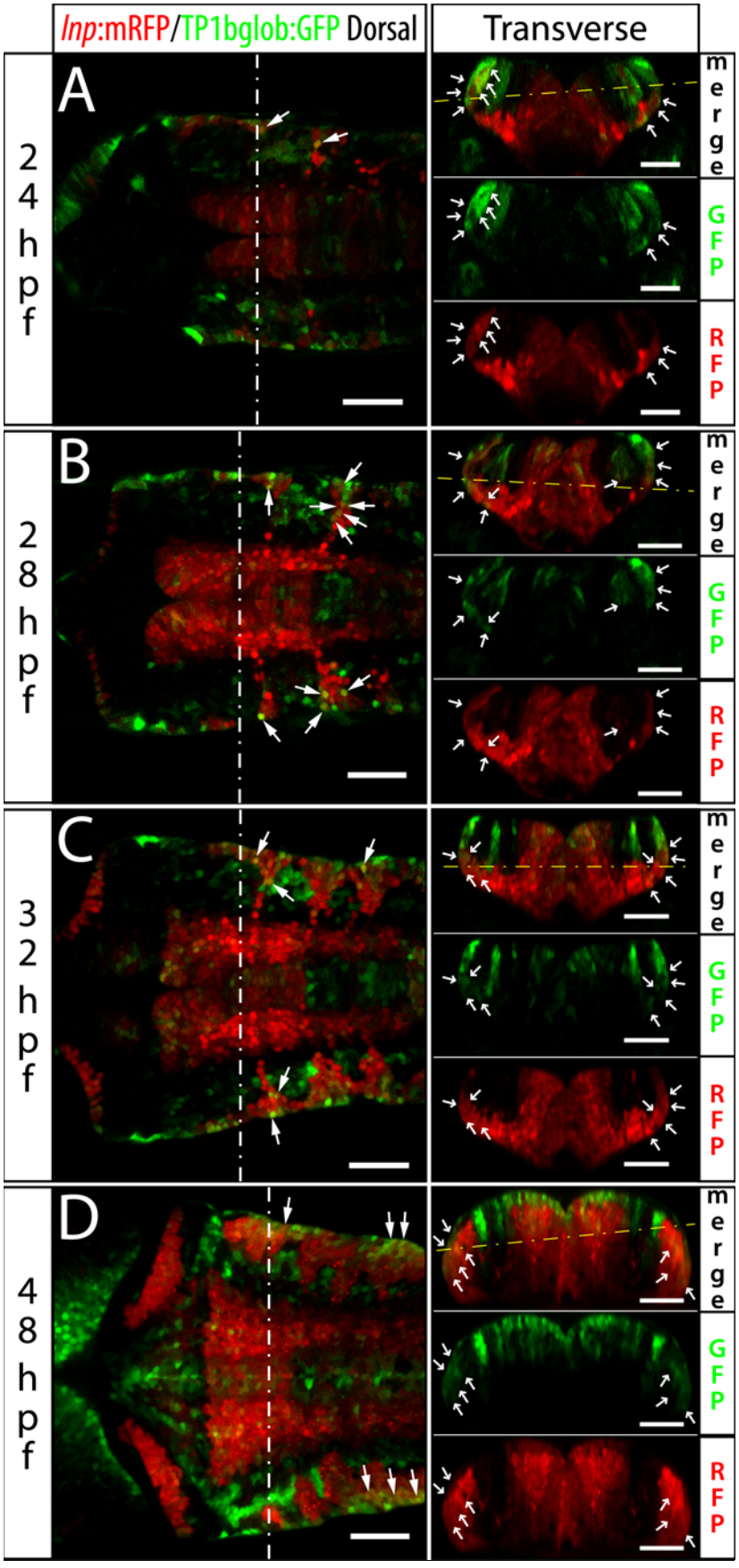

Figure 44 Notch signalling is active in *lnp*:mRFP expressing HCIs
A-D Image stacks recorded by confocal microscopy (dotted circles; white arrows) of double transgenic *lnp*:mRFP/Notch reporter line (TP1bglob:GFP) at indicated stages. Right panel: dorsal view, single plane. Left panel: digital transverse sections. White arrows mark cells with overlapping mRFP and GFP expression. Dashed white line indicates section plane of transverse figures; dashed yellow line indicates position of dorsal section plane. Scale bars 50 µm.

and the first GFP fluorescence signal as well as the high stability of GFP does not allow to precisely delineate the time course of active Notch signalling in *lnp*:mRFP expressing HCIs, but these findings nevertheless reveal that HCIs receive Notch signal transduction during their time course of development.

3.6.2. Inhibition of Notch signalling impairs HCI differentiation

To address the function of Notch during HCI development, the influence of conditional Notch inhibition on these cells was analysed. 24 hpf *lnp*:mRFP expressing embryos were incubated either in the γ-Secretase inhibitor DAPT or with DMSO as control. The inhibitor blocks cleavage of the Notch receptor intracellular domain (NICD) and the subsequent transcriptional activation of target genes (Geling et al. 2002). At 48 hpf, the embryos were fixed and HCIs were visualised by immunohistochemistry using the Zn8 antibody. Dorsal view confocal image stacks were recorded from the embryos and displayed as dorsal or lateral maximum intensity projections (Figure 45).

Compared to DMSO control embryos (n=44), DAPT-treated embryos showed a dramatic loss of *lnp*:mRFP-expressing HCIs, particularly in the more anterior rhombomeres (Figure 45 A-D, n=34/35, dashed white circles). Moreover, as shown by the Zn8 antibody staining, Neurolin-expressing commissural interneurons were completely absent in the anterior rhombomeres and severely reduced in posterior rhombomeres in the ventral hindbrain of DAPT-treated embryos (Figure 45 A'-D', n=34/35, dashed white circles). In rhombomere 4, some remaining mRFP and anti-Neurolin positive HCIs could be observed. This most likely reflects the fact that this rhombomere is the first one to develop and therefore may have escaped the full effect of DAPT-mediated inhibition of Notch signalling (Maves et al. 2002).

In order to demonstrate the successful inhibition of Notch signalling during HCI development, double transgenic *lnp*:mRFP/*Tp1bglob*:GFP embryos were incubated in either DMSO alone or DAPT for 24 hours starting at 24 hpf. Dorsal view confocal image stacks were recorded and displayed as maximum intensity projections (Figure 46). In contrast to DMSO treated control fish, the GFP reporter expression was almost entirely lost in DAPT-treated embryos (Figure 46 A,C). In addition, a specific lack of *lnp*:mRFP HCI cells in anterior and posterior rhombomeres was observed (Figure 46 B, D).

It is possible that DAPT causes general cell death and an unspecific loss of HCIs, rather than mediating a direct effect through Notch inhibition. To eliminate this possibility, we assayed for cell death using the dye Acridine Orange (AcO) (Figure 47). *lnp*:mRFP expressing

embryos were treated with DMSO or DAPT as described above and then stained with AcO at

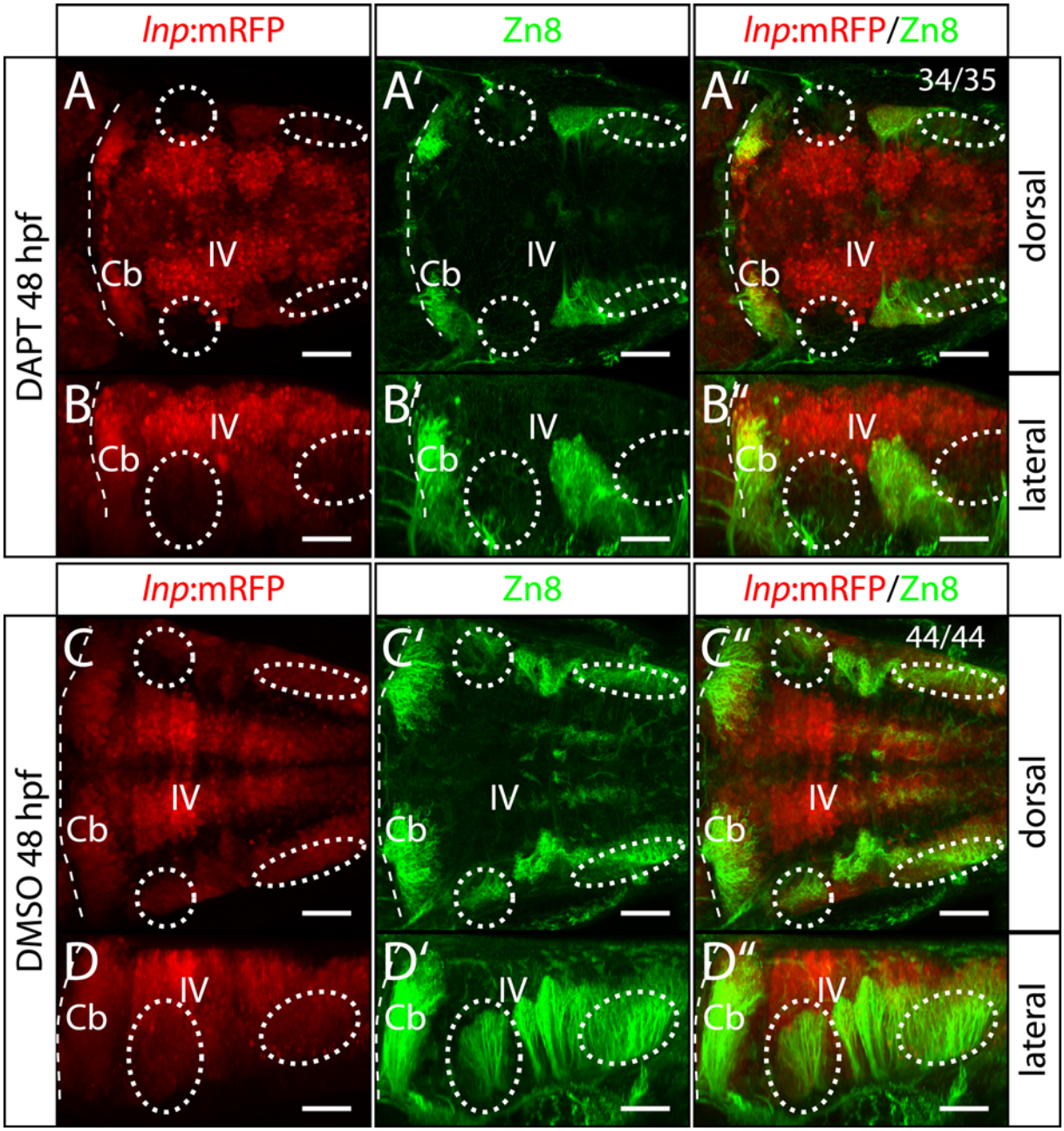

Figure 45 Hindbrain commissural interneurons fail to differentiate upon inhibition Notch signal transduction
Whole-mount immunostainings with anti-RFP and Zn8 antibody of 48 hpf *lnp:*mRFP embryos. Images show **A**, **C** dorsal and **B**, **D** lateral projections of confocal image stacks. Embryos were treated with **A**, **B** DAPT or **C**,**D** DMSO starting at 24 hpf. DAPT treated embryos showed a severe loss of HCIs in areas indicated by dashed ovals. Scale bars 50µm.

28 hpf or 48 hpf. Cells showing intense AcO derived fluorescence (i.e. dying cells) were counted in the hindbrain using images recorded using a confocal microscope. Comparison of the individual values revealed that no increase in cell death could be detected DAPT in treated embryos versus controls (Figure 47). Thus the lack of HCIs is not a result of enhanced cell death, but rather a consequence of the specific inhibition of Notch signalling. In summary,

these findings suggest that Notch signalling is responsible for the generation or differentiation of hindbrain commissural interneurons.

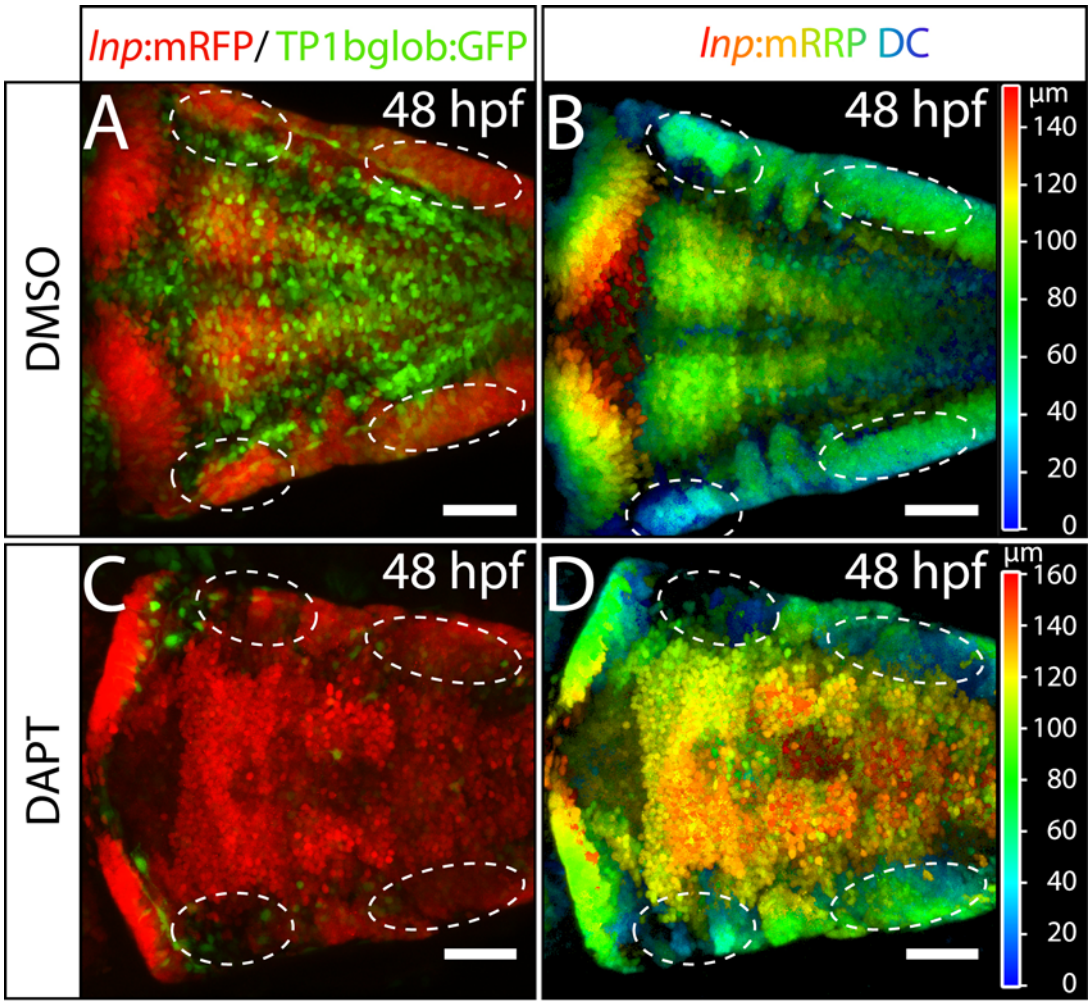

Figure 46 DAPT deactivates Notch signalling in the zebrafish hindbrain

A-D Dorsal view image stacks recorded by confocal microscopy of *lnp*:mRFP/TP1bglob:GFP double transgenic embryos at 48 hpf. Treated with **A-B** DMSO or **C-D** DAPT for 24 h starting at 24 hpf. **A**, **C** Images show maximum intensity projections of mRFP and GFP expression and **B**, **D** pseudo coloured depth coding of mRFP fluorescent signal (dotted circles depict affected areas). Scale bars 50 µm.

3.6.3. HCI progenitors are not maintained after DAPT-mediated Notch inhibition

lnp:mRFP expressing HCIs are derived from the *atonal1a*-expressing rhombic lip and these neurons are lost as a consequence of Notch inhibition. But what happens to the rhombic lip progenitors of the *lnp*:mRFP expressing cells? In order to address this question, 24 hpf *atoh1a*:KalTA4/UAS:GFP embryos were incubated with DAPT for 24 hpf. Dorsal view confocal image stacks of these embryos demonstrated that the GFP expression was lost in the anterior and posterior rhombomeres of DAPT-treated embryos (Figure 48 B,B' dashed circles; n=81/82) as compared to animals treated with DMSO only (Figure 48 A,A' dashed circles; n=157/157). In addition, the absence of differentiated HCIs could be confirmed by immunostaining with the Zn8 antibody (Figure 48 A,A'' & B,B'' dashed circles). Consistent

with the results obtained from the DAPT treatment of *lnp*:mRFP expressing embryos, some differentiated HCIs in rhombomere 4 could still be observed, but they were positioned more

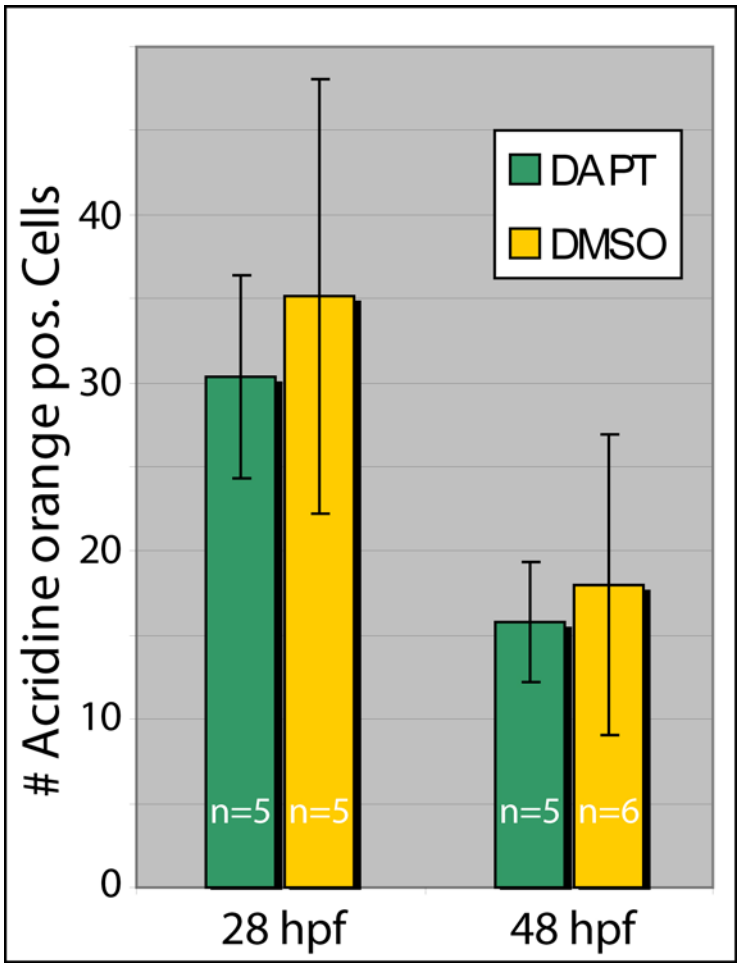

Figure 47 DAPT treatment does not cause increased apoptosis in the hindbrain
Zebrafish embryos treated with DMSO or DAPT for 24 h starting at 24 hpf were analysed for cell death in the hindbrain by acridine orange staining followed by observation with a confocal microscope. Acridine orange positive cell were counted and the results were summarised in the graph. An increase in cell death could not be observed in zebrafish embryos treated with DAPT compared to DMSO treated control embryos (n=5).

dorsally than in controls, as demonstrated by depth coding analysis of the confocal image stacks. Furthermore, these neurons projected their axons ectopically. Rather than crossing to the contralateral side across the ventral floorplate, axons from rhombomere 4 of DAPT-treated fish grew across the dorsal midline (Figure 48 B'-B'').

This suggests that Notch signalling in the hindbrain is important for several steps of HCI differentiation: First, it is required to maintain *atonal1a*-expressing HCI progenitors inside the rhombic lip. Second, it is necessary to mediate HCI migration along rhombomere boundaries to ventral positions in the hindbrain.

3.6.4. Activation of Notch impairs HCI differentiation by prolonged progenitor state maintenance

DAPT-mediated inhibition of the Notch signal transduction pathway inhibited differentiation of HCIs. To address the effects of a prolonged activation of Notch signalling, we generated triple transgenic *atoh1a*:KalTA4/UAS:GFP/UAS:NICD embryos, which express GFP and the

Notch intracellular domain (NICD) under the control of *atonal1a* enhancer-activated Gal4.

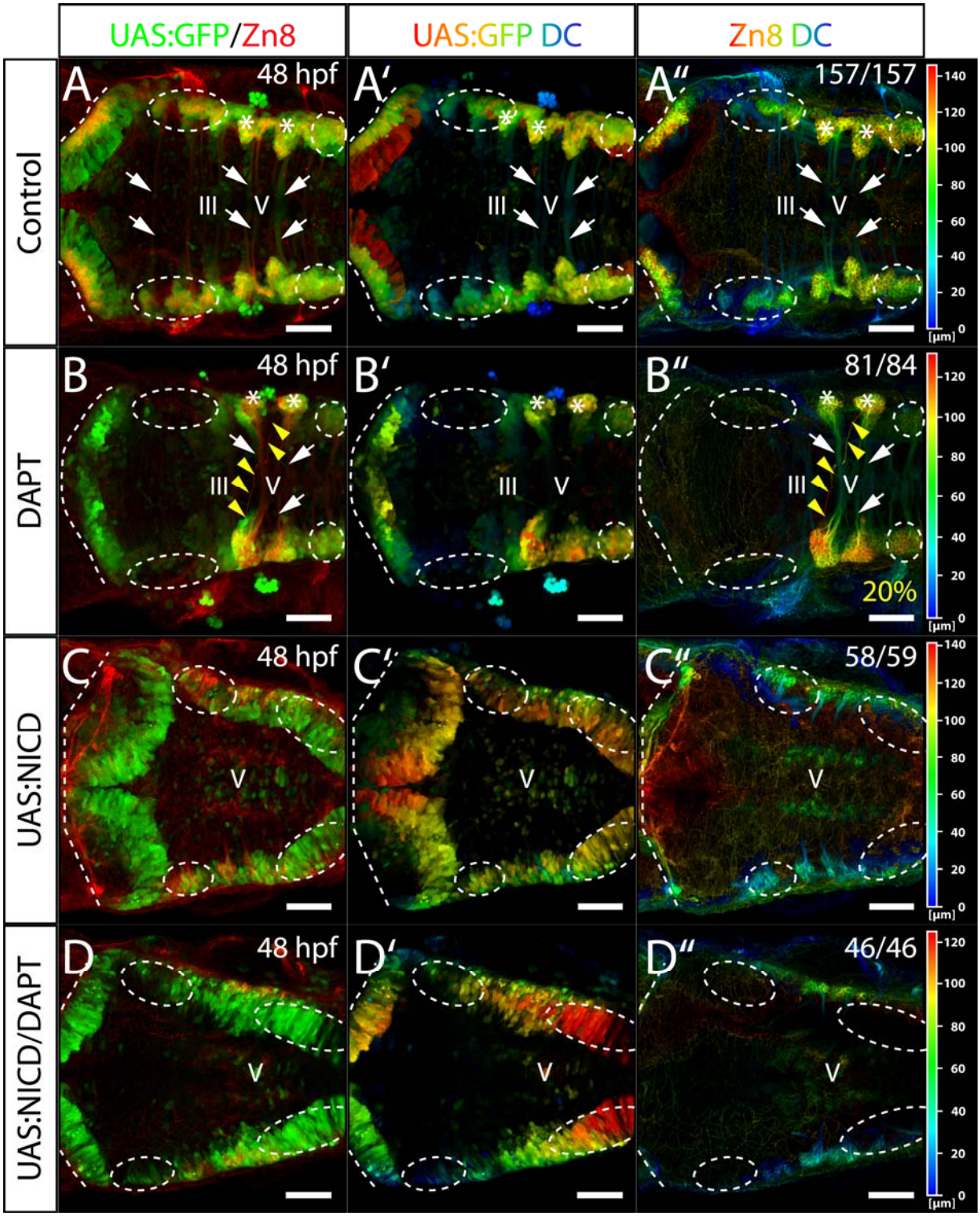

Figure 48 Continuous activation or conditional inhibition of Notch signalling in rhombic lip cells impairs differentiation and migration of HCIs

A-D'' Immunostainings using Zn8 antibody in 48 hpf *atonal1a*:KalTA4/UAS:GFP transgenic zebrafish embryos crossed into **A-B''** WT or **C-D''** UAS:NICD transgenic background treated with **A-A''**,**C-C''** DMSO or **B-B''**,**D-D''** DAPT. Images show merge of confocal image stacks of the red Zn8 and the green GFP fluorescence (dorsal view) (**A**, **B**, **C**, **D**) pseudo coloured depth coding (DC) image of GFP fluorescence (**A'**, **B'**, **C'**, **D'**) or Zn8 antibody signal (**A''**, **B''**, **C''**, **D''**), dashed circles indicate areas populated by HCIs in WT, white arrows indicate commissural axons; yellow arrows indicate ectopic axons. Scale bars 50 µm.

The NICD acts as a constitutively active form of Notch, activating target genes without any external stimulus. (Fortini et al. 1993; Lieber et al. 1993; Struhl et al. 1993). Heterozygous *atoh1a*:KalTA4/UAS:GFP carriers were crossed with homozygous UAS:NICD fish (Scheer and Campos-Ortega 1999) and HCI differentiation in the resulting embryos was analyzed by observation of GFP expression and Zn8 immunostaining.

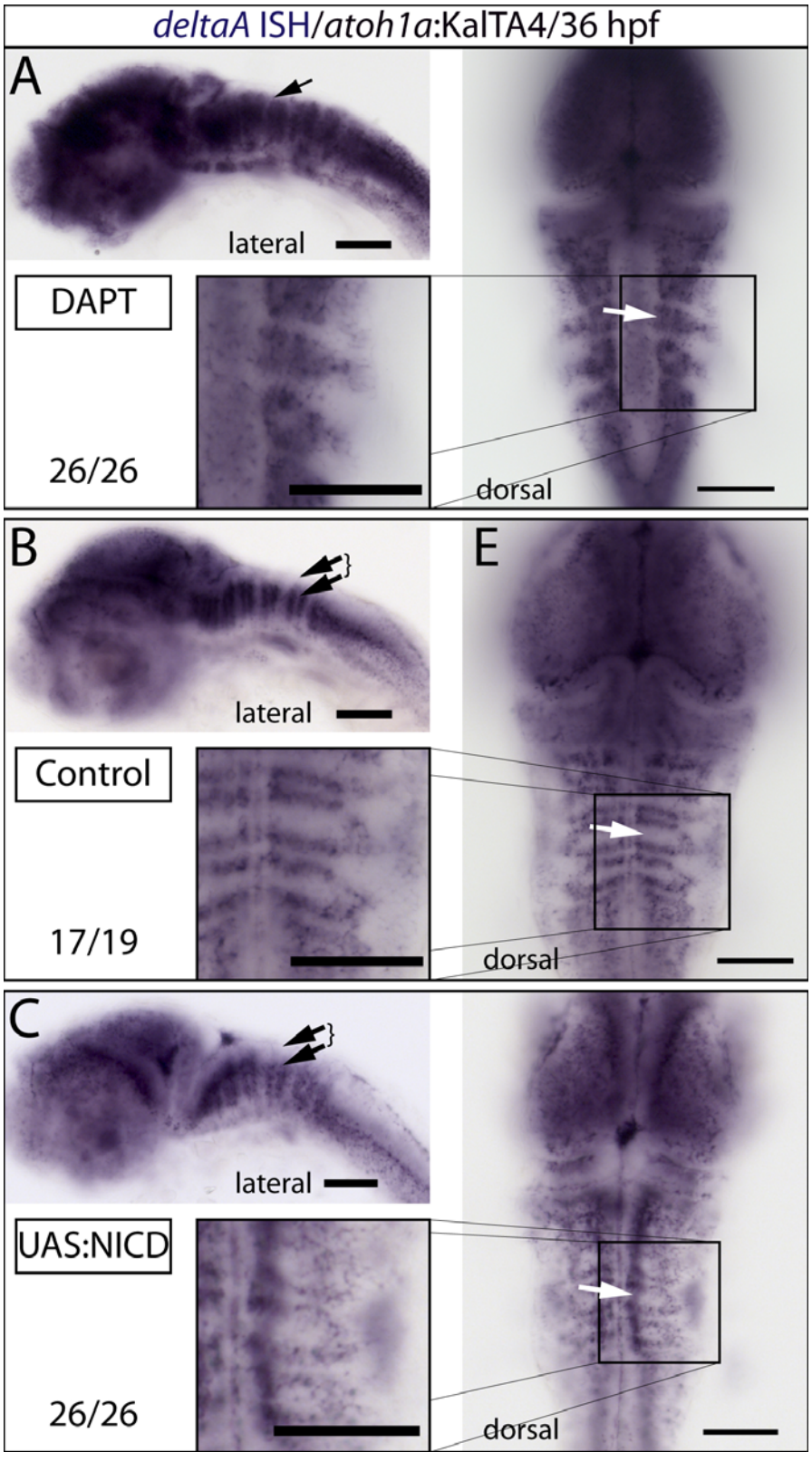

Figure 49 Inhibition of Notch signalling results in an increase and dorsal shift of *deltaA* mRNA expression
mRNA *in situ* hybridisation to detect *deltaA* gene expression in either **A-C** DAPT treated, **D-F** control (DMSO only) or **G-I** NICD expressing (*atoh1a*:KalTA4/UAS:NICD) 36 hpf zebrafish embryos. White arrows indicate segment centres; black arrows indicate dorsal hindbrain region free of *deltaA* expression. **C**, **F**, **I** magnification of boxed area in corresponding picture.
Scale bars 50 µm.

Confocal image stacks were recorded at 48 hpf and displayed as maximum intensity projections as an overlay of the green GFP signal and the red Zn8 antibody signal. Additional false colour depth coding diagrams were created from the individual channels. These images revealed that throughout the rhombic lip, *atonal1a* enhancer-mediated GFP expression was strongly maintained; however, condensation of HCI progenitors at sites of rhombomere boundaries did not occur. Moreover, depth coding showed that HCIs did not migrate to their ventral sites of differentiation, but remained in dorsal positions (Figure 48 C, C'). In addition, differentiation into HCIs was impaired as demonstrated by the absence of Neurolin-expressing commissural projections in the hindbrain of these embryos at 48 hpf.

To show that the observed DAPT phenotypes were indeed mediated by Notch signalling, 24 hpf *atoh1a*:KalTA4/UAS:GFP/UAS:NICD embryos were treated for 24 hours with DAPT and then stained with the Zn8 antibody. DAPT inhibits the γ-Secretase and thereby prevents cleavage of the Notch receptor. Thus NICD acts downstream of the inhibition target, and consequently endogenous expression of the intracellular domain should constitutively activate Notch signalling and rescue the DAPT effect.

Confocal image stacks demonstrated that DAPT treatment of these triple transgenic embryos neither rescued HCI differentiation nor abolished *atonal1a* enhancer-driven GFP expression in the rhombic lip (Figure 48 D, D'). These embryos showed the same phenotype as untreated NICD over-expressing embryos (Figure 48 C, C'). This demonstrates two points: First, DAPT mediates its effect on HCI differentiation via inhibiting the Notch receptor and second, maintenance of rhombic lip cell derived HCI progenitors is indeed mediated by Notch signalling.

In addition the rhombomeric organisation of the hindbrain is not altered. This could be demonstrated by in situ hybridisation against the expression of the neurogenic marker *deltaA* on DAPT-treated (Figure 49 A; n=26/26 embryos) or NICD-expressing embryos (Figure 49 C; n=26/26 embryos). Dorsal and lateral images of these embryos compared to control samples revealed that the segmentation of the expression pattern and therefore of the rhombomeres is not altered. During development, the rhombomere boundaries are formed long before 24 hpf, which means also before DAPT was applied or NICD became overexpressed. These experiments show that the boundaries remain intact even after interference with Notch signalling in the hindbrain. Taken together, this data suggests that Notch signal transduction has to be temporally active in the rhombic lip progenitors; however, maintained Notch activity will prevent HCI progenitors from condensing at and migrating along the boundaries and from terminally differentiating at their target regions. Therefore we

conclude that Notch signalling has to be carefully orchestrated in the rhombic lip in order to allow for HCI development to proceed properly.

3.6.5. Inhibition of Notch signalling leads to premature neuronal differentiation

DAPT-induced Notch inhibition leads to a dramatic loss of differentiated HCIs as well as of the HCI progenitor population. As cell death could be excluded as a potential cause for this effect, it might be possible that the fate of these cells is altered. In order to address this question, we used an antibody against Proliferating Cell Nuclear Antigen (PCNA) to analyze

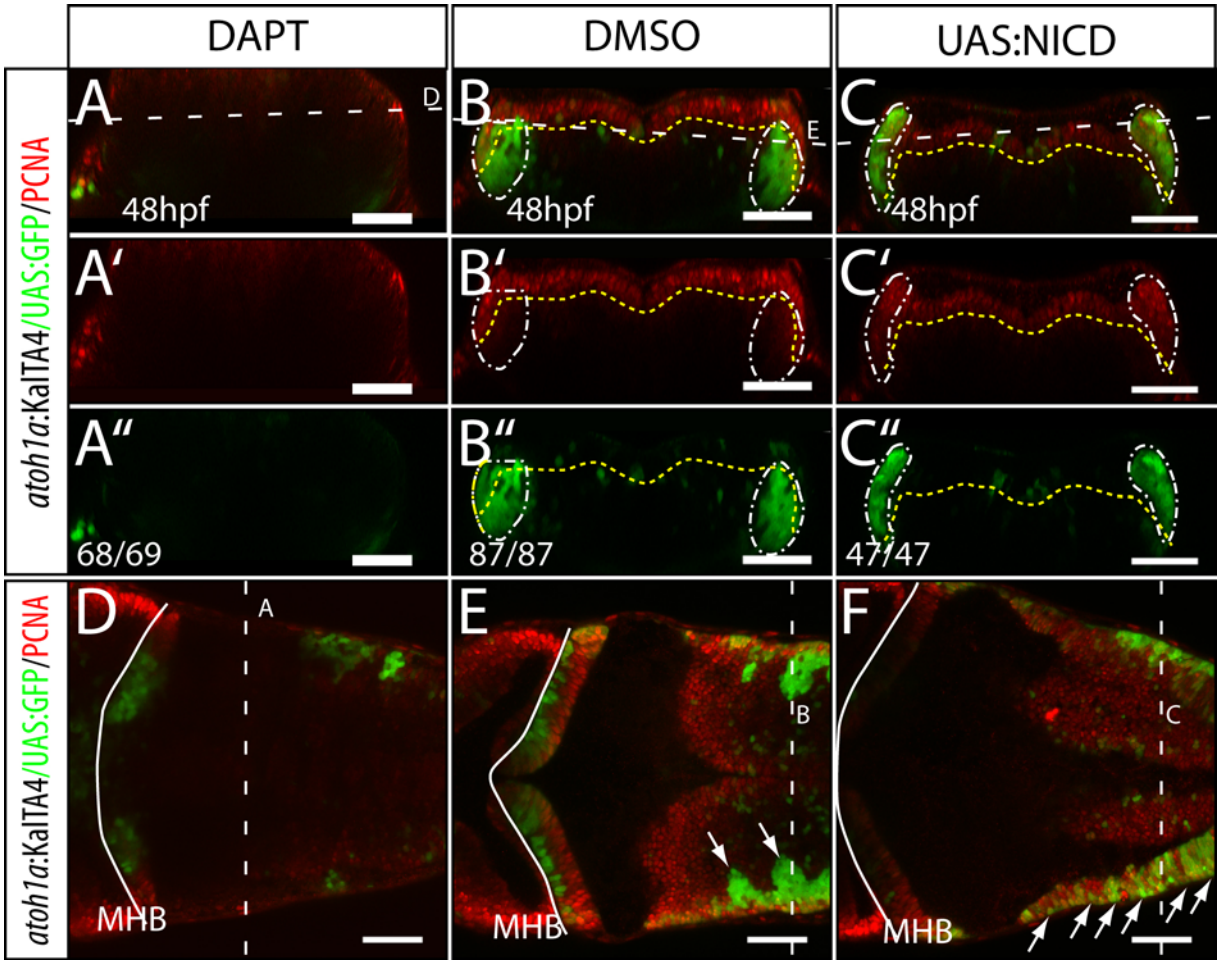

Figure 50 Continuous activation of Notch signalling keeps rhombic lip cells in their proliferating progenitor state
Whole-mount immunostainings against PCNA at 48 hpf in *atoh1a*:KalTA4/ UAS:GFP embryos in **A-B''**, **D-E** wild type or **C-C''**, **F** UAS:NICD transgenic background. For inhibition of Notch signalling *atoh1a*:KalTA4/ UAS:GFP embryos were treated with **A-A''**, **D** DAPT or **B-C''**, **E-F** DMSO as control for 24 h starting at 24 hpf. Images show **A-C''** transverse or **D-F** dorsal image sections recorded by confocal microscopy of the hindbrain region. (Position of the section planes are indicated by dashed white lines) Note: GFP expressing rhombic lip cells fail to condensate at rhombomere boundaries (**F**; white arrows) in triple transgenic *atoh1a*:KalTA4/ UAS:GFP/ UAS:NICD embryos. Dashed white ovals indicate GFP expression mediated by the *atoh1a* enhancer, dashed yellow lines **B-C''** indicate ventral limit of proliferation zone. Scale bars 50 µm.

cell proliferation in transgenic *atoh1a*:KalTA4/UAS:GFP fish treated with DAPT or DMSO. Dorsal confocal images of DAPT-treated 48 hpf embryos showed that PCNA expression in the hindbrain was lost as a result of Notch inhibition (Figure 50 A-A'', D). Moreover,

similarly treated embryos labelled with the radial glia fibre staining antibody cocktail Zrf 1-4 gave further proof for the loss of hindbrain progenitors, as no Zrf 1-4 signal could be detected in 2 day old DAPT treated embryos (Figure 51 A-C). In contrast, in DMSO only treated control embryos numerous proliferating (Figure 50 B-B'', E) and radial glia fibre positive cells could be detected in the dorsal hindbrain (Figure 51 D-F).

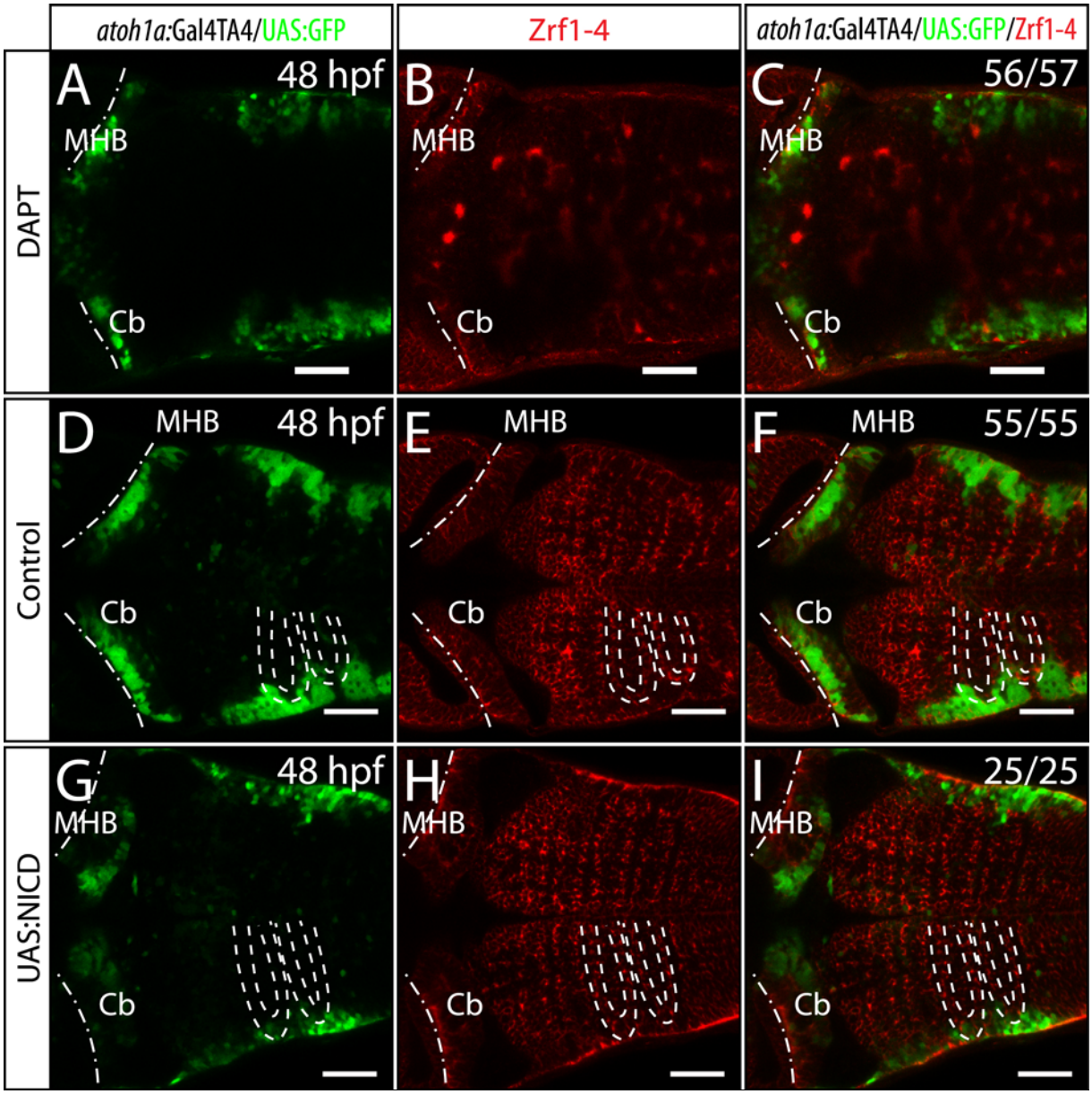

Figure 51 Glial marker expression in embryos with conditionally inhibited or activated Notch signalling
Whole-mount immunostainings using Zrf 1,2,3,4 antibody cocktail in 48 hpf *atoh1a*:KalTA4/UAS:GFP embryos in **A-F** wild type or **G-I** UAS:NICD transgenic background. Embryos were treated with DAPT **A-C** or DMSO only as control **D-I** for 24 h starting at 24 hpf. Images show dorsal optical sections of the hindbrain region. Dashed white lines indicate location of glial curtain. Scale bars 50 µm.

As shown before, the lack of proliferating progenitors is not due to enhanced cell death. In order to clarify whether premature differentiation of these cells might be responsible for this phenotype, the expression of the postmitotic neuronal marker HuC/D was investigated.

Digital sections of confocal image stacks of DAPT-treated embryos showed that almost every cell in the hindbrain expressed HuC/D, whereas in control animals the dorsal most cells in the germinal zone and the areas of the glial curtain are devoid of HuC/D antigen expression (Figure 52 A,A'). Similarly, the expression domain of the neurogenic marker *deltaA* is expanded into the dorsal-most areas of the hindbrain in DAPT-treated embryos, as shown by in situ hybridisation (Figure 49 A black arrow). In summary, this data suggests that conditional inhibition of Notch leads to the premature differentiation of rhombic lip progenitors at the expense of later arising cell types such as HCIs.

3.6.6. Notch signalling is essential for progenitor maintenance in the hindbrain

Activation of Notch signal transduction by conditional overexpression of NICD prevents rhombic lip cells from differentiating into mature HCIs. Unlike in DAPT-treated animals, where differentiation is also impaired, GFP expression is maintained in NICD overexpressing animals. This suggests that rather than premature differentiation, the cause of HCI loss is prolonged progenitor maintenance by NICD over activation.

In order to investigate if rhombic lip cells are arrested in the progenitor state, cell proliferation was analysed by immunohistochemistry against the mitotic marker PCNA. Confocal image sections of triple transgenic *atoh1a*:KalTA4/UAS:GFP/UAS:NICD compared with *atoh1a*:KalTA4/UAS:GFP control embryos at 48 hpf showed that in both embryos proliferating cells could be detected with the anti-PCNA antibody in the dorsal hindbrain (Figure 50 F). In contrast to the control embryos the GFP positive HCI progenitors of NICD embryos however stayed in dorsal positions and showed a broad overlap with the PCNA expression (Figure 50 C-C'').

In control embryos, most GFP expressing cells did not co-localise with PCNA (Figure 50 B-B''). That the maintenance of mitotic progenitor cells was autonomous to rhombic lip cells in the hindbrain of NICD-expressing transgenic embryos was further confirmed by Zrf1-4 stainings, revealing glia curtains (white dashed lines) lining rhombomere boundaries in these embryos (Figure 51 G-I) that were unaltered in position and size when compared to controls (Figure 51 D-F). Similarly, expression of neurogenic marker gene *deltaA* was unaltered in its spatio-temporal distribution in the rhombomere centres of rhombic lip-specific NICD-expressing embryos compared to wild type controls (Figure 49 B, C)

Due to the increase of the PCNA overlap with the GFP reporter in triple transgenic *atoh1a*:KalTA4/UAS:GFP/UAS:NICD, it can be assumed that these cells no longer express the postmitotic neuronal marker HuC/D. In order to prove this idea, immunohistochemistry

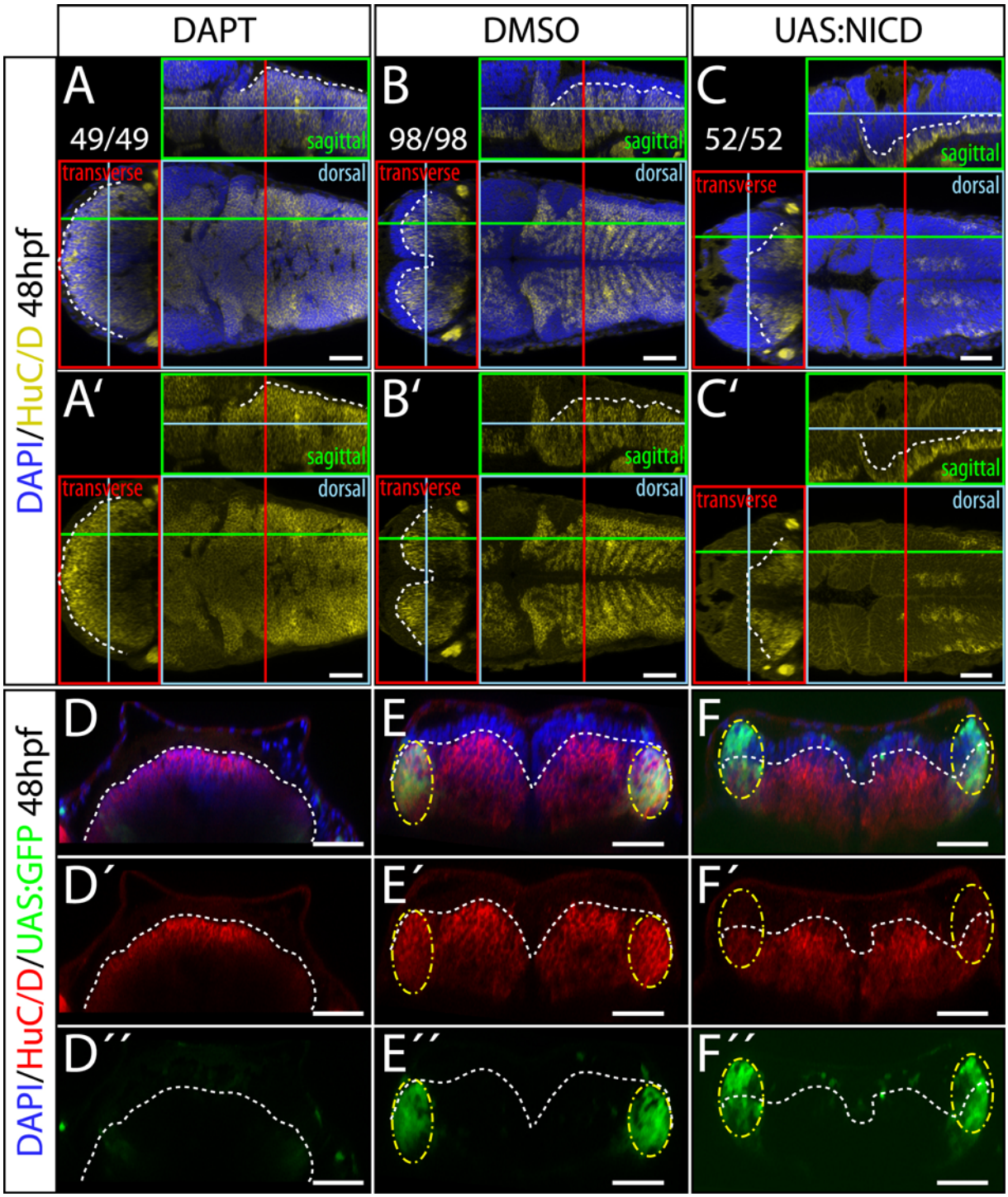

Figure 52 Notch signalling controls neurogenesis of HCIs

A-C' Immunostainings against HuC/D in 48 hpf *atoh1a*:KalTA4 embryos in **A-B'** wild type or **C-C'**UAS:NICD background treated with **A-A'**DAPT or **B-C'**DMSO only as control for 24 h starting at 24 hpf. Embryos were counterstained with DAPI. Images show dorsal, transverse and sagittal sections generated from image stacks recorded by confocal microscopy. Dashed white lines indicate dorsal border of HuC/D expression domain.
D-F'' Immunostainings against HuC/D in *atoh1a*:KalTA4/ UAS:GFP embryos at 48 hpf in wild type (**D-E''**) or UAS:NICD background (**F-F''**) treated with DAPT (**D-D''**) or DMSO only as control (**E-F''**). Embryos were counterstained with DAPI. Images show digital cross sections; dashed white lines indicate dorsal border of HuC/D expression domain; yellow circles depict GFP expression domain mediated by the *atoh1a* enhancer. Scale bars 50 µm.

using the anti HuC/D antibody was performed. As expected zebrafish embryos overexpressing NICD under the control of *atonal1a* regulatory element showed strongly

reduced HuC/D expression, especially in the dorsal and lateral hindbrain regions (Figure 52 C,C'). In addition the number of double positive GFP/HuC/D was strongly reduced in NICD expressing embryos (Figure 52 F-F'') compared to wildtype (Figure 52 E-E'').

In summary, the data showed that the progenitor pool in the rhombic lip has to be maintained in order to give rise to later born neuronal subtypes, and that Notch mediated regulation of differentiation time points is important for the maintenance of the hindbrain embryonic neural progenitors.

Nevertheless, subsequent downregulation of Notch signalling is likewise essential for HCI progenitors in the rhombic lip to condense at rhombomere boundaries, to initiate neuronal differentiation, and to terminally differentiate into mature HCIs

3.6.7. Over-activation of Notch under control of the *atonal1a* enhancer element may lead to an increase in brain size

Constitutive activation of Notch signalling results in the maintenance of dividing progenitors in the rhombic lip at expense of the HCIs. So far, the differentiation of HCIs has been analysed only at early embryonic stages. But does the loss of HCIs have any detectable physiological relevance in older embryos, or are there are any compensatory mechanisms that allow them to recover? In order to address this question, some preliminary data from 5-7 day old larvae continuously expressing NICD under the control of the *atonal1a* enhancer was acquired. Brightfield images of these embryos show that they probably have an increased hindbrain size compared to control animals although precise measurements are still missing to underline these findings (Figure 53 red outlines). In addition to the brain, the tissue surrounding the eye was expanded and large heart oedema were observed in the mutant embryos. The enlargement of the heart and the tissue surrounding are likely a result of fluid accumulation rather than an alteration in cell number. This might rather represent an artefact of sustained transgene expression also because the *atoh1a* driven GFP is not expressed in the heart or in the tissue surrounding the eye. Furthermore the occurrence of the phenotype strongly varied in respect to severity from very mild (Figure 53 C,D n =12/51) to quite strong (Figure 53 A,B n=27/51). In rare cases, (n=7/51) animals developed heart oedema exceeding the size of the head, and also the size of the tissue surrounding the eye was dramatically increased (data not shown). These animals were no longer capable of swimming and were sacrificed.

In contrast to the heart and eye alterations the increase in brain size might represent a more specific effect as the optical appearance of the tissue was not altered. The increase might be a

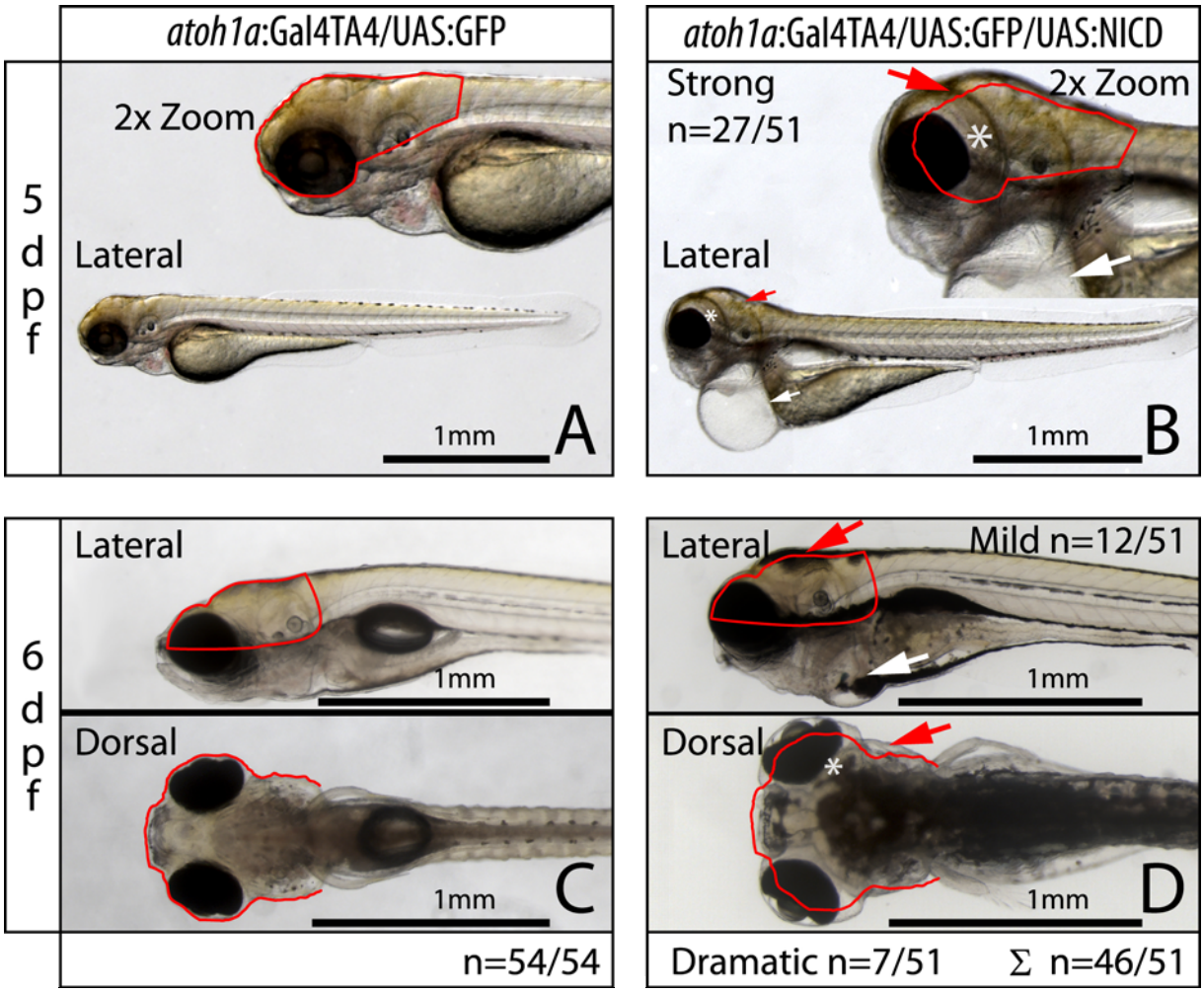

Figure 53 Morphology of 5-6 dpf *atoh1a*:KalTA4/UAS:GFP/UAS:GFP embryos

Brightfield images recorded from **A**, **B** 5 dpf or **C**, **D** 6 dpf old **A**, **C** wild type or **B**, **D** *atoh1a*:KalTA4/ UAS:GFP/ UAS:NICD zebrafish larvae show that NICD expressing embryos develop heart oedema, enlargement of the tissue surrounding the eye and slightly larger brains indicated by the red lines.

result of the maintenance of proliferating progenitor induced by *athonal1a* enhancer mediated NICD overexpression. Except for the tissues described, the mutant embryos appeared to be normal and viable; in particular the trunk region was indistinguishable from control.

3.6.8. Inhibition of HCI differentiation impairs escape response after sound and vibration stimuli

Conditional activation of Notch resulted in an impairment of hindbrain commissural interneurons. These neurons most likely receive lateral line and inner ear input (Sassa et al. 2007) and they connect contralaterally to the midbrain torus semicircularis and caudally to unknown targets. Aside from sound, the inner ear and the lateral line (LL) detect vibrations and water flow. Very early in their development (i.e. starting at 2-3 dpf), zebrafish are capable of reacting to these stimuli by performing an escape response, in which they turn away from the source. Thus, we predicted that zebrafish embryos whose HCIs have failed to differentiate

by constitutive Notch signal transduction through NICD overexpression would be unable to integrate and reply to lateral line signals if challenged via sound and vibration stimuli (SVS). Before addressing this question it had to be clarified if the tissue alterations in the mutant embryos did impair their ability to swim and therefore to perform an escape response. Therefore the escape reflex was triggered by an alternative stimulus not received through the lateral line.

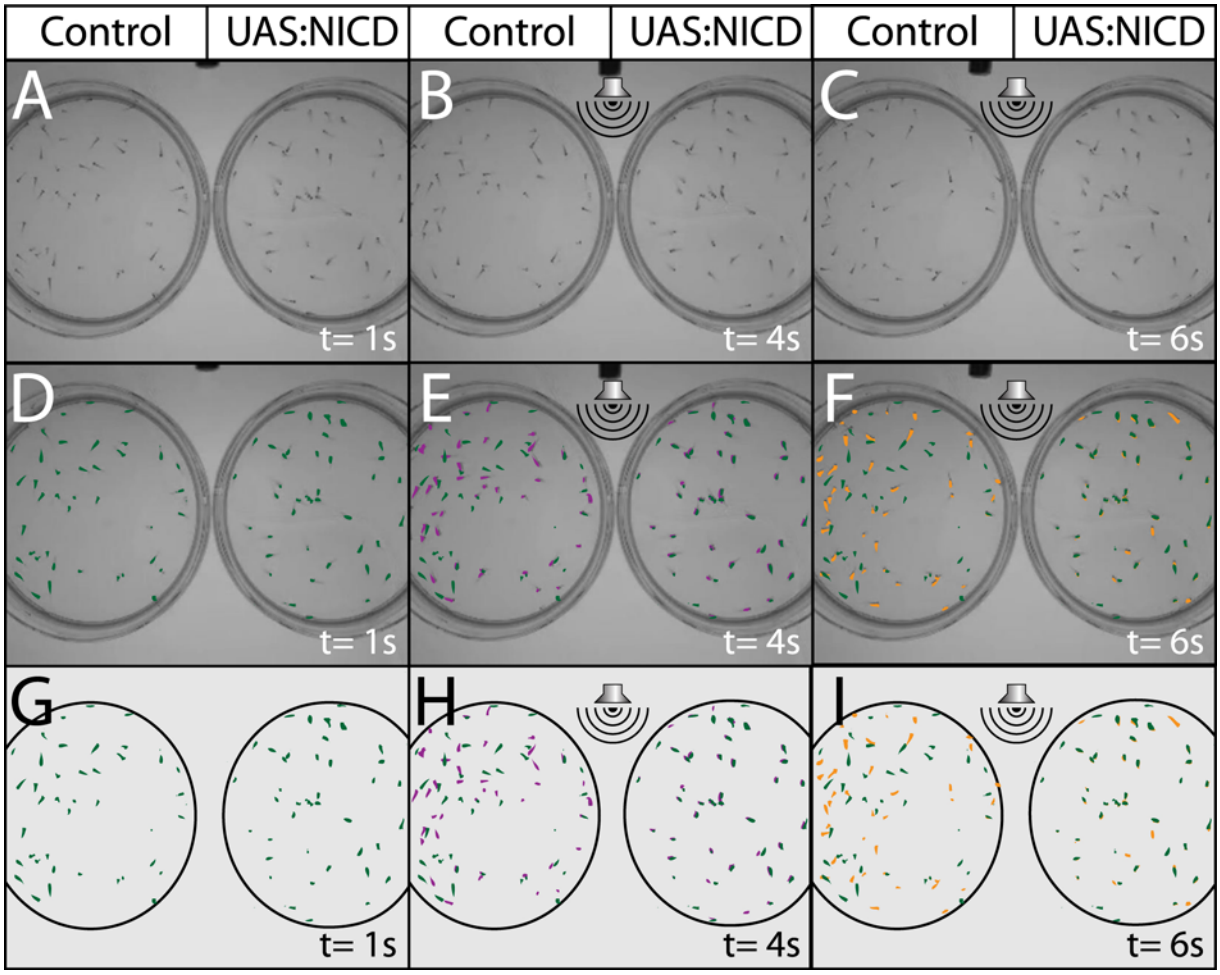

Figure 54 Embryos expressing NICD under the control of *atoh1a* enhancer show impaired escape response after sound and vibration stimuli (SVS)
Images of three individual time points from a time lapse movie showing 5 dpf wild type (left petri dish) or *atoh1a*:KalTA4/ UAS:GFP/ UAS:NICD (right petri dish) larvae. Between each time point a stimulus was applied indicated by the speaker symbol. **A**, **B**, **C** Brightfield images grey spots are the zebrafish embryo. **D**, **E**, **F** Each zebrafish embryo was labelled with a coloured spot with an individual colour for every time point allowing the observation of changes after the SVS. **G**, **H**, **I** Extracted traces from (**D**, **E**, **F**). Note: The position of wild type embryos changes after every SVS as indicated by the colour labels. In contrast the vast majority of UAS:NICD expressing larvae did not alter their position.

The tail of control and *atoh1a*:Gal4TA4/UAS:NICD/UAS:GFP were poked with a needle to clarify if these embryos are able to perform a touch mediated escape response and are therefore able to swim at all. (Movie 12 Control & Movie 13 NICD). Although the control embryos reacted much faster when they were touched, NICD expressing embryos were able to swim away from the needle. Only the very dramatically effected embryos (see one example

in Movie 13) failed to escape. This suggests that *atoh1a*:Gal4TA4/UAS:NICD/UAS:GFP transgenic fish are in general capable of swimming and performing directed escape responses.

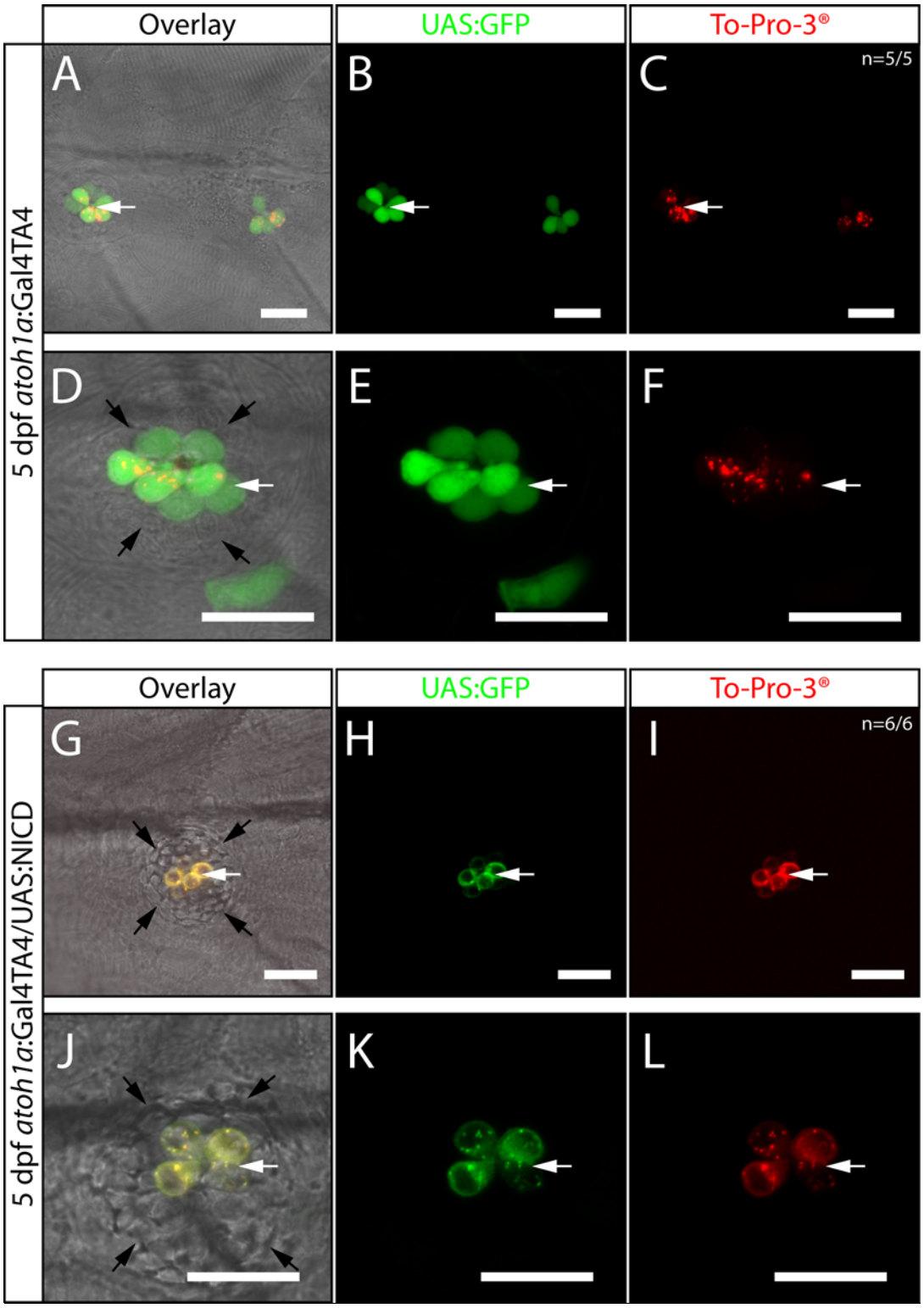

Figure 55 NICD overexpression in hair cells leads to their reduction in number but does not cause a complete loss

Images of neuromasts of *atoh1a*:KalTA4/UAS:GFP embryos recorded by confocal microscopy in a **A-F** wildtype or **G-H** UAS:NICD background. GFP expressing hair cells counterstained with To-Pro-3® (white arrow) are surrounded by support cells. In NICD expressing embryos hair cells are still present but their number seems to be reduced. In contrast, the number of support cells seems to be increased in these animals.

Next, 5-6 dpf old zebrafish triple transgenic *atoh1a*:KalTA4/UAS:GFP/UAS:NICD and *atoh1a*:KalTA4/UAS:GFP control larvae were placed in separate petri dishes and challenged with sound and vibration stimuli (SVS) caused by hitting either the rim of the petri dish directly with the tip of a needle or the surface in close proximity with the bar end of the needle. The procedure was repeatedly performed and the embryo movements were recorded over time. Control animals responded by showing a characteristic escape response (Movie 10), while zebrafish expressing NICD driven by the *atonal1a* enhancer (Movie 11) generally did not respond at all. An additional movie (Movie 12) shows the direct side by side comparison of NICD expressing zebrafish larvae on the left and control animals on the right. Again the control fish responded intensely to the vibration stimuli, whereas NICD overexpressing specimens did not. This was underlined by a tracing analysis of their movements. Images of the tested animals at three different time points (Figure 54 A-C) were extracted from Movie 12 and compared by false colouring with an individual colour for each time point (Figure 54 D-E). Between each time point, embryos were challenged once simultaneously. The initial positions of individual embryos are indicated in green and used as reference for later time points. In the petri dish with the NICD overexpressing animals, almost no change in the position of the animals could be detected as indicated by the fact that the coloured spots representing individual time points are almost completely congruent. In contrast, animals in the control dish clearly left their initial position in response to SVS, as hardly any overlap between spots of different colours could be observed. This data demonstrate that zebrafish larvae expressing NICD under the control of the *atonal1a* enhancer are no longer able to integrate SVS. And that this might by due to the loss of HCI caused by constitutive activation of Notch signalling in rhombic lip cells. This finding also suggests that HCIs are integrating lateral line and auditory input.

3.6.9. NICD overexpression in haircells leads to their reduction but does not cause a complete loss of these cells

These preliminary behavioural experiments revealed that triple transgenic *atoh1a*:KalTA4/UAS:GFP/UAS:NICD larvae show an impairment in the escape response triggered by SVS. This lack of reaction is most probably due to an inability of the lateral line and auditory system to conduct the signal to downstream neuronal systems that could initiate the reflex. There are several possible explanations for why the lateral line is unable to conduct the input in *atoh1a*:KalTA4/UAS:GFP/UAS:NICD larvae. On reason might be that in these animals HCIs fail to terminally differentiate, and therefore signal transmission would be

impaired. A second explanation could be that the lateral line sensory organs are affected directly. Intriguingly, GFP expression can also be observed in the hair cells of the inner ear and the lateral line neuromasts starting at 4 dpf as they are known to express *atonal1a* during their development. Consequently these cells also overexpress NICD. Earlier findings have shown that *atonal1a* and *athonal1b* expression as well as Delta-Notch signalling have to be carefully orchestrated in the inner ear in order to allow the two cell types, hair cells and support cells, to form properly (Millimaki et al. 2007). A lack of hair cells as well as functional impairment in the inner ear or lateral line neuromasts would obviously lead to a lack of SVS-mediated flight response. In order to investigate if hair cells are still present in *atoh1a*:KalTA4/UAS:GFP/UAS:NICD, these animals were counterstained with TO-PRO® 3, a far red dye that specifically labels hair cells.

Lateral view confocal images demonstrated that NICD expressing embryos developed neuromasts with two different cell types. In the middle of the neuromasts, identified by red TO-PRO® 3 fluorescent signals, hair cells were located with their typical cone like shape (Figure 55 G-M white arrows). They were surrounded by cells that are most likely support cells (Figure 55 G-M black arrows).

Although this provided the impression that the neuromasts developed quite normally, there were some differences if compared to the control embryos. The total number of neuromasts in individual larvae seemed to be reduced (not shown) and in addition the neuromasts of larvae with NICD overexpression mediated by the *atonal1a* enhancer seemed to have an increased number of supporting cells. It has been shown before that *atonal* mediated (*atonal1a*/*atonal1b*) regulation of Notch signal transduction is required to produce support cells and hair cells from a progenitor population via lateral inhibition. (Millimaki et al. 2007).

These results are preliminary and we could not clarify if the neuromast hair cells are functional. Therefore further experiments have to be carried out to dissect if the observed behavioural phenotype is due to the lack of HCIs or due to the reduced number or impaired functionality of lateral line hair cells.

4. Discussion

4.1. Zebrafish Lunapark is highly conserved and potentially functions in neuronal development by mediating membrane fusion events

4.1.1. Lunapark expression pattern and peptide sequences are highly conserved

The vertebrate brain is an organ of almost infinite complexity. The human brain, for example, contains an estimated amount of 50-100 billion neurons, consisting of hundreds of different subtypes. These neurons pass signals to each other via the approximately 1,000 synaptic connections made by each neuron. In the generation of a functional brain, the developing organism has to face the overall challenge of transforming a fertilised egg with comparably low complexity into a highly organised multi cellular organism. This is achieved by the precise regulation and carefully orchestrated interaction of more than 20,000 genes encoded by the vertebrate genome. In this study we analysed one of this genes, *lunapark,* in the developing zebrafish embryo.

Although the function of Lunapark has not been studied intensively so far, its sequence is highly conserved from yeast to humans. It was first described in mammals, where it is part of the *lnp-evx2-hoxd* cluster and *lnp* is expressed in neuronal structures at a developmental time point when critical migratory and differentiation steps are occurring (Spitz et al. 2003, this work). In addition, *lnp* is expressed in developing limbs and the urogenital system. In humans, breakpoints within the vicinity of this cluster result in, among other defects, severe cerebellar hypoplasia, (Dlugaszewska et al. 2006), suggesting that *lunapark* has a role in vertebrate hindbrain development. Furthermore, fluorescent reporter genes expressed in *C. elegans* under the control of an *lnp* enhancer element ($_p$*lnp*) were localised to various neuronal cell types and some muscle cells. The expression pattern, subcellular distribution and behavioural phenotypes in *C. elegans* point to a role for LNP-1 in vesicular trafficking in developing neurons (Ghila and Gomez 2008).

In this study, we identified and isolated two novel *lunapark* homologues from the zebrafish genome by sequence comparison and RT-PCR. *lunaparkA* localises to chromosome 23 and *lunaparkB* was found to be located on chromosome 6. The second homologue is most likely a paralogue resulting from the teleost genome duplication (Amores et al. 1998; Robinson-Rechavi et al. 2001; Taylor et al. 2003), since in all other vertebrate species the *lnp* genes exist as single copies. Comparison of the amino acid sequences of different species revealed a very high degree of conservation between the Lunapark homologues. Characteristic for the

Lnp peptide sequences is a short N-terminus followed by two transmembrane domains, and a longer C-terminus harbouring an 80 amino acid region that represents an atypical zinc finger domain (Spitz et al. 2003; Ghila and Gomez 2008). This latter domain shows the highest degree of conservation among the Lnp proteins, of more than 88% across a number of vertebrate species. Analysis of the peptide sequence showed that the N-terminus of zebrafish Lnp proteins harbours a signal anchor sequence, suggesting that these proteins are integrated into the plasma membrane. Moreover, the analysis revealed that a large majority of the peptide sequence is facing the cytosol with less then 10 AA located in the lumen of membrane containing organelles. This prediction although requires experimental verification of the topology of the Lunapark protein. Due to the small size of the luminal domain it is unlikely that Lnp functions as a receptor capable of receiving extracellular signals. Lnp proteins are more likely to function as scaffolding or adaptor proteins located on the inner cell membrane or on the surface of organelles or vesicles.

Both zebrafish *lunapark* genes are expressed maternally. While *lnpA* expression persists up to two days after fertilisation, *lnpB* transcripts disappear during early somitogenesis. In other vertebrate species, *lnp* is part of the regulatory landscape of the *evx2/hoxd* cluster. While the genomic organisation of *lnpA* is syntenic to other vertebrates with respect to the location of *evx2* and the *hoxd* genes, no additional copy of *evx2* or the *hoxd* cluster can be found in the vicinity of the zebrafish *lnpB* gene or anywhere else in the zebrafish genome. It was suggested that these additional copies have been lost during evolution by a deletion event (Woltering and Durston 2006). Such a modulation of genes or genomic regions after duplication is very common because the redundancy provides the second copy with an increased freedom for mutation events (Amores et al. 1998; Wagner et al. 2003; Hoegg and Meyer 2005). This deletion and the resulting rearrangement of the genomic area may have altered the expression pattern of the *lnpB* gene, restricting it to very early development. Regarding the temporal distribution of *lnpB* it is even possible, that it is only expressed maternally.

In contrast to *lnpB*, *lnpA* mRNA is also detectable at later stages using mRNA in-situ hybridisation. *lnpA* showed very distinct expression patterns that are spatially and temporally well defined in the developing trunk muscles and the hindbrain. The expression of *lnpA* is conserved in mice and even in *C.elegans lunapark* is expressed in similar cell types (Spitz et al. 2003; Ghila and Gomez 2008). Furthermore, similar to mouse, zebrafish *lnpA* expression greatly overlaps with that of *evx2* (except for the muscles) and partly overlaps with some of the genes of the *hoxd* cluster (data not shown) indicating that gene regulation over the entire genomic landscape is preserved.

The hindbrain expression domain of *lnpA* is populated by neuronal progenitors that become postmitotic and start to differentiate at a time point that correlates with an upregulation of *lnpA* expression. Of note, the expression in the muscle correlates with developmental period when individual muscle cells fuse to syncitia.

Furthermore, in the anterior cerebellum extensive cell migration is occurring when *lnpA* is expressed (Volkmann et al. 2010). Therefore, concerning its expression *lnpA* might play a role in neuronal migration and differentiation in the developing zebrafish hindbrain. While in skeletal muscle it might be involved in the fusion of muscle cells.

Except for teleost, which have a second copy of *lunapark* derived from a genome duplication event, in all other investigated vertebrate *lunapark* is a single copy gene that does not belong to a gene family. Nevertheless there is a high degree of similarity between the peptide sequences of different vertebrate species and the gene expression is very carefully regulated thereby also showing a high degree of conservation concerning the developmental time point and the tissue specificity. These aspects argue for an important role of Lunapark during the development of the zebrafish embryo.

4.1.2. LunaparkA localises to late endosomal/lysosomal compartments

Bioinformatic analyses showed that Lunapark proteins are anchored to the membrane, but the precise subcellular localisation remained unclear. In experiments expressing fluorescent LunaparkA fusion constructs together with known cellular markers in cultured zebrafish PAC2 cells, we aimed to determine the subcellular localisation of the protein.

Unfortunately, the fluorescent Lnp fusion proteins formed irregular large vesicle/vacuole-like structures occupying most of the cell, and co-expressing ER markers. These aggregates are not observed in normal cells and are therefore likely to be overexpression artefacts from which we cannot predict the proper cellular localisation of LnpA proteins. The formation of the aggregates may occur for several reasons.

First, immunoprecipitation assays showed that Lnp proteins can specifically and strongly interact in a homotypic manner, thereby forming dimers or oligomers. Overexpression could therefore result in a strong and uncontrolled clustering of Lunapark proteins. An alternative explanation could be that the polypeptide sequence fails to fold properly in the ER, due to either the strong overexpression or a lack of available binding partners required for the correct formation of secondary and tertiary protein structures. This second hypothesis is supported by the fact that the vacuole-like aggregates are positive for ER proteins. In the ER, misfolded proteins become bound to chaperones and are eventually degraded (Blond-Elguindi et al.

1993; Cox et al. 1993; Hammond et al. 1994; Brewer and Diehl 2000; Shen et al. 2002), but strong overexpression of the misfolded protein might lead to accumulation in the ER. A third explanation could be that Lnp enhances either membrane fusion of initially separated compartments or membrane metabolism and thereby extension of the endomembrane system. Strong overexpression might then lead to an imbalance in these processes, causing organelles to fuse or grow in an uncontrolled manner and creating enlarged vesicular structures. Similar structures were observed in HeLa cells strongly overexpressing wild type Rab7 GFP or mutant dominant active Rab7 GFP (Bucci et al. 2000).

The formation of enlarged vesicle by LnpA expression was highly dependent on the cell type. In PAC2 cells strongly overexpressing Lnp, these structures were highly abundant. In contrast, NIH3T3 cells seemed to be less prone to the Lnp overexpression and only a minority of cells in a transfected batch formed the described structures. In addition, a reduction in ER retention could be observed. NIH3T3 cells are relatively big and show a spread out morphology compared to other cultured cell lines and are therefore capable of handling larger amounts of ectopically expressed protein or they perhaps express the interaction partners required for Lnp folding and regulation that are not present in PAC2 cells. We therefore decided that NIH3T3 cells were more suitable for LnpA co-localisation studies. Interestingly, we found that Lnp fusion proteins co-localised with the late endosomal/lysosomal markers Rab7 and Rab9. Furthermore, high resolution brightfield images showed that Lnp partially co-localises with dark vesicular structures that could be identified as lysosomes. Moreover, a truncated version of Lnp containing only the N-terminus and the two transmembrane domains fused to a fluorescence protein (NTM-cherry) localised to rather small and highly motile vesicular structures identified as late endosomes/lysosomes without forming any vacuole-like aggregates. In contrast, expression of the C-terminus of Lunapark fused to mCherry resulted in a distribution of the red fluorescent signal all over the cytosol. This indicates that the C-terminus does not contain any specific cell sorting signal. Also no evidence of aggregates formation could be found with this truncated variant.

The NTM-cherry overexpression studies support the finding that LnpA localises to the membrane of lysosomes and late endosomes. In addition it can be concluded that the N-terminus is required for proper targeting of the protein, while the C-terminus is responsible for aggregate formation or membrane fusion, but only if the protein is targeted to the endomembrane system.

4.1.3. The interactome of Lunapark shows a bias for vesicle trafficking proteins

One strategy to characterise a gene or protein of unknown function is to identify its potential binding partners as they may be attributable to a specific cellular process. Putative interactors with known properties can provide information about the functional context of the uncharacterised binding partner. The state of the art method to screen for new interactors in mammalian cells involves the use of tandem affinity purification based pull down assays with subsequent mass spectrometry analysis. In the case of zebrafish LunaparkA, we created two constructs with N-terminal and C-terminal fusions of a tandem affinity tag consisting of a double Streptavidin and a single FLAG peptide (Gloeckner et al. 2009b; Gloeckner et al. 2009a). Both versions were tested successfully for robust cell culture overexpression and efficient tandem purification. Subsequent mass spectrometry analysis of the purified samples identified a large number of proteins. Among those proteins, LunaparkA itself could be discovered with a very high reproducibility and sequence confidence. The experiment was performed in human cells using the zebrafish LnpA as a bait protein, and so the mass spectrometry data was analysed using a human protein database. Due to the high degree of conservation, it was not unexpected that the zebrafish LunaparkA bait was identified using the human database. Further, this finding confirmed the initial testing that the TAP-tagged Lnp proteins could be purified efficiently from the crude lysate.

Analysis of the putative interactors of Lunapark revealed a strong bias towards proteins involved in vesicle trafficking like the small Rab GTPases Rab7A, known to initiate endosomal/lysosomal tethering and docking (Luzio et al. 2007), and Rab15, a marker for recycling endosomes (Strick and Elferink 2005). Other candidates are members of the SNARE family of genes responsible for endosomal/lysosomal fusion, e.g. Syntaxin7 (Stx7) or factors associated with SNAREs like Syntaxin binding protein 5 (StxB5) Vesicle-associated membrane protein-associated protein A and B. Further analysis with a database of confirmed interactions was used to determine second order binding partners of Lunapark, and revealed several other Syntaxins (e.g. Stx1A, Stx4), Vesicle associated membrane proteins (Vamp/Synaptobrevin) 1 & 2 and various SNAP proteins.

The SNARE proteins and their adaptors SNAP form the core complex that mediates the fusion of vesicles with the membrane or with target compartments such as lysosomes (Hanson et al. 1997; Hay and Scheller 1997; Fasshauer et al. 1998). The high abundance of various SNARE and related proteins in the screen for Lnp interaction partners suggests a role for Lunapark in vesicle fusion processes. Furthermore, strong overexpression of Lnp in cultured

cells resulted in the formation of large vesicular structures potentially caused by uncontrolled fusion events.

In order to obtain an idea in which vesicle fusion events Lnp might be involved, direct and second order candidates were further analysed by screening the literature to see if they could be summarised to a functional pathway. In humans, over 30 distinctly localised SNARE family members exist and each intracellular fusion reaction seems to require a distinct subset (for review see (Ungar and Hughson 2003)). One set of SNAREs found in the interaction screen and known to be functionally related are Synaptobrevin/Vamp 1&2, Syntaxin1a, Vap A/B and Rab3. These proteins are well known to play a key role in the fusion of synaptic vesicles with the membrane in order to promote synaptic vesicle release. Syntaxin 1 and one of the two Synaptobrevins, together with Snap25, form the trans-SNARE complex necessary for the fusion process.

Although this might be a possible explanation, there are other findings that argue against a direct role of Lnp in synaptic transmission. In *C.elegans* LNP-1 was found to promote the localisation of two synaptic proteins, Synaptobrevin/Vamp-1 (Syn-1) and Rab3 (also identified here as second order interactors of LnpA), and disruption of LNP-1 resulted in a mild redistribution of the two proteins towards the cell body (Ghila and Gomez 2008). However, although Ghila and co-workers found that Lnp has an effect on synaptic proteins in *C.elegans*, they excluded the possibility that Lnp is a synaptic protein itself. They rather claimed that Lnp positive vesicles are distributed all over the cell body and that the protein is more likely required for the transport of the synaptic proteins, as *C.elegans lnp* mutants show a similar phenotype to the UNC51 mutant (Ghila and Gomez 2008). UNC51 is a kinase that regulates the trafficking of endosomes and their axon guidance molecular cargo (Sann et al. 2009). The fact that Lnp is not a synaptic protein is in line with the findings from our cell culture co-localisation studies, which showed that Lnp is present in late endosomes/lysosomes. Additionally, these results are further supported by the fact that at least two known late endosomal/lysosomal proteins are found to directly bind to Lnp. Rab7A, a well known marker for these compartments (Davies et al. 1997; Kashuba et al. 1997), and Syntaxin7 (Prekeris et al. 1999; Xie et al. 2010). Moreover, the expression of Lunapark is spatially and temporally restricted to neuronal progenitors undergoing migration and neurite outgrowth excluding a role for Lnp in synaptic transmission in mature neurons. It is well established that endosomal trafficking is crucial for growth cone extension and axon guidance through either the directed delivery of essential cargo like RNA or proteins to their site of action or by promoting vesicle fusion with the surface membrane (Pfenninger et al. 1991; Pfenninger et al. 2003; Alberts et al.

2006; Pfenninger 2009). Studies in cell culture demonstrated that overexpression of Vamp2 drives neurite elongation, while Snap25A promotes neurite sprouting (Kimura et al. 2003). TI-VAMP (Vamp7), identified as second order interactor and present in late endosomes, mediates fusion of intracellular vesicles with the plasma membrane and is crucial for neurite outgrowth. (Martinez-Arca et al. 2000; Martinez-Arca et al. 2001; Alberts et al. 2003; Alberts et al. 2006). Thus, Lnp may facilitate vesicle fusion for the delivery of cargo to the growth cone or for the addition of plasma membrane needed for neurite elongation.

Another potential role for Lnp is in the regulation of lipid storage. A whole genome siRNA screen performed in *C.elegans* to detect molecules that reduce the lipid content within the animal identified 305 genes whose knock down caused a reduction in body fat (Ashrafi et al. 2003). Among these 305 candidate genes *lunapark*, as well as some putative direct and second order interactors of Lnp, such as *synaptobrevin*, *rab7*, *vps16*, and *vapA/B* were found. Whether these genes directly regulate lipid metabolism or if the reduced body fat is an indirect effect caused by a failure of membrane expansion still has to be clarified.

Alternatively or in addition, Lnp might be involved in the promotion of late endosomal-lysosomal fusion events, as we found a second set of SNARE proteins that represent possible interactors of Lnp and these are known to be involved in this process. These include Syntaxin7, Rab7A, VAMP7 and VAMP8. Syntaxin7 is of special interest in that it is the protein that showed the highest confidence level in the interaction screen. Further, the binding of zebrafish Syntaxin7-like to Lnp could be confirmed by immunoprecipitation. Co-expressed Lnp and Syntaxin7-like did co-localise in cell culture and Lnp fusion proteins showed reduced aggregate formation if co-transfected with Stx7l. Moreover, Avalanche, the *Drosophila* homologue of Syntaxin7, was shown to attenuate the Notch signalling pathway by targeting the endocytosed Notch receptor for degradation (Lu and Bilder 2005). Interestingly, we showed that Notch signalling is indeed present in the progenitors of Lnp-expressing cells in the zebrafish hindbrain and that Notch has to be downregulated in order to allow these neurons to differentiate and migrate to their target regions.

Summarizing the data from the co-localisation studies and the mass spectrometric analysis, we can conclude that Lunapark is a protein involved in the regulation of vesicle fusion, most likely in the homotypic endosomal and heterotypic endosomal/lysosomal fusion events. In addition, the developmental time course of *lunapark* gene expression suggests that Lnp may also function in the fusion of vesicles at the cell membrane, driving membrane extension during neurite outgrowth. Finally, a third function of Lnp might be the attenuation of the Notch signal transduction pathway through Syntaxin7-like.

These data strongly support the high sequence conservation and that Lunapark is an important protein crucial for embryonic development.

4.1.4. The Morpholino artefacts

In order to determine the in vivo function of Lnp during development, a knock-down approach using sequence-specific Morpholino phosphorodiamidate antisense oligonucleotides (Morpholinos Mo) was used. Mo are a commonly used platform to study gene function, especially in zebrafish embryos (Summerton 1999; Nasevicius and Ekker 2000). During the course of this thesis though, reasonable doubts arose about possible severe undesirable off-target effects of Mo (Robu et al. 2007). Morpholino injection can result in p53-mediated apoptosis, an effect particularly pronounced in the hindbrain. The enhanced cell death can lead to secondary effects that are easily misunderstood to be specific phenotypes. For example, the expansion of the *rfng* expression domain is a phenotype that results from Morpholino injections independent of the target sequence (this study; David Wilkinson personal communication). This expansion of *rfng* expression has long been taken as evidence for a specific perturbation of rhombomere boundary expression domains. As long as one is aware of this issue, the problem can often be resolved by rescuing the unspecific apoptosis through co-injection of an anti *p53* Morpholino (*p53* Mo). Sooner or later, the *p53* Mo injection will become a standard control for Morpholino-mediated gene knock down, especially if the investigation concerns the hindbrain.

In this study, three independent Morpholinos targeting the *lunaparkA* mRNA sequence were used. They were intensively tested and showed specific and efficient downregulation of the target gene mRNA. In the hindbrain, postmitotic commissural interneurons (HCIs) that are supposed to express *lnp* disappear after *lnpA* Mo treatment. The loss of this specific type of neurons is accompanied by highly abundant cell death throughout the CNS. Cell death as well as the loss of those neurons could be rescued with *p53* Mo co-injection. While for most genes the co-injection of p53 Mo solves the problems caused by off-target effects, thereby revealing the real phenotype, this is sometimes more problematic. In the rare cases that specific knock down of the gene itself would cause hindbrain cell death mediated by p53, for example a p53 inhibitor. *p53* Morpholino injection would eliminate specific and unspecific apoptosis simultaneously. If this is indeed the case for the *lunapark* gene, and the loss of endogenous *lunapark* would activate *p53* and subsequently apoptosis it could theoretically be tested by co-injection of the *lnpA* mRNA. The injected *lnpA* mRNA could then substitute the endogenous *lnpA* mRNA which was knocked down by *lnpA* Mo, thereby rescuing the specific apoptosis

and resulting in a reduction of overall cell death (Robu et al. 2007). In the case of *lunaparkA*, mRNA did not rescue the apoptotic effect. Arguing that the Mo induced cell death is an unspecific off-target effect.

In summary, it is impossible to make a legitimate conclusion about the function of LunaparkA in development based on the results of the Morpholino experiments. The only way to solve this problem is to obtain zebrafish embryos mutant for the *lunaparkA* gene. This could be achieved either by TILLING (Targeting Induced Local Lesions in Genomes) (McCallum et al. 2000b, 2000a; Draper et al. 2004) or by using Zinc finger nucleases (Kim et al. 1996; Ekker 2008). Tilling is a method that combines a standard technique of random mutagenesis using a chemical mutagen such as ENU with a sensitive DNA screening-technique that identifies single base mutations in a target gene. In order to guarantee a successful TILLING process the gene of interest should contain an exon of at least 350 bp of coding sequence that lies within the 5' two-thirds. Ideal target fragments correspond to single large exons near the 5' ends of target genes, where nonsense mutations are most likely to be deleterious (Moens et al. 2008). The Intron-Exon structure of *lunaparkA* does not fulfil these requirements because *lunaparkA* consists of 13 relatively short exons. Especially in the N-terminus none of *lnpA* Exon is longer than 188 bp. Therefore *lunaparkA* is a rather poor candidate for a successful TILLING approach and Zinc Finger nucleases mediated targeted mutagenesis will be the method of choice.

4.1.5. Lunapark: Summary & Future perspective

In this part of the study we aimed to determine the function of the so far undescribed LunaparkA in central nervous system development. We could show that the *lunaparkA* gene is highly conserved especially among vertebrate species not only in concern of sequence similarity but also in regards to gene regulation and its expression profile. The fact that the gene has been preserved to such a degree, suggests an important role during development. Concerning the spatial and temporal distribution of its expression pattern it is likely that LunaparkA is involved in migration, differentiation and axonogenesis of specific hindbrain neuronal progenitors which are at least partially derived from the rhombic lip.

In cell culture assays we could demonstrate, that the LunaparkA protein localises to late endosomes/lysosomes. A screen for putative interactors of the LunaparkA protein identified several candidates that are known to be part of the endosomal pathway and a great number of these putative interactors are known to be involved in vesicular fusion events. In addition, if strongly overexpressed, LunaparkA fusion proteins tend to form large vesicular structures

within the cell, which could result from enhanced membrane fusion. For that reason we believe that LunaparkA is mediating membrane fusions of endosomal vesicles either with other vesicles or the plasma membrane.

Based on genetic evidence from *Drosophila* and our results from the screen for interaction partners a possible developmental role of LunaparkA could be the attenuation of the Notch signal to allow neuronal progenitors to exit the cell cycle and to differentiate. Alternatively or in addition LunaparkA could direct membrane dynamics by regulation of membrane fusion during axonogenesis or neuronal migration.

In order to prove this hypothesis on the one hand the putative interactors have to be further analysed in terms of their binding behaviour and their gene expression. More importantly ways of inhibiting LunaparkA function have to be achieved. Knock down using antisense oligo Morpholinos has its limitations as demonstrated in this work.

Alternatively though, several different approaches based on results presented in this thesis are feasible:

In this work we have analysed carefully the properties of the *lnp* regulatory element in zebrafish embryos. We could show that the expression of fluorescent reporters driven by the *lnp* enhancer did nicely recapitulate the CNS expression of endogenous *lunaparkA* mRNA.

Establishing of transgenic zebrafish strains expressing an optimised variant of the Gal4 transcription factor (KalTA4) under the control of the *lnp* enhancer would allow to use combinatorial Gal4 genetics in order to express shRNA targeting *lnp* mRNA to interfere with Lnp translation. In order to monitor effective transactivation of the shRNA transgene the generated zebrafish strain could in addition express a fluorescent reporter (for example Venus a yellow fluorescent protein). An example for a transgenic construct that could be used to generate a anti-*lnp*-shRNA zebrafish strain could be UAS:anti-*lnp*-shRNA_UAS-*venus*. UAS (upstream activator sequence) is the sequence where the Gal4 transcription factor specifically binds in order to activate gene expression (Brand and Perrimon 1993).

An alternative to RNA interference is tissue specific expression of a dominant negative version of LnpA. We could show that LnpA is able to form dimers or even oligomers and that LnpA is also capable of binding to other proteins. In order to map these binding domains immunoprecipitation assays using truncated LnpA variants could be performed. Deletion of the binding domains could result in a dominant negative version of LnpA protein that could be used in combination with the *lnp*:KalTA4 line to inhibit endogenous LnpA function in the CNS.

Another promising approach is a mutagenesis method based on zinc finger nucleases. Zinc finger nucleases are artificial fusion proteins that consist of a zinc finger DNA binding domain and the non-specific cleavage domain from the restriction endonuclease FokI. Zinc finger domains can be engineered to target desired DNA sequences, which enables zinc-finger nucleases to target unique sequence within a complex genome resulting in a DNA double strand break. Incomplete repair of this DNA cleavage results in a targeted mutation of the targeted locus.

Any of these three methods will allow us to address the function of Lunapark independent from Morpholino knock down which is crucial to understand the role of Lunapark in central nervous system development.

4.2. *atonal1* expressing rhombic lip cells migrate tangentially along the rhombomere boundaries in the zebrafish hindbrain

4.2.1. The global regulatory element of *lunapark* and the *hoxd* cluster drives reporter gene expression in migrating hindbrain commissural interneurons

Important landmarks of embryonic neural development include the birth and differentiation of neurons from stem cell precursors, the migration of immature neurons from their birthplaces to their final positions in the embryo, the outgrowth and guidance of axons and dendrites, and the generation of synapses. Due to advanced bio-imaging techniques and tissue specific expression of fluorescent molecules, these processes can be observed under highly dynamic in vivo conditions in developing zebrafish embryos.

In order to achieve the tissue specific expression necessary to distinguish between different neuronal subtypes, regulatory elements need to be identified and isolated. The large size and high complexity of such enhancers often make this a challenging task. Recently, a global control region (GCR) that regulates several genes, including the *hoxd* cluster, *evx2* and *lunapark,* was identified in mice (Spitz et al. 2003; Spitz and Duboule 2008). Strikingly, organisation of the entire genomic landscape around the *hoxd* cluster, including the GCR, shows a high degree of conservation among vertebrates and the GCR isolated from Tetraodon was able to drive reporter gene expression in mice embryos in a pattern that was CNS specific and closely resembled *evx2* and *lnp* expression. It is known that the genome of the pufferfish is among the smallest of the vertebrate genomes, about one-eighth the size of the human genome despite a similar repertoire of genes (Brenner et al. 1993). Many regulatory elements are conserved in pufferfish, but are rather small compared to the ones found in human and

other vertebrate genomes, thus facilitating the handling and cloning of these fragments. For that reason, we used the Tetraodon GCR to generate transgenic zebrafish strains expressing fluorescent proteins in the central nervous system (*lnp*:mRFP and *lnp*:Kaede). The fluorescent protein expression in these strains nicely resembles the endogenous gene expression of *lnpA* and *evx2*. Careful analysis revealed that the enhancer element drives expression in migrating neurons that differentiate into hindbrain commissural interneurons (HCI).

4.2.2. HCIs are derived from the rhombic lip and migrate tangentially along rhombomere boundaries to their ventral target areas

Hindbrain commissural interneurons are part of the sensory system. Previous studies suggested that these neurons are linking lateral line and auditory input to higher brain areas.

Interestingly, in the same study they showed that HCIs fail to properly differentiate after Morpholino-mediated knock down of *atoh1a* (Sassa et al. 2007). If the differentiation of HCIs is dependent on *atoh1a*-expressing cells located at the rhombic lip or if *atonal1a* is expressed in HCIs itself acting in a cell autonomous manner remained however unclear.

In order to address this question we generated triple transgenic (*atoh1a*:Gal4TA4/ UAS:GFP/ *lnp*:mRFP) zebrafish animals with *atoh1a* Enhancer element driven GFP expression in the rhombic lip and mRFP expression in HCIs. These experiments showed that HCIs are born in the dorsal hindbrain as progeny of from rhombic lip progenitors. 3D time lapse imaging revealed further that the migration of the HCIs does not occur over the entire rhombencephalon, but follows a stereotypic pattern strictly along the rhombomere boundaries. The rhombomere boundaries had not previously been recognised as a pathway for migratory neurons in zebrafish embryos. They are rather known for maintaining boundary lineage restriction and for their function as local organisers. Thus, our results assign a new role to rhombomere boundaries providing a permissive territory for HCI progenitor migration.

The migratory routes of *atonal1* expressing rhombic lip cells have been intensely investigated in other vertebrate species especially in chick and mouse embryos showing that these neuronal progenitors do not migrate from all over the rhombic lip they rather follow strictly defined routes with a distinct anterior posterior pattern (Wingate 2001; Bloch-Gallego et al. 2005; Landsberg et al. 2005; Wang et al. 2005; Ray and Dymecki 2009). How this anterior posterior pattern although develops as remained elusive so far. Concerning the conservation of neuronal progenitor migration in the cerebellum it might well be that the hindbrain migratory routes are also conserved and that rhombomere boundaries might play also role in the anterior posterior pattern of other vertebrates like mice for example.

One reason why until now the rhombomeric pattern of this migration route was not observed in mice or chicken might be due to the function of the HCIs in the animal. Preliminary data obtained from behavioural assays performed in this study, as well as retrograde axon tracing of HCIs in the developing zebrafish (Sassa et al. 2007), strongly supports the fact that the HCIs are interneurons of the lateral line and auditory system. During the evolution from fish to mammals and birds, the auditory system was preserved while the lateral line organ was lost. It might therefore be possible that the HCIs required for relaying lateral line information together with their migration routes were lost as well.

However, what about the neurons of the auditory system? In mice it is well established that all neurons contributing to the cochlear nucleus are derived from the *atonal1* expressing caudal rhombic lip. In order to reach their target area, they follow a well defined extramural migration stream similar to the pathway of the HCIs in the fish hindbrain, but whether this stream runs along the rhombomere boundaries has not yet been investigated. As the migration in mouse was elucidated through lineage tracing analysis on fixed tissues sections rather than by time lapse, it is still possible that the mouse rhombomere boundaries have an unrecognised function in providing a migration pathway for differentiating neurons.

The guidance molecules or mechanical forces that drive HCI migration in zebrafish embryos along rhombomere boundaries remain unknown. Evidence obtained from mouse shows that the guidance molecules Netrin-1 and Slit act as a chemoattractant factors for neurophilic migration of precerebellar neurons (PCN) and neurons from the cochlear nucleus that are derived from the rhombic lip directing dorso ventral migration(Causeret et al. 2004; Bloch-Gallego et al. 2005; Howell et al. 2007; Marcos et al. 2009). However, an involvement in anterior posterior patterning of the migration streams as not been demonstrated. Interestingly, zebrafish *netrin1a* is expressed in the floor plate showing a pronounced dorsal expansion of its expression domain at the rhombomere boundaries, (Park et al. 2005; Vanderlaan et al. 2005; Ke et al. 2008) thus providing a good candidate for restricting the migration of *atonal* expressing rhombic lip neuronal progenitors to the rhombomere boundaries.

It is one possibility, that ventral guidance factors provide instructive cues to direct HCI migration, or it may be that the boundaries represent the best permissive territory for HCI migration in comparison to the repulsive and differential adhesion properties of rhombomere cells mediated by Eph receptor tyrosine kinases (Eph) and their Ephrin ligands (Cooke et al. 2001; Cooke et al. 2005). The strong Eph-Ephrin interaction within the individual rhombomers might physically prevent HCIs to invade the rhombomers themselves. At the interface of two adjacent rhombomeres with different adhesive properties the HCIs might be

able to migrate freely. During the time of HCI migration, a defined pattern of radial glial fibres spans the hindbrain in a dorso ventral direction adjacent to the rhombomere boundaries. Although HCIs migrate to final ventral positions in close proximity to the glial fibres, it is clear that they do not undergo radial migration. Instead, time lapse images clearly showed that HCIs migrate tangentially, forming chain-like structures along the outer border of the neuroepithelium were glial fibres are absent.

4.2.3. HCIs form a complex meshwork of differentially projecting axons

HCIs that reach their target areas settle in clusters at the rhombomere boundaries and start to extend commissural axons across the ventral floorplate. During the migration process, HCIs appear to be a very homogeneous population and so it was surprising that the axonal projections of individual HCIs are actually quite diverse. It had previously been shown that these neurons project over the midline and then follow distinct longitudinal fascicles to terminate in the midbrain torus semicircularis (Sassa et al. 2007). To more carefully analyze the axonal projections of individual HCIs, we used a zebrafish line that expresses the photoconvertible fluorescent protein Kaede in HCIs. Small clusters of Kaede positive cells were converted from green to red fluorescence and the outgrowth of their axons was monitored. These experiments showed that axons from HCIs within the same cluster project to a variety of targets by turning either rostrally or caudally in the contra-lateral hindbrain and joining different longitudinal axon fascicles. The caudal projections, which had not previously been recognised, could represent circuitries directly connecting the lateral line and auditory inputs to the spinal chord motor system, promoting locomotive reflex responses to sound and vibration stimuli. This idea is further supported by our preliminary results obtained from behavioural experiments, where the depletion of HCIs induced by Notch over activation resulted in a failure to respond to sound and vibration.

Several explanations are possible for how a homogenous population of cells can produce a projection pattern of such high diversity. It could for example be that the growth cone of an axon is not predetermined to reach a particular destination and instead initially follows general projection rules. On its way, it may be able to make crucial decisions upon reaching certain critical points, like for example longitudinal fascicles on the contralateral side, thereby integrating the projection patterns of HCI axons that arrived earlier. Alternatively, the temporal order at which HCIs arrive in ventral hindbrain positions after tangential migration along rhombomere boundaries may pose a distinct fate onto terminally differentiating HCIs and thus instructs them to contribute to certain circuitries by establishing a distinct axon

projection pattern. Thus, an analysis of the molecular and cell biological processes of zebrafish HCI axon projections promises to reveal important insights into the mechanisms of axon guidance, afferent selection and neuronal circuitry establishment. In vivo imaging of axonogenesis in zebrafish using photoconvertible fluorescent proteins provides a powerful tool to gain access to these answers.

4.3. Differentiation and migration of the *atonal1* expressing HCI progenitors depends on Notch signalling

4.3.1. Notch signalling is required for RL progenitor maintenance and for the differentiation of late born hindbrain neurons

In vivo time lapse analysis performed in this study showed that hindbrain commissural interneurons are born in the caudal rhombic lip and migrate to ventral positions where they terminally differentiate. In order to understand how this process is regulated on a molecular level, the Notch signal transduction pathway was conditionally manipulated. Depletion of Notch signalling by DAPT treatment of 24 hpf embryos resulted in premature differentiation of all rhombic lip progenitors and a loss of later born neurons, such as the HCIs. Strikingly, if Notch signalling is constitutively activated inside the rhombic lip by expression of *athonal1* enhancer-driven NICD, HCIs also fail to differentiate but in this case due to enhanced progenitor maintenance in the rhombic lip. Thus Notch signalling is required to establish and maintain a HCI progenitor pool in the rhombic lip, but at the same time must eventually be downregulated to allow for the differentiation of HCIs.

The role of Notch in maintaining progenitors while ensuring constant neuronal differentiation has been described for various neuroepithelia (Bertrand et al. 2002; Ross et al. 2003; Kageyama et al. 2008; Kopan and Ilagan 2009; Imayoshi et al. 2010). This study is the first to show that the progenitor pool of the caudal rhombic lip also relies on Notch signal transduction for maintenance. This finding is of particular interest, as the rhombic lip is a unique germinal zone that produces different types of neurons in a highly organised spatio-temporal manner (Wang et al. 2005; Volkmann et al. 2008; Volkmann et al. 2010). Interestingly, in the upper rhombic lip of mouse embryos, Notch signalling was found to be critical for controlling the timing of the induction of upper rhombic lip neurons from the progenitor pool, in addition to its role in progenitor maintenance (Machold et al. 2007). Specification of the rhombic lip-derived neurons thus appears to occur within the rhombic lip itself and prior to migration. Consistent with this idea is that early born HCI progenitors, which escape the full effect of DAPT-treatment, are able to differentiate but are located at

ectopic positions and show ectopic axon projections. Moreover, recent cell tracing studies of migrating granule cells in the differentiating zebrafish cerebellum showed that the spatial pattern in the upper rhombic lip predicts the final contribution of granule neurons to different cerebellar compartments, indicating again that the cells have already been specified by the time they leave the rhombic lip (Volkmann et al. 2008).

In summary, cell fate specification of rhombic lip-derived neurons likely occurs within the dorsal neuroepithelium, and Notch signalling is required for progenitor maintenance in order to ensure the generation of later born neurons. In addition Notch signalling may be also required to control the timing of the differentiation of different neuronal subtypes emanating from the rhombic lip.

4.3.2. Notch activity in neuronal migration

We have observed that some rhombic lip cells when treated with DAPT were still able to differentiate. Although, these cells expressed Neurolin and formed commissural axonal processes, they remained in dorsal positions instead of migrating ventrally and their axons projected to ectopic dorsal locations. This finding suggests two independent roles for Notch signalling. First, Notch is required for the maintenance of HCI progenitors within the rhombic lip, but has to be turned off in cells that are determined to differentiate into HCIs. Second, with ongoing development, Notch becomes required for proper cell migration at the rhombomere boundaries. Because HCIs that escape the full effect of DAPT are still able to differentiate but they fail to migrate to their ventral target areas.

While the involvement of Notch signalling in cell differentiation is well described, its role in neuronal migration has not been systematically explored. Recently however, some evidence concerning this issue has emerged. For example, analysis of mice Presenilin-1 mutants revealed widespread neuronal migration phenotypes (Louvi et al. 2004; Wines-Samuelson et al. 2005). Presenilin-1 is a crucial component of the γ-Secretase complex and is therefore required for Notch receptor activation. As a consequence of the inability to activate Notch signal transduction, target genes of the pathway are downregulated in several migratory neuronal populations like telencephalic cortical neurons, midbrain dopaminergic neurons, cerebellar granule neurons and lower rhombic lip-derived precerebellar neurons. All of these neurons fail to find their proper locations due to severe migration defects (Louvi et al. 2004). However, in view of the complex relationship between Presenilin and specific cellular events and biochemical pathways that affect neuronal migration, it is unlikely that these defects are all dependent on misregulation of Notch activity (Louvi and Artavanis-Tsakonas 2006). More

recent findings show that regulation of Notch activity is important for Reelin-dependent neuronal migration. Reelin-deficient mice have reduced levels of the cleaved form of the Notch intracellular domain (NICD) and this loss of Notch signalling in migrating neurons results in migration and morphology defects. Furthermore, overexpression of NICD reduces the laminar and morphological abnormalities of migrating neurons in Reeler mice and thus partly rescues Reelin deficient mice (Hashimoto-Torii et al. 2008a). Interestingly, in situ hybridisation experiments on the zebrafish hindbrain show that *reelin* is expressed in close proximity to the rhombomere boundaries, along which HCIs do migrate (Costagli et al. 2002). These findings together with our results suggest a so far barely recognised role of Notch signal transduction in neuronal migratory processes.

4.3.3. Rhombic lip progenitor and Notch regulation: Summary & Future perspective

Using in vivo time lapse analysis of fluorescent zebrafish transgenic lines in combination with conditional genetics, we were able to show that hindbrain commissural interneurons are rhombic lip derived. They show intense dorso ventral migration behaviour and follow precisely defined migratory routes along the rhombomere boundaries. These neurons generate a complex meshwork of axonal projections and seem to be important if not necessary for promoting the sensory input of the lateral line and auditory system. We could demonstrate that the differentiation of these neurons is dependent on the precise temporal attenuation of Notch signalling in their progenitors. Sustained Notch activity in HCI precursors prevents differentiation, while blocking Notch globally within the organism results in premature differentiation of those cells. In addition to the importance of Notch signalling in progenitor cell maintenance in the rhombic lip, a role of Notch activity which has been well described in other systems, we found that Notch signalling is also required for proper HCI migration. Whether this effect is cell autonomous or mediated by the surrounding cells e.g. rhombomere boundary cells still has to be clarified. An experiment that could provide further insight in this mechanism is the conditional inactivation of Notch signalling in HCI progenitors by *atoh1*:Gal4 driven overexpression of dominant negative Suppressor of hairless dnSu(H).

The zebrafish hindbrain is probably the brain region with the easiest accessibility to neuro-imaging techniques. Our transgenic Kaede line in combination with Gal4 genetics provides a very good model not only to address questions concerning HCI migration and axon guidance but it might also help to understand general mechanisms concerning these developmental processes. In addition, it could be interesting to perform experiments that interfere with Netrin1a signalling or Eph-Ephrin mediated cell adhesion in the zebrafish hindbrain using for

example, Morpholinos that are well established for various *eph* and *ephrin* genes (Cooke et al. 2001; Cooke et al. 2005; Kemp et al. 2009), to find out if these factors are important for rhombomere boundary restricted migration. Thereby getting new insights the important developmental processes of axon guidance and path finding of migrating neurons and neuronal progenitors

5. Appendix

5.1. Supplementary Figures

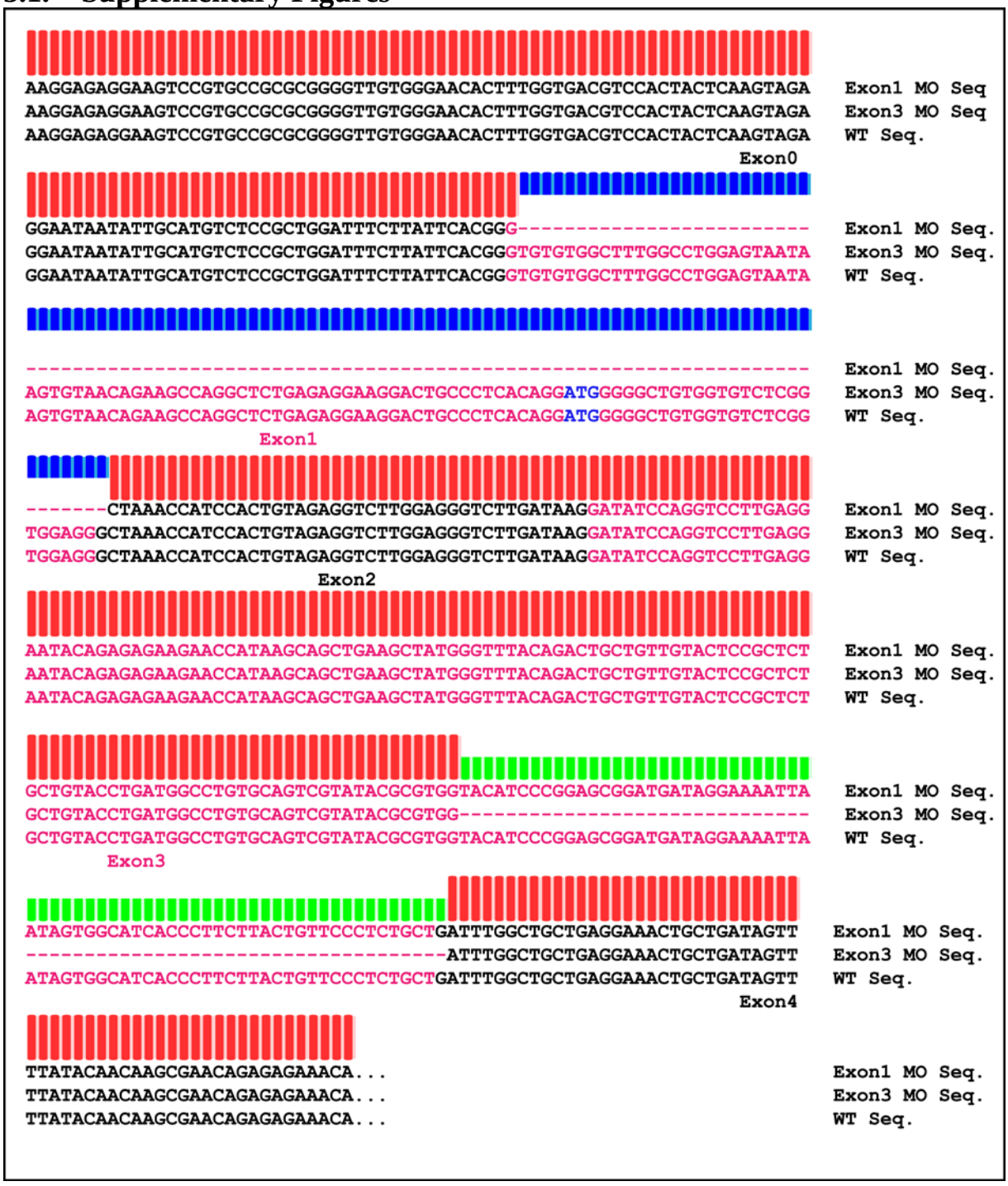

Figure 1 Sequence analysis of zebrafish embryos injected with Exon2 Mo & Exon4 Mo

lnpA mRNA transcripts obtained by RT-PCR after splice Morpholino injection were separated by agarose gel-electrophoresis, extracted and subsequently sequenced. Blue area indicates the sequence section excised by Exon2 Morpholino injection. Green labels show the part of the transcript removed upon injection of the Exon4 Morpholino.

5.2. Abbrevations

AA	amino acid
AcO	Acridine Orange
ATP	adenosine triphosphate
BCIP	5-bromo-4-chloro-3'-indolyphosphate p-toluidine
bp	base pair
BSA	bovine serum albumine
CB	cerebellum
CNS	central nervous system
cRL	caudal rhombic lip
DAB	diaminobenzidine
DMSO	dimethylsulfoxid
DNA	deoxyribonucleic Acid
DNAse	desoxyribonuclease
dNTP	deoxynucleotide triphosphate
dpf	days past fertilization
E.coli	Escherichia coli
EGL	external granular layer
ENU	N-ethyl-N-nitrosourea
EtOH	ethanol
GFP	green fluorescent protein
GCR	global control region
h	hour
H2B	Histone 2B
HCI	hindbrain commissural interneurons
hpf	hours past fertilization
IGL	inner granular layer
IsO	isthmic organiser
IPTG	isopropyl-β-D-thiogalactopyranosid
IV	fourth ventricle
kD	kilo dalton
LB	Luria-Bertani medium
µ	micro-
MeOH	methanol
MHB	mid-hindbrain boundary
min	minutes
mRFP	monomeric red fluorescent protein
mRNA	messenger RNA
n	nano-
NBT	nitro-blue tetrazolium chloride
NGS	normal goat serum
OD	optical density
PBS	phosphate-buffered saline
PC	purkinje cells
PCR	polymerase chain reaction
PFA	paraformaldehyd
PTU	phenylthiourea
PTW	PBS with Tween
RA	retinoic acid
Rh	rhombencephalon
RNA	ribonucleic acid
RNase	ribonuclease
rpm	rounds per minute
rRL	rostral rhombic lip
RT	room temperature
RT-PCR	reverse transcription-polymerase chain reaction
sec	seconds
SP	signal peptide
TAP	tandem affinity purification
Tris	2-Amino-2-hydroxymethyl-1,3-propandiol
Tween®20	poly(oxyethylen)n-sorbitan-monolaurate
U	units
UAS	upstream activating sequence
URL	upper rhombic lip
UTP	Uridine Triphosphate
UV	ultra violette
V	volt
YFP	yellow fluoresce

5.3. Movie legends

Movie 1 LnpA-YFP in PAC2 cells
360° projection of an image stack recorded by confocal microscopy of a single PAC2 cell transiently transfected with Lnp-YFP shows large vacuole-like structures within the cell. Scale bar 10 µm.

Movie 2 NTM-mCherry localisation
Images recorded by confocal microscopy of a PAC2 cell transiently transfected wit NTM-mCherry recorded over time. Left panel shows fluorescent signal only, right panel shows brightfield image in addition. NTM-mCherry is localises to dark vesicular structures that are highly motile. Scale bars 10 µm.

Movie 3, 4, 5. Projection patterns of hindbrain commissural interneurons
Time lapse sequence of dorsal view projections of image stack recorded by confocal microscopy of *lnp:*Kaede expressing embryos. Cells at multiple (1) or individual rhombomere boundaries (2-3) have been repetitively converted by UV laser light in areas indicated by dotted rectangles and recorded over time. Arrows depict axonal growth cones. Scale bars 50 µm

Movie 6.
3D overview a *lnp*:mRFP expressing zebrafish hindbrain and migratory behaviour at rhombomere boundaries 3D reconstruction of time series of image stacks recorded by confocal microscopy of a *lnp:*mRFP zebrafish hindbrain. The first part shows an 3D overview of the *lnp:*mRFP hindbrain expression pattern. Starting from a dorsal view, the embryo is first rotated 180° around the x-axis and then back to starting position, followed by a rotation of 180° around the y-axis. In the second part the movie shows dorso-ventral migration of *lnp:*mRFP expressing cells along rhombomere boundaries (black arrows) Scale bars 50 µm

Movie 7. Migration of individual clusters of HCI along rhombomere boundaries
Maximum intensity projections of time lapse image stacks recorded by confocal microscopy during the main phase oh HCI migration. Single clusters were converted at approx. 24 hpf in the dorsal hindbrain of *lnp:*Kaede expressing embryos. Individual cells migrate in a bow like structure in a narrow extramural migration stream along rhombomere boundaries (white arrows). Scale bars 50 µm

Movie 8. Migration of HCIs dorsal view
Time-lapse movie of dorsal view stacks recorded from the hindbrain of a *lnp:*Kaede expressing embryo by confocal microscopy. At 24 hpf the dorsal domain was completely converted using UV laser light excitation. Left panel: Maximum intensity projection of red and green channel. Middle panel: Anaglyph visualisation of the green channel. Left panel: Anaglyph visualisation of the red channel. (To achieve the 3D effect red green goggles are required). Scale bars 50 µm

Movie 9. Migration of HCIs lateral view
Time-lapse movie of lateral projections of image stacks recorded by confocal microscopy stacks from the hindbrain of a *lnp:*Kaede expressing embryo. The dorsal *lnp*:Kaede expression domain was converted using UV laser light excitation at 24 hpf. Cells migrate from the rhombic lip along rhombomere boundaries to populate the ventral commissural interneuron clusters (white arrows). Scale bars 50 µm

Movie 10 Response of wildtype embryos to Sound and vibration stimuli (SVS)
Time lapse recordings of wildtype zebrafish embryos at 6 dpf. The embryos were repetitively exposed to SVS induced by tapping the rim of the petri dish with the tip of a needle. The majority of the embryos showed extensive escape response after individual stimuli.

Movie 11 *atoh1a*:KalTA4/UAS:NICD show impaired escape response after SVS
Time lapse recordings of *atoh1a*:KalTA4/UAS:NICD transgenic zebrafish embryos at 6 dpf. The embryos were repetitively exposed to SVS induced by tapping the rim of the petri dish with the tip of a needle. Most embryos fail to perform an escape response after SVS.

Movie 12 Comparison of wildtype and *atoh1a*:KalTA4/UAS:NICD embryos in regards to their early escape response
Simultaneous time lapse recordings of wildtype (left dish) *atoh1a*:KalTA4/UAS:NICD (right dish) zebrafish embryos at 6 dpf. The embryos were repetitively exposed to SVS induced by hitting the surface between the two petri dishes with the bar end of a needle. Wildtype embryos show intense and synchronous flight response after SVS whereas transgenic embryos showed almost no reaction. See also Results Figure 54.

Movie 13 Touch response of wildtype embryos
Time lapse recordings of wildtype zebrafish embryos at 6 dpf. Individual embryos tapped with the tip of a needle showed normal escape response.

Movie 14 *atoh1a*:KalTA4/UAS:NICD are capable of a touch induced escape response
Individual *atoh1a*:KalTA4/UAS:NICD transgenic zebrafish embryos at 6 dpf were teased with the tip of a needle and recorded over time. Most of the excited embryos were capable of performing an escape response.

5.4. List of publications

5.4.1. Publications

- Chu, Y., **Senghaas, N.**, Köster, R.W., Wurst, W., Kühn, R. (2008), Novel caspase-suicide proteins for tamoxifen-inducible apoptosis.
Genesis 46(10), 530-6.

- **Senghaas, N.**, Köster, R.W. (2009), Culturing and Transfecting Zebrafish PAC2 Fibroblast Cells.
CSH Protocols 4(6):725-731

- Rieger, S., **Senghaas, N.**, Walch, A., and Koster, R. W. (2009). Cadherin-2 controls directional chain migration of cerebellar granule neurons.
PLoS Biol 7, e1000240.

5.4.2. Publications in Preparation

- **Senghaas,N.**, Solchenberger,B., Köster,R.W. Notch-dependent differentiation of hindbrain interneurons involves rhombomere boundary migration

5.5. Lebenslauf

AKADEMISCHER WERDEGANG

Mai/2006 bis Aug/2010

Promotion in der Zebrafisch Neuroimaging Gruppe von Dr. Reinhard Köster am Helmholtz Zentrum München unter der Betreuung von Prof. Dr. Wolfgang Wurst
http://www.helmholtz-muenchen.de/en/idg/group-neuroimaging/goal/index.html

Titel: *Regulation, Biochemistry and functional Analysis of the conserved Lunapark Protein in Central Nervous System Development*

Schwerpunkte:
- *In vivo confocal Bioimaging*
- Durchlicht und Epifluoreszenz Mikroskopie
- Zebrafisch Neurogenetik
- Protein *Pulldown* für Massenspektrometrie

Nov/2005

Diplom der Biologie an der Albert-Ludwigs-University Freiburg, Abschluss 1,1 (sehr gut).
Titel der Diplomarbeit: *Acetylierung des Wnt-Effektorproteins TCF4 durch die Co-Aktivatoren und Histonacetyltransferasen p300/CBP*

Schwerpunkte:
- Proteinbiochemie
- Proteinaufreinigung
- Zellkultur

Sept/2001

Vordiplom an der Albert-Ludwigs-Universität Freiburg mit 1,7 (gut)

Okt/2000

Studienwechsel von Lehramt auf Diplombiologie.
Hauptfach: Entwicklungsbiologie Nebenfächer: Genetik, Biochemie und Organische Chemie

Okt/1998 bis Okt/2000

Lehramtsstudium in den Hauptfächern Biologie, Englisch und Mathematik an der Albert-Ludwigs-Universität in Freiburg

SCHULAUSBILDUNG

Aug/1988 bis Juni/1997

Allgemeine Hochschulreife am Robert-Mayer-Gymnasium Heilbronn, Abschluss: 2,4 (gut)

LEHRTÄTIGKEITEN

Jan/2009 bis Okt/2010

Betreuung einer Masterstudentin während ihrer Abschlussarbeit im Fach Molekulare Biotechnologie an der TU München

Hauptstudium bis Ende Promotion

Betreuung diverser Hochschulpraktika als Kursassistent.
Beispiele
- *Grundkurs IV-Histologie, Anatomie und Embryologie der Wirbeltiere und niederen Deuterostomier* 2002 (Universität Freiburg)
- *Forschungspraktikum Neurogenetik* 2007 (TUM)
- *Entwicklungsbiologisches Grundpraktikum* 2007/2008/2009 (TUM)

AUSLANDSERFAHRUNG

Sept/2003 bis Dez/2003

Viermonatiges Großpraktikum an der Universität Calgary in Alberta, Kanada im Labor von Dr. Sarah Childs, unterstützt von der Universität Calgary und dem DAAD

Juni/2007

Zwei Wochen Kurs *Advanced Bioimaging* am Zentrum für molekulare Medizin, Singapur

Eidesstattliche Erklärung

Ich erkläre hiermit an Eides statt, dass ich die vorliegende Arbeit selbständig ohne unzulässige fremde Hilfe angefertigt habe. Die verwendeten Literaturquellen sind im Literaturverzeichnis vollständig zitiert.

Heilbronn, 01. 11. 2010

_____

(Niklas Senghaas)

6. References

Adolf B, Bellipanni G, Huber V, Bally-Cuif L (2004) atoh1.2 and beta3.1 are two new bHLH-encoding genes expressed in selective precursor cells of the zebrafish anterior hindbrain. Gene Expr Patterns 5(1): 35-41.

Ahn D, Ho RK (2008) Tri-phasic expression of posterior Hox genes during development of pectoral fins in zebrafish: implications for the evolution of vertebrate paired appendages. Dev Biol 322(1): 220-233.

Alberts B, Johnson A, Lewis J, Raff M, Roberts K et al. (2002) The Compartmentalization of Cells. Molecular Biology of the Cell. 4th Edition ed. New York: Garland Science.

Alberts P, Rudge R, Irinopoulou T, Danglot L, Gauthier-Rouviere C et al. (2006) Cdc42 and actin control polarized expression of TI-VAMP vesicles to neuronal growth cones and their fusion with the plasma membrane. Mol Biol Cell 17(3): 1194-1203.

Alberts P, Rudge R, Hinners I, Muzerelle A, Martinez-Arca S et al. (2003) Cross talk between tetanus neurotoxin-insensitive vesicle-associated membrane protein-mediated transport and L1-mediated adhesion. Mol Biol Cell 14(10): 4207-4220.

Alder J, Cho NK, Hatten ME (1996) Embryonic precursor cells from the rhombic lip are specified to a cerebellar granule neuron identity. Neuron 17(3): 389-399.

Alder J, Lee KJ, Jessell TM, Hatten ME (1999) Generation of cerebellar granule neurons in vivo by transplantation of BMP-treated neural progenitor cells. Nat Neurosci 2(6): 535-540.

Altman J, Bayer SA (1997) Development of the Cerebellar
System: In Relation to its Evolution, Structure, and Functions. Boca Raton, FL: CRS Press.

Amores A, Force A, Yan YL, Joly L, Amemiya C et al. (1998) Zebrafish hox clusters and vertebrate genome evolution. Science 282(5394): 1711-1714.

Amoyel M, Cheng YC, Jiang YJ, Wilkinson DG (2005) Wnt1 regulates neurogenesis and mediates lateral inhibition of boundary cell specification in the zebrafish hindbrain. Development 132(4): 775-785.

Amsterdam A, Burgess S, Golling G, Chen W, Sun Z et al. (1999) A large-scale insertional mutagenesis screen in zebrafish. Genes Dev 13(20): 2713-2724.

Ando R, Hama H, Yamamoto-Hino M, Mizuno H, Miyawaki A (2002) An optical marker based on the UV-induced green-to-red photoconversion of a fluorescent protein. Proc Natl Acad Sci U S A 99(20): 12651-12656.

Apps R, Garwicz M (2005) Anatomical and physiological foundations of cerebellar information processing. Nat Rev Neurosci 6(4): 297-311.

Ashrafi K, Chang FY, Watts JL, Fraser AG, Kamath RS et al. (2003) Genome-wide RNAi analysis of Caenorhabditis elegans fat regulatory genes. Nature 421(6920): 268-272.

Baek JH, Hatakeyama J, Sakamoto S, Ohtsuka T, Kageyama R (2006) Persistent and high levels of Hes1 expression regulate boundary formation in the developing central nervous system. Development 133(13): 2467-2476.

Begemann G, Schilling TF, Rauch GJ, Geisler R, Ingham PW (2001) The zebrafish neckless mutation reveals a requirement for raldh2 in mesodermal signals that pattern the hindbrain. Development 128(16): 3081-3094.

Ben-Arie N, Bellen HJ, Armstrong DL, McCall AE, Gordadze PR et al. (1997) Math1 is essential for genesis of cerebellar granule neurons. Nature 390(6656): 169-172.

Bernardos RL, Raymond PA (2006) GFAP transgenic zebrafish. Gene Expr Patterns 6(8): 1007-1013.

Bertrand N, Castro DS, Guillemot F (2002) Proneural genes and the specification of neural cell types. Nat Rev Neurosci 3(7): 517-530.

Bloch-Gallego E, Causeret F, Ezan F, Backer S, Hidalgo-Sanchez M (2005) Development of precerebellar nuclei: instructive factors and intracellular mediators in neuronal migration, survival and axon pathfinding. Brain Res Brain Res Rev 49(2): 253-266.

Blond-Elguindi S, Cwirla SE, Dower WJ, Lipshutz RJ, Sprang SR et al. (1993) Affinity panning of a library of peptides displayed on bacteriophages reveals the binding specificity of BiP. Cell 75(4): 717-728.

Bolivar F, Backman K (1979) Plasmids of Escherichia coli as cloning vectors. Methods Enzymol 68: 245-267.

Bong YS, Park YH, Lee HS, Mood K, Ishimura A et al. (2004) Tyr-298 in ephrinB1 is critical for an interaction with the Grb4 adaptor protein. Biochem J 377(Pt 2): 499-507.

Bonifacino JS, Glick BS (2004) The mechanisms of vesicle budding and fusion. Cell 116(2): 153-166.

Brand AH, Perrimon N (1993) Targeted gene expression as a means of altering cell fates and generating dominant phenotypes. Development 118(2): 401-415.

Bray SJ (2006) Notch signalling: a simple pathway becomes complex. Nat Rev Mol Cell Biol 7(9): 678-689.

Brenner S, Elgar G, Sandford R, Macrae A, Venkatesh B et al. (1993) Characterization of the pufferfish (Fugu) genome as a compact model vertebrate genome. Nature 366(6452): 265-268.

Brewer JW, Diehl JA (2000) PERK mediates cell-cycle exit during the mammalian unfolded protein response. Proc Natl Acad Sci U S A 97(23): 12625-12630.

Broccoli V, Boncinelli E, Wurst W (1999) The caudal limit of Otx2 expression positions the isthmic organizer. Nature 401(6749): 164-168.

Bucci C, Thomsen P, Nicoziani P, McCarthy J, van Deurs B (2000) Rab7: a key to lysosome biogenesis. Mol Biol Cell 11(2): 467-480.

Bullock WO, Fernandex JM, Short JM (1987) Xl1-Blue: A High Efficiency Plasmid Transforming recA Escherichia coli Strain With Beta-Galactosidase Selection. BioTechniques 5: 376-379.

Cambronero F, Puelles L (2000) Rostrocaudal nuclear relationships in the avian medulla oblongata: a fate map with quail chick chimeras. J Comp Neurol 427(4): 522-545.

Causeret F, Hidalgo-Sanchez M, Fort P, Backer S, Popoff MR et al. (2004) Distinct roles of Rac1/Cdc42 and Rho/Rock for axon outgrowth and nucleokinesis of precerebellar neurons toward netrin 1. Development 131(12): 2841-2852.

Chandrasekhar A (2004) Turning heads: development of vertebrate branchiomotor neurons. Dev Dyn 229(1): 143-161.

Chandrasekhar A, Moens CB, Warren JT, Jr., Kimmel CB, Kuwada JY (1997) Development of branchiomotor neurons in zebrafish. Development 124(13): 2633-2644.

Chedotal A (2010) Should I stay or should I go? Becoming a granule cell. Trends Neurosci 33(4): 163-172.

Cheng YC, Amoyel M, Qiu X, Jiang YJ, Xu Q et al. (2004) Notch activation regulates the segregation and differentiation of rhombomere boundary cells in the zebrafish hindbrain. Dev Cell 6(4): 539-550.

Chi CL, Martinez S, Wurst W, Martin GR (2003) The isthmic organizer signal FGF8 is required for cell survival in the prospective midbrain and cerebellum. Development 130(12): 2633-2644.

Chitnis AB, Kuwada JY (1990) Axonogenesis in the brain of zebrafish embryos. J Neurosci 10(6): 1892-1905.

Chu Y, Senghaas N, Köster RW, Wurst W, Kühn R (2008) Novel caspase-suicide proteins for tamoxifen-inducible apoptosis. Genesis 46(10): 530-536.

Cooke J, Moens C, Roth L, Durbin L, Shiomi K et al. (2001) Eph signalling functions downstream of Val to regulate cell sorting and boundary formation in the caudal hindbrain. Development 128(4): 571-580.
Cooke JE, Kemp HA, Moens CB (2005) EphA4 is required for cell adhesion and rhombomere-boundary formation in the zebrafish. Curr Biol 15(6): 536-542.
Corbin JG, Nery S, Fishell G (2001) Telencephalic cells take a tangent: non-radial migration in the mammalian forebrain. Nat Neurosci 4 Suppl: 1177-1182.
Costagli A, Kapsimali M, Wilson SW, Mione M (2002) Conserved and divergent patterns of Reelin expression in the zebrafish central nervous system. J Comp Neurol 450(1): 73-93.
Cowan CA, Henkemeyer M (2001) The SH2/SH3 adaptor Grb4 transduces B-ephrin reverse signals. Nature 413(6852): 174-179.
Cowan CA, Yokoyama N, Saxena A, Chumley MJ, Silvany RE et al. (2004) Ephrin-B2 reverse signaling is required for axon pathfinding and cardiac valve formation but not early vascular development. Dev Biol 271(2): 263-271.
Cox JS, Shamu CE, Walter P (1993) Transcriptional induction of genes encoding endoplasmic reticulum resident proteins requires a transmembrane protein kinase. Cell 73(6): 1197-1206.
Davies JP, Cotter PD, Ioannou YA (1997) Cloning and mapping of human Rab7 and Rab9 cDNA sequences and identification of a Rab9 pseudogene. Genomics 41(1): 131-134.
De Reuck AVS, Cameron MP (1963) Ciba Foundation for the Promotion of International Cooperation in Medical and Chemical Research:
Lysosomes. Churchill, London: J&A.
Distel M, Köster RW (2007) In vivo time-lapse imaging of zebrafish embryonic development. CSH Protocols doi:10.1101/pdb.prot4816.
Distel M, Wullimann MF, Köster RW (2009) Optimized Gal4 genetics for permanent gene expression mapping in zebrafish. Proc Natl Acad Sci U S A 106(32): 13365-13370.
Dlugaszewska B, Silahtaroglu A, Menzel C, Kubart S, Cohen M et al. (2006) Breakpoints around the HOXD cluster result in various limb malformations. J Med Genet 43(2): 111-118.
Draper BW, McCallum CM, Stout JL, Slade AJ, Moens CB (2004) A high-throughput method for identifying N-ethyl-N-nitrosourea (ENU)-induced point mutations in zebrafish. Methods Cell Biol 77: 91-112.
Ekker SC (2008) Zinc finger-based knockout punches for zebrafish genes. Zebrafish 5(2): 121-123.
Elsen GE, Choi LY, Prince VE, Ho RK (2009) The autism susceptibility gene met regulates zebrafish cerebellar development and facial motor neuron migration. Dev Biol 335(1): 78-92.
Elsen GE, Choi LY, Millen KJ, Grinblat Y, Prince VE (2008) Zic1 and Zic4 regulate zebrafish roof plate specification and hindbrain ventricle morphogenesis. Dev Biol 314(2): 376-392.
Emanuelsson O, Brunak S, von Heijne G, Nielsen H (2007) Locating proteins in the cell using TargetP, SignalP and related tools. Nat Protoc 2(4): 953-971.
Fader CM, Colombo MI (2009) Autophagy and multivesicular bodies: two closely related partners. Cell Death Differ 16(1): 70-78.
Farago AF, Awatramani RB, Dymecki SM (2006) Assembly of the brainstem cochlear nuclear complex is revealed by intersectional and subtractive genetic fate maps. Neuron 50(2): 205-218.
Fashena D, Westerfield M (1999) Secondary motoneuron axons localize DM-GRASP on their fasciculated segments. J Comp Neurol 406(3): 415-424.

Fasshauer D, Sutton RB, Brunger AT, Jahn R (1998) Conserved structural features of the synaptic fusion complex: SNARE proteins reclassified as Q- and R-SNAREs. Proc Natl Acad Sci U S A 95(26): 15781-15786.
Flasza M, Nguyen Huu NS, Mazaleyrat S, Clemence S, Villemant C et al. (2006) Regulation of the nuclear localization of the human Nedd4-related WWP1 protein by Notch. Mol Membr Biol 23(3): 269-276.
Fortini ME, Rebay I, Caron LA, Artavanis-Tsakonas S (1993) An activated Notch receptor blocks cell-fate commitment in the developing Drosophila eye. Nature 365(6446): 555-557.
Fox MA, Sanes JR (2007) Synaptotagmin I and II are present in distinct subsets of central synapses. J Comp Neurol 503(2): 280-296.
Fraser SE, Koster RW (2009) Time-Lapse Microscopy of Brain Development. In: Westerfield M, Zon L, Detrich H, editors. Essential Zebrafish Methods: Cell and Developmental Biology: Academic Press. pp. 584.
Fujiyama T, Yamada M, Terao M, Terashima T, Hioki H et al. (2009) Inhibitory and excitatory subtypes of cochlear nucleus neurons are defined by distinct bHLH transcription factors, Ptf1a and Atoh1. Development 136(12): 2049-2058.
Garcia-Bellido A, Ripoll P, Morata G (1973) Developmental compartmentalisation of the wing disk of Drosophila. Nat New Biol 245(147): 251-253.
Gavalas A, Krumlauf R (2000) Retinoid signalling and hindbrain patterning. Curr Opin Genet Dev 10(4): 380-386.
Gazit R, Krizhanovsky V, Ben-Arie N (2004) Math1 controls cerebellar granule cell differentiation by regulating multiple components of the Notch signaling pathway. Development 131(4): 903-913.
Geling A, Steiner H, Willem M, Bally-Cuif L, Haass C (2002) A gamma-secretase inhibitor blocks Notch signaling in vivo and causes a severe neurogenic phenotype in zebrafish. EMBO Rep 3(7): 688-694.
Ghila L, Gomez M (2008) The evolutionarily conserved gene LNP-1 is required for synaptic vesicle trafficking and synaptic transmission. Eur J Neurosci 27(3): 621-630.
Gloeckner CJ, Boldt K, Ueffing M (2009a) Strep/FLAG tandem affinity purification (SF-TAP) to study protein interactions. Curr Protoc Protein Sci Chapter 19: Unit19 20.
Gloeckner CJ, Boldt K, Schumacher A, Ueffing M (2009b) Tandem affinity purification of protein complexes from mammalian cells by the Strep/FLAG (SF)-TAP tag. Methods Mol Biol 564: 359-372.
Godinho L, Mumm JS, Williams PR, Schroeter EH, Koerber A et al. (2005) Targeting of amacrine cell neurites to appropriate synaptic laminae in the developing zebrafish retina. Development 132(22): 5069-5079.
Gonzalez-Quevedo R, Lee Y, Poss KD, Wilkinson DG (2010) Neuronal regulation of the spatial patterning of neurogenesis. Dev Cell 18(1): 136-147.
Gonzalez F, Duboule D, Spitz F (2007) Transgenic analysis of Hoxd gene regulation during digit development. Dev Biol 306(2): 847-859.
Gould A, Itasaki N, Krumlauf R (1998) Initiation of rhombomeric Hoxb4 expression requires induction by somites and a retinoid pathway. Neuron 21(1): 39-51.
Gould GW, Lippincott-Schwartz J (2009) New roles for endosomes: from vesicular carriers to multi-purpose platforms. Nat Rev Mol Cell Biol 10(4): 287-292.
Graham FL, Smiley J, Russell WC, Nairn R (1977) Characteristics of a human cell line transformed by DNA from human adenovirus type 5. J Gen Virol 36(1): 59-74.
Gressens P (2006) Pathogenesis of migration disorders. Curr Opin Neurol 19(2): 135-140.
Guthrie S (2004) Neuronal development: putting motor neurons in their place. Curr Biol 14(4): R166-168.
Guthrie S (2007) Patterning and axon guidance of cranial motor neurons. Nat Rev Neurosci 8(11): 859-871.

Guthrie S, Lumsden A (1991) Formation and regeneration of rhombomere boundaries in the developing chick hindbrain. Development 112(1): 221-229.
Haines N, Irvine KD (2003) Glycosylation regulates Notch signalling. Nat Rev Mol Cell Biol 4(10): 786-797.
Hallonet ME, Teillet MA, Le Douarin NM (1990) A new approach to the development of the cerebellum provided by the quail-chick marker system. Development 108(1): 19-31.
Hammond C, Braakman I, Helenius A (1994) Role of N-linked oligosaccharide recognition, glucose trimming, and calnexin in glycoprotein folding and quality control. Proc Natl Acad Sci U S A 91(3): 913-917.
Hanson PI, Heuser JE, Jahn R (1997) Neurotransmitter release - four years of SNARE complexes. Curr Opin Neurobiol 7(3): 310-315.
Hashimoto-Torii K, Torii M, Sarkisian MR, Bartley CM, Shen J et al. (2008a) Interaction between Reelin and Notch signaling regulates neuronal migration in the cerebral cortex. Neuron 60(2): 273-284.
Hashimoto-Torii K, Torii M, Sarkisian M, Bartley C, Shen J et al. (2008b) Interaction between Reelin and Notch signaling regulates neuronal migration in the cerebral cortex. Neuron 60(60): 273-284.
Hashimoto T, Zhang XM, Chen BY, Yang XJ (2006) VEGF activates divergent intracellular signaling components to regulate retinal progenitor cell proliferation and neuronal differentiation. Development 133(11): 2201-2210.
Hatta K, Tsujii H, Omura T (2006) Cell tracking using a photoconvertible fluorescent protein. Nat Protoc 1(2): 960-967.
Hatten ME, Heintz N (1995) Mechanisms of neural patterning and specification in the developing cerebellum. Annu Rev Neurosci 18: 385-408.
Hay JC, Scheller RH (1997) SNAREs and NSF in targeted membrane fusion. Curr Opin Cell Biol 9(4): 505-512.
Heijne L (1988) A description of hydatidiform mole with ultrasound case studies. Radiography 54(614): 70-73.
Higashijima S, Hotta Y, Okamoto H (2000) Visualization of cranial motor neurons in live transgenic zebrafish expressing green fluorescent protein under the control of the islet-1 promoter/enhancer. J Neurosci 20(1): 206-218.
His (1891) Die Entwicklung des menschlichen Rautenhirns vom
Ende des ersten bis zum Beginn des dritten Monats. I Verlangertes Mark Abhandlungen der koniglicher sachsischen Gesellschaft der
Wissenschaften Mathematische-physikalische Klasse (29): 1-74.
Hoegg S, Meyer A (2005) Hox clusters as models for vertebrate genome evolution. Trends Genet 21(8): 421-424.
Hollemann T, Chen Y, Grunz H, Pieler T (1998) Regionalized metabolic activity establishes boundaries of retinoic acid signalling. Embo J 17(24): 7361-7372.
Hoshino M, Nakamura S, Mori K, Kawauchi T, Terao M et al. (2005) Ptf1a, a bHLH transcriptional gene, defines GABAergic neuronal fates in cerebellum. Neuron 47(2): 201-213.
Howell DM, Morgan WJ, Jarjour AA, Spirou GA, Berrebi AS et al. (2007) Molecular guidance cues necessary for axon pathfinding from the ventral cochlear nucleus. J Comp Neurol 504(5): 533-549.
Ikawa T, Hirose S, Masuda K, Kakugawa K, Satoh R et al. An essential developmental checkpoint for production of the T cell lineage. Science 329(5987): 93-96.
Imayoshi I, Sakamoto M, Yamaguchi M, Mori K, Kageyama R (2010) Essential roles of Notch signaling in maintenance of neural stem cells in developing and adult brains. J Neurosci 30(9): 3489-3498.

Isaacs HV, Pownall ME, Slack JM (1998) Regulation of Hox gene expression and posterior development by the Xenopus caudal homologue Xcad3. Embo J 17(12): 3413-3427.
Jekely G, Rorth P (2003) Hrs mediates downregulation of multiple signalling receptors in Drosophila. EMBO Rep 4(12): 1163-1168.
Joyner AL, Liu A, Millet S (2000) Otx2, Gbx2 and Fgf8 interact to position and maintain a mid-hindbrain organizer. Curr Opin Cell Biol 12(6): 736-741.
Jukkola T, Lahti L, Naserke T, Wurst W, Partanen J (2006) FGF regulated gene-expression and neuronal differentiation in the developing midbrain-hindbrain region. Dev Biol 297(1): 141-157.
Kadrmas JL, Beckerle MC (2004) The LIM domain: from the cytoskeleton to the nucleus. Nat Rev Mol Cell Biol 5(11): 920-931.
Kageyama R, Ohtsuka T, Kobayashi T (2008) Roles of Hes genes in neural development. Dev Growth Differ 50 Suppl 1: S97-103.
Kageyama R, Ohtsuka T, Hatakeyama J, Ohsawa R (2005) Roles of bHLH genes in neural stem cell differentiation. Exp Cell Res 306(2): 343-348.
Kageyama R, Ohtsuka T, Shimojo H, Imayoshi I (2009) Dynamic regulation of Notch signaling in neural progenitor cells. Curr Opin Cell Biol 21(6): 733-740.
Kani S, Bae YK, Shimizu T, Tanabe K, Satou C et al. (2010) Proneural gene-linked neurogenesis in zebrafish cerebellum. Dev Biol 343(1-2): 1-17.
Kashuba VI, Gizatullin RZ, Protopopov AI, Allikmets R, Korolev S et al. (1997) NotI linking/jumping clones of human chromosome 3: mapping of the TFRC, RAB7 and HAUSP genes to regions rearranged in leukemia and deleted in solid tumors. FEBS Lett 419(2-3): 181-185.
Kawakami K (2004) Transgenesis and gene trap methods in zebrafish by using the Tol2 transposable element. Methods Cell Biol 77: 201-222.
Kawakami K, Shima A (1999) Identification of the Tol2 transposase of the medaka fish Oryzias latipes that catalyzes excision of a nonautonomous Tol2 element in zebrafish Danio rerio. Gene 240(1): 239-244.
Kawakami K, Koga A, Hori H, Shima A (1998) Excision of the tol2 transposable element of the medaka fish, Oryzias latipes, in zebrafish, Danio rerio. Gene 225(1-2): 17-22.
Ke Z, Kondrichin I, Gong Z, Korzh V (2008) Combined activity of the two Gli2 genes of zebrafish play a major role in Hedgehog signaling during zebrafish neurodevelopment. Mol Cell Neurosci 37(2): 388-401.
Kemp HA, Cooke JE, Moens CB (2009) EphA4 and EfnB2a maintain rhombomere coherence by independently regulating intercalation of progenitor cells in the zebrafish neural keel. Dev Biol 327(2): 313-326.
Kerenyi L, Gallyas F (1972) A highly sensitive method for demonstrating proteins in electrophoretic, immunoelectrophoretic and immunodiffusion preparations. Clin Chim Acta 38(2): 465-467.
Kiecker C, Lumsden A (2005) Compartments and their boundaries in vertebrate brain development. Nat Rev Neurosci 6(7): 553-564.
Kim YG, Cha J, Chandrasegaran S (1996) Hybrid restriction enzymes: zinc finger fusions to Fok I cleavage domain. Proc Natl Acad Sci U S A 93(3): 1156-1160.
Kimmel CB, Ballard WW, Kimmel SR, Ullmann B, Schilling TF (1995) Stages of embryonic development of the zebrafish. Dev Dyn 203(3): 253-310.
Kimura K, Mizoguchi A, Ide C (2003) Regulation of growth cone extension by SNARE proteins. J Histochem Cytochem 51(4): 429-433.
Kolm PJ, Apekin V, Sive H (1997) Xenopus hindbrain patterning requires retinoid signaling. Dev Biol 192(1): 1-16.
Kopan R, Ilagan MX (2009) The canonical Notch signaling pathway: unfolding the activation mechanism. Cell 137(2): 216-233.

Korner U, Fuss V, Steigerwald J, Moll H (2006) Biogenesis of Leishmania major-harboring vacuoles in murine dendritic cells. Infect Immun 74(2): 1305-1312.
Köster RW, Fraser SE (2001a) Direct imaging of in vivo neuronal migration in the developing cerebellum. Curr Biol 11(23): 1858-1863.
Köster RW, Fraser SE (2001b) Tracing transgene expression in living zebrafish embryos. Dev Biol 233(2): 329-346.
Krishna SS, Majumdar I, Grishin NV (2003) Structural classification of zinc fingers: survey and summary. Nucleic Acids Res 31(2): 532-550.
Krumlauf R, Marshall H, Studer M, Nonchev S, Sham MH et al. (1993) Hox homeobox genes and regionalisation of the nervous system. J Neurobiol 24(10): 1328-1340.
Kulesa PM, Lu CC, Fraser SE (2005) Time-lapse analysis reveals a series of events by which cranial neural crest cells reroute around physical barriers. Brain Behav Evol 66(4): 255-265.
Lambert de Rouvroit C, Goffinet AM (2001) Neuronal migration. Mech Dev 105(1-2): 47-56.
Landsberg RL, Awatramani RB, Hunter NL, Farago AF, DiPietrantonio HJ et al. (2005) Hindbrain rhombic lip is comprised of discrete progenitor cell populations allocated by Pax6. Neuron 48(6): 933-947.
Lawrence PA (1973) A clonal analysis of segment development in Oncopeltus (Hemiptera). J Embryol Exp Morphol 30(3): 681-699.
Lewis J (1998) Notch signalling and the control of cell fate choices in vertebrates. Semin Cell Dev Biol 9(6): 583-589.
Lichtman JW, Fraser SE (2001) The neuronal naturalist: watching neurons in their native habitat. Nat Neurosci 4 Suppl: 1215-1220.
Lieber T, Kidd S, Alcamo E, Corbin V, Young MW (1993) Antineurogenic phenotypes induced by truncated Notch proteins indicate a role in signal transduction and may point to a novel function for Notch in nuclei. Genes Dev 7(10): 1949-1965.
Lin JW, Biankin AV, Horb ME, Ghosh B, Prasad NB et al. (2004) Differential requirement for ptf1a in endocrine and exocrine lineages of developing zebrafish pancreas. Dev Biol 274(2): 491-503.
Liu A, Joyner AL (2001) Early anterior/posterior patterning of the midbrain and cerebellum. Annu Rev Neurosci 24: 869-896.
Louvi A, Artavanis-Tsakonas S (2006) Notch signalling in vertebrate neural development. Nat Rev Neurosci 7(2): 93-102.
Louvi A, Sisodia SS, Grove EA (2004) Presenilin 1 in migration and morphogenesis in the central nervous system. Development 131: 3093-3105.
Louvi A, Alexandre P, Metin C, Wurst W, Wassef M (2003) The isthmic neuroepithelium is essential for cerebellar midline fusion. Development 130(22): 5319-5330.
Lu H, Bilder D (2005) Endocytic control of epithelial polarity and proliferation in Drosophila. Nat Cell Biol 7(12): 1232-1239.
Lu Q, Sun EE, Klein RS, Flanagan JG (2001) Ephrin-B reverse signaling is mediated by a novel PDZ-RGS protein and selectively inhibits G protein-coupled chemoattraction. Cell 105(1): 69-79.
Lumsden A, Krumlauf R (1996) Patterning the vertebrate neuraxis. Science 274(5290): 1109-1115.
Luzio JP, Pryor PR, Bright NA (2007) Lysosomes: fusion and function. Nat Rev Mol Cell Biol 8(8): 622-632.
Machold R, Fishell G (2005) Math1 is expressed in temporally discrete pools of cerebellar rhombic-lip neural progenitors. Neuron 48(1): 17-24.
Machold RP, Fishell G (2009) Math1: waiting to inhale. Neuron 64(3): 293-295.
Machold RP, Kittell DJ, Fishell GJ (2007) Antagonism between Notch and bone morphogenetic protein receptor signaling regulates neurogenesis in the cerebellar rhombic lip. Neural Dev 2: 5.

Maden M, Gale E, Zile M (1998a) The role of vitamin A in the development of the central nervous system. J Nutr 128(2 Suppl): 471S-475S.
Maden M, Sonneveld E, van der Saag PT, Gale E (1998b) The distribution of endogenous retinoic acid in the chick embryo: implications for developmental mechanisms. Development 125(21): 4133-4144.
Manzanares M, Cordes S, Kwan CT, Sham MH, Barsh GS et al. (1997) Segmental regulation of Hoxb-3 by kreisler. Nature 387(6629): 191-195.
Marcos S, Backer S, Causeret F, Tessier-Lavigne M, Bloch-Gallego E (2009) Differential roles of Netrin-1 and its receptor DCC in inferior olivary neuron migration. Mol Cell Neurosci 41(4): 429-439.
Maricich SM, Xia A, Mathes EL, Wang VY, Oghalai JS et al. (2009) Atoh1-lineal neurons are required for hearing and for the survival of neurons in the spiral ganglion and brainstem accessory auditory nuclei. J Neurosci 29(36): 11123-11133.
Marin O, Rubenstein JL (2001) A long, remarkable journey: tangential migration in the telencephalon. Nat Rev Neurosci 2(11): 780-790.
Martinez-Arca S, Alberts P, Zahraoui A, Louvard D, Galli T (2000) Role of tetanus neurotoxin insensitive vesicle-associated membrane protein (TI-VAMP) in vesicular transport mediating neurite outgrowth. J Cell Biol 149(4): 889-900.
Martinez-Arca S, Coco S, Mainguy G, Schenk U, Alberts P et al. (2001) A common exocytotic mechanism mediates axonal and dendritic outgrowth. J Neurosci 21(11): 3830-3838.
Marusich MF, Furneaux HM, Henion PD, Weston JA (1994) Hu neuronal proteins are expressed in proliferating neurogenic cells. J Neurobiol 25(2): 143-155.
Mathis L, Bonnerot C, Puelles L, Nicolas JF (1997) Retrospective clonal analysis of the cerebellum using genetic laacZ/lacZ mouse mosaics. Development 124(20): 4089-4104.
Maves L, Jackman W, Kimmel CB (2002) FGF3 and FGF8 mediate a rhombomere 4 signaling activity in the zebrafish hindbrain. Development 129(16): 3825-3837.
Mayor S, Pagano RE (2007) Pathways of clathrin-independent endocytosis. Nat Rev Mol Cell Biol 8(8): 603-612.
McCallum CM, Comai L, Greene EA, Henikoff S (2000a) Targeting induced local lesions IN genomes (TILLING) for plant functional genomics. Plant Physiol 123(2): 439-442.
McCallum CM, Comai L, Greene EA, Henikoff S (2000b) Targeted screening for induced mutations. Nat Biotechnol 18(4): 455-457.
Mellman I (1996) Endocytosis and molecular sorting. Annu Rev Cell Dev Biol 12: 575-625.
Metin C, Vallee RB, Rakic P, Bhide PG (2008) Modes and mishaps of neuronal migration in the mammalian brain. J Neurosci 28(46): 11746-11752.
Millimaki BB, Sweet EM, Dhason MS, Riley BB (2007) Zebrafish atoh1 genes: classic proneural activity in the inner ear and regulation by Fgf and Notch. Development 134(2): 295-305.
Miyata T, Kawaguchi A, Okano H, Ogawa M (2001) Asymmetric inheritance of radial glial fibers by cortical neurons. Neuron 31(5): 727-741.
Moens CB, Prince VE (2002) Constructing the hindbrain: insights from the zebrafish. Dev Dyn 224(1): 1-17.
Moens CB, Donn TM, Wolf-Saxon ER, Ma TP (2008) Reverse genetics in zebrafish by TILLING. Brief Funct Genomic Proteomic 7(6): 454-459.
Morata G, Lawrence PA (1975) Control of compartment development by the engrailed gene in Drosophila. Nature 255(5510): 614-617.
Morris NR, Efimov VP, Xiang X (1998) Nuclear migration, nucleokinesis and lissencephaly. Trends Cell Biol 8(12): 467-470.
Mukherjee S, Ghosh RN, Maxfield FR (1997) Endocytosis. Physiol Rev 77(3): 759-803.
Mumm JS, Kopan R (2000) Notch signaling: from the outside in. Dev Biol 228(2): 151-165.

Nadarajah B, Brunstrom JE, Grutzendler J, Wong RO, Pearlman AL (2001) Two modes of radial migration in early development of the cerebral cortex. Nat Neurosci 4(2): 143-150.
Narita Y, Rijli FM (2009) Hox genes in neural patterning and circuit formation in the mouse hindbrain. Curr Top Dev Biol 88: 139-167.
Nasevicius A, Ekker SC (2000) Effective targeted gene 'knockdown' in zebrafish. Nat Genet 26(2): 216-220.
Nikolaou N, Watanabe-Asaka T, Gerety S, Distel M, Koster RW et al. (2009) Lunatic fringe promotes the lateral inhibition of neurogenesis. Development 136(15): 2523-2533.
Nishio T (2009) Axonal regeneration and neural network reconstruction in mammalian CNS. J Neurol 256 Suppl 3: 306-309.
Okajima T, Irvine KD (2002) Regulation of notch signaling by o-linked fucose. Cell 111(6): 893-904.
Okajima T, Xu A, Lei L, Irvine KD (2005) Chaperone activity of protein O-fucosyltransferase 1 promotes notch receptor folding. Science 307(5715): 1599-1603.
Okano HJ, Darnell RB (1997) A hierarchy of Hu RNA binding proteins in developing and adult neurons. J Neurosci 17(9): 3024-3037.
Ono K, Yasui Y, Ikenaka K (2004) Lower rhombic lip-derived cells undergo transmedian tangential migration followed by radial migration in the chick embryo brainstem. Eur J Neurosci 20(4): 914-922.
Pagnon-Minot A, Malbouyres M, Haftek-Terreau Z, Kim HR, Sasaki T et al. (2008) Collagen XV, a novel factor in zebrafish notochord differentiation and muscle development. Dev Biol 316(1): 21-35.
Park KW, Urness LD, Senchuk MM, Colvin CJ, Wythe JD et al. (2005) Identification of new netrin family members in zebrafish: developmental expression of netrin 2 and netrin 4. Dev Dyn 234(3): 726-731.
Parsons MJ, Pisharath H, Yusuff S, Moore JC, Siekmann AF et al. (2009) Notch-responsive cells initiate the secondary transition in larval zebrafish pancreas. Mech Dev 126(10): 898-912.
Pasini A, Wilkinson DG (2002) Stabilizing the regionalisation of the developing vertebrate central nervous system. Bioessays 24(5): 427-438.
Pfenninger KH (2009) Plasma membrane expansion: a neuron's Herculean task. Nat Rev Neurosci 10(4): 251-261.
Pfenninger KH, de la Houssaye BA, Helmke SM, Quiroga S (1991) Growth-regulated proteins and neuronal plasticity. A commentary. Mol Neurobiol 5(2-4): 143-151.
Pfenninger KH, Laurino L, Peretti D, Wang X, Rosso S et al. (2003) Regulation of membrane expansion at the nerve growth cone. J Cell Sci 116(Pt 7): 1209-1217.
Pownall ME, Tucker AS, Slack JM, Isaacs HV (1996) eFGF, Xcad3 and Hox genes form a molecular pathway that establishes the anteroposterior axis in Xenopus. Development 122(12): 3881-3892.
Prekeris R, Yang B, Oorschot V, Klumperman J, Scheller RH (1999) Differential roles of syntaxin 7 and syntaxin 8 in endosomal trafficking. Mol Biol Cell 10(11): 3891-3908.
Prince VE, Moens CB, Kimmel CB, Ho RK (1998) Zebrafish hox genes: expression in the hindbrain region of wild-type and mutants of the segmentation gene, valentino. Development 125(3): 393-406.
Puelles E, Acampora D, Lacroix E, Signore M, Annino A et al. (2003) Otx dose-dependent integrated control of antero-posterior and dorso-ventral patterning of midbrain. Nat Neurosci 6(5): 453-460.
Purves D, Augustine GJ, Fitzpatrick D, Katz LC, LaMantia A et al. (2001) Neuroscience; Purves D, Augustine GJ, Fitzpatrick D, Katz LC, LaMantia A et al., editors. Sunderland (MA): Sinauer Associates.
Rakic P (1990) Principles of neural cell migration. Experientia 46(9): 882-891.

Ray RS, Dymecki SM (2009) Rautenlippe Redux -- toward a unified view of the precerebellar rhombic lip. Curr Opin Cell Biol 21(6): 741-747.
Rhinn M, Brand M (2001) The midbrain--hindbrain boundary organizer. Curr Opin Neurobiol 11(1): 34-42.
Richardson SC, Winistorfer SC, Poupon V, Luzio JP, Piper RC (2004) Mammalian late vacuole protein sorting orthologues participate in early endosomal fusion and interact with the cytoskeleton. Mol Biol Cell 15(3): 1197-1210.
Rieger S, Senghaas N, Walch A, Köster RW (2009) Cadherin-2 controls directional chain migration of cerebellar granule neurons. PLoS Biol 7(11): e1000240.
Rigaut G, Shevchenko A, Rutz B, Wilm M, Mann M et al. (1999) A generic protein purification method for protein complex characterization and proteome exploration. Nat Biotechnol 17(10): 1030-1032.
Robinson-Rechavi M, Marchand O, Escriva H, Laudet V (2001) An ancestral whole-genome duplication may not have been responsible for the abundance of duplicated fish genes. Curr Biol 11(12): R458-459.
Robu ME, Larson JD, Nasevicius A, Beiraghi S, Brenner C et al. (2007) p53 activation by knockdown technologies. PLoS Genet 3(5): e78.
Rose MF, Ahmad KA, Thaller C, Zoghbi HY (2009a) Excitatory neurons of the proprioceptive, interoceptive, and arousal hindbrain networks share a developmental requirement for Math1. Proc Natl Acad Sci U S A 106(52): 22462-22467.
Rose MF, Ren J, Ahmad KA, Chao HT, Klisch TJ et al. (2009b) Math1 is essential for the development of hindbrain neurons critical for perinatal breathing. Neuron 64(3): 341-354.
Ross SE, Greenberg ME, Stiles CD (2003) Basic helix-loop-helix factors in cortical development. Neuron 39(1): 13-25.
Rubinsztein DC (2006) The roles of intracellular protein-degradation pathways in neurodegeneration. Nature 443(7113): 780-786.
Rupp RA, Snider L, Weintraub H (1994) Xenopus embryos regulate the nuclear localization of XMyoD. Genes Dev 8(11): 1311-1323.
Saghatelyan A, de Chevigny A, Schachner M, Lledo PM (2004) Tenascin-R mediates activity-dependent recruitment of neuroblasts in the adult mouse forebrain. Nat Neurosci 7(4): 347-356.
Sakata T, Sakaguchi H, Tsuda L, Higashitani A, Aigaki T et al. (2004) Drosophila Nedd4 regulates endocytosis of notch and suppresses its ligand-independent activation. Curr Biol 14(24): 2228-2236.
Sambrook aF (2001) Molecular Cloning: Cold Spring Harbor.
Sann S, Wang Z, Brown H, Jin Y (2009) Roles of endosomal trafficking in neurite outgrowth and guidance. Trends Cell Biol 19(7): 317-324.
Sasamura T, Sasaki N, Miyashita F, Nakao S, Ishikawa HO et al. (2003) neurotic, a novel maternal neurogenic gene, encodes an O-fucosyltransferase that is essential for Notch-Delta interactions. Development 130(20): 4785-4795.
Sassa T, Aizawa H, Okamoto H (2007) Visualization of two distinct classes of neurons by gad2 and zic1 promoter/enhancer elements in the dorsal hindbrain of developing zebrafish reveals neuronal connectivity related to the auditory and lateral line systems. Dev Dyn 236(3): 706-718.
Sato T, Takahoko M, Okamoto H (2006) HuC:Kaede, a useful tool to label neural morphologies in networks in vivo. Genesis 44(3): 136-142.
Scheer N, Campos-Ortega JA (1999) Use of the Gal4-UAS technique for targeted gene expression in the zebrafish. Mech Dev 80(2): 153-158.
Seaman MN (2008) Endosome protein sorting: motifs and machinery. Cell Mol Life Sci 65(18): 2842-2858.

Senghaas N, Koster RW (2009) Culturing and transfecting zebrafish PAC2 fibroblast cells. CSH Protoc 2009(6): pdb prot5235.
Shen J, Chen X, Hendershot L, Prywes R (2002) ER stress regulation of ATF6 localization by dissociation of BiP/GRP78 binding and unmasking of Golgi localization signals. Dev Cell 3(1): 99-111.
Shi S, Stanley P (2003) Protein O-fucosyltransferase 1 is an essential component of Notch signaling pathways. Proc Natl Acad Sci U S A 100(9): 5234-5239.
Shin J, Park HC, Topczewska JM, Mawdsley DJ, Appel B (2003) Neural cell fate analysis in zebrafish using olig2 BAC transgenics. Methods Cell Sci 25(1-2): 7-14.
Sibbe M, Förster E, Basak O, Taylor V, Frotscher M (2009) Reelin and Notch1 cooperate in the development of the dentate gyrus J Neurosci 29: 8578-8585.
Skromne I, Thorsen D, Hale M, Prince VE, Ho RK (2007) Repression of the hindbrain developmental program by Cdx factors is required for the specification of the vertebrate spinal cord. Development 134(11): 2147-2158.
Sleptsova-Friedrich I, Li Y, Emelyanov A, Ekker M, Korzh V et al. (2001) fgfr3 and regionalization of anterior neural tube in zebrafish. Mech Dev 102(1-2): 213-217.
Solecki DJ, Liu XL, Tomoda T, Fang Y, Hatten ME (2001) Activated Notch2 signaling inhibits differentiation of cerebellar granule neuron precursors by maintaining proliferation. Neuron 31(4): 557-568.
Spitz F, Duboule D (2008) Global control regions and regulatory landscapes in vertebrate development and evolution. Adv Genet 61: 175-205.
Spitz F, Gonzalez F, Duboule D (2003) A global control region defines a chromosomal regulatory landscape containing the HoxD cluster. Cell 113(3): 405-417.
Spitz F, Herkenne C, Morris MA, Duboule D (2005) Inversion-induced disruption of the Hoxd cluster leads to the partition of regulatory landscapes. Nat Genet 37(8): 889-893.
Strick DJ, Elferink LA (2005) Rab15 effector protein: a novel protein for receptor recycling from the endocytic recycling compartment. Mol Biol Cell 16(12): 5699-5709.
Struhl G, Fitzgerald K, Greenwald I (1993) Intrinsic activity of the Lin-12 and Notch intracellular domains in vivo. Cell 74(2): 331-345.
Summerton J (1999) Morpholino antisense oligomers: the case for an RNase H-independent structural type. Biochim Biophys Acta 1489(1): 141-158.
Taber-Pierce E (1975) Histogenesis of the deep cerebellar nuclei
in the mouse: an autoradiographic study Brain Res 95: 503–518.
Tamamaki N, Nakamura K, Okamoto K, Kaneko T (2001) Radial glia is a progenitor of neocortical neurons in the developing cerebral cortex. Neurosci Res 41(1): 51-60.
Taylor JS, Braasch I, Frickey T, Meyer A, Van de Peer Y (2003) Genome duplication, a trait shared by 22000 species of ray-finned fish. Genome Res 13(3): 382-390.
Todaro GJ, Green H (1963) Quantitative studies of the growth of mouse embryo cells in culture and their development into established lines. J Cell Biol 17: 299-313.
Trevarrow B, Marks DL, Kimmel CB (1990) Organization of hindbrain segments in the zebrafish embryo. Neuron 4(5): 669-679.
Tsai LH, Gleeson JG (2005) Nucleokinesis in neuronal migration. Neuron 46(3): 383-388.
Tucker B, Lardelli M (2007) A rapid apoptosis assay measuring relative acridine orange fluorescence in zebrafish embryos. Zebrafish 4(2): 113-116.
Ungar D, Hughson FM (2003) SNARE protein structure and function. Annu Rev Cell Dev Biol 19: 493-517.
Valiente M, Marin O (2010) Neuronal migration mechanisms in development and disease. Curr Opin Neurobiol 20(1): 68-78.
Vanderlaan G, Tyurina OV, Karlstrom RO, Chandrasekhar A (2005) Gli function is essential for motor neuron induction in zebrafish. Dev Biol 282(2): 550-570.

Volkmann K, Rieger S, Babaryka A, Köster RW (2008) The zebrafish cerebellar rhombic lip is spatially patterned in producing granule cell populations of different functional compartments. Dev Biol 313(1): 167-180.
Volkmann K, Chen YY, Harris MP, Wullimann MF, Köster RW (2010) The zebrafish cerebellar upper rhombic lip generates tegmental hindbrain nuclei by long-distance migration in an evolutionary conserved manner. J Comp Neurol 518(14): 2794-2817.
Wagner GP, Amemiya C, Ruddle F (2003) Hox cluster duplications and the opportunity for evolutionary novelties. Proc Natl Acad Sci U S A 100(25): 14603-14606.
Wakamatsu Y, Weston JA (1997) Sequential expression and role of Hu RNA-binding proteins during neurogenesis. Development 124(17): 3449-3460.
Wang VY, Rose MF, Zoghbi HY (2005) Math1 expression redefines the rhombic lip derivatives and reveals novel lineages within the brainstem and cerebellum. Neuron 48(1): 31-43.
Watanabe H, Murakami F (2009) Real time analysis of pontine neurons during initial stages of nucleogenesis. Neurosci Res 64(1): 20-29.
Weber HS, Cyran SE (1998) Transvenous "snare-assisted" coil occlusion of patent ductus arteriosus. Am J Cardiol 82(2): 248-251.
Weber T, Zemelman BV, McNew JA, Westermann B, Gmachl M et al. (1998) SNAREpins: minimal machinery for membrane fusion. Cell 92(6): 759-772.
Wessel D, Flugge UI (1984) A method for the quantitative recovery of protein in dilute solution in the presence of detergents and lipids. Anal Biochem 138(1): 141-143.
Westerfield M (1995) The Zebrafish Book. A Guide for the Laboratory Use of Zebrafish (Danio rerio). Eugene, OR: University of Oregon Press. p.
Wettstein DA, Turner DL, Kintner C (1997) The Xenopus homolog of Drosophila Suppressor of Hairless mediates Notch signaling during primary neurogenesis. Development 124(3): 693-702.
Wilkin MB, Carbery AM, Fostier M, Aslam H, Mazaleyrat SL et al. (2004) Regulation of notch endosomal sorting and signaling by Drosophila Nedd4 family proteins. Curr Biol 14(24): 2237-2244.
Wilson LJ, Wingate RJ (2006) Temporal identity transition in the avian cerebellar rhombic lip. Dev Biol 297(2): 508-521.
Wines-Samuelson M, Handler M, Shen J (2005) Role of presenilin-1 in cortical lamination and survival of Cajal-Retzius neurons. Dev Biol 277(2): 332-346.
Wingate RJ (2001) The rhombic lip and early cerebellar development. Curr Opin Neurobiol 11(1): 82-88.
Woltering JM, Durston AJ (2006) The zebrafish hoxDb cluster has been reduced to a single microRNA. Nat Genet 38(6): 601-602.
Wullimann MF, Reichert H, Rupp B (1996) Neuroanatomy of the Zebrafish Brain: A Topological Atlas: Birkhauser Verlag.
Wurst W, Bally-Cuif L (2001) Neural plate patterning: upstream and downstream of the isthmic organizer. Nat Rev Neurosci 2(2): 99-108.
Xie LX, Calafat J, Janssen H, de la Iglesia-Vicente J, Mollinedo F (2010) Intracellular location of syntaxin 7 in human neutrophils. Immunol Lett.
Yamamoto N, Yamamoto S, Inagaki F, Kawaichi M, Fukamizu A et al. (2001) Role of Deltex-1 as a transcriptional regulator downstream of the Notch receptor. J Biol Chem 276(48): 45031-45040.
Zecchin E, Mavropoulos A, Devos N, Filippi A, Tiso N et al. (2004) Evolutionary conserved role of ptf1a in the specification of exocrine pancreatic fates. Dev Biol 268(1): 174-184.